INFORMATION TO USERS

This manuscript has been reproduced from the microfilm master. UMI films the text directly from the original or copy submitted. Thus, some thesis and dissertation copies are in typewriter face, while others may be from any type of computer printer.

The quality of this reproduction is dependent upon the quality of the copy submitted. Broken or indistinct print, colored or poor quality illustrations and photographs, print bleedthrough, substandard margins, and improper alignment can adversely affect reproduction.

In the unlikely event that the author did not send UMI a complete manuscript and there are missing pages, these will be noted. Also, if unauthorized copyright material had to be removed, a note will indicate the deletion.

Oversize materials (e.g., maps, drawings, charts) are reproduced by sectioning the original, beginning at the upper left-hand corner and continuing from left to right in equal sections with small overlaps.

ProQuest Information and Learning
300 North Zeeb Road, Ann Arbor, MI 48106-1346 USA
800-521-0600

UMI®

University of Alberta

MOMENT REDISTRIBUTION IN REINFORCED CONCRETE STRUCTURES

by

Adnan Shakir ©

A thesis submitted to the Faculty of Graduate Studies and Research in partial fulfillment of the requirements for the degree of Doctor of Philosophy

in

Structural Engineering

Department of Civil and Environmental Engineering

Edmonton, Alberta

Spring 2005

Canada

DEDICATION

This thesis is dedicated to my parents Shakir Ali and Mehmooda Begum, wife Talat, and children Maha, Omar, and Asher to appreciate their sacrifices, love, and support without which it would not have been possible for me to achieve these goals.

ABSTRACT

Moment redistribution provides an attractive alternative to the non-linear methods of analysis. CSA A23.3-94 provisions for moment redistribution neglect the effects of important parameters and can be conservative. Significant differences exist among design standards on the provisions for moment redistribution. The lack of consensus suggests that as a profession we do not fully understand the problem. This work attempts to establish appropriate limits on allowable moment redistribution in reinforced concrete structures.

An analytical model is developed for computing β, the permissible percentage reduction in moment at a section due to moment redistribution. Important parameters affecting β are identified and incorporated in the model. The model is validated against experimental results and shows good agreement. Comparison between CSA A23.3-94 and the model limits shows that the code is conservative. The maximum code limit for β is 20%. For the ultimate limit-state, with favourable combination of parameters, the model would allow β in excess of 50%. The serviceability limit state, however, can restrict β to 21% to 34%.

The code considers β as a function of c/d, the ratio of the depth of neutral axis to the effective depth of beam cross-section, only. For 20% moment redistribution, the standard allowable c/d is only 0.2. By comparison, the model allowable c/d for 20% moment redistribution is at least 0.38 and can be as high as 0.6.

A parametric study shows that the β depends upon various parameters, in addition to c/d. It is thus inappropriate to express β as a function of c/d alone.

A set of empirical equations for β is developed to provide an alternative to the code equation. The equations consider the explicit effects of ω, the mechanical reinforcement ratio, and L/d, the span to depth ratio, on β, with implicit effects from other parameters.

Design moment coefficients for continuous reinforced concrete beams are developed. Use of these coefficients vs code coefficients can provide savings in the amount of flexural reinforcement. It is demonstrated that considering moment redistribution can eliminate the need for pattern live-load analysis, in the design of continuous reinforced concrete beams with c/d less than 0.4.

ACKNOWLEDGEMENTS

This research was conducted under the supervision of Dr. D.M. Rogowsky. His able guidance and untiring support in the writing of this thesis and the work that preceded it are greatly appreciated.

I would like to express my appreciation of Dr. S.D.B Alexander and Dr. G.Y Grondin who provided a critical review of the draft of this thesis. Professors J. G. MacGregor and P. Marti also provided valuable comments during the course of this work. Their assistance is gratefully acknowledged.

It would not have been possible to conduct this research without the financial support provided by the University of Alberta, Natural Sciences and Engineering Research Council, and Concrete Canada. Their support is greatly appreciated.

A special thank goes out to my friends and their families, especially Nadeem Khattak, Agha Hasan, Azer Mashhood, and Kishwer Sultana, for being there in time of need and providing moral support and motivation during the course of my candidature.

I remain forever indebted to my parents Shakir Ali and Mehmooda Begum, brothers Nadeem and Navaid, and sisters Yasmeen and Sohaila for their endless support, love, and encouragement. Their prayers certainly kept me going.

Last but not least, my deepest gratitude is due to my wife Talat, and children Maha, Omar, and Asher for keeping my spirits alive. They showed unlimited patience, understanding and tolerance during the course of my candidature. Their love, encouragement, and untiring support provided me with the strength to stay on course and were the biggest source of inspiration in completing this research.

Finally, I would like to thank Almighty Allah on giving me the endurance and courage to accomplish this work.

TABLE OF CONTENTS

LIST OF FIGURES

LIST OF TABLES

LIST OF ABBREVIATIONS AND SYMBOLS

Abbreviations

ACI American Concrete Institute

BS British Standards

CEB Comité Euro-International du Béton (Euro-International Concrete Committee)

CSA Canadian Standards Association

DIN Deutsches Institut fur Normung E.V. (German Standards Institute)

FIP Fédération Internationale de la Précontrainte (International Federation for Prestressing)

JSCE Japan Society of Civil Engineering

Symbols

a depth of equivalent rectangular stress block at ultimate

A'_s area of compression reinforcement

A_{cef} effective area of concrete in tension

A_s area of tension reinforcement

A_{sb} area of reinforcement corresponding to the balanced steel ratio

A_{si} area of steel for i^{th} steel layer

A_{vs} cross-section area of one leg of stirrup

b beam width

b' beam flange width

b_o width of concrete core measured to outside of the peripheral ties

b_s centre to centre width of the stirrup

b_{so} width to the outside of stirrup

b_w beam web width

c depth of neutral axis (distance from the extreme compression fiber to the neutral axis of the section)

C_c	compressive force in concrete
c_o	concrete cover in mm
c_y	depth of neutral axis at first yield
d	effective depth of section (distance from the extreme compression fiber to the centroid of the tension reinforcement)
d_b	diameter of reinforcing bar
d_i	depth of ith steel layer from extreme compression fibre
d_x	differential element of reinforced concrete member
E_c	modulus of elasticity of concrete
EI	flexural stiffness of reinforced concrete section
EI_{cr}	cracked flexural stiffness
E_s	modulus of elasticity of steel
E_{sh}	modulus of strain hardening
f_c'	compressive strength of concrete
f_{ct}	tensile strength of concrete
f_s	steel stress
f_{si}	steel stress for i^{th} steel layer
f_{su}	ultimate strength of steel
f_t	tensile stress in concrete
Ft	force in tension steel
f_y	yield strength of steel
f_{yh}	yield strength of steel hoops
h_s	centre to centre height of the stirrup
h_{so}	height to the outside of stirrup
I_{av}	average cracked moment of inertia $= (I_{su}+I_{sp})/2$
I_{cr}	cracked moment of inertia
I_{sp}	cracked moment of inertia at the span
I_{su}	cracked moment of inertia at the support
jd	distance from the centroid of compressive forces in steel and concrete to the centroid of tension steel
K	factor that takes into account the effect of confinement on concrete strength

K_1	parameter depending upon the support conditions and loading
k_1	factor taken as 0.7 for mild steel, 0.9 for cold rolled steel
K_2	parameter that defines the effective plastic hinge length
k_2	$1+0.5p_u/p_o$
k_3	factor taken as 0.6 for a concrete cube strength of 40 MPa, 0.9 for 15 MPa
kd	depth of neutral axis corresponding to yielding of steel.
K_p	plastic hinge length factor
k_s	spring stiffness
L	centre to centre span
L_n	clear span
L_p	plastic hinge length
L_t	bond transfer length
M	bending moment
M_a	ultimate moment at support
M_{des}	design moment
M_{eL}	elastic envelope moment at left support
M_{emid}	elastic envelope moment at mid-span
M_{eR}	elastic envelope moment at right support
M_f	factored elastic moment
M_{min}	moment resistance corresponding to minimum area of flexural reinforcement
M_o	static span moment
M_r	nominal moment of resistance
M_{rL}	moment resistance of a critical section at left support
M_{rmid}	moment resistance of a critical section at mid-span
M_{rR}	moment resistance of a critical section at right support
M_s	service elastic moment
M_{total}	total span moment
M_u	moment at ultimate load
M_x	bending moment at a distance x from the support
M_y	moment at first yield

n	modular ratio (E_s/E_c)
P	axial load
P_o	axial compressive strength of member without bending moment
P_u	axial load at ultimate
q	uniformly distributed load
q_p	uniformly distributed load corresponding to formation of first plastic hinge
q_u	uniformly distributed load at beam failure
q_y	uniformly distributed load at yielding of steel
s	centre to centre spacing of the stirrups
s_b	spacing of longitudinal bars
s_m	average crack spacing
T_i	tension force in i^{th} steel layer
V_c	shear carried by the concrete
V_r	shear resistance of the beam
V_s	shear carried by the stirrups crossing 45^0 crack
V_{sx}	shear carried by the stirrups crossing cracks within the distance d_v
V_x	shear at a given section
w_d	uniformly distributed dead load
w_L	uniformly distributed live load
w_f	uniformly distributed factored load
w_i	crack width at section i
x_j	yield safety parameter for section j
x_{L1}	left hand side region of a cracked element in which $\tau_b = \tau_{b1}$
x_{L2}	left hand side region of a cracked element in which $\tau_b = \tau_{b2}$
x_{R1}	right hand side region of a cracked element in which $\tau_b = \tau_{b1}$
x_{R2}	right hand side region of a cracked element in which $\tau_b = \tau_{b2}$
x_u	depth of compression zone at ultimate limit stage
z	distance of critical section to the point of contraflexure
Z_m	factor defining slope of falling branch of concrete stress-strain curve
α	unfactored live load to dead load ratio

α_1	ratio of average stress in the rectangular compression block to the specified concrete strength = $0.85 - 0.0015 f_c'$
β	allowable percentage reduction in the elastic bending moment
β_c	global factor to take into account the different ultimate concrete strains
β_L	allowable percentage reduction in the left support elastic moment
β_{mid}	allowable percentage reduction in the mid-span elastic moment
β_n	22.5 (global factor to take into account the non-linearity
β_R	allowable percentage reduction in the right support elastic moment
β_s	0.0740 for high ductile steel, 0.0476 for normal ductile steel
β_1	ratio of the depth of stress block, a, to the depth of neutral axis at ultimate = $0.97 - 0.0025 f_c'$.
γ	ratio of adjacent spans
ε_c	concrete strain
ε_{cu}	ultimate concrete strain at extreme compression fibre
ε_{cy}	strain in concrete at the yielding of steel
ε_{k50u}	concrete strain corresponding to $0.5 f_c'$
ε_{k50h}	additional concrete strain due to confinement at $0.5 f_c'$
ε_s	steel strain
ε_{si}	steel strain for i^{th} steel layer
ε_{sm}	average steel strain
ε_{su}	ultimate strain in steel
ε_{suk}	characteristic value of steel strain at maximum strength (0.05)
ε_{suk}^*	steel strain at ultimate taking into account tension stiffening
ε_{sx}	steel strain at a given section
ε_{syk}	characteristic steel strain at yield point
η	ratio of shear carried by steel to the total shear (v_s/v_r)
θ	rotation of a section
θ_{free}	unrestrained rotation
θ_p	plastic rotation capacity
θ_{pL}	plastic rotation capacity for one side of hinge

θ_{preqd}	required plastic rotation capacity
θ_{rest}	restrained rotation
$\Theta_{R,pl}$	plastic rotation capacity (din 1045)
θ_{tu}	total inelastic rotation in length z
θ_u	ultimate rotation in plastic hinge length
θ_y	yield rotation in plastic hinge length
κ_1	coefficient defining the influence of the bond properties of the bars
κ_2	coefficient dependent on the distribution of tensile stress within the section
λ	limiting moment coefficient
λ_q	shear slenderness
μ	moment coefficient
μ_d	ductility moment coefficient
μ_{des}	design moment coefficient
μ_f	factored elastic moment coefficient
μ_{red}	redistributed moment coefficient
μ_s	serviceability moment coefficient
ρ	tension reinforcement ratio = a_s/bd
ρ'	compression reinforcement ratio = A'_s/bd
ρ_b	balanced reinforcement ratio = A_b/bd
ρ_r	ratio of the area of tension steel to the effective area of concrete, A_{cef}
ρ_v	volumetric percentage of transverse steel = $2(b_s+h_s)A_{vs}/b_{so}h_{so}s$
σ_s	stress in steel for cracked element
σ_{scrL}	steel stress at left face of the cracked element
σ_{scrR}	steel stress at right face of the cracked element
σ_{smin}	minimum steel stress within the cracked element
τ_b	bond shear
τ_{bave}	average bond shear stress
τ_{b1}	bond shear when $f_s<f_y$
τ_{b2}	bond shear when $f_s>f_y$
ϕ	curvature

ϕ_c capacity reduction factor for concrete

ϕ_p plastic curvature

ϕ_s capacity reduction factor for steel

ϕ_u ultimate curvature

ϕ_x curvature at a given section

ϕ_y curvature at first yield

ω mechanical reinforcement index $= A_s f_y / bdf_c'$

ω' mechanical compression reinforcement index $= A_s' f_y / bdf_c'$

ω_b mechanical reinforcement index at balanced condition $= A_{sb} f_y / bdf_c'$

ω_{eff} effective mechanical reinforcement index $= \left(A_s - A_s' \right) f_y / bdf_c'$

1. INTRODUCTION

1.1 Introduction

This work considers moment redistribution and ductility of indeterminate reinforced concrete structures. Moment redistribution occurs in reinforced concrete structures due to cracking of concrete and yielding of steel. Moment redistribution can be used to reduce the design moments in indeterminate reinforced concrete structures. Today the focus of our work is not only the design and construction of new structures but also the evaluation and rehabilitation of existing structures. Moment redistribution can be used to tap into the reserves of strength which otherwise could not be rationalised by the elastic methods of analysis. CSA A23.3-94 provisions for moment redistribution are conservative and do not account for the effect of the main parameters. A need exists for a ductility model that can assess the allowable moment redistribution in reinforced concrete structures and provide a more rational limit than the current standard limit.

The actual behaviour of reinforced concrete is non-linear. As a result, elastic analysis does not predict the behaviour of reinforced concrete structures at ultimate. For redundant concrete structures, there is a reserve of strength that can be best utilised through non-linear analysis and design. A number of non-linear analysis and design methods exist. These are often referred to as the limit design methods. True non-linear-analysis methods are generally not used in design practice due to complexity of the analysis procedures. Since these methods utilise all the strength reserves, there is also a concern among the design engineers about the safety margins provided by these methods.

Moment redistribution is a form of non-linear analysis in which the calculated elastic bending moment at a critical section may be reduced or increased provided that the bending moments in the adjoining critical sections are increased or decreased to satisfy equilibrium for the loading case under consideration. Since the load cases that give the maximum moments at support are usually different from those which give the maximum moments at mid-span, allowing for moment redistribution reduces maximum negative

1

and maximum positive moments of the elastic moment envelope. This results in a reduction in the amount of flexural reinforcement required and congestion of reinforcement at supports locations.

Recognizing the non-linear behavior of concrete structures at the ultimate load stage, structural design standards allow limited redistribution of elastic moments. There are several issues that need to be addressed regarding the use of such relations. The following outlines the issues related to the provisions of the Canadian standard (CSA A23.3-94) in particular.

(1)   The CSA A23.3-94 limit for allowable moment redistribution is conservative compared to most design standards. It gives a maximum allowable moment redistribution of 20%. British (BS8110-1988) and European (CEB-FIP Model Code-1990) design standards allow up to 30% moment redistribution, while the Danish standard (DS411-1986) allows as much as 66% moment redistribution. Japanese standards (JSCE-1986) set an upper limit of 15%. Thus significant differences exist among the design standards on the amount of allowable moment redistribution.

(2)   CSA A23.3-94 assumes that β is only a function of the c/d ratio. As the literature review will reveal, this is not true. The amount of moment redistribution depends upon the plastic rotation capacity, which in turn depends upon a number of other factors. Some of the important factors identified in the literature include; structure geometry, loading, presence of shear cracks, bond-slip relationship, concrete confinement, and material constitutive relationships.

(3)   CSA A23.3-94 places a restriction on the increase in moment, while performing moment redistribution. Since increasing the design moment above the elastic moment does not pose any ductility demand on the section, this restriction is unwarranted.

2

There is a need to improve the provisions of A23.3-94. Furthermore, the revised moment redistribution provisions can be used to improve the approximate frame analysis coefficients in section 9.3.3 of A23.3-94.

1.2 Research Objective and Scope

The research objective is to develop a rational moment redistribution provision, suitable for incorporation in the design standard.

The following scope of work is identified.

(1)   Perform an analytical assessment of CSA A23.3-94 provisions for moment redistribution to demonstrate the need for a rational ductility model.

(2)   Develop a comprehensive analytical model for computing the plastic rotation capacity and determining the allowable limit for moment redistribution.

(3)   Perform a parametric study to understand and quantify the effects of different parameters on allowable moment redistribution.

(4)   Evaluate the moment redistribution limits with respect to the ductility limit condition.

(5)   Evaluate the moment redistribution limits with respect to the serviceability limit condition.

(6)   Develop alternate equations for moment redistribution by considering both ductility and serviceability limit conditions. These equations would reflect the effects of various parameters in addition to the c/d ratio.

(7)   Derive moment coefficients for flexural design of continuous beams.

3

(8)   Examine the need for pattern load analysis in continuous reinforced concrete beams.

The scope of work is limited to reinforced concrete beams and braced frames subjected to static gravity loads only. Lateral load analysis and stability consideration are beyond the scope of this work.

1.3 Outline of the Thesis

As with all research, the search for a solution started with a review of existing literature. An overview of the existing literature on moment redistribution and ductility of reinforced concrete continuous beams is presented in Chapter 2. The purpose of the review is to identify the important parameters affecting ductility and moment redistribution and review the concepts that will be used later in the thesis to develop the analytical model. A critical review of the existing provisions for moment redistribution in different design standards is also done to point out the discrepancies and deficiencies associated with these provisions. Anomalies in the A23.3-94 requirements for moment redistribution are especially pointed out.

Chapter 3 examines the standard (CSA A23.3-94) limit for moment redistribution and assesses the need for a ductility model that can provide a realistic estimate of plastic rotation capacity and allowable moment redistribution in continuous reinforced concrete beams. Ductility equations from plane-section analysis, combined with classical equilibrium methods of analysis and subsequent hinge moment analysis, is used to establish the allowable c/d for given amount of moment redistribution.

An analytical model is developed in Chapter 4 to predict the plastic rotation capacity and moment redistribution limit of reinforced concrete sections. The model is developed by considering the mechanics of reinforced concrete, constitutive laws, which include a bond-slip law that allows computation of stresses and strains within the cracked elements. An effort is made to incorporate all the important variables identified in the literature

4

review, especially beam slenderness, concrete confinement, ultimate concrete strain, steel ductility, shear cracking, and type of loading.

A parametric study is done in Chapter 5 to understand and quantify the effects of various parameters on plastic rotation capacity and allowable moment redistribution. The study is carried out using the model developed in Chapter 4. The parametric study provides guidelines for safe incorporation of moment redistribution in design practice. The data generated from the parametric study is used to develop a set of ductility-based empirical equations for allowable moment redistribution.

Although ductility condition may allow very high amount of moment redistribution under favorable conditions, the serviceability limit-state must be checked to establish an upper limit on allowable moment redistribution. In Chapter 6, moment redistribution limits are determined by evaluating the maximum elastic service load moments at critical sections under different load combinations, adjacent span ratios, and live load to dead load ratios. Empirical equations for allowable moment redistribution are derived considering both serviceability and ductility requirements.

Redistributed design moment coefficients are derived in Chapter 7 by considering the ultimate limit-state and the serviceability limit-state. The effects of pattern loads, span configurations and live load to dead load ratios are considered. The maximum coefficients from the two provide the design moment coefficients.

The need for pattern load analysis is assessed in Chapter 7 to determine if continuous reinforced concrete beams can be analyzed and designed for a single load case. This is accomplished by comparing the maximum elastic moments from a non-pattern single load analysis with the redistributed design moments from pattern load analysis.

Chapter 8 presents a summary of the research, conclusions, and recommendations for future research.

5

2. LITERATURE REVIEW

2.1 Introduction

This chapter reviews the concepts and literature on the behaviour of reinforced concrete structures that will be used and referred to in the remainder of the thesis. A review of the classical methods of non-linear analysis provides a tool for initial assessment and comparison of standard (CSA A23.3-94) limit for moment redistribution. A review of the existing ductility models identifies the major parameters influencing allowable moment redistribution. A review of the concrete stress-strain models helps selecting a constitutive relationship for modelling the behaviour of confined concrete. A review of the moment redistribution provisions of different standards provides a notion of differences among these standards on this subject matter.

2.2 Classical Methods For Non-Linear Design of Concrete Structures

Reinforced concrete is not an elastic material and hence the application of elastic analysis concepts to reinforced concrete structures is a matter of pure convenience. Even if the elastic behaviour may be accepted as an idealised model for statically determinate reinforced concrete members, such a model can not reflect the actual behaviour of redundant structures. Redundant structures, subjected to a large number of loading conditions, have strength reserve that can be utilised through non-linear methods of analysis.

Elastic theory of concrete structures can not provide answers to such questions as; what is the behaviour of a structure after the yield occurs at a critical section? What is the load at which a redundant reinforced concrete structure actually collapses? What is the deflection of a structure on the verge of its collapse? Answers to such questions can only be provided through inelastic methods of analysis.

6

Fundamental concepts and theories of the non-linear analysis of reinforced concrete structures were developed in late fifties and sixties (Baker 1956, Maachi 1960, Sawyer 1964, Cohn 1964). These methods of non-linear analysis are often referred to as the "limit design" methods.

The limit design approach allows any distribution of bending moments at ultimate load to be used, provided the following conditions are met (Park and Paulay 1975).

1. The distribution of bending moments is statically admissible. That is, the bending moment pattern chosen does not violate the laws of equilibrium for the structure as a whole or for any part of it.

2. The rotation capacity of the plastic hinge regions is sufficient to enable the assumed distribution of moments to be developed at the ultimate load. That is, the required plastic rotations at critical sections do not exceed the available plastic rotations, for all possible loading schemes.

3. The cracking and deflections at the service load are not excessive.

The requirements of items 1 to 3 can be stated as limit equilibrium, rotation compatibility, and serviceability (Park and Paulay 1975). Most limit design methods consider one or two of these conditions initially, the remaining condition or conditions being the object of a subsequent check.

In proceedings of the International symposium on Non-linear design of concrete structures, Cohn (1979) classified the limit design methods into two broad classes, depending on the way they satisfy the three fundamental requirements. The "compatibility methods" are essentially concerned with the satisfaction of equilibrium and rotation compatibility at ultimate load and require a subsequent check of serviceability. The "equilibrium methods" are primarily concerned with the satisfaction

7

of equilibrium and serviceability and require a subsequent check of rotation compatibility.

Classical inelastic methods in the compatibility group have been proposed by Baker (1956), Macchi (1960), and Sawyer (1964). Methods in the equilibrium group have been proposed by Cohn (1964, 1968), and Furlong (1970). The following presents a brief review of some of the limit design methods, done by Park and Paulay (1975) and Cohn (1979).

2.2.1 Compatibility methods

Compatibility methods satisfy, in the first place, the equilibrium and rotation compatibility of critical sections under ultimate loads. The serviceability criterion is not considered initially and is a matter of subsequent checks. The compatibility methods aim at controlling the deformation capacity of structures, for the worst loading combinations, at the ultimate limit state. Various authors differ on two major assumptions; the idealised behavioural model of reinforced concrete sections and the definition of the ultimate state.

Baker (1971) adopted the bilinear moment-curvature relationship, as shown in Fig. 2.1(a), with points A and B corresponding to the incipient yielding of the tension steel and the crushing of the compression zone of concrete, respectively. Baker assumed that the ultimate limit-state of a structure is reached when it develops a collapse mechanism by the formation of a sufficient number of plastic hinges.

The design is commenced by determining a distribution of ultimate bending moments, which is in equilibrium with the ultimate loads. This may be obtained by drawing the free bending moment diagram for the members supporting the ultimate loads when the ends are free of rotational restraint, and drawing the fixing moment line at some convenient position, as shown in Fig. 2.2. The sections are reinforced for those ultimate moments. Note that a collapse mechanism has developed at the ultimate load. The rotation capacity of the plastic hinge regions is then checked to ensure that the chosen distribution of bending moments can be developed at the ultimate load. The pattern of moments at the

8

service load is determined and the stresses checked to ensure that the members are serviceable. The assumed distribution of ultimate moments may need to be modified if inadequate rotation capacity or unsatisfactory serviceability is found.

Sawyer (1964) adopted the bilinear model, as shown in Fig. 2.1(b), with points C and D corresponding to the elastic and ultimate limit states of the section, respectively. The carrying capacity of a structure is reached when at least one of its critical sections is defined by point D in Fig. 2.1(b). Sawyer proposed that the statically indeterminate beams and frames be designed for suitably low probabilities of failure for two failure stages. One stage would be crushing-spalling of concrete and the other would be wide cracking of concrete.

The method uses a rotational compatibility analysis indirectly by adjusting the elastic envelope moments obtained from the various design-loading combinations at ultimate load, to establish a bending moment pattern for which reinforcement is provided. For each possible loading combination at ultimate load, using any set of adjusted moments that satisfies static equilibrium and falls within the ultimate resisting moments of the sections, the inelastic rotations at all plastic sections are calculated. A moment-curvature curve with a yield moment of 0.85 of the ultimate moment is assumed. Elastic theory is then used to calculate the moments resulting from these inelastic bending angles and the external loading imposed on the structure. If the calculated moments exceed the ultimate resisting moments of the sections, the reinforcement is revised by adding reinforcement to regions in which the ultimate moment is exceeded or to regions in which the inelastic angle developed is excessive. The moments introduced by the inelastic angles and the external loading are recalculated, and the reinforcement is adjusted, until the adequacy of the ultimate moments of resistance has been demonstrated. The design is then checked by elastic theory to ensure that the steel stresses and cracks at service load are not excessive.

2.2.2 Equilibrium methods

Equilibrium methods of analysis satisfy equilibrium and serviceability criteria in the first place while compatibility is a matter of subsequent checks. These methods aim at

9

ensuring convenient margins of safety against local section failures and against structural collapse. The main aspects of equilibrium methods may be summarised as follows.

(1)   Under-reinforced concrete sections are idealised by the elastic-plastic model, as shown in Fig. 2.1(a).

(2)   Design moments are defined as percentages of the corresponding elastic envelope moments calculated for the ultimate loads.

(3)   A satisfactory criterion for the ultimate limit state is required to provide safety against any possible mode of plastic collapse.

(4)   An appropriate serviceability criterion is required to provide sufficient safety against yielding, cracking, and deflection when subjected to worst loading combination.

Cohn (1964, 1968) developed a limit design method based on the requirements of limit equilibrium and serviceability. In this method, the solution is obtained by scaling down the elastic envelope moments obtained from the various ultimate load combinations, by multiplying by appropriate parameter $x_j \leq 1$, where x_j is the yield safety parameter for section j. The value of x_j is set by the following requirements: at service load, the critical sections of the frame must remain in the elastic range; at the ultimate load, the internal forces must be in equilibrium with the external loads and one or more collapse mechanisms must form; and the overall moment reductions from the elastic envelope must be a maximum. A typical design seeks the minimum value for x_j consistent with acceptable service load behaviour and the equilibrium conditions at the ultimate load. The sections are designed on the basis of the determined distribution of bending moments, and the plastic hinge regions are checked to ensure that they have sufficient rotation capacity to develop the assumed moment redistribution at the ultimate load.

Furlong (1970) developed a limit design method that involved assigning ultimate moments for structures braced against side sway. The worst cases of different types and

10

arrangements of loading on various arrangements of spans were analysed by Furlong to determine the possible patterns of design moments in continuous beams that would satisfy the requirements of serviceability and limit equilibrium. Then the plastic rotations resulting from these distributions of ultimate moments were analysed to determine the curvature ductility requirements. The possible distributions of design moments so found were used to derive the moment coefficients and a simple equation was given for curvature ductility requirements.

$$\frac{\phi_u}{\phi_y} \geq 1 + 0.25 \frac{L_n}{d} \qquad\qquad [2.1]$$

where

ϕ_u = ultimate curvature

ϕ_y = curvature at first yield

L_n = clear span

D = effective depth of section.

Later, Furlong and Rezende (1979) proposed an alternate system of moment coefficients and equations for determining beam shears and beam and column moments in order to determine design values for beams and one way slabs in braced frames. This alternate set of analysis coefficients can be applied to a broad range of structures involving live to dead load ratios as high as five and almost any combination of span lengths. The alternate system is derived with requirements that every component is ductile and strong enough to resist a minimum limit state of strength, with provisions that no reinforcement will yield under any service limit state of loading.

Modern equilibrium methods are those proposed by Marti (1999). Marti proposed a simple consistent approach to the design of plain, reinforced and prestressed concrete structures. It utilises both static (lower bound) and kinematic (upper bound) methods of limit analysis. The static method uses discontinuous stress fields and a truss model (Marti 1991) to model the flow of forces within the member and is particularly suitable for new

11

structures. The method allows for some assumed level of redistribution. The kinematic method on the other hand enables quick check of essential dimensions and details of an existing design or structure. In the kinematic method the concrete is treated as an isotropic, perfectly plastic material, and the governing failure mechanisms are derived by using the Mohr-Coulomb failure envelope (Marti 1980).

According to Marti, after cracking the structural response is governed mainly by the tension chord deformations. The tension chord model developed by Marti et al. (1998) permits a unified treatment of the problems of cracking, minimum reinforcement, tension stiffening, deformation capacity and permissible redistribution of forces and moments. The cracked membrane model (Kaufmann and Marti 1998) combines the basic concepts of modified compression field approach and the tension chord model to predict the behaviour of cracked members.

Marti pointed out that the response of the structure changes with the loading history because the member starts cracking at earlier loads. However, provided that sufficiently ductile behaviour is ensured, ultimate strengths are unaffected by the loading and restraining history. Hence, to obtain reliable results from limit stress analysis, the ductility of the structure must be ensured through the selection of appropriate materials, as well as adequate dimensioning and detailing of the structures. Marti indicated that the behaviour of a structural member under service loads could be improved by prestressing some of the reinforcement.

2.3 Arbitrary Moment Redistribution

The "arbitrary redistribution of moments" is an alternate method of inelastic design that has gained more acceptance than the limit design methods. In moment redistribution, the calculated elastic bending moment at a critical section may be reduced or increased provided that the bending moments in the adjoining critical sections are adjusted appropriately to maintain equilibrium for the loading case under consideration. Figure 2.3 illustrates the adjustment in the elastic bending moment diagram for a two-span continuous beam (Park and Paulay 1975). Since the load cases that give the maximum

12

moments at support are usually different from those which give the maximum mid-span moments, allowing for moment redistribution will result in reduction of maximum negative and maximum positive moments as compared to the elastic moment envelope.

There are two main advantages associated with the use of moment redistribution; the designer can select patterns of bending moment that avoid congestion of the reinforcement at the supports of beams, and improved economy from the reduction of the peaks of the elastic bending moment envelope. If large adjustments to the peak bending moments in Fig. 2.3 can be made, significant savings will result, particularly if the ratio of live load to dead load is high.

2.4 Moment Redistribution Provisions in Design Standards

Design standards recognise the non-linear behaviour of reinforced concrete and acknowledge it by allowing some moment redistribution from an elastic analysis. Different formulae for the redistribution of elastic moments have been proposed by various standards of practice. A summary of such formulae is presented here:

I.   ACI 318-95

$$\beta = 20\left(1 - \frac{\rho - \rho'}{\rho_b}\right)$$
[2.2]

But, $\rho - \rho'$ should not exceed $0.5\rho_b$

where,

β =   amount of moment redistribution expressed as a percentage of the elastic moment

ρ =   tension reinforcement ratio = A_s / bd

ρ' =   compression reinforcement ratio = A_s' / bd

A_s =   tension reinforcement

A_s' =   compression reinforcement

13

ρ_b = reinforcement ratio under balanced conditions

II.   CSA A23.3-94

$$\beta = 30 - 50\frac{c}{d} \le 20\% \qquad\qquad [2.3]$$

where

c   = the depth of neutral axis

d   = the effective depth of the section.

III.   BS 8110-85

$$\beta = \left(0.6 - \frac{c}{d}\right) \times 100 \le 30\% \qquad\qquad [2.4]$$

For structures more than four storeys high, in which the frame provides the lateral stability, the reduction in moment is restricted to 10%.

IV.   CEB Model Code 1990

For concrete strengths between 12 MPa and 35 MPa

$$\beta = \left(0.56 - 1.25\frac{c}{d}\right) \times 100 \qquad\qquad [2.5a]$$

For concrete strengths between 40 MPa to 60 MPa

$$\beta = \left(0.44 - 1.25\frac{c}{d}\right) \times 100 \qquad\qquad [2.5b]$$

For continuous beams and non-sway frames

14

$$0 < \beta < 30\%$$

For sway frames

$$0 < \beta < 10\%$$

V.   Din 1045-78 (German)

$$\beta \leq 15\% \qquad\qquad\qquad\qquad\qquad\qquad\qquad\qquad\qquad\qquad [2.6]$$

VI.   JSCE-1986 (Japan)

$$\beta < 15\% \qquad\qquad\qquad\qquad\qquad\qquad\qquad\qquad\qquad\qquad [2.7]$$

when, $\rho - \rho' \leq 0.5\rho_b$

VII.   DS 411-1986 (Danish)

$$\beta \leq 66\% \qquad\qquad\qquad\qquad\qquad\qquad\qquad\qquad\qquad\qquad [2.8]$$

when $\omega < \omega_b$

where

ω =   mechanical reinforcement index ($A_s f_y / bd f_c'$)

ω_b =   mechanical reinforcement index under balanced conditions.

2.5 Review of Codes Provisions For Moment Redistribution

Figure 2.4 gives a graphical representation of all the standards formulae presented above. The comparison shows that significant differences exist, among the various design standards, on the amount of allowable moment redistribution. The Japanese and the German standards are most conservative, allowing only 15% moment redistribution. The

15

American Standard (ACI 318-95) allows a maximum of 20% moment redistribution for $(\rho - \rho') = 0$ (equal amount of tension and compression reinforcement) and the redistribution limit decreases linearly to 10% as the reinforcement ratio reaches half of the balanced value. The Canadian Standard (A23.3-94) allows a maximum of 20 % moment redistribution which reduces linearly from 20% at $c/d = 0.2$ to 0% for $c/d = 0.6$. The British Standard and the CEB Model Code are more liberal as they allow a maximum of 30% moment redistribution, depending upon the c/d ratio.

The most liberal of the above standards is the Danish standard (not shown in Fig. 2.4) that allows a maximum moment redistribution of 66%, with the only restriction that the reinforcement index is less than the balanced value. This may look too generous, however if the conclusions of Macchi (1960) and others are remembered in that high moment redistribution is possible due to flexural cracking and compatibility, then the progressive recommendation of the Danish standard may be within the realm of possibility for certain structures.

Cohn and Lounis (1991) raised the concern that these standard formulations are aimed only at satisfying the compatibility criterion along with the equilibrium at the ultimate limit-state. No condition that satisfies the serviceability (crack width, deflection, allowable stresses) is specified and no consideration is given to live load to dead load ratio and the degree of prestressing. Furthermore because of the significant differences in the partial safety factors adopted on the loads and materials, completely different conditions at both ultimate and service loads are reached when the same amount of moment redistribution is allowed for by various standards. The relative depth of neutral axis calculated for each individual standard would be different and so is the factored moment capacity of critical section. The ultimate concrete strains vary from one standard to another. The concrete stress blocks, for section analysis at ultimate limit-state, adopted by various standards are also different. Hence the allowable moment redistribution proposed by different standards is related to the specific design parameters.

16

Cohn and Lounis (1991) pointed out the following major differences between various design standards:

1. The CSA and CEB-FIP standards consider the redistribution to be independent of the degree of prestressing. This implies that both reinforced concrete (RC) and prestressed concrete (PC) can accommodate the same amount of moment redistribution, a conclusion that can be justified from ductility point of view, but not from a serviceability point of view. Allowing moment redistribution for a high degree of prestressing may violate the crack width requirement, especially for lightly reinforced members.

2. The ACI and BS standards implicitly consider the moment redistribution as a function of γ (mixed reinforcement index) by giving different formulae for the two extreme cases of RC and PC. Both ACI and BS allow less moment redistribution for PC than RC, which may be understood to reflect the more severe service condition imposed on PC structures. In the BS standard the maximum moment redistribution decreases from 30% for reinforced concrete to 20% for prestressed concrete.

3. In the CSA, ACI and CEB-FIP standards, the moment redistribution is a function of concrete grades; for high strength concrete the permissible moment redistribution is reduced in all three standards. However this reduction is very small in the ACI and CSA standards, while it is considerable in the CEB-FIP standard. In the BS standard, the same amount of moment redistribution applies for both low and high concrete grades.

Experimental studies conducted by Mattock (1959) showed that redistribution of bending moments by up to 25% does not result in performance (cracking and deflection) inferior to that of the beams designed for the distribution of bending moments predicted by elastic theory.

17

The review of standards provisions on moment redistribution reveals that design standards consider c/d ratio or reinforcement index as the only parameter influencing the amount of moment redistribution. Research has shown that although c/d ratio is an important factor influencing moment redistribution, it is not the only factor governing moment redistribution. The review of the ductility models for plastic rotation capacity, which follows, reveals other important factors that influence the plastic rotation capacity and the amount of moment redistribution in reinforced concrete structures.

2.6 Existing Ductility Models

The amount of moment redistribution that can be allowed at a section depends upon the plastic rotation capacity of that section. Several experimental and analytical studies have been conducted to assess the plastic rotation capacity, θ_p, and allowable moment redistribution, β, of reinforced concrete sections. This section reviews the main phases in the development of calculation models for deformation capacity of reinforced concrete members.

2.6.1 Constant curvature models

The classical expressions for plastic rotation capacity, θ_p, in the literature were of the type:

$$\theta_p = \left(\phi_u - \phi_y\right)L_p \tag{2.9}$$

which could be rewritten as:

$$\theta_p = \left(\frac{\varepsilon_{cu}}{c} - \frac{\varepsilon_{cy}}{kd}\right)L_p \tag{2.10}$$

where

ϕ_y = curvature at yield

ϕ_u = curvature at ultimate

18

L_p = effective hinge length

ε_{cu} = strain in concrete at ultimate

ε_{cy} = strain in concrete at the yielding of steel

kd = depth of neutral axis corresponding to yielding of steel.

c = depth of neutral axis at ultimate moment resistance

The above equations give an idealised plastic rotation capacity by considering constant curvature over an effective plastic hinge length. The concept of this idealised plastic rotation is described in various texts (Park and Paulay 1975) and is elaborated in Fig. 2.5. The figure shows part of a reinforced concrete beam that has reached the ultimate curvature and bending moment at the critical section. End A of the member, for example, is the free end of a cantilever or a point of contraflexure, and end B is a column face. The distribution of curvature along the member is apparent. The region of inelastic curvature is spread over a length of beam in which the bending moment exceeds the yield moment of the section. The curvature fluctuates along the beam because of the increased rigidity of the member between the cracks. Each of the peaks of curvature corresponds to a crack location. The actual curvature distribution at ultimate can be idealised into elastic and inelastic regions, as shown in Fig. 2.5c. The shaded area of Fig. 2.5c is the inelastic rotation that can occur at the plastic hinge in the vicinity of the critical section. Thus, the shaded area represents the plastic rotation that occurs in addition to the elastic rotation at the ultimate stage of the member. The inelastic area at the ultimate stage can be replaced by an equivalent rectangle of height $(\phi_u - \phi_y)$ and width L_p, having the same area as the actual inelastic curvature distribution. The width L_p is the effective length of the plastic hinge over which the plastic curvature is considered to be constant. Using moment area theorem, the plastic rotation equals the area of the curvature diagram and the resulting equation is exactly of the same form as Eq.2.9 or Eq. 2.10.

To estimate θ_p from Eq. 2.9, the effective plastic hinge length L_p is required. Investigators have proposed various empirical expressions for the effective plastic hinge length and the maximum concrete strain ε_{cu} at ultimate curvature. Baker and Amarakone (1964) conducted one of the first large scale investigations to explore the parameters

19

affecting rotation capacity of concrete sections. The experimental program was conducted with the collaboration of several universities and research institutes. The prime variables investigated were the compressive strength of concrete, the yield strength of the reinforcement, the relative amounts of longitudinal and transverse reinforcement, the presence of axial and shear force, and the type of loading the sections were subjected to. Two types of load patterns were studied: a single point load at midspan and two point loads spaced at roughly one third of the span. All beams were simply supported. In all, there were ninety-four beams for which results were correlated. The cross-sections of the beams varied between 150mm x 200mm and 300mm x 300mm. The concrete compressive strength ranged from 17 MPa to 40 MPa, the yield stress of the reinforcement from 270 MPa to 590 MPa. The relative amounts of tensile, compressive and transverse reinforcement ranged from 2.5% to 65.7%, 0.96% to 24.8%, and 0.051% to 1.51% respectively, with the tensile and compressive reinforcement percentages being expressed in terms of the reinforcement index ($\omega = \rho f_y / f_c'$). The span lengths varied from 1.4 m to 2.9 m. Sixty-two beams were tested in pure flexure while the remaining thirty-two were subjected to an additional axial force. Approximately half of the beams tested were reinforced with mild reinforcement, the remaining with cold rolled reinforcement. For members subjected to an axial load, the ratio of the neutral axis depth to the effective section depth was held constant throughout the test. As the axial load was increased, the bending moment was adjusted accordingly.

The authors gave the following equation for L_p, for members with unconfined concrete, based on the initial assessment of the test results:

$$L_p = k_1 k_2 k_3 \left(\frac{z}{d}\right)^{1/4} d \qquad [2.11]$$

where,

k_1 = 0.7 for mild steel, 0.9 for cold rolled steel

k_2 = $1 + 0.5 P_u / P_o$, where P_u = axial compressive force in member and P_o = axial compressive strength of member without bending moment

20

k_3 = 0.6 for a concrete cube strength of 40 MPa, 0.9 for 15 MPa

z = distance of critical section to the point of contraflexure

d = effective depth of member

For use of above equation in conjunction with Eq. 2.10, the value of ε_{cu} = 0.0035. The authors concluded that for the range of span/d and z/d ratios normally found in practice, L_p lies in the range between 0.4d and 2.4d.

After correlation of the test data, the authors proposed a revised expression for computing the plastic rotation capacity of members confined by transverse steel.

$$\theta_p = 0.8(\varepsilon_{cu} - \varepsilon_{cy})k_1 k_3 \left(\frac{z}{d}\right)$$ [2.12]

where

ε_{cy} = 0.002 or the actual calculated value

$$\varepsilon_{cu} = 0.0015\left\{1.45 + 1.5\rho_s + (0.7 - 0.1\rho_s)\frac{1}{c/d} - \frac{f_c'}{10^4}\right\}$$ [2.12a]

ρ_s = volumetric percentage of transverse steel

f_c' = compressive strength of concrete in psi.

The major conclusions that the authors drew from the correlated data were:

(1) The compressive strain in concrete at ultimate is the major parameter influencing the plastic rotation capacity.

(2) It is better to use a tri-linear moment-curvature relationship rather than the usual bilinear model.

(3) Confined concrete is more ductile than the unconfined concrete.

21

(4) It can be dangerous to apply plastic theory to reinforced concrete frames without checking hinge rotations.

(5) It is possible to achieve high rotations and moments redistribution by suitable detailing.

(6) Long-term creep has a favourable effect with regard to the distribution of bending moments.

Mattock (1964) carried out a series of tests to investigate the rotation capacity of hinging regions in reinforced concrete members. In all, 37 beams were tested. The following variables were considered: compressive strength of concrete (28 MPa to 41 MPa), yield strength of reinforcement (325 MPa and 414 MPa), relative amounts of longitudinal reinforcement (1% to 3%), effective depth of beam (254 mm and 508 mm), span of beam (1397 mm, 2795 mm, and 5588 mm), and distance from point of maximum moment to point of zero moment. All the beams tested were 152 mm wide. Most of the test specimens were simple-span beams subjected to a concentrated load at mid-span, to simulate the distribution of bending moments adjacent to an interior support in a continuous beam. For reference purposes, six additional specimens were tested as simple-span beams with equal concentrated loads applied at each third point. Following conclusions were drawn from the test results:

(1) The ultimate curvature decreases with an increase in percentage of the tensile reinforcement.

(2) The ultimate curvature decreases with an increase in the ratio c/d.

(3) The maximum compressive strain in concrete can be very much in excess of the usually assumed value of 0.003. For most test specimens, the maximum concrete compression strains recorded were in excess of 0.01. In a few specimens the maximum concrete compressive strains recorded were in excess of 0.02. Mattock

22

(1964) proposed the following tentative equation for computing the maximum compression strain in concrete:

$$\varepsilon_{cu} = 0.003 + \frac{0.5}{z}$$ [2.13]

where z is measured in inches. Mattock himself pointed out that the above equation is not dimensionally consistent and is a subject of further refinement, as additional test data become available.

(4) The inelastic deformations extend at least a distance d/2 on either side of the section of maximum moment. The extent to which plasticity extends beyond the distance d/2 from the point of maximum moment depends primarily on the ratio z/d and the amount of flexural reinforcement at the section. The plastic hinge length was found to increase with increase in the ratio z/d, for beams with the same amount of flexural reinforcement.

(5) The influence of the range of stirrups spacing, considered in the tests (64 mm, 127 mm, and 254 mm), on the maximum concrete compression strain was found to be negligible.

Mattock adopted a conservative value of d/2 as the plastic hinge length, to each side of the critical section, and proposed following equation for computing the total inelastic rotation in the hinging region:

$$\frac{\theta_{tu}}{\theta_u} = 1 + \left(1.14\sqrt{\frac{z}{d}} - 1\right)\left[1 - \left(\frac{\omega - \omega'}{\omega_b}\right)\sqrt{\frac{d}{16.2}}\right]$$ [2.14]

where,

θ_{tu} = total inelastic rotation in length z

θ_u = inelastic rotation in length d/2

23

ω = tension reinforcement index = $\rho f_y / f_c'$

ω' = compression reinforcement index = $\rho' f_y / f_c'$

ω_b = balanced tension reinforcement index = $\rho_b f_y / f_c'$

ρ, ρ', and ρ_b are the tension reinforcement ratios, compression reinforcement ratios, and balanced tension reinforcement ratios respectively.

Based on his findings, Mattock suggested that complete redistribution of moments might be assumed to occur in continuous beams, provided the net tension reinforcement index at critical sections is kept below $0.5\omega_b$.

Sawyer (1964) proposed following expression for the effective plastic hinge length, based on the interpretation of existing test results:

$$L_p = 0.25d + 0.075z \qquad [2.15]$$

This equation is based on the assumptions that the maximum moment in the member is the ultimate moment, that $M_y / M_u = 0.85$, and that the zone of yielding is spread d/4 past the section in which the bending moment is reduced to M_y.

Corley (1966) designed his test series as a continuation to that of Mattock. For the test series, the specimen size ranged from 75 mm x 125 mm to 300 mm x 750 mm, the concrete compressive strength from 28 MPa to 40 MPa, the yield strength of the steel reinforcement from 300 MPa to 550 MPa, and the span lengths from 0.9 m to 8.4 m. In all 40 simply supported beams were tested to examine the effect of cross section size, and of transverse reinforcement volume on the rotational capacity of reinforced concrete. Corley noted from Mattock's test series that the rotations were greater for a beam subjected to shear, in addition to moment, as opposed to one subjected to a constant moment with zero shear. From his own work Corley noted that the effect of size of the specimen did not seem to have a great deal of influence on the rotational capacity. He

24

also noted that a beam with closely spaced stirrups develop greater rotation capacity than a beam with fewer stirrups. Corley pointed out that a premature shear failure would drastically reduce the rotation capacity of a beam and hence it is necessary to provide proper shear reinforcement to develop full rotation capacity.

From the test results, Corley proposed the following expression for the effective length of the plastic hinge:

$$L_p = 0.5d + 0.2\sqrt{d}\left(\frac{z}{d}\right) \qquad [2.16]$$

He also suggested the following as a lower bound for the maximum concrete strain:

$$\varepsilon_{cu} = 0.003 + 0.02\frac{b}{z} + \left(\frac{\rho_s f_y}{20}\right)^2 \qquad [2.17]$$

where all the notations have the same meanings as described before, b is the beam width, and f_y is expressed in ksi. The plastic rotation may be computed by substituting these values for L_p and ε_{cu} into Eq. 2.10.

Mattock (1967), in discussing Corley's paper, suggested simpler forms of Eq. 2.16 and Eq. 2.17 that fitted the trend of the data reasonably well:

$$L_p = 0.5d + 0.05z \qquad [2.18]$$

$$\varepsilon_{cu} = 0.003 + 0.02\frac{b}{z} + 0.2\rho_s \qquad [2.19]$$

When using these values in strength calculations, the spalling of the cover concrete at high strains was ignored and the ACI concrete compressive stress block parameters were employed. It was also emphasised that at large ultimate curvatures the steel strains are high, and the steel may be in the strain hardening range. The increased tensile force due

25

to strain hardening will increase the neutral axis depth and should be taken into account in calculating c; otherwise the ultimate curvature may be overestimated.

Dilger (1966) was the first to incorporate the effects of inclined shear cracks on plastic rotation capacity. As shown in Fig. 2.6, the rotation capacity was divided into two parts: the rotation due to bending, calculated from the section moment-curvature diagram, and the rotation due to the shear force effect, approximated using the shift in the tensile force line (rotation A and B in Fig. 2.6). In estimating the length of the plastic area, which is activated due to shear cracks, the influence of the crack inclination and of the angle between stirrups and beam axis was taken into account. The angle of the inclined cracks was calculated according to the criteria of minimum deformation energy. With such an approach an inclined-crack-dependent part of the rotation capacity could be computed as a product of length of the plastic hinge due to inclined cracks and the plastic curvature of the most strained section. Using a truss model and a compression strut angle of 45^0, Dilger showed that the shift in the tension force diagram due to inclined shear cracks is approximately d/2.

Dilger verified his method with several previously tested reinforced concrete beams and then proceeded to design a series of two span T-beams for moment redistribution. Each beam was designed for a different amount of moment redistribution. Each span of the beam was subjected to a single concentrated load in the middle. Full redistribution of moment was achieved in almost all the specimens. What is even more interesting is that all of the test beams were designed for a balanced failure and were thus not under-reinforced. Other researchers considered under-reinforced members a necessity for achieving full moment redistribution.

The following observations were made from the test series:

(1)   Shear deformations made up approximately half of the total deformation.

26

(2) It is unconservative to neglect the comparison between the available rotation capacity and that required for a given redistribution of moments.

(3) High percentages of moment redistribution can be achieved without slender members or ductile sections as long as one properly designs for shear and anchorage.

Later Abele (1974) showed that shear deformations in T-sections increase at a much higher rate in time than flexural deformations and that shrinkage has a major influence on the total deformation.

2.6.2 Variable curvature models

A further improvement in modelling the rotation capacity followed from the observation that deformations along the plastified part of the member are discontinuous and that curvature is concentrated in the cracks, while the contribution of the member parts between the cracks is very small (tension stiffening). This finding had important implications for the evolution of calculation models. Consequently, the member deformations could not be calculated by simple integration, along the member axis, of the curvature diagram derived directly from the bending moment diagram. Plastic rotation had to be computed as a sum of the rotations of cracked elements within the plastic hinge region. Rotation of each element followed from the integration of strains along the beam element taking into account tension stiffening between cracks. The maximum plastic deformation (i.e. the maximum rotation capacity) was obtained when in the most stressed cracked beam element the steel stress reached the ultimate value or when the rotation angle that marked failure of the concrete compression zone was exceeded. Good examples of this type of modelling are the models according to Eifler (1969) and Bachmann (1970).

While studying the influence of inclined cracking on the development of plastic hinge rotation, refined methods of discretization of the hinge region were proposed. Figure 2.7 schematically shows the discrete crack model proposed by Eifler (1969). In Fig. 2.8, the

27

example of bending and shear crack hinge discretization after Bachmann (1970) is given. Bachmann separated plastic hinges into two categories and noted that:

(1) Flexural crack hinges develop relatively small rotational capacities and are generally centred about one dominant crack; and

(2) Shear crack hinges develop much higher rotational capacities since the hinge length is extended because of the fan-like pattern.

Bachmann tested ten two-span continuous beams; five with rectangular sections, and five with T-sections. The percentage of steel reinforcement was varied at critical sections such that two failure mechanisms were possible. Two of the beams formed failure mechanisms with the first hinge forming in the span, while the remaining eight developed their first hinge over the central support. Eight of the test beams reached a failure load that exceeded that which was predicted using the familiar bilinear moment-rotation assumption.

Bachmann developed equations for calculating the rotation of a section depending upon the type of crack pattern expected (flexure or shear). For example, for a flexural crack hinge:

$$\theta = \sum_{i=1}^{n} \frac{w_i}{d-c} \qquad\qquad [2.20]$$

where w_i is the crack width at a section, d is the effective depth, and c is the depth of neutral axis. The crack width and spacing were determined through several equations relating bond stress, slip, and steel strain. The strain in the concrete between cracks was ignored. For a shear crack hinge the calculations were drawn from the well-known truss analogy.

28

Bachmann concluded that the theories used by the ACI standard and researchers such as Corley and Mattock were unrealistic since they did not account for the effects of shear. Also, the bar length over which the tension reinforcement is yielded is considerably greater in shear crack hinges than in flexural crack hinges. The latter conclusion being the same as Dilger's horizontal shift in the tension force diagram resulting from shear cracking.

Using the strut-and-tie approach Michalka (1986) proposed a truss-model, shown in Fig. 2.9, to analyse the support region and determine the plastic hinge rotation capacity. Michalka concluded that shear deformation (compression of the struts) has a prominent influence on the rotation capacity only for very high shear stresses. Furthermore he emphasised that resistance against shear force, sufficient to prevent a premature failure, is required (e.g. by adequate stirrup reinforcement) in order to utilise the rotation capacity of plastic hinges. If shear failure occurs before the bending moment capacity is reached, the strain in the tension reinforcement and in the compression reinforcement is reduced, thus leading to a reduced plastic rotation. Therefore design and detailing provisions must ensure that the shear capacity of a structure is well above the bending capacity, even when taking into account the usual over strength of tension reinforcement.

In the eighties and nineties extensive research on the ductility of reinforced concrete was conducted in Europe and some interesting models were proposed for computing the plastic rotation capacity. A brief summary of some of the models is given below.

Model STUTTGART for calculating the rotation capacity of reinforced and prestressed concrete was developed by Langer (1987) and extended by Li (1995). Langer emphasised that an accurate representation of the material behaviour is an indispensable condition for a mathematical model that produces reliable results. Langer's model was therefore based on a very accurate representation of the concrete and steel stress-strain relationships.

In Langer's model, a statically determinate beam with a length equal to the distance between two adjacent points of zero moment is cut out of the real indeterminate system.

The distribution of moments along the beam is determined. If shear cracks are expected, the shifting of the tensile force is taken into account assuming an angle of the inclined compression struts according to Dilger (1966). The curvatures at the location of cracks and between the cracks are determined and integrated over the beam length to obtain the rotation capacity (see Fig. 2.10).

The Model NAPLES is related to the work of Cosenza et al. (1991). The model is similar in principle to the one proposed by Langer (1987). The characteristics of the model are:

(1)   Because of the slip between the two materials, the deformations of concrete and steel in tension are different.

(2)   the concrete in tension that collaborates with the steel is restricted to an effective area with constant stress.

(3)   the Bernoulli hypothesis is assumed for compressed concrete and steel in tension.

(4)   the distance between the flexural cracks is assumed constant.

The bending moment diagram is made considering a 45^0 diffusion of applied load to the centroidal axis, as shown in Fig. 2.11. The effect of inclined cracking is taken into account by varying the bending moment diagram as shown in Fig. 2.12.

The ZURICH model is based on the work of Sigrist and Marti (1994). The model uses discontinuous stress fields to compute the distribution of forces in the member. A tension chord model is developed to determine the distribution of bond-stress and steel strains over the member length. The curvatures at the crack location and between the cracks are determined using the steel strains, and are integrated over the plastic hinge length to obtain the plastic rotation capacity. Sigrist concluded that for steel with good ductility characteristics and normal strength concrete, moment redistribution of up to 20% can be

30

permitted without an explicit check of rotation capacity provided that the c/d ratio is less than 0.333.

2.6.3 Other ductility models in literature

Researchers have presented various ductility models in an attempt to include the influence of important parameters on moment redistribution and ductility. Kemp (1981) proposed the following equation for moment redistribution that considers the effect of beam slenderness in addition to the c/d ratio.

$$\beta = \frac{1}{\left[1 + \frac{K_1}{K_2} \frac{L}{d} \frac{1}{(\phi_u/\phi_y) - 1}\right]} \times 100 \qquad [2.21]$$

where

K_1 = parameter depending upon the support conditions and loading ($K_1 = 1$ for fixed ended beam under uniform load)

K_2 = parameter that defines the effective plastic hinge length

For low reinforcement ratios, the above equation allows maximum moment redistribution as high as 62% of the elastic value.

Scholz (1993) conducted an analytical study to investigate the influence of beam slenderness and stiffness variation along the span of a beam, on allowable moment redistribution. He proposed the following relationship:

$$\frac{c}{d} \leq \frac{1.33KC}{1 + 0.7KC + \frac{\{\beta/(100 - \beta)\}}{0.027 + 0.5(L/d)}} \qquad [2.22]$$

where

31

$$K = \frac{\varepsilon_{cu}}{0.0035} \times \frac{450}{f_y}$$

$$C = \frac{I_{av}}{I_{su}} \text{ in which } I_{av} = \frac{I_{su} + I_{sp}}{2}$$

I_{su} = cracked moment of inertia at the support

I_{sp} = cracked moment of inertia at the span

I_{av} = average cracked moment of inertia.

ε_{cu} = ultimate strain in concrete

In the above formula, no upper bound on the percentage of moment redistribution is imposed from strength considerations. Scholz, however, recognised that deflection and cracking under service loads would introduce a variable limit in this regard.

Riva and Cohn (1994) developed a non-linear analysis model based on realistic materials laws. The model was then used to carry out parametric study of beams with various bending moment distributions, section shapes and amounts of reinforcement. The parametric investigation consists of the non-linear analysis of 30 cantilevered reinforced concrete beams under distributed load and 16 simply supported reinforced concrete beams under either distributed or concentrated load. A non-linear regression analysis resulted in the following expression for the plastic hinge length in terms of the ductility factor ϕ_p/ϕ_y, the shape factor M_u/M_y, the reinforcement index ω, and the compression flange to web width ratio b/b_w.

For $1.0 \leq \phi_p/\phi_y < 7.0$

$$\frac{L_p}{z} = \left(A - \frac{B}{800\omega} \right) \left(\frac{\phi_p}{\phi_y} \right)^{-(0.9-0.8\gamma)} \left(\frac{b'}{b_w} \right)^{\left(-D/640\omega^2 \right)} f(\gamma) \qquad [2.23]$$

and for $\phi_p/\phi_y > 7.0$

32

$$\frac{L_p}{z} = \frac{E}{\phi_p/\phi_y}(1.25\omega)^F + G\left(\frac{Mu}{M_y} - 1\right)\left(\frac{b}{b_w}\right)^H \qquad [2.24]$$

The constants A, B, C, D, E, F, G, H, and the function f(γ) were determined for three different bending moment distributions. The plastic rotation capacity is calculated from the formula:

$$\theta_p = \left(\frac{L_p}{z}\right)\phi_p z \qquad [2.25]$$

where z is the shear span. After comparing with the existing rotation capacity formulations, the authors concluded that neglecting the influences of the loading distribution and the ratio z/d may lead to non-conservative results. This aspect becomes particularly relevant for support sections of continuous beams under distributed loads, which are characterized by hogging moment distributions and low z/d ratios. For prestressed members it may not be possible to achieve higher moment redistribution due to presence of secondary moments. The authors provided a comparison of available plastic rotation formulae, which are reproduced in Table 2.1.

Riva and Cohn pointed out that the validity of CEB (1990), Mattock (1983) and Baker and Amarakone (1964) models is limited as they are based on experimental results on simply supported beams under concentrated load at mid span, in which only a few parameters were considered. Furthermore, with only few exceptions, the experimental beams were characterised by z/d ratios larger than 5 that are not likely to be critical in the neighbourhood of a support section of a continuous beam.

The FIP (1984) and Naaman et al.(1986) models are independent of z/d and, although simpler, they are non-conservative for low z/d values that characterise the support sections.

33

Table 2.1 Summary of available expressions for plastic rotations (Riva and Cohn 1994)

Model	Expression for plastic rotation capacity
Riva and Cohn (1994)	$\theta_p = \left(\dfrac{L_p}{z}\right)\phi_p z$ For $1.0 \le \phi_p/\phi_y < 7.0$ $\dfrac{L_p}{z} = \left(A - \dfrac{B}{800\omega}\right)\left(\dfrac{\phi_p}{\phi_y}\right)^{-(0.9-0.8\gamma)}\left(\dfrac{b}{b_w}\right)^{\left(-D/640\omega^2\right)} f(\gamma)$ For $\phi_p/\phi_y > 7.0$ $\dfrac{L_p}{z} = \dfrac{E}{\phi_p/\phi_y}(1.25\omega)^F + G\left(\dfrac{Mu}{M_y}-1\right)\left(\dfrac{b}{b_w}\right)^H$ The constants A, B, C, D, E, F, G, H, and the function $f(\gamma)$ depends upon bending moment distribution
Naaman et al. (1986)	$\theta_p = \dfrac{1.05-(\omega-\omega')}{850(\omega-\omega')-35}\dfrac{L_p}{d/2}$ (upper bound) $\theta_p = \dfrac{1.05-1.65(\omega-\omega')}{1300(\omega-\omega')-40}\dfrac{L_p}{d/2}$ (lower bound) where $L_p = d/2$
FIP (1984)	$\theta_p = \dfrac{0.004}{c/d}$
Mattock (1983)	$\theta_p = 0.0086\left(1 + 0.1\dfrac{L}{d}\right)\left(\dfrac{\omega_b}{\omega + \omega_p - \omega'}\right)$
Corley (1966)	$\theta_p = (\phi_u - \phi_y)\left(0.5d + 0.2\sqrt{d}\dfrac{z}{d}\right)$
Mattock (1964)	$\dfrac{\theta_{tu}}{\theta_u} = 1 + \left(1.14\sqrt{\dfrac{z}{d}}-1\right)\left[1-\left(\dfrac{\omega-\omega'}{\omega_b}\right)\sqrt{\dfrac{d}{16.2}}\right]$
Baker and Amarakone (1964)	$\theta_p = 0.8(\varepsilon_{cu} - \varepsilon_{cy})k_1 k_3 \dfrac{z}{d}$ ($k_1 k_3 = 0.5$)

34

Ahner and Kliver (1999) used an analytical model to provide a simplified formula for computing the plastic rotation capacity of reinforced concrete structures.

$$\Theta_{R,pl} = \beta_n \beta_s \frac{\varepsilon_{suk}^{*} - \varepsilon_{syk}}{1 - \dfrac{x_u}{d}} \sqrt{\frac{\lambda_q}{3}}$$

[2.26]

where

x_u = depth of compression zone at ultimate limit stage

d = effective depth

λ_q = shear slenderness

β_n = 22.5 (global factor to take into account the non-linearity)

β_s = 0.0740 for high ductile steel

= 0.0476 for normal ductile steel

ε_{syk} = Characteristic steel strain at yield point

$$\varepsilon_{suk}^{*} = \min \left\{ \begin{array}{l} 0.28\left(\beta_c - \dfrac{x_u}{d}\right)\varepsilon_{suk} \rightarrow \text{steel} - \text{failure} \\[3mm] 1.75\left(\dfrac{x_u}{d}\right)^{\frac{2}{3}}\left(\dfrac{d}{x_u} - 1\right)\varepsilon_{cu} \rightarrow \text{concrete} - \text{failure} \end{array} \right\}$$

ε_{suk}^{*} = steel strain at ultimate limit state using a simplified approach to take into account tension stiffening effects

ε_{suk} = characteristic value of steel strain at maximum strength (taken as 0.05 by the authors)

ε_{cu} = ultimate concrete strain

β_c = global factor to take into account the different ultimate concrete strains

35

The size effect, relating to the beam depth, was not considered and it was assumed that the size effect is small as compared to the effects of slenderness and material properties. The confinement effect was also not considered. The authors concluded that the most important parameters affecting plastic rotation capacity are member slenderness, ultimate concrete strength and strain, steel strength and ultimate steel strain. Furthermore, the authors pointed out that the model yields values that appear to be unsafe in comparison with a mechanically accurate model. Further research was recommended, particularly on maximum concrete strain and bond behaviour after steel yielding.

2.7 Further Studies on Moment Redistribution and Ductility

Researchers have conducted numerous experimental and analytical studies on moment redistribution in reinforced concrete members to understand the phenomena and the parameters influencing it. Rangan and Hall (1984) considered moment redistribution in flat plate floors. A series of large-scale tests were conducted on flat plate panels subjected to uniformly distributed loads. The authors noted that between the uncracked condition and the ultimate load condition, there was considerable amount of moment redistribution. The two support moments and the mid-span moments vary by about 50% from the elastic value. The authors concluded that the flat plates can tolerate higher amounts of moment redistribution and hence any sophistication in the analysis and design of flat plate is not really necessary.

Sveinson (1989) conducted analytical studies using the program "NONARCS" that he developed to study moment redistribution in reinforced concrete structures. The studies showed that, from the ultimate strength perspective, very high amounts of moment redistribution may be achieved, however serviceability criteria ceased to be met for redistribution of about 40% from the elastic distribution. Results indicate that a moment redistribution of 35% may be easily achieved and will satisfy serviceability criteria such that deflections and steel stresses at service load are not critical.

Cohn and Lounis (1991) reviewed the moment redistribution provisions of American and European standards and concluded that major differences exist among the various design

36

standards. The existing formulae neglect the ratio of live load to dead load, degree of prestressing and permissible crack-widths, resulting in possibly unsafe, unserviceable and uneconomic designs. For prestressed members it may not be possible to achieve high amounts of moment redistribution without adverse cracking. The potential for moment redistribution increases with high live load to dead load ratios. On the other hand where dead loads prevail, a small amount of moment redistribution is possible without violating crack width criteria. The major factors influencing plastic rotation capacity are the c/d or reinforcement index ω, allowable crack width and the live load to dead load ratio.

Cohn and Riva (1992) studied the effect of moment redistribution on serviceability. They introduced a yield safety parameter to control both cracking under service conditions and the permissible moment redistribution under ultimate loads. The limiting values of these safety parameters that ensure satisfaction of the standard specified cracking criteria were derived from the results of a comprehensive computer investigation. A subsequent parametric study showed that the reinforcement index ω, allowable crack width w_a, and the degree of prestressing are the governing factors in crack control. These factors, along with the live load to total load ratio, determine the permissible moment redistribution in reinforced concrete and prestressed concrete members.

Wyche et al. (1992) conducted an analytical study to understand the interaction between prestress secondary moments and moment redistribution in prestressed concrete members. The authors concluded that the secondary moments from prestressing can be beneficial or detrimental, depending upon the sign of these moments. Positive secondary prestress moments at supports would assist in moment redistribution while negative moments would prohibit higher moment redistribution and cause premature failure due to rupture of steel. The authors noted that some standards do not make a distinction between reinforced concrete members and prestressed concrete members. This can be very un-conservative when designing prestressed concrete members for moment redistribution. Thus while redistributing bending moments, the factored elastic moments must include the moments due to superimposed loads as well as the secondary moments due to prestressing.

The effect of the yield strength of reinforcing steel on curvature ductility was studied by Al-Haddad (1995) through parametric study. The study considers the actual properties of reinforcing steel under both low and high strain rates of loading. The study shows that the ductility reduces as the yield stress increases. There is an average reduction in curvature ductility of 12% for an increase of 34.5 MPa in the yield stress. The code-specified yield value falls in the lower tail of the probability density function of the yield stress. For conservative estimate of ductility the yield value should be the one that falls in the upper tail of its probability density function. He concluded that using code-specified yield strength of the reinforcing steel will lead to an overestimation of the ductility capacity of reinforced concrete sections. The study highlights that the definition of yield stress used for evaluation of curvature ductility is an unsettled issue and needs further research.

Dishongh (1995) proposed a method (inelastic moment redistribution or IMR) for obtaining redistributed moments in continuous bridge girders, using "shake down" analysis. The IMR procedure makes use of the conjugate beam method to relate the inelastic hinge rotations to both the resulting redistributed moments and the resulting residual deflections. The process consists of performing moment redistribution for various cycles of loading, representing passage of live load across the bridge. A complete cycle consists of moving load along the girder, one by one unlocking each plastic hinge and allow it to rotate inelastically while other hinges are held locked. After a few cycles, when the inelastic rotations at every hinge remain unchanged, shakedown is reached, and residual deformations can be determined. Details of the procedure can be obtained from the above reference.

Alca et al. (1997) investigated the size effect on the behaviour of flexural members subjected to pure bending. The need for investigation of size effect arises due to different conclusions reached by Corley (1966) and Hillerborg (1988). Corley concluded that there is no effect of size on the ductility of reinforced concrete sections. Hillerborg, on the other hand, used a fracture mechanics approach and Corley's test data to conclude that the rotational capacity of the hinge is inversely proportional to the effective depth of the member.

38

The authors conducted tests on 12 simply supported, under-reinforced, high strength concrete beams under two-point loading. Three different effective depths and two different concrete strengths were considered. It was concluded through measured rotations, extreme compression fibre strains, and flexural strengths that there was no apparent effect of size on deformation capacity or flexural strength. The authors attributed the size effect noted by others to the mid point loading, and confinement from stirrups and loading plate.

Pisanty and Regan (1998) conducted a series of tests to determine the effect of moment redistribution on the entire loading history, from serviceability to ultimate limit-state. The results indicate that the redistribution of moments in reinforced concrete elements is not a phenomena associated with the formation of plastic hinges only. Once an element is designed and loaded with the view of taking into consideration moment redistribution, it will affect its entire loading history. They suggested that redistribution of moments should be considered from the serviceability limit-state through the entire loading history up to the ultimate limit-state.

Kemp (1998) reviewed the effects of lateral confinement, longitudinal strain gradient, size effect, concrete strength and nature of loading on ductility through non-linear analysis of 94 beam-tests conducted by other authors. He concluded that the ultimate strain in concrete is increased by the confinement of concrete provided by the stirrups. With proper confinement much higher concrete ultimate strains can be achieved than those given by the normal code limitations of 0.003 to 0.004. Kemp noted that the lengthening of longitudinal strain gradient has a beneficial effect on the ductility of reinforced concrete beams. The size of the specimen affects the concrete stress-strain properties of concrete in flexure. The maximum concrete stress reduces as the size of the specimen is increased. Kemp further noted that the concentrated loads have a beneficial localized effect on the ductility of concrete.

Alvarez et al. (2000) conducted bending tests on a series of continuous slab strips to determine the effects of cold-formed reinforcing bars on ductility. The experimental and numerical analysis revealed that the low ductility of cold-formed steel may result in dangerous strain localization, impairing rotation capacity, permissible moment redistribution and ultimate strength.

2.8 Stress-Strain Relationship for Confined Concrete

The application of limit design methods requires computation of available and required plastic rotations at critical sections of the beam. The plastic rotation capacity of a hinge depends upon various material and structural parameters, concrete stress-strain law being one of them. CSA A23.3-94 uses a linear strain distribution with a limit of 0.0035 on ultimate concrete strain and an equivalent rectangular stress block is used for computing the ultimate flexural strength and curvature. Reinforced concrete beams usually contain transverse reinforcement in the form of stirrups. These stirrups provide confinement to the compression zone of concrete and result in an increase in the strength and ultimate strain of the concrete. The slope of the falling branch of stress-strain curve for confined concrete is quite moderate as compared to that for unconfined concrete. The standard does not account for the beneficial effects of confinement. Concrete strains much higher than 0.0035 have been reported in tests (Mattock 1964). Researchers agree that ultimate concrete strain is the most important parameter that effects the plastic rotation capacity. It is therefore necessary to have a stress-strain model that takes into account the effect of confinement on ductility and ultimate strain of concrete.

Concrete may be confined by transverse reinforcement in the form of closely spaced steel spirals or hoops. Such confinement is passive. At low levels of axial concrete stress the transverse reinforcement is hardly stressed and thus the concrete is unconfined. The concrete becomes confined when at stresses approaching the uniaxial strength it commences to increase in volume due to progressive internal fracturing. The volumetric expansion causes the concrete to bear outward against the transverse reinforcement, which then applies a confining reaction to the concrete. Tests by many investigators in the past (Chan 1955, Roy and Sozen 1964, Soliman and Yu 1967) have shown that such

40

confinement can considerably improve the stress-strain characteristics of concrete. Circular spirals confine concrete more effectively than rectangular ties or hoops as they apply a uniform radial pressure to the concrete, whereas a rectangle tends to confine the concrete mainly at corners (Fig. 2.13). Nevertheless, rectangular ties do produce a significant increase in ductility of the concrete core as a whole. A comparative study of the confined concrete models, proposed by Chan (1955), Roy and Sozen (1964), Soliman and Yu (1967), Sargin (1971), Kent and Park (1971), Vallenas et al. (1977), Sheikh and Uzumeri (1980), was done by Sheikh (1982).

Chan (1955) suggested a tri-linear curve for confined and unconfined concrete, as shown in Fig. 2.14(a). The only variable considered in this model is the volumetric ratio of lateral steel to concrete core. The OAB part approximates the curve for unconfined concrete. The slope BC depends upon the lateral confinement. For unconfined concrete the slope is negative. For confined concrete the slope is positive with ultimate concrete strains attaining values much higher than for unconfined concrete. Comparison between experimental and analytical results (Sheikh 1982) shows that Chan's model overestimates the strength and ultimate strain of confined concrete in several cases, particularly for specimens with large tie spacing. Conversely for specimens with closely spaced ties the model underestimates the strength and ultimate strain. This might be attributed to the fact that no consideration is given to the tie spacing and steel configurations.

Roy and Sozen (1964) proposed a stress-strain relationship for concrete as shown in Fig. 2.14(b). The co-ordinates of the peak point are 0.002 and f'_c, where f'_c is the strength of concrete in a plain specimen. An equation for the strain value corresponding to 50 percent of the maximum stress is suggested to define the descending part of the bilinear curve. The variables considered in the model are the volumetric ratio of lateral steel to concrete core and the ratio of the shorter dimension of the section to the tie spacing. Comparisons with experimental results (Sheikh 1982) show that the model underestimates the strain at the maximum stress and ignores the increase in strength due to confinement. The slope of the descending part has a slower rate of drop than shown by experiments.

41

Soliman and Yu (1967) proposed the stress-strain curve shown in Fig. 2.14(c). The variables considered in the model are the area of ties, tie spacing, and section geometry. No consideration is given to the steel configuration. Comparisons with experimental results (Sheikh 1982) show that the model underestimates the increased concrete strength due to confinement. The model predicts the maximum strain corresponding to the maximum stress reasonably well. The slope of the descending part is too steep compared with the experimental curves.

Sargin (1971) proposed a general equation to give a continuous stress-strain curve of confined concrete as shown in Fig. 2.14(d). The variables recognised in the model are the volumetric ratio of lateral steel to concrete core, ratio of width of concrete core to tie spacing, yield strength of steel, and concrete cylinder strength. The strain value at peak stress is also assumed to depend on the strain gradient at the section. Comparison with test results (Sheikh 1982) shows that the model underestimates the increase in concrete strength due to confinement. The effect of tie spacing, it seems, is also not appropriately accounted for. The increase in concrete strength is directly related to the stress in the ties. The test data does not support this assumption.

The stress-strain curve proposed by Kent and Park (1971), shown in Fig. 2.14(e), is based on the data reported by Roy and Sozen (1964), and Soliman and Yu (1967) and combined many features of the previously proposed curves. The ascending portion of the curve is represented by a second-degree parabola and is unaffected by the confinement of concrete. The maximum concrete stress is assumed equal to the cylinder strength f'_c and the corresponding strain is 0.002. The falling branch of the curve is a straight line whose slope is specified by determining the strain at $0.5f'_c$. The slope of the falling branch is a function of concrete cylinder strength, ratio of width of confined concrete to spacing of ties, and ratio of volume of tie steel to volume of concrete core. The descending curve extends to $0.2f'_c$, beyond which a horizontal line to infinity represents the concrete behaviour. The model recognises the effect of confinement on ductility but does not recognise the effect on concrete strength. Comparison with test data (Sheikh 1982) shows

42

that the model reasonably estimates the slope of the descending branch. The model however underestimates the maximum stress and corresponding strain.

The model proposed by Vallenas et al. (1977), Fig. 2.14(f), is similar in form to Kent and Park's (1971) model, with the difference that it considers the concrete strength enhancement due to confinement. The variables included in the model are the volumetric ratio of tie steel to concrete core, ratio of area of longitudinal steel to area of cross-section, sizes of tie bar and longitudinal bar, ratio of core dimension to tie spacing, steel strength, and strength of concrete. Comparison with test data (Sheikh 1982) shows that the model reasonably estimates the slope of the falling branch. Since this model takes into account the increase in concrete strength due to confinement, the predictions are better than the Kent and Park's (1971) model. However, the test data shows that the strength of the concrete is not dependent upon the longitudinal steel content and is not directly proportional to the stress in ties, as suggested by the model. The model underestimates the effect of tie spacing on strength and ductility.

The stress-strain model of Sheikh and Uzumeri (1980), for confined concrete, is shown in Fig. 2.14(g). The first part of the curve OA is a second-degree parabola followed by a straight portion AB, at maximum stress level. The descending part of the curve is a straight line extending to 30 percent of the maximum stress, after which a horizontal line represents the concrete behaviour. The variables considered in the model are, volumetric ratio of lateral steel to concrete core, distribution of longitudinal steel around the core perimeter and the resulting tie configuration, tie spacing, characteristics of lateral steel, and strength of plain concrete. The amount of longitudinal steel was recognised as having no significant effect on the behaviour of confined concrete. The analytical behaviour of confined concrete under concentric load, using this model, shows good agreement with experimental results (Sheikh 1982).

Park et al. (1982) improved the original Kent and Park (1971) model by making an allowance for the enhancement in the concrete strength due to confinement. Fig. 2.14(h) shows the modified stress-strain model. The curve consists of two parts. A second-degree

43

parabola represents the ascending portion of the curve and a linear falling branch represents the descending portion of the curve. The maximum stress reached at point B is assumed to be Kf'_c and the corresponding strain is $\varepsilon_o = 0.002K$. The factor K is greater than one and takes into account the effect of confinement on concrete strength. K depends upon the volumetric ratio of tie steel to concrete core, yield strength of ties, and cylinder strength of concrete. The maximum strain is taken as 0.002K, in which 0.002 is the assumed value of the strain at maximum stress of unconfined concrete. This enables the initial curve (parabola AB) to have the same initial slope as the unconfined concrete. The descending branch extends to $0.2Kf'_c$. Comparisons with test results show that this model gives a better prediction of the confined strength of concrete than the original Kent and Park (1971) model. A comparison, given by Park et al (1982), shows that both modified Kent and Park model and Sheikh and Uzumeri (1980) model give excellent agreement with the measured moment capacity. The modified Kent and Park model has the advantage of simplicity of application compared with Sheikh and Uzumeri model.

Sheikh and Yeh's (1986) model is an extension of earlier model, proposed by Sheikh and Uzumeri (1980) for axially loaded members, to include the effects of flexural strain gradient. Tests by Sargin (1971) have concluded that specimens show increased ductility under the flexural strain gradient. The model is shown in Fig. 2.14(i). The curve OABCDE is for confined concrete under concentric compression, while the curve OAB'C'D'E' is for confined concrete under eccentric compression. The model shows good agreement with the experimental results, but is quite complicated for routine applications.

Mander et al. (1988) developed a unified stress-strain model for confined concrete, applicable to both circular and rectangular sections. The concrete section may contain any general type of confining steel, either spiral or circular hoops, or rectangular hoops with or without supplementary cross ties. The model is applicable to static or dynamic loading, applied either monotonically or cyclically. The model takes into account the effects of cyclic loading and strain rate. The proposed model for monotonic loading and slow strain rate is shown in Fig. 2.14(j). A single equation is used to define the stress-

44

strain curve. The influence of confinement is taken into account by defining an effective lateral confining stress. The ultimate strain in concrete is defined as the one corresponding to first fracture of the transverse reinforcement and is based on the energy balance approach. Since this is a unified model applicable to a variety of loading rates, strain rates, and shape and arrangement of ties, its application to specific cases is complicated.

The proposed stress-strain model of Saatcioglu and Razvi (1992) is similar in shape to the Kent and Park (1971) model, as shown in Fig. 2.14(k). The model defines the confined strength in terms of equivalent uniform pressure provided by the reinforcement cage. The slope of the descending branch is obtained by defining the strain corresponding to 85% of the peak stress. A constant residual strength is assumed beyond the descending branch, at the 20% strength level. The variables consider are the size and spacing of ties, arrangement of ties, and dimensions of the cross-section. The model does not take into account the effect of strain gradient. In general the model provides good agreement with the test results.

Literature review of the stress-strain models for confined concrete reveals that the volumetric ratio of lateral steel to concrete core is the most important parameter affecting the concrete behaviour. Other variables affecting concrete behaviour include, tie spacing, section dimensions, cylinder strength, and steel strength.

The modified Kent and Park model (Park et al 1982) and the Sheikh model (Sheikh and Uzumeri 1982) give better predictions of test results than all the other models reviewed here. The Sheikh and Uzumeri model gives good predictions of concrete strength in general but may overestimate the concrete strength in the presence of shear and spalling of concrete cover. It would be logical in that case to use a model that underestimates the increase in concrete strength due to confinement. An appropriate choice in that case would be the modified Kent and Park model (Park et al 1982). The model is easy to apply and gives a very good prediction of the slope of the falling branch.

45

2.9 Ultimate Strain of Concrete

Researchers agree that ultimate concrete strain ε_{cu} is the most important factor that affects the plastic rotation capacity of a concrete section. The standard (A23.3-94) specifies an ultimate concrete strain of 0.0035 for use in the computation of ultimate strength and curvature of concrete section. The presence of transverse reinforcement and strain gradient provides a confinement effect and increases the ductility and hence ultimate strain of concrete. Concrete strains much larger than 0.0035 have been reported in flexural tests of concrete beams. Researchers have proposed empirical equations for computing the ultimate strain at the extreme compression fibre of flexural members. The classical equations for ε_{cu} were given by Baker and Amarakone (1964) (Eq. 2.12a) and Corley (1966) (Eq. 2.17).

$$\varepsilon_{cu} = 0.0015\left\{ 1.45 + 1.5\rho_s + (0.7 - 0.1\rho_s)\frac{1}{c/d} - \frac{f_c'}{10^4} \right\} \qquad [2.12a]$$

$$\varepsilon_{cu} = 0.003 + 0.02\frac{b}{z} + \left(\frac{\rho_s f_y}{20}\right)^2 \qquad [2.17]$$

Park et al. (1982) used the above equations to compare the experimental values of peak strains and the theoretical predictions. The experiments were conducted on axially loaded columns. The minimum strain at first visible crushing at the extreme compression fibre was 0.005, which is well in excess of the standard-specified value of 0.0035. The concrete cover showed no sign of spalling at this stage. The maximum measured strains on the surface of the confined core, when the cover had spalled off, varied between 0.016 and 0.026. Corley's equation gives a very good agreement between the theoretical and experimental values of peak strain. The authors mentioned that the tests were terminated at a stage when the load-deflection curve was still rising and hence greater values of experimental peak strains would have obtained had the tests were continued. Baker's equation provides a highly conservative estimate of ε_{cu} compared to the experimental values.

46

2.10 Summary and Conclusions

A review of the non-linear analysis methods and ductility models for computing the plastic rotation capacity and allowable moment redistribution in reinforced concrete structures is presented. It is found that elastic methods of analysis are not suitable for predicting the ultimate behaviour of reinforced concrete structures. One must resort to non-linear methods for a realistic prediction of the response of reinforced concrete structures at ultimate. These non-linear methods, known as limit design methods, must satisfy equilibrium, rotation compatibility, and serviceability. Two broad classifications of limit design methods are identified, the equilibrium methods, and the compatibility methods. These methods, although provide a sound rationale for predicting the non-linear response of reinforced concrete structures, are quite complicated and laborious. As such these methods have not gain much acceptance within the designers community.

Design standards recognise the non-linear behaviour of reinforced concrete and provide empirical relations for arbitrary moment redistribution. These relations assume a linear relationship between the allowable moment redistribution and the c/d ratio and require no check of compatibility and serviceability. It is noted that a major disagreement exists among different standards on the amount of allowable moment redistribution. The allowable percentage of moment redistribution varies from 15% for the Japanese standard to 66% for the Danish standard.

It is recognised that to establish a limit on permissible moment redistribution one needs a rational model for predicting the plastic rotation capacity of critical sections. Initial models for computing the plastic rotation capacity assume a constant curvature over an equivalent plastic hinge length. Further research showed that deformations along the plastic hinge length are discontinuous and that plastic rotation should be computed as a sum of the rotations of cracked elements within the plastic hinge region. It is recognised that the shear cracking causes a significant shift in the tension force diagram and results in increased rotation capacity. On the other hand, neglecting bond-slip may result in an unconservative estimate of plastic rotation capacity. Researchers emphasise the importance of using accurate constitutive relationships for concrete and steel and

47

recognised ultimate strain of concrete as the most important parameter influencing the plastic rotation capacity. Some suggested member slenderness and shear cracking as important parameters influencing plastic rotation capacity. The effect of loading and prestressing on the plastic rotation capacity has also been recognised.

The literature review helps identifying the important parameters affecting plastic rotation capacity and allowable moment redistribution. It is evident from the literature review that different ductility models emphasise the importance of different parameters affecting moment redistribution. The current standard (CSA A23.3-94) considers c/d to be the only influencing parameter. The need exists for a comprehensive ductility model that incorporates all the important variables to provide a basis for formulating alternate equation for allowable moment redistribution.

48
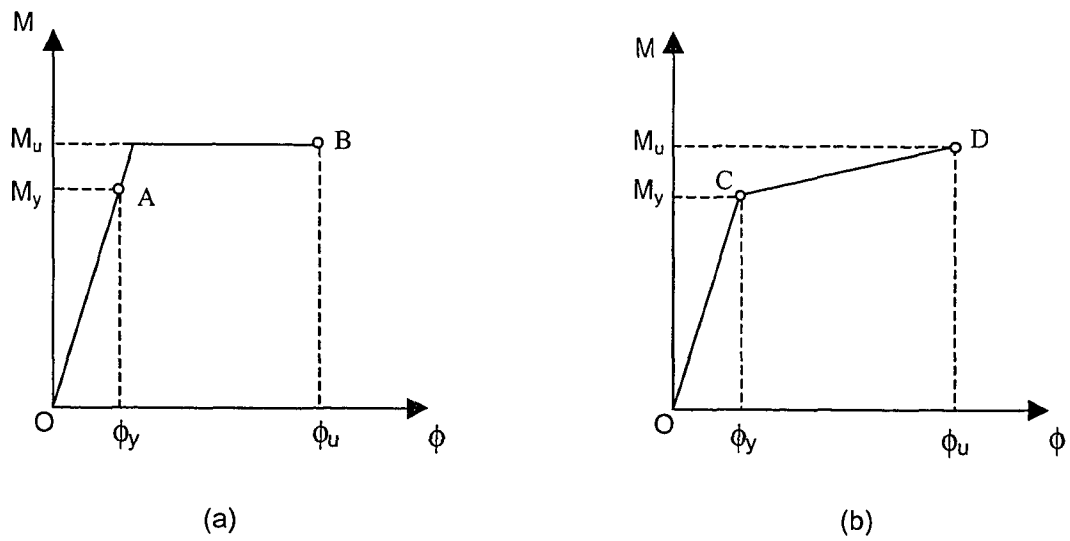
Figure 2.1 Idealized moment-curvature relationships used in non-linear analysis and design of reinforced concrete structures
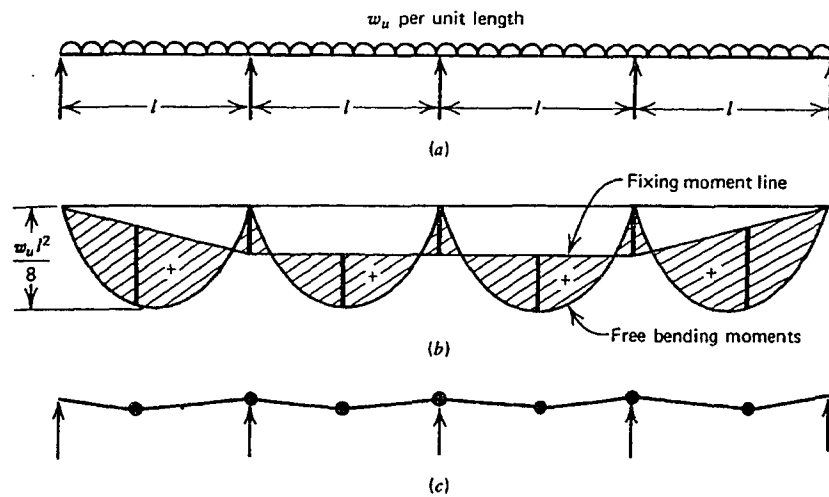
Figure 2.2 Distribution of ultimate bending moments; (a) beam, (b) limit bending moment diagram, (c) collapse mechanism, after Park and Paulay (1975)

49

Live load (on either or both spans) plus dead load

Uniformly loaded continuous beam

Bending moment diagram

a = not less than increase resulting from reduction
of support moment for load case 1 by 20%
b = not more than the reductions resulting from
an increase of support moment for load
cases 2 and 3 by 20% or up to design
envelope, whichever is less

———— Load case 1: dead load and live load on both spans
— — Load case 2: dead load on both spans, live load on right-hand span
—·— Load case 3: dead load on both spans, live load on left-hand span.
———— Bending moment envelope for design

Figure 2.3 Adjustments of elastic theory bending moment diagram for
allowable moment redistribution, after Park and Paulay (1975)

50
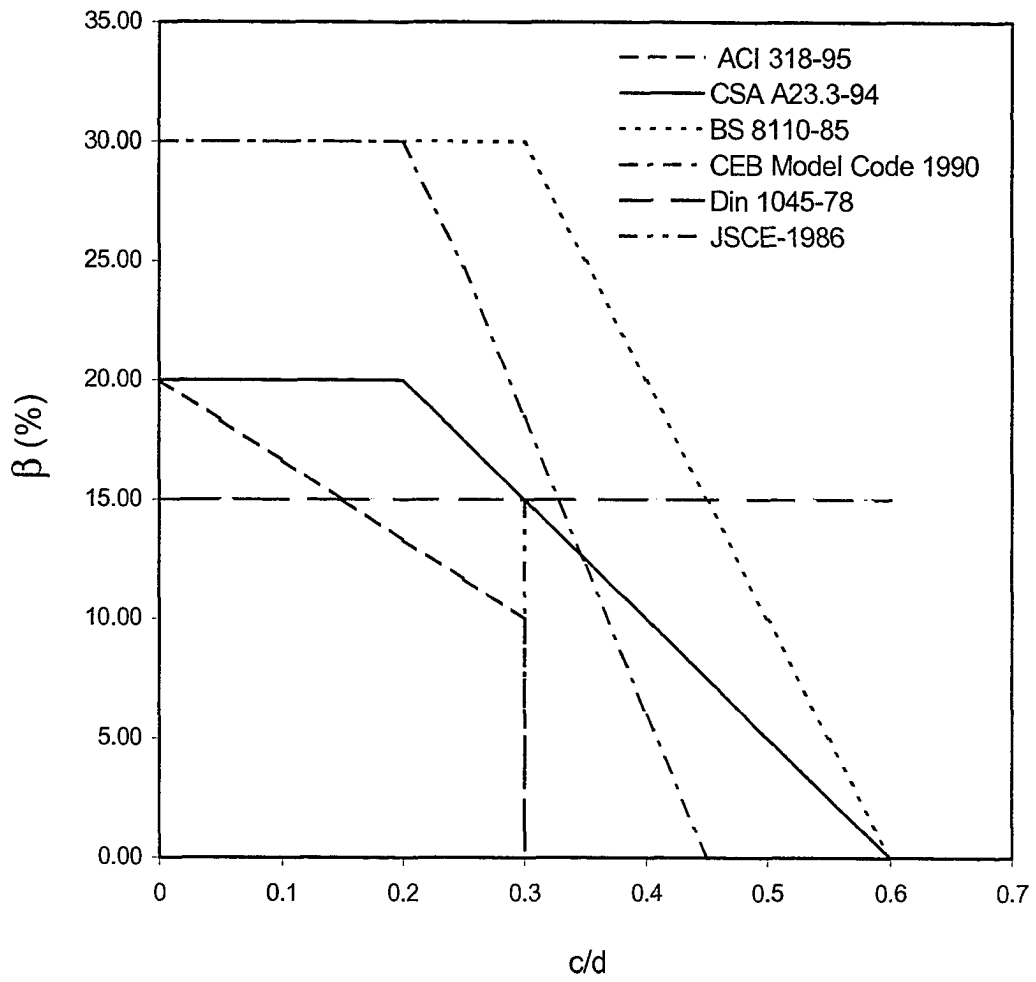
Figure 2.4 Moment redistribution limit according to different design standards
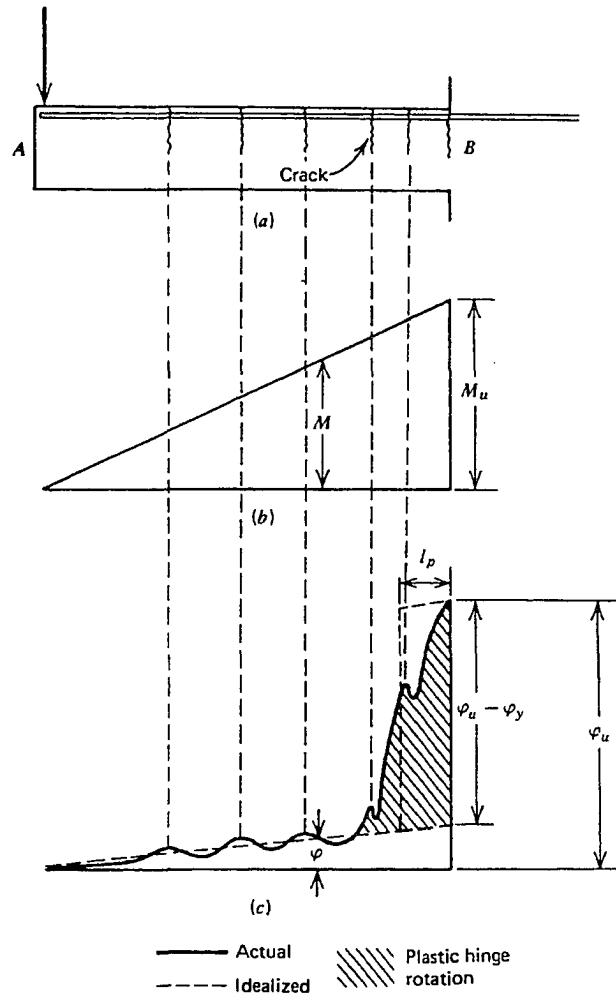
Figure 2.5 Idealized plastic rotation; (a) beam, (b) bending moment diagram, (c) curvature diagram, after Park and Paulay (1975)

52
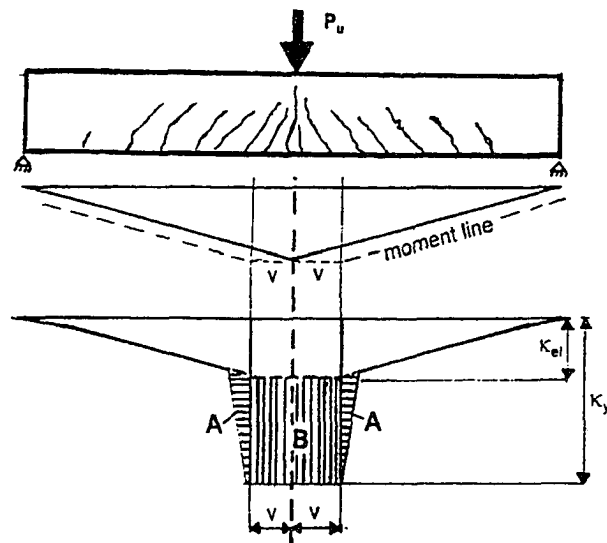
Figure 2.6 Calculation of plastic rotation considering inclined cracking, after Dilger (1966)

cracked beam elements

plastic hinge region
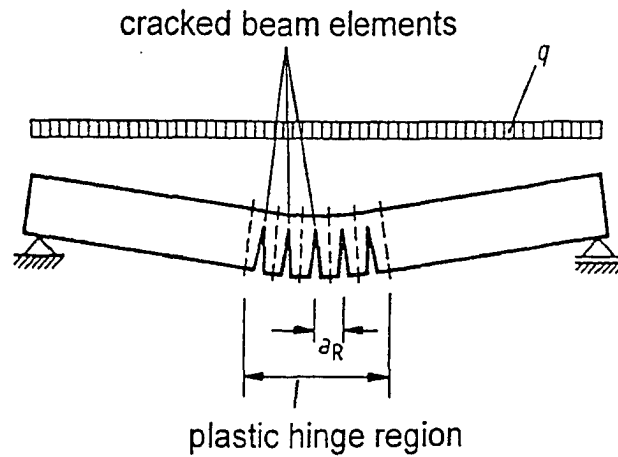
Figure 2.7 Calculation of rotation capacity in discrete crack model, after Eifler (1969)

53
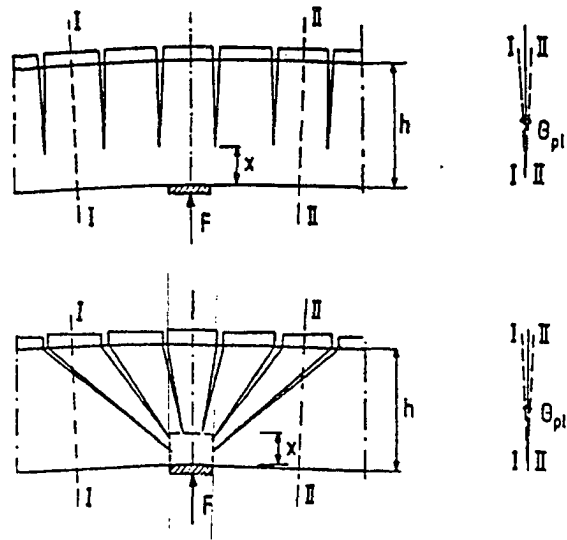
Figure 2.8 Bending (top) and shear crack hinge (bottom) after Bachmann (1967)

stirrup

——— tie
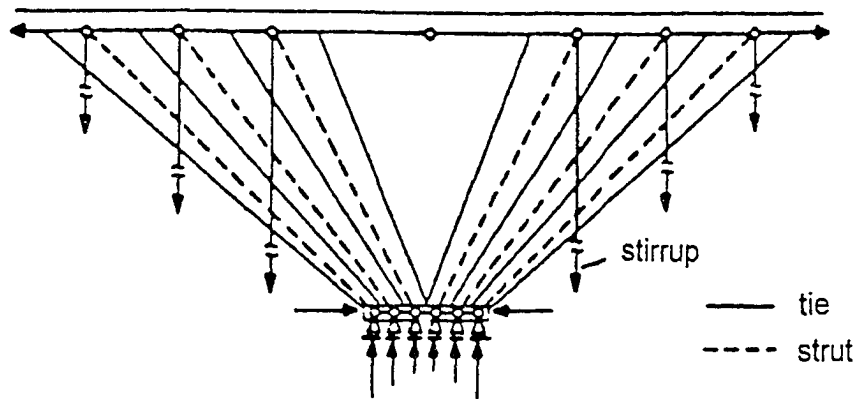
----- strut

Figure 2.9 Strut and tie model for calculating rotation (bending/shear), after Michalka (1986)

54
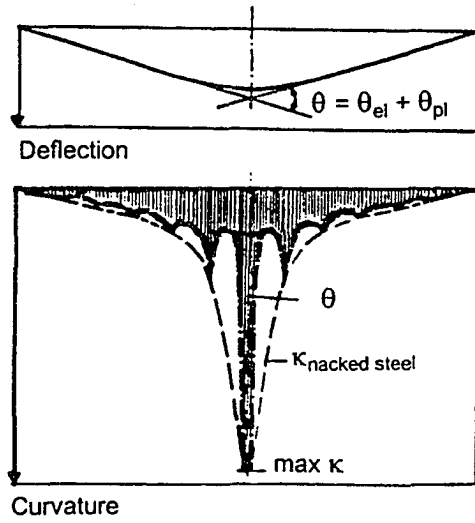
Figure 2.10 Integration of the curvature in numerical model, after Langer (1987)
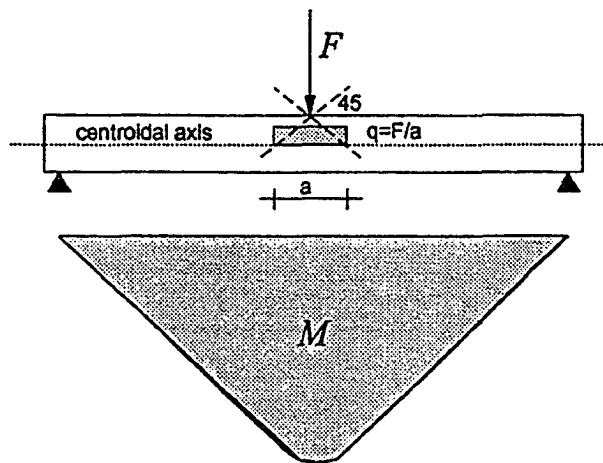
Figure 2.11 Bending moment diagram, after Cosenza et al. (1991)

55
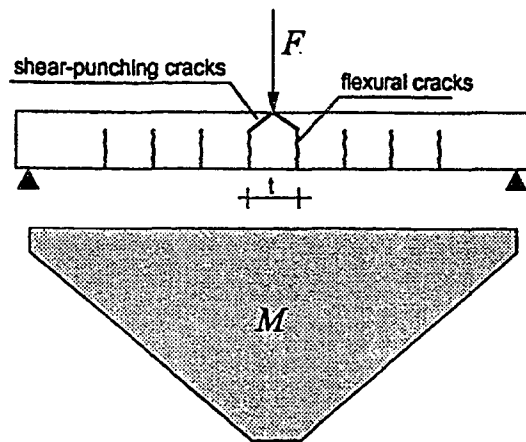
Figure 2.12 Bending moment diagram in the presence of shear-punching cracks, after Cosenza et al. (1991)
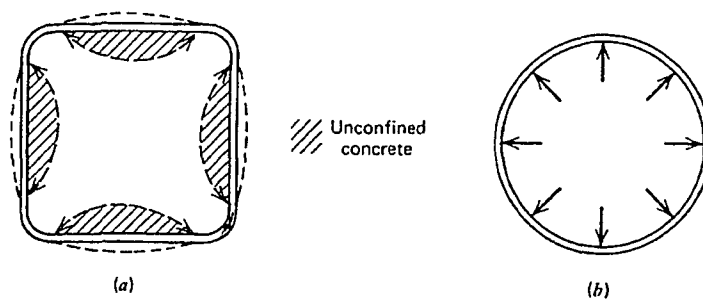
Figure 2.13 Confinement by square hoops and circular spirals; (a) square hoop, (b) circular spiral, after Park and Paulay (1975)

56
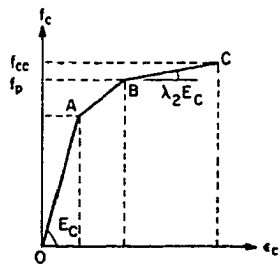
(a) Chan (1955)
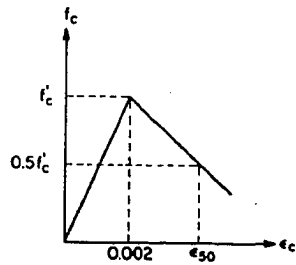
(b) Roy and Sozen (1964)
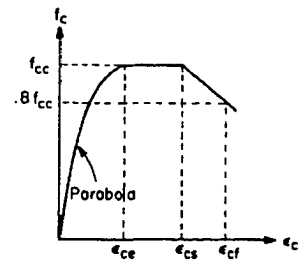
(c) Soliman and Yu (1967)
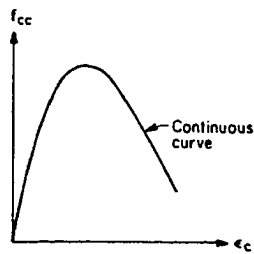
(d) Sargin (1971)
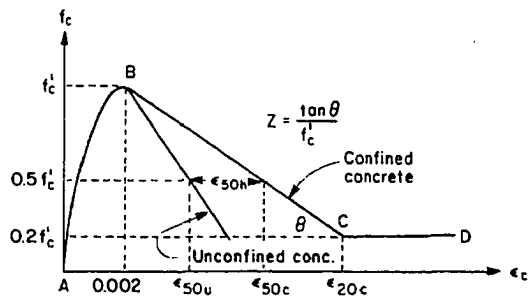
(e) Kent and Park (1971)
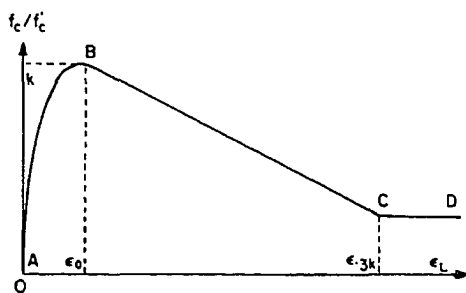
(f) Vallenas et al. (1977)
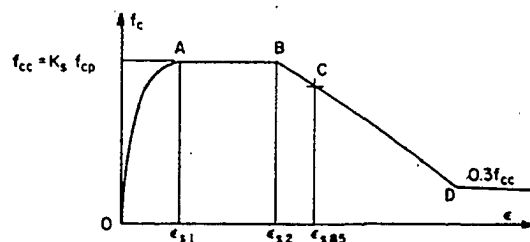
(g) Sheikh and Uzumeri (1980)

Figure 2.14 Stress-strain curves for confined concrete, after Sheikh (1982)
(continued on next page)
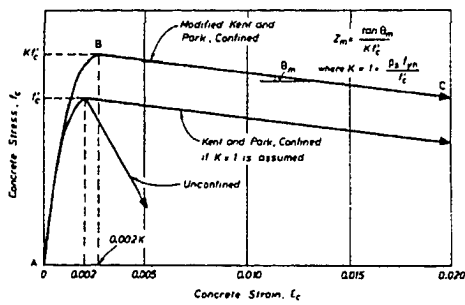
(h) Park et al. (1982)
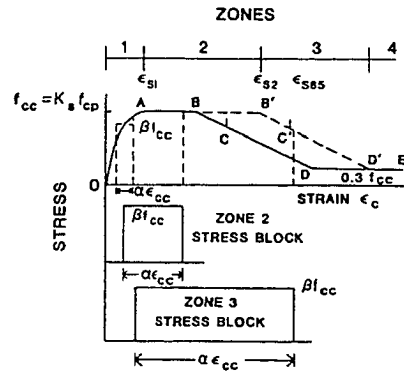
(i) Sheikh and Yeh (1986)
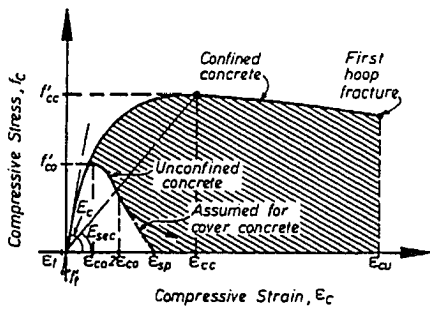
(j) Mander et al. (1988)
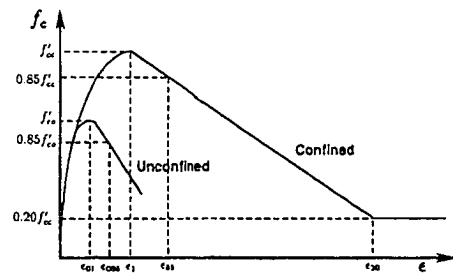
(k) Saatcioglu and Razvi (1992)

Figure 2.14 (contd.) Stress-strain curves for confined concrete

58

3. ASSESSMENT OF CODE PROVISIONS FOR MOMENT REDISTRIBUTION[*]

3.1 Introduction

This chapter examines the code (CSA A23.3-94) limit for moment redistribution and demonstrates that it is not entirely rational.

Because of the ease of computer based structural analysis, structures are now analysed and designed for more load cases than in the past. This leads to an expansion of design bending moment envelope, an increase in flexural reinforcement and a higher construction cost. Moment redistribution can be used to reduce the design moment envelope and the amount of flexural reinforcement required at critical sections. In moment redistribution, the calculated elastic bending moment at a critical section can be reduced or increased provided that the bending moment in the adjoining critical sections are adjusted to satisfy equilibrium for the loading case under consideration. Since the load cases that give maximum moments at supports are different from those which give maximum moments in spans, allowing for moment redistribution will result in reduction of both maximum negative and maximum positive moments of the elastic envelope.

Structural design standards (CSA A23.3-94, ACI 318-95, BS 8110-85, CEB Model code 1990, JSCE 1986, DIN 1045-78, DS411-1986) recognise the non-linear behaviour of reinforced concrete structures and allow limited moment redistribution of elastic moments. Different formulae for the redistribution of elastic moments are proposed by various standards of practice. The literature review revealed that significant differences exist among design standards on the amount of permissible moment redistribution with the Canadian Standard being very conservative. Structural standards consider permissible moment redistribution as a section property and relate it to the relative depth of the compression zone at failure (c/d) or the reinforcement index ($\omega = A_s f_y / b d f'_c$) only.

---

[*] Essentials of this chapter appear as a paper in the proceedings of the Annual Conference of the Canadian Society for Civil Engineering, held in Regina SK, 1999

59

Although, c/d or ω can fairly well represent the combined effects of stress-strain characteristics of the materials, the geometry of the cross-section and the amount of tensile and compressive reinforcement, it is an oversimplification to relate moment redistribution to c/d or ω only. The literature review reveals that there are many other factors that need to be considered.

To take complete advantage of moment redistribution, a realistic estimate of permissible moment redistribution, at critical sections, is required. This chapter examines the Canadian standard (CSA A23.3-94) provision for moment redistribution.

3.2 Moment Redistribution in CSA A23.3-94

The amount of moment redistribution at a critical section depends upon the ductility of that section. For a given amount of moment redistribution to occur at a section, the required plastic rotation must not exceed the available plastic rotation. CSA A23.3-94 accounts for the ductility of section in terms of c/d ratio. The standard requires that the maximum permissible moment redistribution, β, at a section must not exceed 30-50(c/d). This can be restated as:

$$\frac{c}{d}(\text{max}) = \frac{1}{50}(30 - \beta)$$

[3.1]

where c is the depth of neutral axis at ultimate, β is the change in moment expressed as a percentage of the elastic moment. The standard limits the maximum value of β to 20%. To ensure ductility, the design c/d ratio must not exceed the value given by Eq. 3.1, for a given amount of moment redistribution. It is important to note here that the code equation for moment redistribution uses material resistance factors ϕ_c and ϕ_s when computing c/d. The material resistance factors vary from standard to standard. In order to make the work in this thesis generally applicable, all material resistance factors are taken as 1.0; thus Eq.

3.1 is rewritten as Eq. 3.2 and all material resistance factors are dropped from further equations.

$$\frac{c}{d}(max) = \frac{1}{50}(30 - \beta)\frac{\phi_c}{\phi_s}$$

[3.2]

where $\phi_s = 0.85$ is the resistance factor for steel and $\phi_c = 0.6$ is the resistance factor for concrete. The draw back of Eq. 3.2 is that it considers β as a section property and relates it linearly to the c/d ratio, as shown in Fig. 3.1. The literature review reveals that the most important factors, influencing permissible moment redistribution, are the plastic rotation capacity and plastic rotation demand, which in turn depend upon many other factors including structure geometry and loading.

3.3 Allowable c/d Limit From Plane-Section Analysis

In this section an alternate expression for c/d is derived to provide basis for comparison with the code c/d limit. The expression is derived using the established methods of plane-section compatibility analysis. The plastic rotation capacity of a hinge is given as:

$$\theta_p = (\phi_u - \phi_y)L_p$$

[3.3]

where ϕ_y and ϕ_u are the curvatures at the critical section at yield and ultimate respectively and L_p is the effective hinge length. Equation 3.3 assumes a constant curvature within plastic hinge length L_p. The yield curvature can be obtained from a plane-section analysis using the conditions at yield as shown in Fig. 3.2a:

61

$$\phi_y = \frac{f_y / E_s}{d(1 - \frac{c_y}{d})}$$ [3.4]

where f_y is the yield strength of steel; E_s is the modulus of elasticity of steel; d is the effective depth of the section, and c_y/d is the relative depth of neutral axis at yield, given as:

$$\frac{c_y}{d} = \sqrt{\rho^2 n^2 + 2\rho n} - \rho n$$ [3.5]

where ρ is the reinforcement ratio = A_s/bd, b is the width of the beam, n is the modular ratio = E_s/E_c, and E_c is the modulus of elasticity of concrete. The ultimate curvature, ϕ_u, can similarly be obtained from the plane-section analysis using the conditions at ultimate, as shown in Fig. 3.2b.

$$\phi_u = \frac{\varepsilon_{cu}}{c}$$ [3.6]

where ε_{cu} = ultimate concrete strain at extreme compression fibre = 0.0035. Using $L_p = K_p d$, and substituting Eq. 3.4 and 3.6 into Eq. 3.3 gives:

$$\theta_p = \left[\frac{\varepsilon_{cu}}{c} - \frac{f_y / E_s}{d(1 - c_y / d)} \right] K_p d$$ [3.7]

Equating $\theta_p = \theta_{prcqd}$ and rearranging, gives the allowable c/d ratio in terms of the required plastic rotation.

$$\frac{c}{d}(\max) = \frac{\varepsilon_{cu}}{\dfrac{\theta_{prcqd}}{K_p} + \dfrac{f_y / E_s}{1 - (c_y / d)}}$$ [3.8]

62

where θ_{preqd} is the required plastic rotation at a critical section and K_p is a constant defining plastic hinge length. Based on Mattock's (1964) findings that plasticity extends at least a distance d/2 on either side of the section of maximum moment, following values of K_p are assumed:

K_p = 1 for hinge with members on both sides

K_p = 0.5 for hinge with member on one side

Figure 3.3 shows a graphical solution of Eq. 3.8. Equation 3.8 cannot be used directly for comparison with the code Eq. 3.2. The code equation relates c/d to allowable moment redistribution, while Eq. 3.8 relates c/d to the plastic rotation capacity. The procedure used to compare Eq. 3.8 with the code equation is as follows:

1. Obtain elastic moment envelope for the continuous beam, using pattern load analysis.

2. Assume a reasonable value of β, within code allowable limits, at critical sections where reduction in design moments is desired.

3. Reduce elastic envelope moments by applying β and adjusting other moments to satisfy equilibrium.

4. Perform "hinge-moment analysis" for each load case, as outlined in section 3.4.2, to obtain the required plastic rotations at critical sections for each load case.

5. Substitute required plastic rotation values into Eq. 3.8 to obtain the allowable c/d limit at each critical section. (These c/d values correspond to assumed values of β at each critical section).

63

6. Using same value of β as in step 2, determine the code c/d limit for each critical section with Eq. 3.2.

7. Compare the theoretical and the code c/d limits obtained from steps 6 and 7.

This procedure is discussed in detail in the following sections.

3.4 Moment Redistribution Analysis

To perform moment redistribution analysis, one must select a value of β. Experimental and numerical studies (Mattock 1959, Svienson 1989, Sigrist and Marti 1994) have shown that 20% moment redistribution is usually not a problem with continuous beams that are not very heavily reinforced. The code upper limit on moment redistribution is also 20%. The actual redistribution used may be less. The selection of β is somewhat arbitrary. A value of 20% is used in the example in section 3.6. The ductility requirement with $\beta=20\%$ can usually be satisfied at the design stage. This may require the addition of compression reinforcement and/or modifying the beam cross-section to ensure that the design c/d does not exceed the allowable c/d at critical sections.

The proposed procedure is a lower bound solution based on limit analysis methods. A brief review of classical limit design methods is given in the literature review. Any distribution of design bending moments is acceptable provided that the following conditions are met:

1. The distribution of bending moments is statically admissible, i.e. the internal forces must be in equilibrium with the external loads.

2. The rotation capacity of the plastic hinge region is sufficient to enable the assumed distribution of moments to be developed at the ultimate load.

3. The cracking and deflections at the service load are within the allowable limits.

Conditions 1 to 3 can be stated as, equilibrium, ductility, and serviceability. The procedure consists of two phases. In the first phase the design moments are obtained by using β to reduce the elastic envelope moments at selected locations. In the second phase a "hinge-moment analysis" is done for each load case to obtain the redistributed design moments, the redistributed shear and axial forces and the plastic rotations at the critical sections. This procedure is demonstrated in the following sections.

3.4.1 Phase I - Direct reduction of elastic envelope moments

The reduced design moments can be obtained directly from the elastic moment envelope by using β and equilibrium. For a beam of span L, acted upon by a uniformly distributed load w_f, equilibrium requires:

$$M_{total} \geq M_o \tag{3.9}$$

M_{total} is the total span moment demand given as:

$$M_{total} = \frac{M_{eL} + M_{eR}}{2} + M_{emid} \tag{3.10}$$

Where M_{eL}, M_{eR}, and M_{emid} are the elastic envelope moments at the left support, right support, and the mid-span, respectively.

M_o is the static span moment given as:

$$M_o = \frac{w_f L^2}{8} \tag{3.11}$$

Equation 3.9 can be rewritten as:

$$\frac{M_{eL} + M_{eR}}{2} + M_{emid} \geq \frac{w_f L^2}{8} \tag{3.12}$$

65

Note that while Eq. 3.12 is commonly used in design, it is not exact unless $M_{eL} = M_{eR}$. For continuous beams with patterned live loads, the elastic envelope moments are typically in excess of the static span moment. Thus reduction in elastic envelope moments is possible as shown in Fig. 3.4. The solid lines in Fig. 3.4 represent the elastic moment envelope, while the dotted lines represent the reduced design moment envelope. The design moment envelope is obtained by reducing the elastic moment envelope, such that the total span moment is equal to the static span moment. The procedure is described below in detail.

Elastic moment envelope is first obtained from the elastic analysis. Next the total span moment M_{total} and static span moment M_0 for each span are calculated using Eq. 3.10 and 3.11 respectively. The reduction in total span moment for each span can be written as:

$$\left(\frac{\beta_L M_{eL} + \beta_R M_{eR}}{2} + \beta_{mid} M_{emid} \right) \times \frac{1}{100} = M_{total} - M_o \qquad [3.13]$$

where β_L and β_R are the percentage reduction in the left and right support moments respectively and β_{mid} is the percentage reduction in the mid-span moment. There are three β values that need to be established. Two are selected by the designer and the third is computed from Eq. 3.13. As previously discussed, a value of 20% will be used for β_L and β_R. The mid-span moment reduction may then be calculated from Eq. 3.13. Finally, the β values are applied to the elastic moment envelope to obtain the reduced design moments at the critical sections. Assuming no ductility problem, this will produce a plastic collapse capacity no smaller than w_f.

3.4.2 Phase II - Hinge moment analysis

A "hinge-moment" analysis is used to: assess the ductility demand; to obtain the points of inflection, and to obtain the axial forces and shear forces that are consistent with the redistributed moments. The design moments obtained from phase-I are used to perform

the hinge-moment analysis. The analysis is performed with a conventional elastic frame analysis program. In this analysis the structure is modified and analysed for each load case by introducing frictionless plastic hinges and the corresponding design moments at the appropriate critical sections. The procedure is summarised below for a typical load case, with reference to Fig. 3.5:

1. Locations of plastic hinges are identified by comparing the elastic moments at the critical sections with the design moments obtained in Phase I of the analysis. These are the sections at which the elastic moments exceed the design moments. Fig. 3.5a shows a beam with a load case that causes maximum moment at the centre support (node 5). Figure 3.5b shows the elastic bending moment diagram for this load case and the design moment envelope. A hinge will form at section 5 because at this section the elastic moment is greater than the design moment.

2. The structure and the load case are modified by introducing plastic hinges and the associated design moments. Figure 3.5(c) shows the modified structure with a hinge at section 5. The design moment is applied to the ends of the members framing into the plastic hinge.

3. The modified structure is analysed for the modified load case to obtain the redistributed forces and deformations.

4. The redistributed moments at critical sections are checked to ensure that they do not exceed the design moments. More than one hinge-moment analysis may be required to make sure that the final redistributed moments do not exceed the design moments, at any critical section. The final analysis gives the required redistributed forces and deformations. The sum of the member end rotations on either side of a plastic hinge gives the total plastic rotation required by that hinge.

Steps 1 through 4 are repeated to obtain the redistributed moments at critical sections for each load case. The solution provides the redistributed moment envelope as well as the required plastic rotations to be used in Eq. 3.8.

3.5 Serviceability

Formation of a plastic hinge, at service load, would produce unacceptable crack widths. Thus, one should avoid redistributing moment below the service load value. All requirements of serviceability such as crack widths and deflection control must be satisfied as for normal elastic analysis.

3.6 Application of Proposed Procedure for Comparison of c/d Limits

To compare the code c/d limits from Eq. 3.2 with the c/d limits from Eq. 3.8, moment redistribution analysis is done on the beam shown in Fig. 3.6. The beam is analysed for six pattern load cases to obtain the maximum moments at critical sections. The factored elastic envelope moments and the service elastic envelope moments are given in Table 3.1.

In phase 1 of the analysis, the elastic support moments, M_e, are reduced by 20% with span moments adjusted to satisfy the equilibrium requirements. Table 3.1 shows the reduced design moments, M_{des}, and the values of β at critical sections. Note that the elastic moments are not reduced below the service load moments M_s. In the second phase of analysis, the required plastic rotations, θ_{preq}, are obtained by performing hinge-moment analysis. The values of the required plastic rotations at critical sections are shown in Table 3.1.

Table 3.1 Plastic rotations from moment redistribution analysis

Section	2	3	4	5
M_e (kNm)	379	-493	264	-400
M_s (kNm)	271	-357	186	-286
M_{des}(kNm)	353	-394	211	-320
β (%)	6.8	20	20	20
θ_{preqd} (radians)	0.0029	0.00357	0.00355	0.00278

68

Having obtained β and θ_{preq} from moment redistribution analysis, the allowable c/d ratios at the critical sections can be calculated using Eq. 3.8. Table 3.2 shows the comparison of c/d limits obtained from Eq. 3.2 and Eq. 3.8. The code c/d limit is very conservative for most of the sections. Equation 3.8 shows that for the same amount of moment redistribution at sections 3, 4, and 5, the allowable c/d limit varies from one section to the other. This is because the plastic rotation demand at each of these sections is different due to structure geometry and other factors not recognized by the code.

Table 3.2 Comparison of code c/d limit and theoretical c/d limit

Section	2	3	4	5
β (%)	6.8	20	20	20
c/d (code, Eq. 3.2)	0.328	0.14	0.14	0.14
c/d (theory, Eq. 3.8)	0.548	0.5	0.505	0.558
c/d (code)/ c/d (theory)	0.6	0.28	.277	.25

3.7 Simplified Approach for Computing Allowable c/d and β

The procedure outlined above for computing allowable c/d is suitable when one needs to perform moment redistribution analysis to obtain the complete design solution. However, when one needs a quick estimate of allowable c/d or β, the procedure may not be very convenient because complete hinge-moment analysis is required to estimate the required plastic rotations. Instead of considering complete structure, a single span indeterminate beam, shown in Fig. 3.7a, can provide a conservative estimate of required plastic rotation. Since allowable c/d varies inversely with θ_{preqd}, a conservative estimate of θ_{preqd} will yield a conservative estimate of allowable c/d.

Let q_u be the ultimate load on the beam and q_p be the load causing plastic hinge at the fixed support. After the formation of plastic hinge, the beam behaves as a simply supported beam for the load q_u-q_p. The plastic rotation at fixed end of the beam can be calculated as the end rotation caused by the load q_u-q_p acting over a simply supported beam, as shown in Fig. 3.7b. The required plastic rotation is thus given as:

69

$$\theta_{preqd} = \frac{(q_u - q_p)L^3}{24EI}$$ [3.14]

where EI is the flexural stiffness of reinforced concrete section. It is appropriate to use EI of a fully cracked section for getting conservative estimate of required plastic rotation. Substituting $q_u = 8M_e/L^2$, and $q_p = 8[1-(\beta/100)]M_e/L^2$ in Eq. 3.14 to get:

$$\theta_{preqd} = \frac{\beta}{100} \frac{M_e L}{3EI}$$ [3.15]

where M_e is the elastic moment corresponding to ultimate load q_u. Thus with the conservative simplifying assumptions noted, Eq. 3.15 can be used in lieu of hinge-moment analysis. Substituting Eq. 3.15 into Eq. 3.8 gives the expression for allowable c/d in terms of the required moment redistribution.

$$\frac{c}{d}(max) = \frac{\varepsilon_{cu}}{\frac{\beta}{100} \frac{M_e}{3EI} \frac{L/d}{K_p/d} + \frac{f_y/E_s}{1-(c_y/d)}}$$ [3.16]

Equation 3.16 can be used to establish the limiting bounds on c/d and β. The procedure is described as follows.

1. For a given beam with a given amount of reinforcement, A_s, at the support, find the relative depth of neutral axis at ultimate.

$$\frac{c}{d} = \frac{A_s f_y}{bd\alpha_1\beta_1 f_c'}$$ [3.17]

where α_1 is the ratio of average stress in the rectangular compression block to the specified concrete strength = $0.85 - 0.0015 f_c'$ but not less than 0.67. β_1 is the ratio of

70

the depth of stress block, a, to the depth of neutral axis at ultimate, given as: β_1 =0.97-0.0025 f_c'.

2. Find the nominal moment of resistance, M_r.

$$M_r = A_s f_y \left(d - \frac{a}{2} \right) = A_s f_y d \left(1 - 0.5\beta_1 \frac{c}{d} \right)$$

[3.18]

3. Calculate relative depth of neutral axis at yield, c_y/d, using Eq. 3.5.

4. Calculate cracked flexural stiffness EI

$$EI = E_c \frac{1}{3} bc_y^3 + E_c nA_s \left(1 - \frac{c_y}{d} \right)^2$$

[3.19]

5. Assume a value of β.

6. Calculate elastic bending moment, M_e, that is consistent with the section provided (M_r) and assumed β.

$$M_e = \frac{M_u}{1 - \dfrac{\beta}{100}}$$

[3.20]

Where M_u is the moment at ultimate load q_u. Setting $M_u = M_r$, Eq. 3.20 can be rewritten as:

$$M_e = \frac{M_r}{1 - \dfrac{\beta}{100}}$$

[3.21]

71

7. Calculate $(c/d)_{max}$ from Eq. 3.16.

8. Compare c/d and $(c/d)_{max}$ from step 1 and step 7. If the two agree then the assumed value of β in step 5 was the correct limiting value, if not, iterate by assuming a new value of β until the two values of c/d converge. The resulting value of β is the maximum allowable moment redistribution for given c/d ratio in step 1.

3.7.1 Comparison with code limits for c/d and β

Figure 3.8 shows the β vs c/d curves generated for a range of beam slenderness ratios (L/d =6, 12, 21), using Eq. 3.16 and the procedure described in previous section. The beam cross-section and material properties are the same as those used in the previous example (Fig. 3.6). The plot shows that for a given value of c/d the allowable moment redistribution decreases with increasing values of beam slenderness. The code equation (Eq. 3.2) for β is also plotted in Fig. 3.8. The comparison shows that the code c/d limit is very conservative, especially for non slender beams. The plot also shows that the relationship between β and c/d is not unique as implied by the code. For the same c/d ratio, the value of β varies with the beam slenderness.

Equation 3.16 is fundamentally more correct than the code equation for moment redistribution because it takes into account the effects of beam slenderness in addition to the section properties, and material properties. It should, however, be noted here that the equation still does not account for the presence of shear cracking, tension stiffening, confinement and other factors of practical significance.

3.8 Summary and Conclusions

Code c/d and β limits are examined to assess the need for a more rational ductility model. Moment redistribution can be used as a tool to reduce the design moment envelope of continuous reinforced concrete beams. CSA A23.3-94 assumes a linear relationship between c/d and β (β=30-50c/d) and limits the allowable moment redistribution to 20%.

An expression for c/d limit is developed in terms of required plastic rotation at critical sections. The required plastic rotations in turn are determined using moment redistribution analysis with assumed values of β at critical sections. From the required plastic rotations the corresponding c/d limits are computed at each critical section. The c/d limits obtained are compared with the code c/d limits. Code limits are found to be very conservative. In theory, for 20% moment redistribution the allowable c/d limit can be higher than 0.5 while the code limit is only 0.14. Also, the relationship between c/d and β is not unique as implied by the code. The analysis showed that the c/d limit can vary from one critical section to the other, for the same value of β. This is because the plastic rotation demand at each of these sections is different due to structure geometry and other factors not recognized by the code. There is no unique relationship between β and c/d as implied by the code.

While moment redistribution analysis provides complete solution, using the entire structure and loading, a conservative estimate of c/d and β limit can be obtained by using a single span indeterminate beam model. An expression for the allowable c/d is developed using this model. The expression takes into account: the elastic moment at critical section; beam slenderness; plastic hinge length; section properties and material properties in addition to β. The code equation and the derived equation for allowable moment redistribution were plotted on the same graph (Fig. 3.8) for comparison purposes. The comparison shows that the code c/d limit is very conservative, especially for non-slender beams. The plot also shows that there is no unique relationship between β and c/d as implied by the code. For the same c/d ratio, the value of β varies with the beam slenderness.

While the equations developed in this chapter for permissible moment redistribution are fundamentally more correct than the code equation, they still do not account for the presence of shear cracking, tension stiffening, confinement and other factors of practical significance.

73

The conservative nature of code and its inability to account for different parameters affecting plastic rotation capacity and allowable moment redistribution points to the need for a comprehensive analytical model for computing permissible limits of θ_p and β.
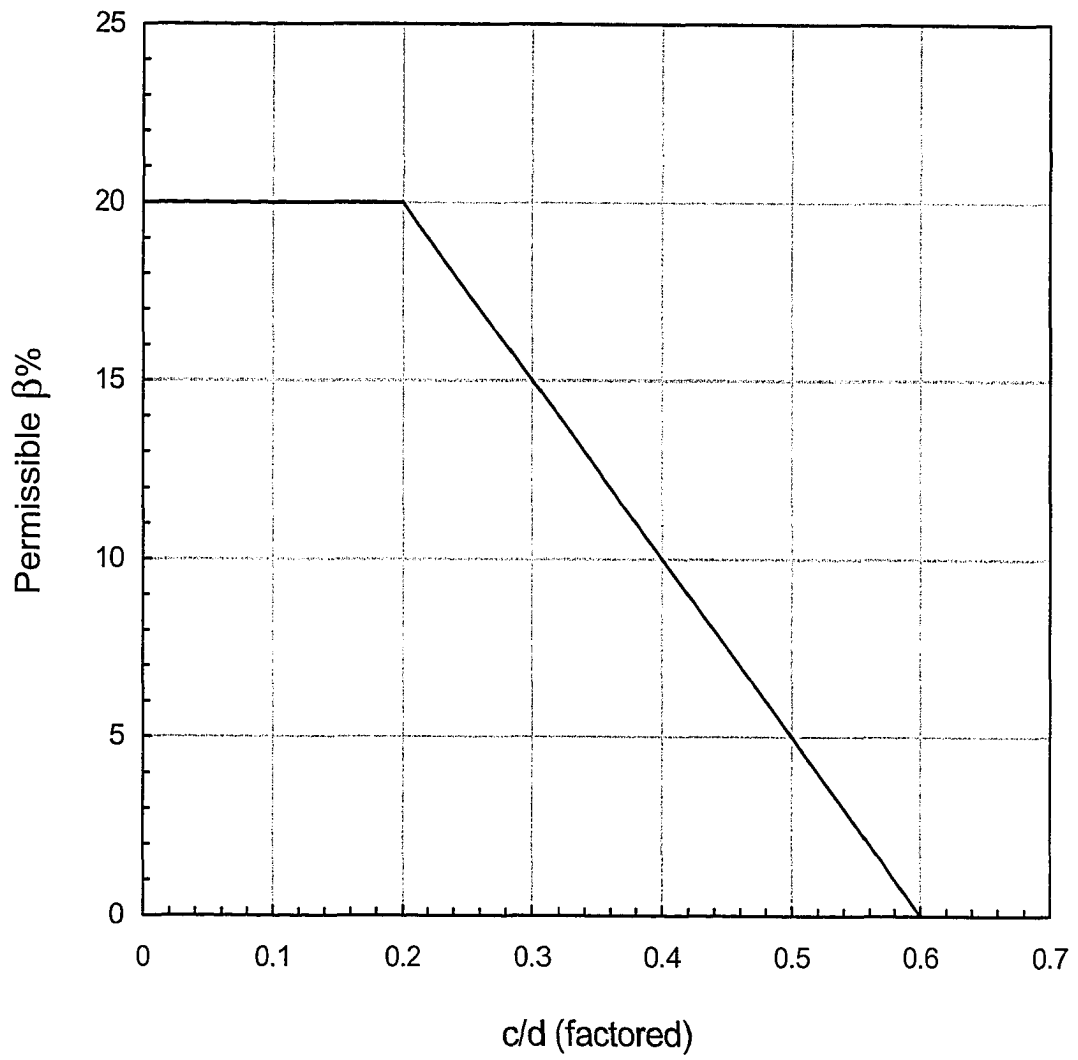
Figure 3.1 Moment redistribution in CSA A23.3-94

75
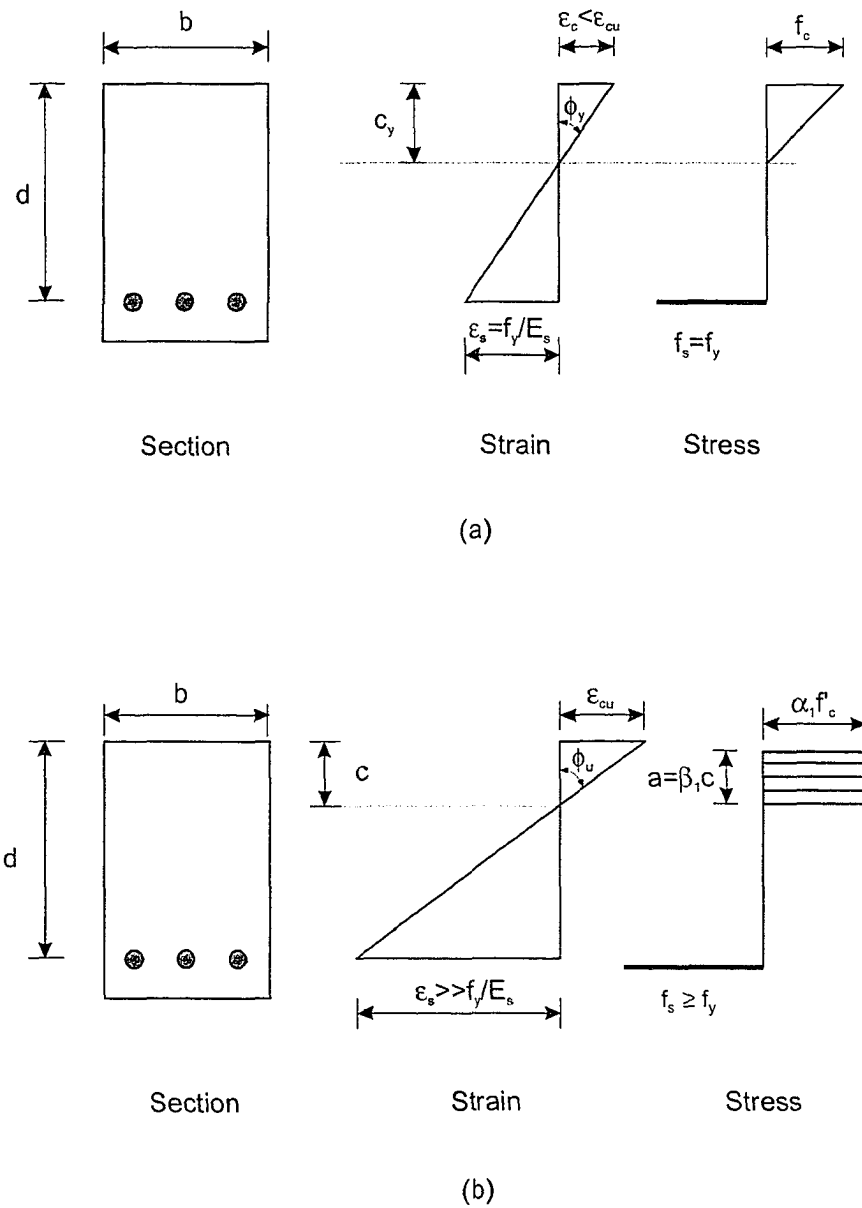
Figure 3.2 Stress and strain distribution in flexure: (a) at first yield; and (b) at ultimate

76
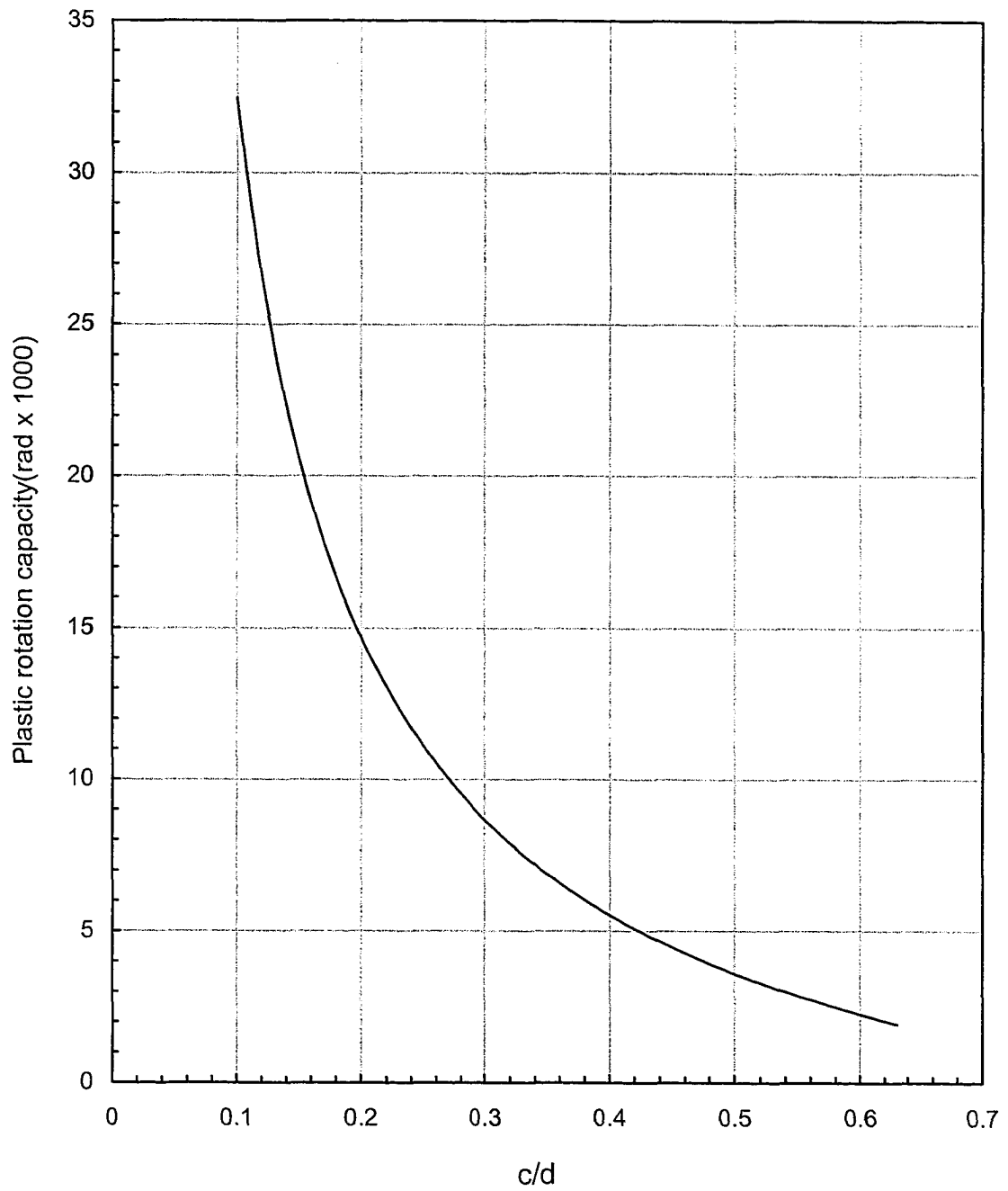
Figure 3.3 Plastic rotation capacity for given c/d based on Eq. 3.8

77

elastic moment envelope

reduced moment envelope
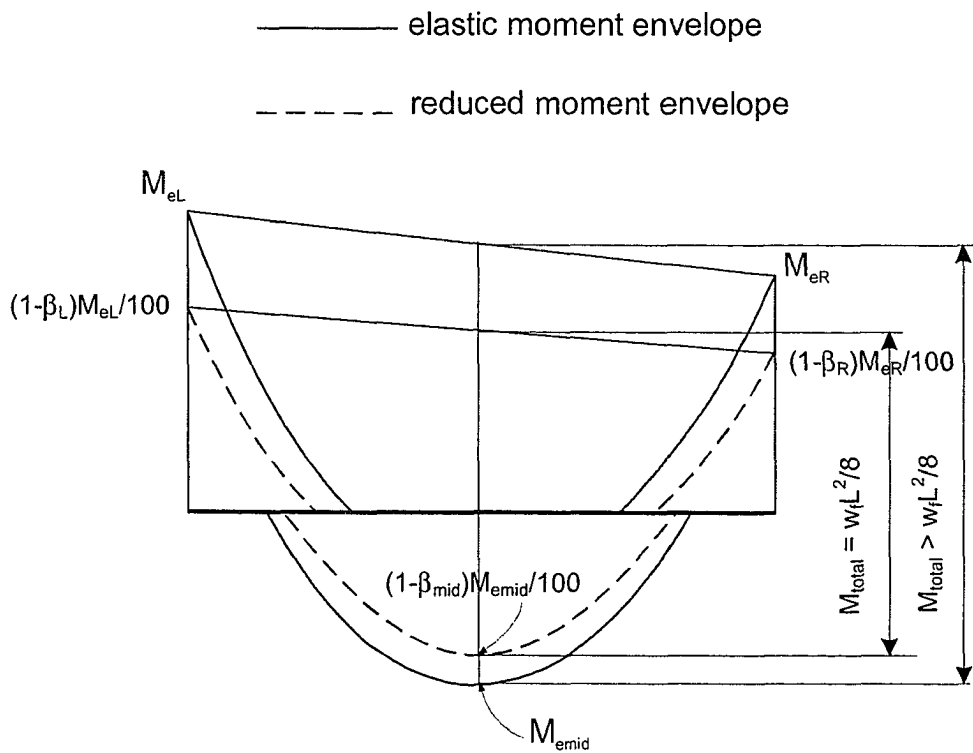
Figure 3.4 Possible moment redistribution, considering equilibrium requirement

78
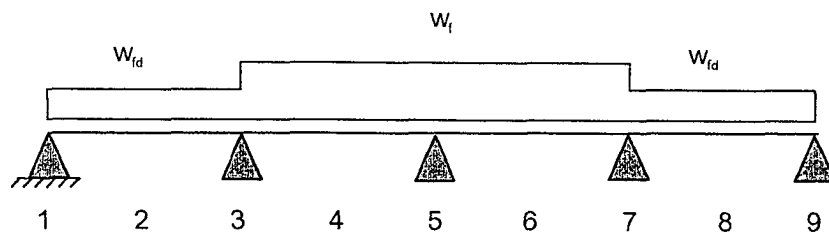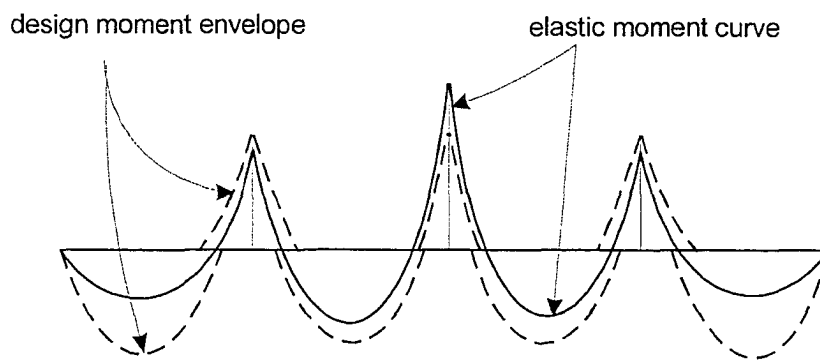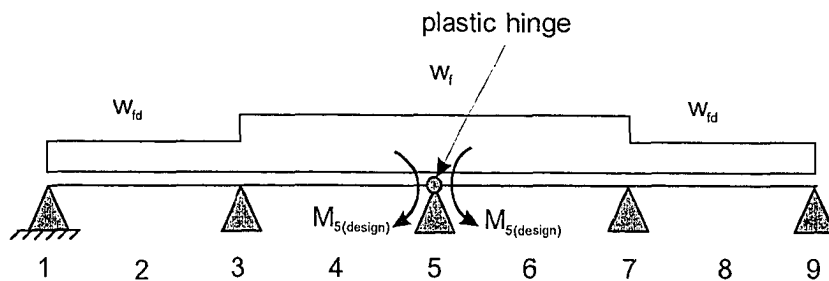
Figure 3.5 Hinge-moment analysis: (a) loading; (b) comparison of elastic moments with design moment envelope; and (c) modified beam with modified loading

79

maximum moment section numbers

1 2 (3) 4 5 6 7 8 9

8.0   8.0   8.0   8.0
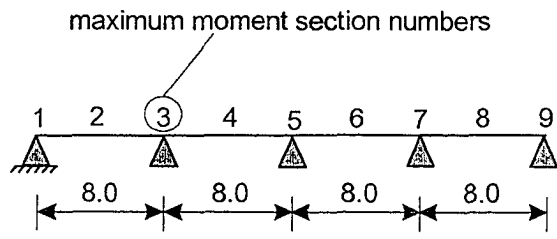
(a)
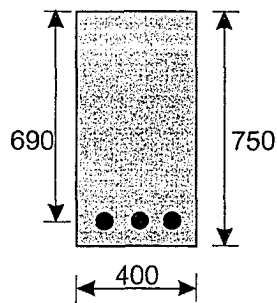
Material properties
f'_c =25 MPa
f_y =400 MPa

Loading
service dead load = 25 kN/m
service live load   = 25 kN/m
100% pattern live loading

690   750

400

(b)

Figure 3.6 Example beam: (a) beam geometry and location of critical sections; and (b) beam cross-section, material properties and loading

80
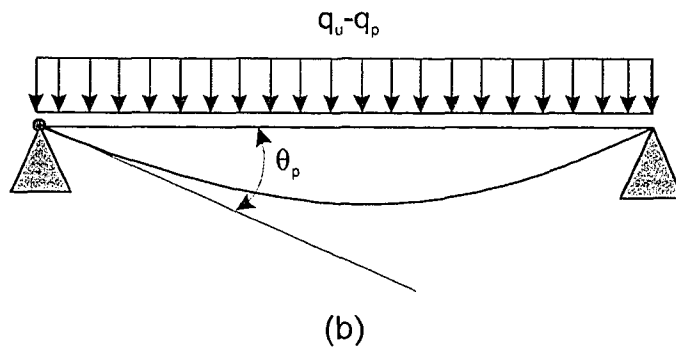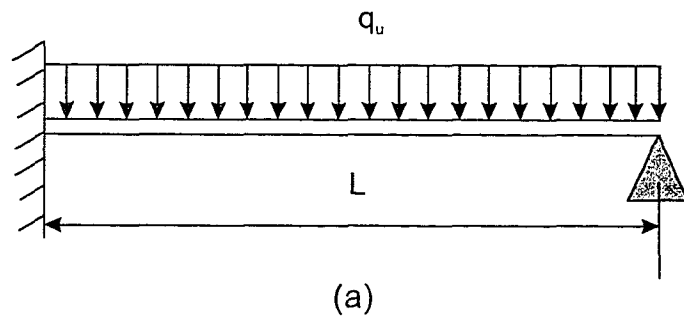
Figure 3.7 Computation of θ_p at support for fixed-hinge beam: (a) beam and loading; and (b) statical system and loading for computing required plastic rotation
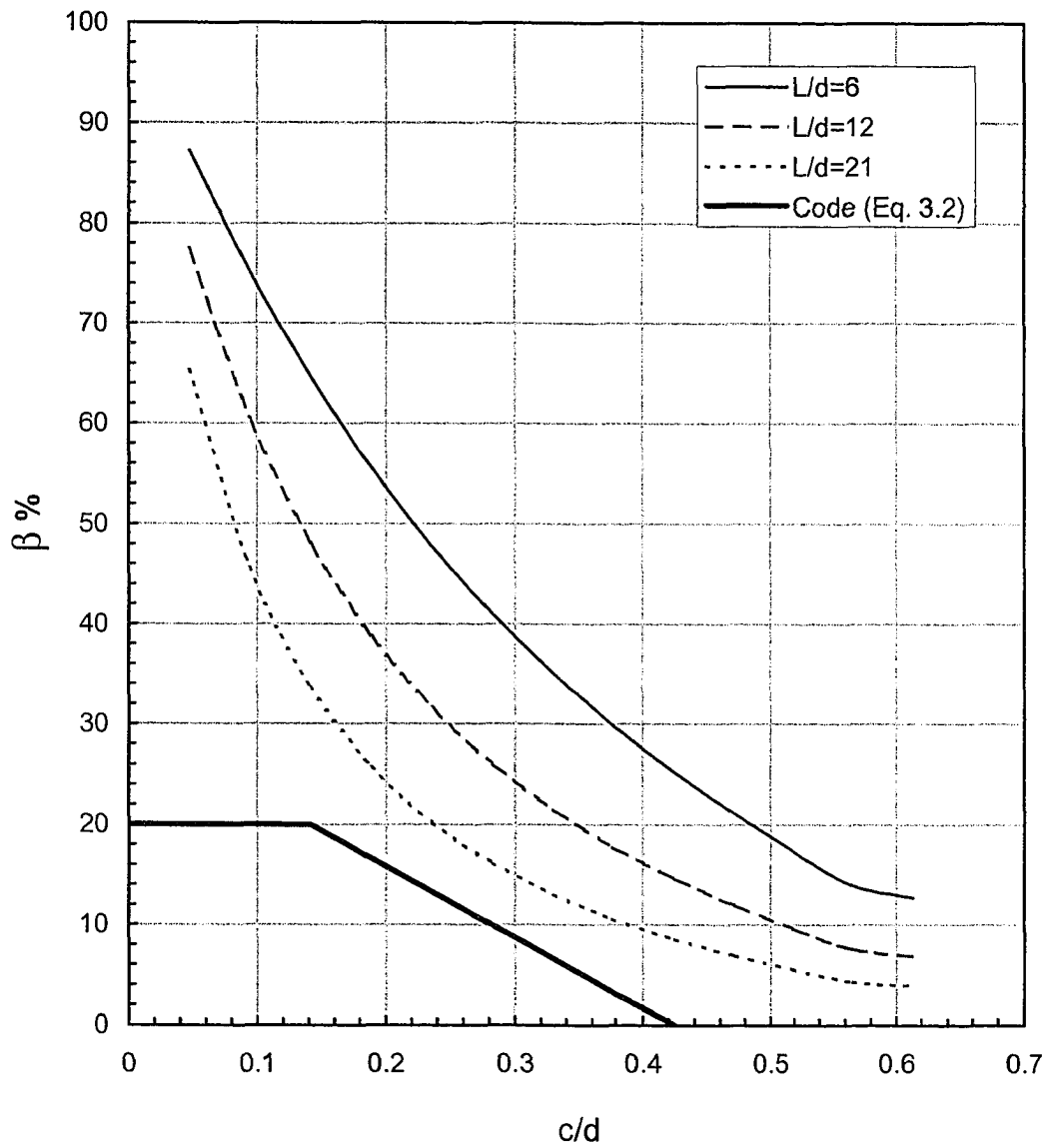
Figure 3.8 Moment redistribution, code vs theory

82

4. ANALYTICAL MODEL[*]

4.1 Introduction

This chapter deals with the development of an analytical model for computing plastic rotation capacity, θ_p, and allowable moment redistribution, β, in reinforced concrete structures. CSA A23.3-94 provisions for moment redistribution were assessed in the previous chapter and were found to be conservative. The model developed in this chapter eliminates much of the unnecessary conservatism of the code.

The possible distribution of design bending moments in indeterminate concrete structures depends upon the amount of moment redistribution that can occur at critical sections, which in turn depends upon the ductility of the section. For a given amount of moment redistribution to occur at a critical section, the required plastic rotation at a section must not exceed the available plastic rotation at that section. Thus, to establish a limit on permissible moment redistribution an estimate of plastic rotation capacity is required.

To understand the concept of ductility and its influence on moment redistribution, consider a two-span reinforced concrete beam subjected to a uniformly distributed load as shown in Fig. 4.1a. A plastic hinge forms at the critical section, at a load q_y, when the tension steel stress at that section reaches the yield value. Assuming the first plastic hinge to form is at the interior support, the idealized beam thereafter is shown in Fig. 4.1b. As the load on the beam increases further, the steel undergoes yielding thereby causing inelastic rotation at the interior support. The moment at the support no longer increases elastically with the applied load. The inelastic rotation causes much of the post yield elastic moment at the center support to be redistributed to the adjacent spans. The amount of moment that can be redistributed depends upon the stiffness of the plastic hinge and the amount of inelastic rotation it can accommodate. The ultimate rotation capacity and the moment redistribution capacity at the support are reached when either the compression concrete crushes or the tension steel ruptures at an ultimate load of q_u. The

---

[*] Essentials of this chapter appear as a paper in the Canadian Journal of Civil Engineering, Vol 27, no. 6, December 2000

elastic moment distribution at yield and ultimate and the inelastic moment distribution at ultimate are shown in Fig. 4.1c. The deformations at yield and ultimate are shown in Fig. 4.1d. The plastic rotation capacity θ_p is defined as the difference of the ultimate rotation and the yield rotation occurring over a length, referred to as plastic hinge length, in which the stress in tension steel is greater than or equal to the yield value. The allowable moment redistribution β is defined as:

$$\beta = \frac{M_e - M_u}{M_e} \times 100\% \qquad [4.1]$$

Where M_e is the elastic moment at ultimate and M_u is the nominal moment of resistance. The code (CSA A23.3-94) considers β to be the function of relative depth of compression zone at failure (c/d) or the reinforcement index (ω) only. The literature review and subsequent assessment in Chapter 3 reveals that θ_p and β depends upon a number of other parameters. Evaluation of θ_p and β is a complex issue because of the interaction of these parameters. Due to the wide range of these parameters, experimental results show large variation of the measured values of plastic rotation capacity. An analytical model is an attractive alternative to experimental investigations in studying member behaviour and allows one to study influences of various parameters in an independent and systematic manner.

In this chapter an analytical model is developed to predict the plastic rotation capacity and moment redistribution limit of reinforced concrete sections. An effort is made to include the major parameters influencing plastic rotation capacity and moment redistribution in reinforced concrete structures.

4.2 Parameters Affecting Plastic Rotation Capacity

The literature review revealed that the following parameters govern the non-linear behaviour of a reinforced concrete member.

(1) *Material parameters:* Stress-strain laws for concrete and steel, concrete-steel bond-slip law.

(2) *Geometric parameters:* Shape of the section, reinforcement index (ω), stirrup percentage.

(3) *Structural parameters:* Structural layout (equal/ unequal span lengths), members' slenderness ratios (L/d), supports conditions.

(4) *Loading parameters:* Load intensity and distribution.

(5) *Type of plastic hinge:* Flexural crack hinge, shear crack hinge. A flexural crack hinge is one that contains flexural cracks, while a shear crack hinge is one that contains inclined shear cracks in addition to the flexural cracks.

The effects of all the above parameters need to be considered in order to develop a realistic model for computing plastic rotation capacity and allowable moment redistribution in reinforced concrete structures.

4.3 Types of Ductility Models

There are two fundamental types of ductility models for the computation of plastic rotation capacity, the constant curvature model and the variable curvature model.

4.3.1 Constant curvature model

The classical models for computation of θ_p assume constant plastic curvature over an equivalent plastic hinge length as shown in Fig. 4.2. Typical expression for computing the plastic rotation capacity is of the form:

$$\theta_p = (\phi_u - \phi_y)L_p \tag{4.2}$$

85

where ϕ_y and ϕ_u are the curvatures at yield and ultimate respectively, at the critical section at which θ_p is required, and L_p is the effective hinge length.

The ultimate curvature and the yield curvature in the above equation are obtained from strain compatibility and equilibrium analysis at the critical section, while L_p is determined from empirical expressions. Examples of such models are those proposed by Baker (1964), Mattock (1964), Sawyer (1964), Corley (1966), and Mattock (1967). Details of such models can be found in the literature review.

4.3.2 Variable curvature model

In variable curvature models, the deformations of reinforced concrete flexural members are calculated from the rotations of elements between cracks rather than from the curvature at the section of maximum moment. Examples of such models are those proposed by Bachmann (1970), Eifler (1969), and Langer (1987). In these models, the member is divided into a series of cracked elements as shown in Fig. 4.3a. Consider a cracked element from the member subjected to a moment and in-plane load, as shown in Fig. 4.4. At the location of a crack, the tensile stress is resisted completely by the reinforcement. Between cracks, bond between the concrete and the reinforcing bars restrains the elongation of the steel and thus a part of the tensile stress in the reinforcement is transmitted to the concrete situated between the cracks. Thus, the stress and strain in a reinforcing bar varies from a maximum value at the cracks to a minimum value between the cracks. This phenomenon is called tension stiffening as it results in an apparent increase in the stiffness of the cracked element. Tension stiffening results in a decrease in the overall deformations of the member. (CEB Manual 1985)

For given steel strains at the cracks, using a suitable steel-concrete bond shear relationship, one can estimate the steel strain distribution between cracks. Integrating steel strain over the cracked element gives the crack width and dividing crack width by the depth of the crack gives the rotation of individual cracked element. The crack widths and the rotations for each individual cracked element are calculated from which the total

rotation θ between the ends of a length of member consisting of n elements is calculated as shown in Fig. 4.3b:

$$\theta = \sum_{i=1}^{n} \theta_i = \sum_{i=1}^{n} \frac{w_i}{d - k_i d}$$

[4.3]

where d is the effective depth to the tension steel, w_i is the elongation of the steel between the ends of elements i, and $k_i d$ is the neutral axis depth at the crack in element i.

The variable curvature methods are more rational and transparent than the constant curvature methods in depicting the deformations of reinforced concrete members. They allow the incorporation of various factors that affect the ductility of reinforced concrete members.

4.4 Analytical Model

The proposed analytical model is based on the variable curvature model. It is understood that the elongation of tension steel is the primary source of plastic rotation; therefore one, needs a model that accurately predicts the elongation of tension steel. The elongation of tension steel depends upon the steel strain distribution between the cracks. This in turn depends upon the magnitude of tensile forces at the cracks, stress-strain law adopted for the steel and the concrete, and the bond-slip law.

The material constitutive relationships and the bond model adopted for the development of the analytical model are described in the following sections. Expressions are derived to determine the distribution of tension steel force at cracks along the member and the distribution of steel strain between the cracks.

The model is general and applies to any loading and continuity conditions. However, for the purpose of this study, it is developed for the interior support of a two-span continuous beam subjected to uniformly distributed load. The principal ductility requirement for beams exists at the support regions of continuous beams, and the condition is most severe

87

when tangents at the ends must retain a slope of zero (Furlong 1979). This would typically be the case for the interior support of a two-span continuous beam with equal spans. Occasionally, the first hinge may form at or near mid-span. Such cases do not govern as the ductility requirements for positive moment or span regions are not as critical as those for the support regions (Cohn 1965).

4.4.1 Constitutive relationship for concrete

The main factors affecting concrete behaviour are; concrete strength, lateral reinforcement (confinement), strain gradient, size of specimen, and type of loading. Lateral confinement of concrete may significantly improve the characteristics of stress-strain curve, resulting in an increase in concrete strength and ultimate strain. The slope of the falling branch of stress-strain curve for confined concrete is also quite moderate as compared to that for unconfined concrete. Strain gradient (such as in flexure) also contributes to the confinement of concrete (Scott, Park and Priestley 1982).

Modified Park et al. model (1982) for confined concrete, shown in Fig. 4.5, is used to incorporate the beneficial effects of confinement. While the model is developed primarily for columns with concentric and eccentric loads, it's use for flexural members is conservative (Scott et al.1982). For the purpose of this study, the ultimate concrete strain is limited to 0.005. The curve consists of two parts. A second-degree parabola represents the ascending portion of the curve and a linear falling branch represents the descending portion of the curve. The maximum stress reached at point B is assumed to be $K f_c'$ and the corresponding strain is $\varepsilon_o = 0.002K$. The factor K is greater than one and takes into account the effect of confinement on concrete strength. K depends upon the volumetric ratio of tie steel to concrete core, yield strength of ties, and cylinder strength of concrete. The first part of the curve (half parabola AB) has the same initial slope as the unconfined concrete. The descending branch extends to $0.2 K f_c'$. The factor K is given as:

$$K = 1 + \frac{\rho_v f_{yh}}{f_c'}$$

[4.4]

88

where ρ_v = ratio of volume of rectangular steel hoops to volume of concrete core measured to outside of the peripheral hoop; f_{yh} = yield strength of steel hoops; and $f_c^{'}$ = concrete compressive cylinder strength. Equation 4.4 assumes that rectangular hoops cause an increase in strength of the concrete of $\rho_v f_{yh}$. The modified Kent and Park stress-strain curve is defined by the following two equations, with reference to Fig. 4.5.

Region AB ($\varepsilon_c < 0.002K$)

$$f_c = Kf_c^{'}\left[\frac{2\varepsilon_c}{0.002K}-\left(\frac{\varepsilon_c}{0.002K}\right)^2\right]$$ [4.5]

Region BC ($\varepsilon_c > 0.002K$)

$$f_c = Kf_c^{'}[1-Z_m(\varepsilon_c-0.002K)]\geq 0.2Kf_c^{'}$$ [4.6]

where Z_m defines the slope of the falling branch, and is given as:

$$Z_m = \frac{0.5}{\varepsilon_{k50u}+\varepsilon_{k50h}-0.002K}$$ [4.7]

in which,

$$\varepsilon_{k50u} = \frac{3+0.29f_c^{'}}{145f_c^{'}-1000}$$ [4.8]

and

$$\varepsilon_{k50h} = \frac{3}{4}\rho_v\sqrt{\frac{b_o}{s}}$$ [4.9]

89

where f_c' is in MPa; K is as given in Eq. 4.4; b_o = width of the concrete core measured to outside of the peripheral ties; and s = centre to centre spacing of the hoops.

The slope of the falling branch in Eq. 4.7 is specified by the strain when the stress has fallen to $0.5 f_c'$. Equation 4.8 for ε_{k50u}, takes into account the effect of concrete strength on the slope of the falling branch of unconfined concrete, high-strength concrete being more brittle than low-strength concrete. Equation 4.9 for ε_{k50h} gives the additional ductility due to rectangular hoops.

Based on test results (Mattock 1964, Park et al. 1982), the extreme fibre concrete strain limit is taken as 0.005 rather than 0.0035 as used in CSA A23.3-94. While the 0.0035 code limit is adequate for computing moment resistance, it is too conservative for computing hinge rotation capacity. In Mattock's tests the experimental concrete strains at ultimate were found to be in the vicinity of 0.008 with few as high as 0.02. In Park et al. (1982) tests, conducted on a series of axially loaded columns, the maximum concrete strains recorded were between 0.016 and 0.026 while the load deformation curve was still rising. Higher values of experimental peak strains would have been obtained had the tests continued further. The minimum concrete strain at first visible crushing of concrete cover was 0.005. In flexural members the strain gradient and the shear reinforcement, if present, increase the maximum concrete strain at ultimate moment resistance. On the basis of the experimental evidence, the assumption of an ultimate concrete strain of 0.005 would be conservative for typical rectangular beams. However, it must be noted that for some specific cases, such as box girders, where the stress state in compression flange approaches uniform compression, and beams with a constant moment region, the limit of 0.005 might be unconservative. For the later cases, the designer should use a value approaching that for the ultimate concrete strain in uniaxial compression.

4.4.2 Stress-strain relationship for reinforcing steel

In plastic hinge regions the steel strains are usually high and the steel may strain harden. Strain hardening causes steel force to increase beyond yield value resulting in an increase in the depth of neutral axis. Neglecting strain hardening can lead to unconservative estimates of plastic rotation capacity and allowable moment redistribution. A bilinear stress-strain diagram, shown in Fig. 4.6 is adopted to include the effects of strain hardening. There are two regions, which may be represented by the following equations:

Region AB: $\varepsilon_s \leq \varepsilon_y$

$$f_s = \varepsilon_s E_s \qquad\qquad [4.10]$$

Region BC: $\varepsilon_y \leq \varepsilon_s \leq \varepsilon_{su}$

$$f_s = f_y + (\varepsilon_s - \varepsilon_y)E_{sh} \qquad\qquad [4.11]$$

where, E_{sh} is the modulus of strain hardening, given as:

$$E_{sh} = \frac{f_{su} - f_y}{\varepsilon_{su} - \varepsilon_y} \qquad\qquad [4.12]$$

The notations used in Eqs. 4.10 to 4.12 are illustrated in Fig. 4.6.

4.4.3 Moment-Rotation relationship

Classical theories for limit analysis assume frictionless hinges at the sections where the steel has yielded. In general, there is an increase in the resisting moment past the yield value due to strain hardening of steel and shift of neutral axis. A more realistic behaviour of plastic hinge is modelled by a linear hardening rotational spring of stiffness k_s, as shown in Fig. 4.7. θ_u is the ultimate rotation corresponding to ultimate moment M_u and q_y

is the yield rotation corresponding to yield moment M_y. The relationship between moment and rotation after yielding is given as:

$$M = M_y + k_s(\theta - \theta_y)$$

[4.13]

4.4.4 Strain compatibility analysis of reinforced concrete sections

The strain distribution, location of neutral axis, and curvature of a reinforced concrete section for given external loading can be determined from strain compatibility and equilibrium of forces. While strain compatibility analysis is textbook material, it is presented here to facilitate further discussion and development in this thesis. The following assumptions of flexural theory are used:

(1) Plane sections before bending remain plane after bending.

(2) Stress-strain curves for concrete and steel are known.

Figure 4.8 shows a reinforced concrete section with axial load and flexure. For a given concrete strain in the extreme compression fibre ε_c and neutral axis depth c, the steel strains $\varepsilon_{s1}, \varepsilon_{s2}, \varepsilon_{s3}$....., can be determined from similar triangles of the strain diagram. For example for bar i at depth d_i:

$$\varepsilon_{si} = \varepsilon_c \frac{c - d_i}{c}$$

[4.14]

The stresses f_{s1}, f_{s2}, f_{s3},....., corresponding to strains $\varepsilon_{s1}\varepsilon_{s2}\varepsilon_{s3}$....., may then be found from the stress-strain curve for the steel. Steel forces T_1, T_2, T_3,...., T_n may be found from the steel stresses and the area of steel. For example for bar i, the force equation is:

$$T_i = f_{si}A_{si}$$

[4.15]

92

The distribution of concrete stress over the compressed part of the section of Fig. 4.8 may be found from the strain diagram and the stress-strain curve for the concrete. For any given concrete strain ε_c in the extreme compression fibre, the concrete compressive Force C_c is given as:

$$C_c = \int_0^c bf_c dy \tag{4.16}$$

where b is the width of the compression zone and the vertical distance dy is measured from the neutral axis, and upward positive. The compressive stress f_c can be obtained from concrete stress-strain curve, using Eqs. 4.5 and 4.6. The force equilibrium equation for the axial force and moment can be written as:

$$\int_0^c bf_c dy + \sum_{i=1}^n f_{si} A_{si} = P \tag{4.17}$$

$$\int_0^c bf_c (\frac{h}{2} - c + y) \, dy + \sum_{i=1}^n f_{si} A_{si} (\frac{h}{2} - d_i) = M \tag{4.18}$$

In the above expressions, the sign convention considers compression as positive and tension as negative.

The curvature is given from the strain diagram as:

$$\phi = \frac{\varepsilon_c}{c} = \frac{\varepsilon_s}{d - c} \tag{4.19}$$

For a given value of ε_c or ε_s the neutral axis depth is found through iteration by adjusting c until the internal force resultants P and M calculated using Eq. 4.17 and 4.18 match the desired axial force and moment. The internal forces and neutral axis depth so found are used to determine the moment M and curvature ϕ from Eq. 4.18 and 4.19 respectively. By

93

carrying out the calculations for a range of ε_c or ε_s values, the moment-curvature curve can be plotted. A spreadsheet formulation has been done to carry out the section analysis, using the procedure described above.

For the purpose of evaluating ductility we are often interested in the curvature at yield and the curvature at ultimate only. The stress-strain curve for concrete is approximately linear up to $0.7 f_c'$. The concrete stress usually does not exceed this value when the steel reaches yield strength. Hence, the neutral axis depth and the curvature may be computed by assuming the linear stress distribution, as shown in Fig. 4.9. For a doubly reinforced concrete section, the relative neutral axis depth c/d can be found from transformed section analysis as:

$$\frac{c}{d} = \left[(\rho + \rho')^2 n^2 + 2 \left(\rho + \frac{\rho' d'}{d} \right) n \right]^{1/2} - (\rho + \rho') n \qquad [4.20]$$

Moment M_y at first yield is given as:

$$M_y = A_s f_y j d \qquad [4.21]$$

and the curvature ϕ_y at yield is given as:

$$\phi_y = \frac{f_y / E_s}{d - c_y} \qquad [4.22]$$

where,

$\rho \quad = \quad A_s/bd$

$\rho' \quad = \quad A_s'/bd$

$A_s \quad = \quad$ area of tension steel

$A_s' \quad = \quad$ area of compression steel

$c_y \quad = \quad$ depth of neutral axis at yield

94

d   = effective depth of tension steel

d' = distance from the extreme compression fibre to the centroid of compression steel

jd = distance from the centroid of compressive forces in steel and concrete to the centroid of tension steel

n   = E_s/E_c.

4.4.5 Bond-slip constitutive relationship

The tension chord model of Marti et al. (1998) is used to determine the stress and strain distribution within the cracked elements. Acknowledging that the exact distribution of stresses in concrete and steel is not of primary interest as long as the resulting steel stresses and overall member strains reflect the governing influence and match the experimental data, the authors use a rigid-perfectly plastic bond-slip relationship with a stepped descending branch as shown in Fig. 4.10. When the steel stress is less than the yield stress, the bond stress is given as:

$$\tau_{b1} = 2f_{ct} = 0.6f_c^{'2/3} \qquad [4.23]$$

when the steel stress is greater than the yield stress, the bond stress is given as:

$$\tau_{b2} = f_{ct} = 0.3f_c^{'2/3} \qquad [4.24]$$

where f_{ct} is the tensile strength of concrete and $f_c^{'}$ is the compressive strength of concrete. The rate of change of steel stress along the bar can be determined by considering the equilibrium of a small length of bar as shown in Fig. 4.11

$$\sigma_s A_s + \tau_b \pi d_b dx = (\sigma_s + d\sigma_s) A_s \qquad [4.25]$$

From which,

$$\frac{d\sigma_s}{dx} = \frac{4\tau_b}{d_b}$$ [4.26]

where σ_s is the stress in steel, A_s is the area of steel bar, d_b is the diameter of reinforcing bar, and $\tau_b = \tau_{b1}$ for pre-yield region and $\tau_b = \tau_{b2}$ for post-yield region.

4.4.6 Steel stress and strain distribution within cracked element

For a tension element loaded with force F_t at both ends, typical distributions of τ_b, σ_s and ε_s are given in Fig. 4.12. If the end forces are not equal, the stress and strain distributions become non-symmetric but can be readily obtained. There are four cases that need to be considered, as shown in Figs. 4.13 through 4.16. To determine the steel strain distribution between the cracks, distances x_{L1}, x_{L2}, x_{R1}, x_{R2}, and the magnitude of minimum stress within the cracked element must be known. These are determined below using the bond model and Eq. 4.26. Following notations are used:

x_{L1} = distance in which $\sigma_{smin} \le \sigma_s \le f_y$

x_{L2} = distance in which $f_y \le \sigma_s \le \sigma_{scrL}$

x_{R1} = distance in which $\sigma_{smin} \le \sigma_s \le f_y$

x_{R2} = distance in which $f_y \le \sigma_s \le \sigma_{scrR}$

σ_s = stress in steel

σ_{scrL} = steel stress at left face of the cracked element

σ_{scrR} = steel stress at right face of the cracked element

σ_{smin} = minimum steel stress within the cracked element

s_m = average crack spacing

d_b = diameter of steel bar

Case 1: $\sigma_{scrL} > f_y$; $\sigma_{scrR} > f_y$; $\sigma_{smin} > f_y$

From Fig. 4.13,

$$x_{L1} = x_{R1} = 0$$ [4.27]

96

Applying the bond model and Eq. 4.26 to left hand side crack gives,

$$\sigma_{s\,min} = \sigma_{scrL} - \frac{4\tau_{b2}}{d_b} x_{L2}$$
[4.28]

Similarly applying bond model to right hand side crack gives,

$$\sigma_{s\,min} = \sigma_{scrR} - \frac{4\tau_{b2}}{d_b} x_{R2}$$
[4.29]

and from Fig. 4.13a

$$x_{R2} = s_m - x_{L2}$$
[4.30]

Equating Eqs. 4.28 and 4.29 to get,

$$x_{L2} = \frac{(\sigma_{scrL} - \sigma_{scrR})d_b}{4\tau_{b2}} + x_{R2}$$
[4.31]

and substituting x_{R2} from Eq. 4.30 to get,

$$x_{L2} = \frac{(\sigma_{scrL} - \sigma_{scrR})d_b + 4\tau_{b2}s_m}{8\tau_{b2}}$$
[4.32]

Case 2: $\sigma_{scrL} > f_y$; $\sigma_{scrR} > f_y$; $\sigma_{smin} < f_y$

Applying the bond model and Eq. 4.26, as shown in Fig. 4.14, gives:

$$\sigma_{s(min)} = f_y - \frac{4\tau_{b1}}{d_b} x_{L1}$$
[4.33]

97

$$\sigma_{s(min)} = f_y - \frac{4\tau_{b1}}{d_b} x_{R1}$$

[4.34]

$$x_{L2} = \frac{(\sigma_{scrL} - f_y)d_b}{4\tau_{b2}}$$

[4.35]

$$x_{R2} = \frac{(\sigma_{scrR} - f_y)d_b}{4\tau_{b2}}$$

[4.36]

Equating Eq. 4.32 and 4.33 gives,

$$x_{R1} = x_{L1}$$

[4.37]

from which one can write,

$$x_{L1} = \frac{s_m - (x_{L2} + x_{R2})}{2}$$

[4.38]

Case 3: $\sigma_{scrL} > f_y$; $\sigma_{scrR} \le f_y$; $\sigma_{smin} < f_y$

Applying the bond model and Eq. 4.26, as shown in Fig. 4.15, gives:

$$\sigma_{s(min)} = \sigma_{scrR} - \frac{4\tau_{b1}}{d_b} x_{R1}$$

[4.39]

$\sigma_{s(min)}$ from the left hand side is the same as that given by Eq. 4.33 and x_{L2} is the same as that given by Eq. 4.35. From Fig. 4.15a one gets,

$$x_{R2} = 0$$

[4.40]

$$x_{R1} = s_m - (x_{L1} + x_{L2})$$

[4.41]

98

Equating Eq. 4.33 and 4.39 gives,

$$x_{L1} = \frac{\left(f_y - \sigma_{scrR}\right)d_b}{4\tau_{b1}} + x_{R1}$$ [4.42]

and substituting x_{R1} from Eq. 4.41 gives,

$$x_{L1} = \frac{\left(f_y - \sigma_{scrR}\right)d_b + 4\tau_{b1}\left(s_m - x_{L2}\right)}{8\tau_{b1}}$$ [4.43]

Case 4: $\sigma_{scrL} < f_y$; $\sigma_{scrR} < f_y$; $\sigma_{smin} < f_y$

From Fig. 4.16:

$$x_{L2} = x_{R2} = 0$$ [4.44]

Applying the bond model and Eq. 4.26 gives:

$$\sigma_{s(min)} = \sigma_{scrL} - \frac{4\tau_{b1}}{d_b}x_{L1}$$ [4.45]

$\sigma_{s(min)}$ from the right hand side is the same as that given by Eq. 4.39. From Fig. 4.16a one gets,

$$x_{R1} = s_m - x_{L1}$$ [4.46]

Equating Eq. 4.39 and 4.45 to get,

$$x_{L1} = \frac{\left(\sigma_{scrL} - \sigma_{scrR}\right)d_b}{4\tau_{b1}} + x_{R1}$$ [4.47]

99

and substituting x_{R1} from Eq. 4.46 to get,

$$x_{L1} = \frac{\left(\sigma_{scrL} - \sigma_{scrR}\right)d_b + 4\tau_{bl}s_m}{8\tau_{bl}}$$ [4.48]

4.4.7 Determination of average steel strains within cracked elements

The average steel strain, ε_{sm}, within a cracked element is given as:

$$\varepsilon_{sm} = \frac{\int\limits_0^{S_m} \varepsilon_{sx} dx}{S_m}$$ [4.49]

The expressions for average steel strain for the four cases are derived below.

Case 1: $\sigma_{scrL} > f_y$; $\sigma_{scrR} > f_y$; $\sigma_{smin} > f_y$

From figure 4.13c,

$$\varepsilon_{sm} \times s_m = \left(\frac{\varepsilon_{scrL} + \varepsilon_{smin}}{2}\right)x_{L2} + \left(\frac{\varepsilon_{scrR} + \varepsilon_{smin}}{2}\right)x_{R2}$$ [4.50]

Expanding and solving for ε_{sm} gives:

$$\varepsilon_{sm} = \frac{16\tau_{br}\left(\varepsilon_y E_{sh}\delta\sigma_{scrL} - \tau_{br}\right) - \delta\sigma_{scr}^{\ 2}}{16\tau_{br}E_{sh}}$$ [4.51]

where,

$$\delta\sigma_{scrL} = \sigma_{scrL} - f_y$$ [4.52]

$$\delta\sigma_{scr} = \sigma_{scrL} - \sigma_{scrR}$$ [4.53]

100

$$\tau_{br} = \tau_{b2} \frac{S_m}{d_b}$$ [4.54]

E_{sh} is the strain hardening modulus of steel and ε_y, ε_{scrL}, ε_{scrR}, ε_{smin}, are the steel strains corresponding to steel stresses f_y, σ_{scrL}, σ_{scrR}, and σ_{smin} respectively.

Case 2: $\sigma_{scrL} > f_y$; $\sigma_{scrR} > f_y$; $\sigma_{smin} < f_y$

From Fig. 4.14c:

$$\varepsilon_{sm} \times S_m = \left(\frac{\varepsilon_{scrL} + \varepsilon_y}{2} \right) x_{L2} + \left(\frac{\varepsilon_{smin} + \varepsilon_y}{2} \right) x_{L1} +$$
$$\left(\frac{\varepsilon_{smin} + \varepsilon_y}{2} \right) x_{R1} + \left(\frac{\varepsilon_{scrR} + \varepsilon_y}{2} \right) x_{R2}$$ [4.55]

Expanding and solving for ε_{sm} gives:

$$\varepsilon_{sm} = \frac{\left[2\varepsilon_y E_{sh} \left(\delta\sigma_{scrL} + \delta\sigma_{scrR} \right) + \delta\sigma_{scrL}^2 + \delta\sigma_{scrR}^2 \right]}{8\tau_{br} E_{sh}} -$$
$$\frac{\left[\left(\delta\sigma_{scrav} - 2\tau_{br} \right) \right]^2}{2\tau_{br} E_s}$$ [4.56]

where,

$$\delta\sigma_{scrR} = \sigma_{scrR} - f_y$$ [4.57]

$$\delta\sigma_{scrav} = \sigma_{scrav} - f_y$$ [4.58]

$$\sigma_{scrav} = \frac{\sigma_{scrL} + \sigma_{scrR}}{2}$$ [4.59]

101

Case 3: $\sigma_{scrL} > f_y$; $\sigma_{scrR} \leq f_y$; $\sigma_{smin} < f_y$

From Fig. 4.15c:

$$\varepsilon_{sm} \times s_m = \left(\frac{\varepsilon_{scrL} + \varepsilon_y}{2}\right) x_{L2} + \left(\frac{\varepsilon_{smin} + \varepsilon_y}{2}\right) x_{L1} + \left(\frac{\varepsilon_{scrR} + \varepsilon_{smin}}{2}\right) x_{R1} \qquad [4.60]$$

Expanding and solving for ε_{sm} gives:

$$\varepsilon_{sm} = \frac{\left(2\varepsilon_y E_{sh} + \delta\sigma_{scrL}\right)\delta\sigma_{scrL}}{8\tau_{br} E_{sh}} +$$
$$\frac{\left(2\sigma_{scrL} + \delta\sigma_{scrR} - 8\tau_{br}\right)\left(8\tau_{br} - 2\delta\sigma_{scrL} - \delta\sigma_{scrR}\right)}{64\tau_{br} E_s} + \qquad [4.61]$$
$$\frac{\left(\sigma_{scrL} + f_y - 4\tau_{br}\right)\left(8\tau_{br} - 2\sigma_{scrL} + \sigma_{scrR} + f_y\right)}{32\tau_{br} E_s}$$

Case 4: $\sigma_{scrL} < f_y$; $\sigma_{scrR} < f_y$; $\sigma_{smin} < f_y$

From Fig. 4.16c:

$$\varepsilon_{sm} \times s_m = \left(\frac{\varepsilon_{scrL} + \varepsilon_{smin}}{2}\right) x_{L1} + \left(\frac{\varepsilon_{scrR} + \varepsilon_{smin}}{2}\right) x_{R1} \qquad [4.62]$$

Expanding and solving for ε_{sm} gives:

$$\varepsilon_{sm} = \frac{\delta\sigma_{scr}^2 + \sigma_{scrR}^2 - \sigma_{scrL}\sigma_{scrR} + 16\tau_{br}\sigma_{scrL}}{16\tau_{br} E_s} \qquad [4.63]$$

4.4.8 Computation of tension steel force

Depending upon the magnitude of the shear force in the critical moment region of the member, two significantly different types of hinges can be formed, a flexural hinge, and a

102

shear hinge. The flexural crack hinge occurs when the bending moment is predominant, while the shear crack hinge develops when in addition to a bending moment the shear force is sufficient to cause diagonal cracking. Figure 4.17 illustrates the two types of hinges.

In flexural crack hinges the plastic deformations concentrate in a single or very few cracks so that their rotation capacity remains relatively low. The shear crack hinges, on the other hand, exhibit a significantly increased rotation capacity due to flexure-shear cracks, provided that the member possesses a sufficient shear capacity to avoid shear failure. This improvement of the behaviour of the hinge is achieved by the shift of the tensile force along the bars as a result of the inclination of the cracks, enlarging the length of plastic hinge (Dilger 1966).

Since, the shear forces are usually high in the vicinity of plastic hinge at supports, it is assumed that inclined cracks are present in the vicinity of plastic hinge. This assumption may be verified at a later stage when computing the actual shear in concrete. Figure 4.18 illustrates the cracking pattern in the vicinity of a shear crack hinge. At the interior support of a beam the diagonal cracks, instead of being parallel, tend to radiate from the compression zone at the reaction point, forming a fan shaped region. Each of the radiating cracks may be assumed to form the boundary of an inclined compression strut. The angle of inclination (from the horizontal) of the compression struts increases as one goes towards the support. Outside the fan region the cracks are parallel to each other.

A literature review by Park and Paulay (1975) reveals that the optimum angle of the compression strut is about 38^0, based on strain energy considerations. The CEB-FIP Model Code (1990) allows for a choice of θ in the range from 18.4^0 to 45^0. The Canadian Standard (A23.3-94) simplified method provisions for shear design are based on a 45^0 truss model while the "General Method" provisions considers variable θ below 45^0.

A small value of θ allows for larger stirrup spacing, but more longitudinal reinforcement is required. For given amount of longitudinal reinforcement, the smaller the angle the

103

more the elongation of tension steel. To obtain a conservative estimate of steel elongation, an inclination angle of 45^0 is assumed in this study.

Considering Fig. 4.18, for an assumed angle of 45^0, the fan region extends a distance d_v from the support, where d_v is the distance between centroid of the tension steel and centroid of the compression stress block. Outside the fan region, the cracks are parallel to each other at an assumed angle of 45^0.

Dilger (1966) recognized the influence of shear cracking on the tension steel force and proposed an expression that allows one to compute the shift in tensile force due to shear cracking. Based on the same idea, the tensile force distribution can be determined by considering various free body diagrams from Fig. 4.18 (Park and Paulay, 1975). The variation of tension force, F_t, within the fan region is given as:

$$F_t = \frac{M_u}{d_v} - \frac{V_u x^2}{2d_v^2}$$

[4.64]

The variation of F_t outside the fan region ($0 \le x \le d_v$) is given as:

$$F_t = \frac{M_x}{d_v} + \frac{V_x}{2}$$

[4.65]

Where M_x and V_x are the moment and shear at the section being considered. In the derivation of the above expressions, it is assumed that the cracks are inclined at an angle of 45^0, there is no contribution of concrete in resisting shear, and the support reaction is concentrated at a point. Thus it is assumed that the entire shear, except for that within d_v of the support, is resisted by transverse steel and the width of support is neglected. These assumptions will underestimate the plastic hinge length and the tension steel force (Park and Paulay, 1975) and would provide a conservative estimate of plastic rotation capacity.

104

For beams with flexural cracks only, the distribution of tension force F_t along the member is given as:

$$F_t = \frac{M_x}{d_v}$$

[4.66]

4.4.9 Computation of crack spacing

The CEB manual for Cracking and Deformations (1985) indicates that there are several parameters that influence the crack spacing, in particular the cover and bar spacing. The CEB Manual (1985) gives the following empirical equation for determining the average crack spacing.

$$s_m = 2(c_o + \frac{s_b}{10}) + \kappa_1 \kappa_2 \frac{d_b}{\rho_r}$$

[4.67]

where,

s_m = average crack spacing in mm

c_o = concrete cover in mm

s_b = spacing of bars or bundles in mm. For beams this is taken as the web width divided by the number of bars or bundles of bars in one layer

$\kappa 1$ = coefficient defining the influence of the bond properties of the bars. The following values are recommended for $\kappa 1$

high bond bars	0.4
ribbed prestressing wires	0.6
plain bars	0.8

$\kappa 2$ = coefficient dependent on the distribution of tensile stress within the section. Appropriate values are:

| pure bending | 0.125 |
| pure tension | 0.25 |

d_b = bar diameter in mm.

ρ_r = ratio of the area of reinforcement to the effective concrete area, A_{cef}

105

The effective area of concrete, A_{cef}, to be used in Eq.4.67 is described in Fig. 4.19.

4.4.10 Computation of plastic rotation capacity

The plastic rotation capacity is computed for the interior support of a two-span continuous beam subjected to uniformly distributed load, as shown in Fig. 4.1. The procedure for computing the plastic rotation capacity consists of two parts. In the first part θ_p is determined by considering the internal mechanics of plastic hinge region to compute the elongation of tension steel. This involves the application of concrete bond-slip law and the materials constitutive laws defined earlier in the chapter. In the second part θ_p is determined by considering the overall behaviour of structure including the effects of stiffness, geometry and loading of the structure. The correct solution requires iteration in which the values of loading and the steel strain at failure are adjusted to give same value of θ_p from the two approaches.

4.4.10.1 A - Computation of θ_p (capacity) from elongation of tension steel

It is understood that elongation of tension steel is the primary cause of plastic rotation. The elongation of tension steel depends upon the steel strain distribution between the cracks. This in turn depends upon the magnitude of tensile forces at the cracks, stress-strain law adopted for the steel and the concrete, and the concrete bond-slip law. The expressions for computing the tension steel forces at cracks and the distribution of steel strain within the cracks have been developed in the previous sections and will be used here to compute the plastic rotation capacity of critical section. The procedure for determining plastic rotation capacity is described for the interior support of a two-span beam shown in Fig. 4.1. The procedure involves the following steps:

1. Divide the tension zone of the beam in the vicinity of plastic hinge into a number of cracked elements. Usually it is sufficient to consider a length d to each side of the plastic hinge.

106

2. Determine crack spacing from Eq. 4.67.

3. Calculate the yield moment M_y, corresponding to yielding of steel at the interior support, using Eqs. 4.20 and 4.21.

4. Calculate the corresponding load q_y

$$q_y = \frac{8M_y}{L^2}$$ [4.68]

5. Assume a value of ultimate load q_u greater than q_y

6. Determine the depth of neutral axis c and the force lever arm d_v from ultimate conditions at the critical section, using strain compatibility analysis.

7. Determine average steel strain in the first cracked element using strain compatibility analysis

$$\varepsilon_{sm} = \varepsilon_{cu}\left(\frac{d}{c} - 1\right)$$ [4.69]

8. Assume a value of steel strain ε_s at first crack above the support.

9. Determine the tension steel stress σ_s at first crack using a steel stress-strain model.

10. Determine the tension steel force at first crack as $F_t = A_s\,\sigma_s$.

11. Determine the moment at support as $M_u = F_t\,d_v$.

12. Calculate the shear at support corresponding to load q_u and moment M_u as $V_u = (M_u/L) + (q_uL/2)$.

107

13. Calculate the tension steel force F_t at the other end of the first cracked element, using Eq. 4.64.

14. Calculate the value of steel stress at the other end of cracked element as $\sigma_s = F_t/A_s$

15. With the steel stress at both ends of the first cracked element known, determine the steel stress and strain distribution within the cracked element using appropriate bond model equations from 4.27 to 4.48.

16. Determine the average steel strain, ε_{sm}, within the first cracked element using appropriate bond model equations from 4.50 to 4.63.

17. Compare the value of ε_{sm} obtained from step16 to the value determined in step 7. If the two agree, the assumed value of ε_s at the first crack was correct. If not, repeat steps 7 through 16 until the two values of ε_{sm} agree.

18. Having obtained the correct value of ε_s at first crack, for given load q_u, revise the values of steel stress σ_s, steel force F_t and moment M_u at support.

19. Determine the distribution of shear force and moment, at crack locations along the beam, from statics.

20. Determine the distribution of tension steel force F_t at crack locations along the beam, using Eqs. 4.64 and 4.65. Figure 4.21 shows a typical distribution of the tension chord force.

21. Obtain the steel stress and strain distribution within each cracked element, using bond model equations. Only those elements that contain plastic deformations need to be considered. The plastic hinge length is limited to the region in which σ_s at cracks is greater than f_y (or $\varepsilon_s > f_y/E_s$)and can be obtained from stress (or strain)

108

distribution along the length of the beam. The curvature (ϕ_x) distribution can be obtained by dividing the steel strains by the distance (d-c).

$$\phi_x = \frac{\varepsilon_{sx}}{d-c} \qquad\qquad [4.70]$$

22. Figures 4.22, 4.23, and 4.24 show typical distribution of steel stress, strain, and curvature respectively along the member. Note that the steel strains and curvatures drop significantly between the cracks.

23. Integrate curvatures over the plastic hinge length to obtain the ultimate rotation of the hinge:

$$\theta_u = \frac{1}{d-c} \int_0^{L_p} \varepsilon_{sx} d_x \qquad\qquad [4.71]$$

24. Use steps 18 through 22 to calculate the yield rotation θ_y for ε_{sy}, q_y and M_y. All cracked elements within the hinge length need to be considered. Since ε_{sy}, q_y and M_y are known, the calculation of θ_y does not require a trial and error procedure.

25. Calculate plastic rotation of the hinge by subtracting the yield rotations from the ultimate rotations:

$$\theta_p = \theta_u - \theta_y \qquad\qquad [4.72]$$

The plastic rotations calculated in part A are based on assumed values of ultimate load q_u and needs to be verified in the second part of analysis. In the second part of analysis, the plastic hinge rotations are computed considering the overall behaviour of structure including the effects of stiffness, geometry and loading of the structure. The loading, q_u, on the beam is the same as that used in the first part of analysis.

109

4.4.10.2 B - Computation of θ_p (demand) From Structure Geometry and Loading

Consider a two-span continuous beam, as shown in Fig. 4.1. The yielding of reinforcement at the interior support at a moment M_y leads to the formation of plastic hinge. The corresponding load q_y is given by Eq. 4.68.

The moment M_y can be calculated using Eqs. 4.20 and 4.21. With hinge formation the statical system transform to that shown in Fig. 4.1b. The behaviour of plastic hinge is modelled by a linear hardening rotational spring of stiffness k_s. The beam is assumed to act elastically between the hinge and the exterior supports. As the load increases from q_y to q_u the moment at the support increases inelastically from M_y to M_u, the nominal moment of resistance of the support section. This moment is less than the elastic value of the moment at the support, M_e, which is given as:

$$M_e = \frac{q_u L^2}{8}$$

[4.73]

The moment in excess of M_u is redistributed from the support to the adjacent spans, causing an increase in the span moments beyond the elastic value. Moment redistribution occurring at the support is that given by Eq. 4.1.

The plastic hinge rotation at the support can be derived using the M-θ_p relationship and the moment area theorem. Due to symmetry, one could consider a single span, fixed at one end, beam as shown in Fig. 4.25a. The plastic rotation occurs, after the formation of the plastic hinge, due to load $(q_u$-$q_y)$ acting over the beam in which the fixed support has been replaced with a rotational spring of stiffness k_s, as shown in Fig. 4.25b. This plastic rotation can be calculated as a difference of the free rotation due to load $(q_u$-$q_y)$ acting over a simply supported beam (Fig. 4.25c) and the restrained rotation due to rotational spring of stiffness k_s (Fig. 4.25d). From Fig. 4.25c, using moment area theorem, the free rotation, θ_{free}, at the hinge is given as:

110

$$\theta_{free} = \frac{(q_u - q_y)L^3}{24EI_{cr}}$$

[4.74]

Where EI_{cr} is the cracked flexural stiffness of the beam. From M-θ_p relationship, the increase in moment beyond elastic value is:

$$M_u - M_y = k_s \theta_{pL}$$

[4.75]

Where θ_{pL} is the plastic rotation to one side of the hinge and M_u is the moment capacity of support section. From Fig. 4.25d, using moment area theorem, the restrained rotation, θ_{rest} is given as:

$$\theta_{rest} = \frac{k_s L \theta_{pL}}{3EI_{cr}}$$

[4.76]

The plastic hinge rotation θ_{pL} is given as:

$$\theta_{pL} = \theta_{free} - \theta_{rest}$$

[4.77]

Substituting values from Eq. 4.74 and 4.76 gives:

$$\theta_{pL} = \frac{(q_u - q_y)L^3}{24EI_{cr} + 8k_s L}$$

[4.78]

This is plastic rotation to one side of the plastic hinge. For both sides, the plastic hinge rotation is $2\theta_{pL}$:

$$\theta_p = \frac{(q_u - q_y)L^3}{12EI_{cr} + 4k_s L}$$

[4.79]

111

Equating θ_{pL} from Eqs. 4.75 and 4.78, and accounting for both sides of the plastic hinge, one can write the expression for the stiffness of rotational spring, k_s, as:

$$k_s = \frac{12EI_{cr}}{L}\left\{\frac{M_u - M_y}{(q_u - q_y)L^2 - 8(M_u - M_y)}\right\}$$

[4.80]

With q_y, M_y, q_u and M_u known from the first part of the analysis, the value of k_s can be computed using Eq. 4.80 and θ_p can be computed using Eq. 4.79.

Compare the values of θ_p from Parts A and B of the analysis. The solution is correct and the maximum load limit has been found if the two values match. If not, a new value of q_u is assumed and the whole procedure for Parts A and B of the analysis is repeated until convergence.

In the above procedure, a constant cracked stiffness is used for the computation of elastic moment distribution in the beam. In reality, the cracked stiffness of the positive and negative moment regions varies with the amount of reinforcement. The amount of reinforcement provided at the support is typically greater than that provided in the span. For rectangular beams this translates to higher cracked stiffness at the support as compared to the span. However, most beams are cast monolithic with the slab and act as T-beams in the positive moment region. This along with the top flange reinforcement contributes to the cracked stiffness of the span region. Furthermore, in a beam designed for moment redistribution the support moments are typically reduced and the cracked stiffness at the support gets closer to that within the positive moment region in the span. In such situations it is conservative to assume a constant EI over the entire length of the beam.

Due to the complex and iterative nature of the procedure for computing θ_p, a spreadsheet program is developed that incorporates the strain compatibility analysis and the bond-model analysis to calculate the tension chord forces, stresses and strains within cracked elements, the curvatures and the plastic hinge rotation. The input to the program requires

112

the beam span, section properties, material properties including stirrups, amount of tension, compression and hoop reinforcement, and the crack spacing. The spreadsheet calculates the plastic rotation capacity for both parts of the analysis and automatically iterates the values of ε_s and q_u to obtain the correct solution. The design example in the next section uses this spreadsheet.

4.5 Design Example

The plastic rotation capacity is calculated for the interior support of a uniformly loaded two-span continuous beam, using spreadsheet formulation of the ductility model. Each span is 12 m. Section properties, material properties and reinforcement details for the beam are given below:

Beam Geometry

L   = 12 m
L/d = 16

Section Properties:

b   = 300 mm
h   = 800 mm
d   = 750 mm

Material Properties:

Concrete:

f_c' = 30 MPa

ε_{cu} = 0.005

E_c = 27700 MPa

Steel: (CSA G30.18-M92, Grade 400R)

f_y = 400 MPa

E_s = 200,000 MPa

113

f_u = 540 MPa

ε_{su} = 0.1

Amount of Reinforcement:

6 No. 20 top bars at interior support

Stirrups No. 10 @ 150 c/c

ω = 0.108

The tension region is divided into a number of cracked elements. Using Eq. 4.67, the crack spacing, s_m, is calculated as 165 mm. A value of 150 mm is used for crack spacing for the purpose of analysis because cracks are likely to develop at stirrup locations. The bond shear τ_{b1} and τ_{b2} are:

$$\tau_{b1} = 0.6(f_c')^{2/3} = 5.8 \text{MPa} \quad \text{and} \quad \tau_{b2} = 0.3(f_c')^{2/3} = 2.9 \text{MPa}$$

In the first part θ_p (capacity) is computed from the elongation of tension steel. The yielding moment and the corresponding load are calculated as, M_y = 479 kNm and q_y = 26.6 kN/m. Assuming a value of ultimate load q_u greater than q_y, say q_u = 58.2 kN/m, it is found that, ε_s = 0.0469, ε_{sm} = 0.0321 and M_u = 581 kNm. Figure 4.26 shows the variation of steel strain in the first cracked element over the support and corresponding mean strain value. Figures 4.21, 4.22, and 4.23 show the force, stress, and strain distribution respectively in tension steel. The plastic hinge length is limited to the region in which σ_s at cracks is greater than or equal to f_y and can be obtained from Fig. 4.22. For this particular case, the plastic hinge length is 500 mm to either side of the critical section. The curvature distribution is shown in Fig. 4.24. The total rotation and the yield rotation are calculated as, θ_u = 0.03427 rad. and θ_y = 0.00404 rad. and the plastic rotation capacity is obtained as θ_p = 0.03023 rad.

In the second part θ_p (demand) is computed from structure geometry and loading. The rotational spring stiffness is computed, using Eq. 4.80, as, k_s = 3.37x10^9 Nmm/rad and plastic rotation is computed, using Eq. 4.79, as θ_p = 0.03023 rad. Since the two values of

114

θ_p from part one and two of the analysis match, a correct solution has been obtained. Thus, for this example, θ_p = 0.03023 rad. Figure 4.27 shows the variation of θ_p with mechanical reinforcement index ($\omega=A_s f_y/bdf_c'$) for the example beam.

The model can be used to determine the allowable moment redistribution. The model gives the ultimate value of the load q_u, from which the elastic moment at the support can be calculated using Eq. 4.73. The nominal moment resistance can be calculated using Eq. 4.18. The allowable moment redistribution can then be determined, using Eq. 4.1 and is 44.5% for this particular example. Figure 4.28 shows the variation of allowable moment redistribution with mechanical reinforcement index for the example problem.

4.6 Comparison With Experimental Results

Mattock's (1964) and Bosco and Debernardi's (1993) tests were used to validate the proposed model. The Mattock's test series consisted of 37 beams, while the Bosco and Debernardi's test series consisted of 44 beams. The following sections provide a brief review of the test programs and comparison with the model.

4.6.1 Mattock's tests

Mattock carried out a series of tests to investigate the moment-rotation characteristics of reinforced concrete beams in the support region of a continuous beam. Simple span beams, with a concentrated load at mid-span, were used to simulate the distribution of bending moments adjacent to a support in a continuous beam. The half span of a simple-span beam represents the region between the support and the point of contraflexure in a continuous beam. Thirty-one such beams were tested. For reference purposes, six additional beams were tested as simple span beams with equal loads applied at each third point. However, the values of θ_p for these beams were not reported.

The variables included in the test program were as follows:

115

- Concrete strength	28 MPa and 41 MPa
- Reinforcement yield point	324 MPa and 413 MPa
- Effective depth of beam	250 mm and 500 mm
- Span of test beam	1.4, 2.8, and 5.6 m
- Amount of tension reinforcement	between 1% and 3%
- All beams were 150 mm wide.	

Figure 4.29 shows the comparison of calculated and measured plastic rotation capacity. The 45^0 line represents the case where calculated rotation capacity is equal to the measured rotation capacity. All the points plot above the 45^0 line, which shows that the model underestimates the plastic rotation capacity. The relatively high deviation of some plotted points from the 45^0 line is due the fact that very high values of ultimate concrete strains (in the vicinity of 0.02) were reported for some of the tests. A better correlation of the test data is obtained when the test beams having ε_{cu} greater than 0.01 are eliminated from the comparison, as shown in Fig. 4.30. Figure 4.31 plots the ultimate concrete strains reported in the tests, showing that for the majority of the tests the reported values were in the vicinity of 0.01.

For comparing the trend of the variation of test and model θ_p with ω, the beams are divided into four groups. Each group is formed by the beams having same slenderness ratio (L/d) and volumetric ratio of stirrups (ρ_s). Group 1 consists of four beams (ref. Mattock's beams B1, D1, G1, G3) having L/d=5.5 and ρ_s =0.01019. Group 2 consists of five beams (ref. Mattock's beams B4, D4, G2, G4, G5) having L/d = 11 and ρ_s = 0.01019. Group 3 consists of four beams (ref. Mattock's beams A4, C5, E2, F2) having L/d = 11 and ρ_s =0.01224, and group 4 consists of four beams (ref. Mattock's beams A3, A6, C3, C6) having L/d = 22 and ρ_s = 0.005656. θ_p vs ω curves were generated for these beam groups for two values of ε_{cu}, 0.005 and 0.008, and are shown in Figs. 4.32 through 4.35. Since the test values of ε_{cu} were in the vicinity of 0.01, the model curves with ε_{cu} = 0.008 predict test results better than those with ε_{cu} = 0.005. The figures show that the model predicts the trend of the test data well. Both test results and the model indicate that the plastic rotation capacity increases with an increase in slenderness ratio.

In general, the model predicts the trend of the test results well. In particular, the correlation is good when the values of ε_{cu} used in the model are close to the values obtained in the test.

4.6.2 Bosco and Debernardi tests

Bosco and Debernardi (1993) carried out a series of tests to study the influence of steel ductility, section size, and shape of moment diagram on plastic rotation capacity of reinforced concrete beams. The testing program was carried out at the Laboratory of the Department of Structural Engineering of the Politecnico di Torino.

The variables considered were as follows:

- types of steel	Grade B 500 H (high ductility, ε_{su}=0.07)
	Grade B 500 N (normal ductility, ε_{su} =0.042)
- beam cross-section	100X200, 200X400, 300X600
- reinforcement	0.13% to 1.7%
- load conditions	single point load at mid-span
	three symmetrically placed point loads

The beam slenderness ratio and the width to depth ratio of the cross sections were kept constant. The mechanical properties of concrete were reported to be constant during the tests. Stirrup and compressive reinforcement were the same over the whole length of the beams for each beam depth.

The testing program employed 44 simple span beams, subdivided into eleven classes. Each class consisted of four specimens, having the same amount of tension reinforcement. The first specimen of each group contain high ductility steel with one load, the second specimen contain normal ductility steel with one load, the third specimen

117

contain high ductility steel with three loads, and the fourth specimen contains low ductility steel with three loads.

Figure 4.36 shows the comparison of calculated and measured plastic rotation capacity. The plotted points in general follow the 45^0 line. For most beams the model is conservative. However, quite a few points plot below the 45^0 line. This can be attributed to the fact that the measured plastic rotation capacities correspond to the maximum moment values attained in tests. The M-θ_p curves reported show that θ_p continues to increase beyond maximum moment value and at failure the plastic rotation can be many times that of the reported value.

For comparing the trend of the variation of test and model θ_p with ω, the beams are divided into four groups, depending upon the type of steel and loading. Only those beams are included in a group, which have the same L/d and ρ_s. Group 1 contains beams with high ductility steel and single point load at mid span. Group 2 contains beams with normal ductility steel and single point load at mid span. Group 3 contains beams with high ductility steel and three point loads placed symmetrically, at a distance 2h, about mid-span of the beam, where h is the height of the beam. Group 4 contains beams with normal ductility steel and three point loads placed symmetrically, at a distance 2h, about mid-span of the beam. For group 3 and 4, the model assumes that only flexural cracks are present since the shear is small in the vicinity of plastic hinge. Figures 4.37 through 4.40 show the θ_p vs. ω curves for groups 1 through 4 along with the corresponding test results. The figures show that the model predicts the trend of the test data well except for one test in group 2 that plotted much higher on the graph. Tests and model both confirm that in low ductility steel the plastic rotation capacity may be significantly reduced for low values of reinforcement index.

4.7 Summary and Conclusions

An analytical model is developed for evaluating the rotation capacity, θ_p, of plastic hinges and allowable moment redistribution, β. The model accounts for the effects of major parameters on θ_p and β. These include the constitutive relationships, bond-slip law, type

118

of plastic hinge, beam slenderness, concrete confinement, ductility of steel, and the type of loading.

Constitutive relationships were used for concrete and steel to include the effect of concrete confinement and strain hardening. Concrete-steel bond-slip relationship is used to include the effect of tension stiffening. A linear M-θ_p relationship allows accounting for the finite stiffness of hinges. The effect of shear cracking on θ_p and β is taken into account by considering the shift of tension steel force along the reinforcement.

The model considers the tension regions of beam to be composed of individual cracked elements. The analysis to determine θ_p and β consists of two parts. In the first part θ_p is computed by summing up the individual rotations of each cracked element. The steel strain distribution within each cracked element is determined, using the bond-slip law. The steel strain distribution provides the curvature distribution, which is integrated over the plastic hinge length to provide the plastic hinge rotation. In the second part, θ_p is computed using the stiffness, geometry and loading on the structure. The correct solution requires iteration in which the values of loading and the steel strain at failure are adjusted to give same value of θ_p from the two approaches. The correct solution satisfies equilibrium internally and externally, and compatibility of deflections and rotations without violating the failure criteria for the steel and concrete.

The proposed model gives good agreement with experimental results. Both tests and model show the same trend in the variation of θ_p with the reinforcement index.

The concrete strain at ultimate has a significant influence on plastic rotation capacity; θ_p increases with increasing ε_{cu}. The plastic rotation capacity also increases with increasing beam slenderness. A parametric study will be used in the next chapter to quantify the effects of various parameters on θ_p and β.
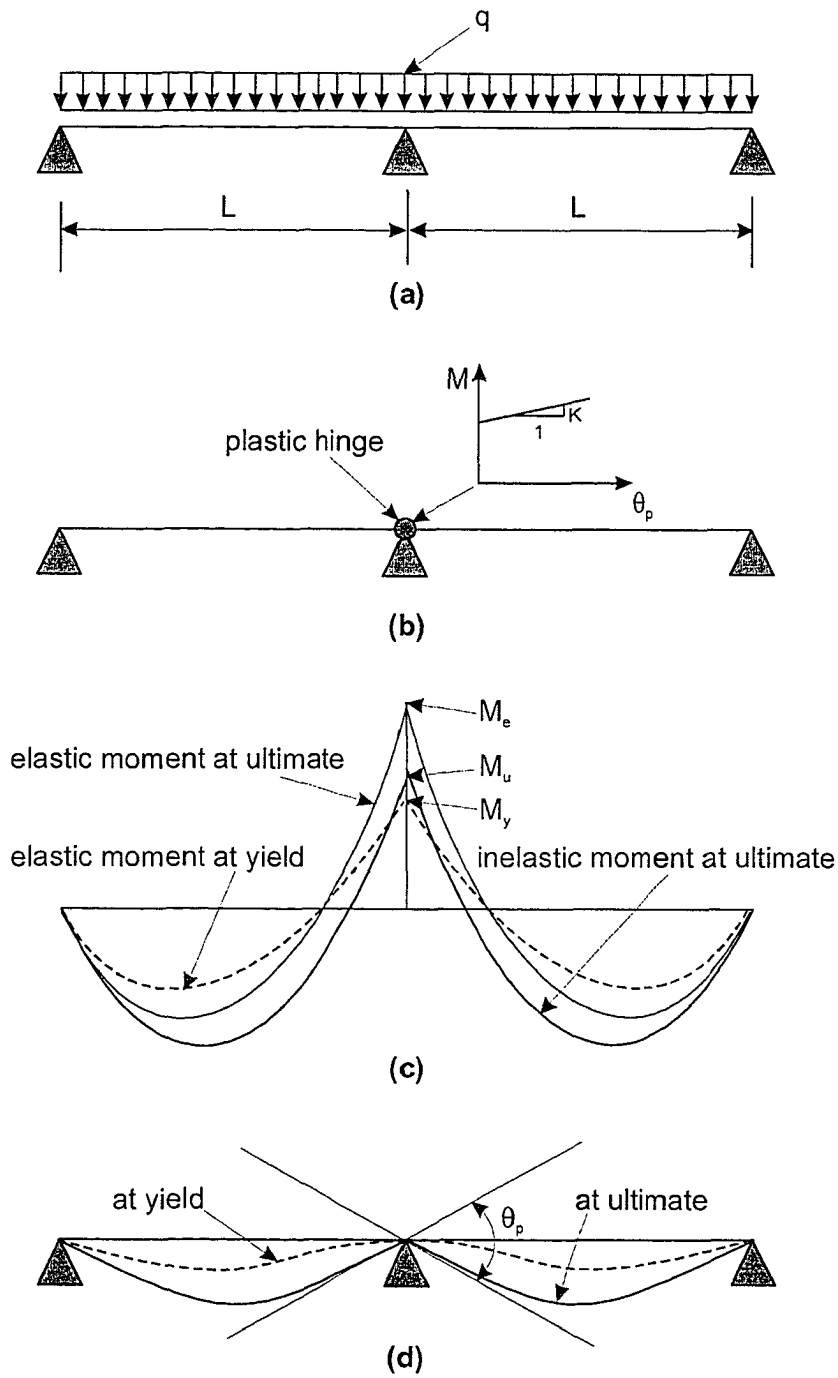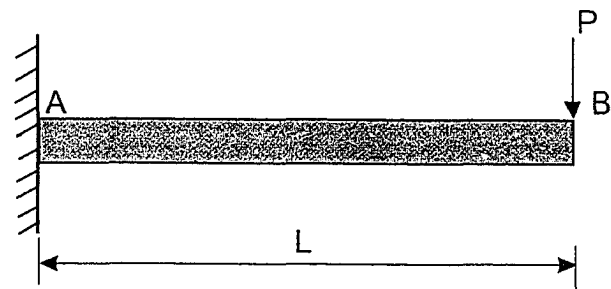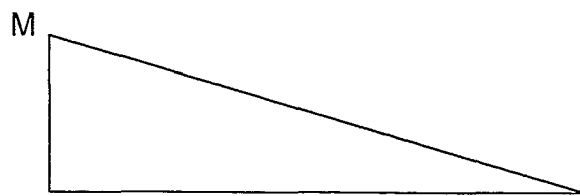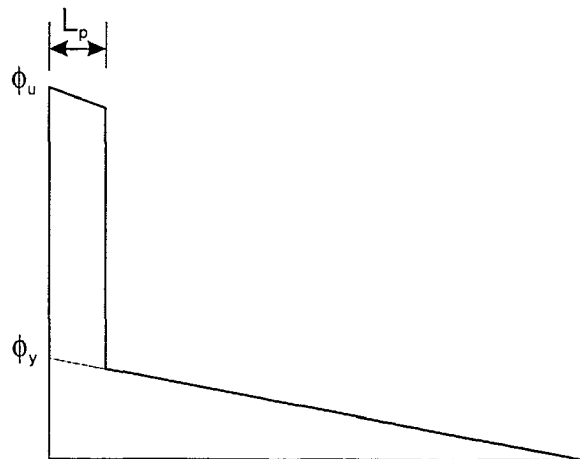
119

Figure 4.1 (a) Two span beam with loading; (b) idealized beam after formation of plastic hinge; (c) distribution of moments; and (d) deformations at yield and ultimate

120

Figure 4.2 Constant curvature model: (a) cantilever beam; (b) bending moment diagram; and (c) curvature distribution
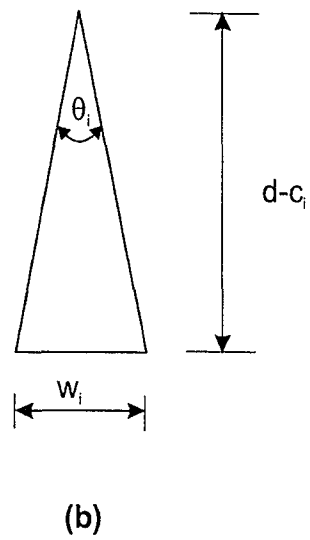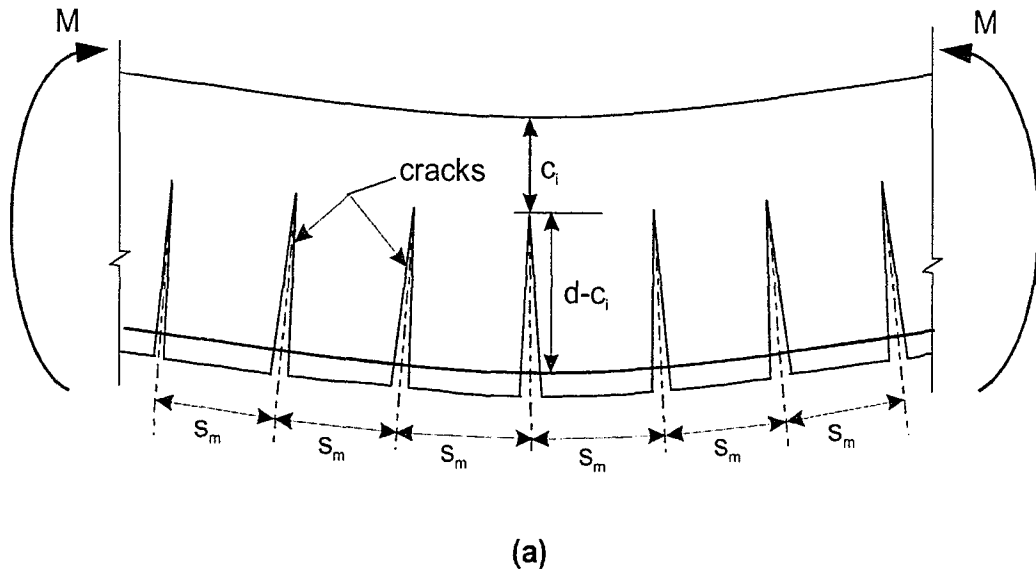
121

Figure 4.3 (a) Flexural member with cracked elements; and (b) rotation of cracked element
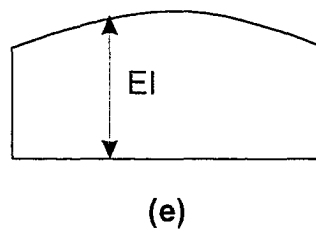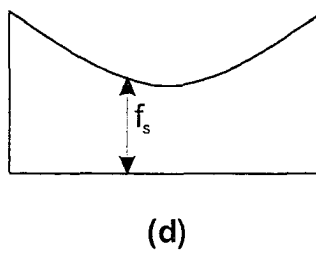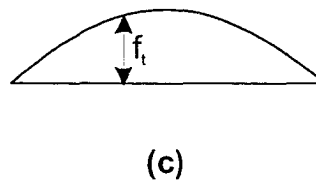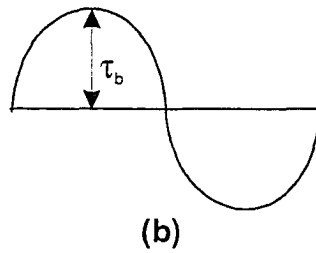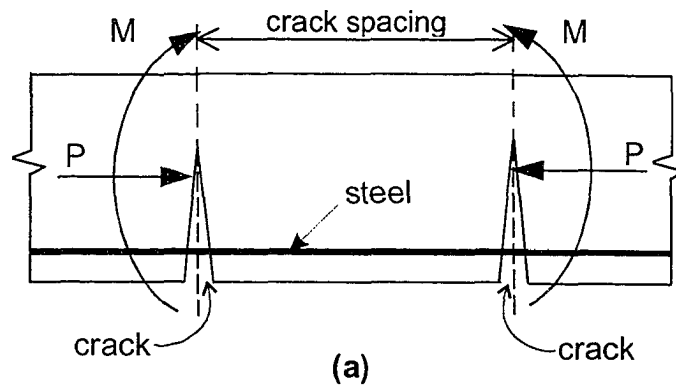
122

Figure 4.4 Tension stiffening effect: (a) cracked element; (b) bond stress; (c) tensile stress in concrete; (d) tensile stress in steel; and (e) flexural rigidity
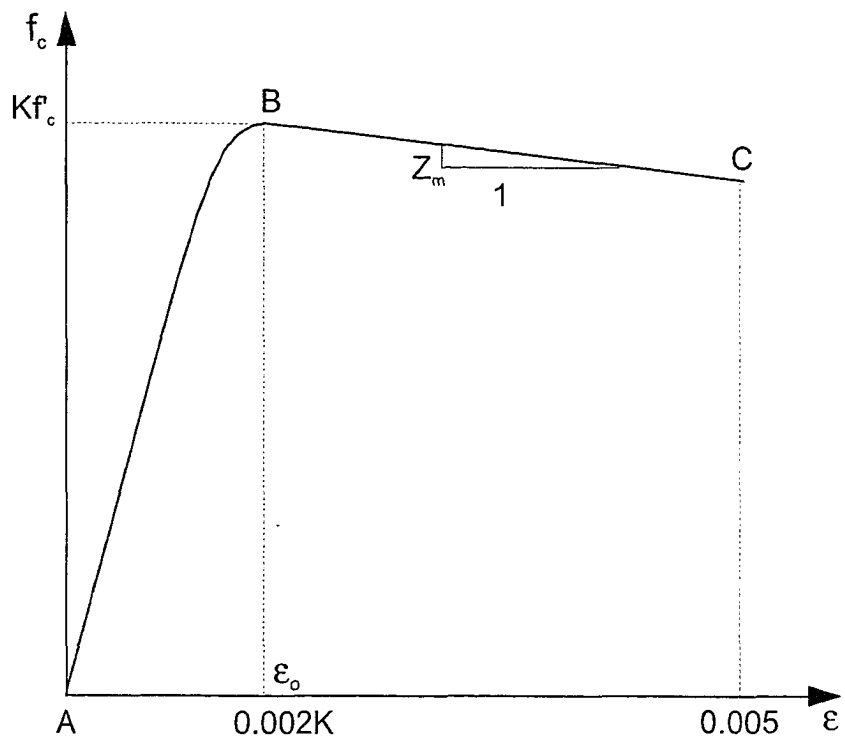
123

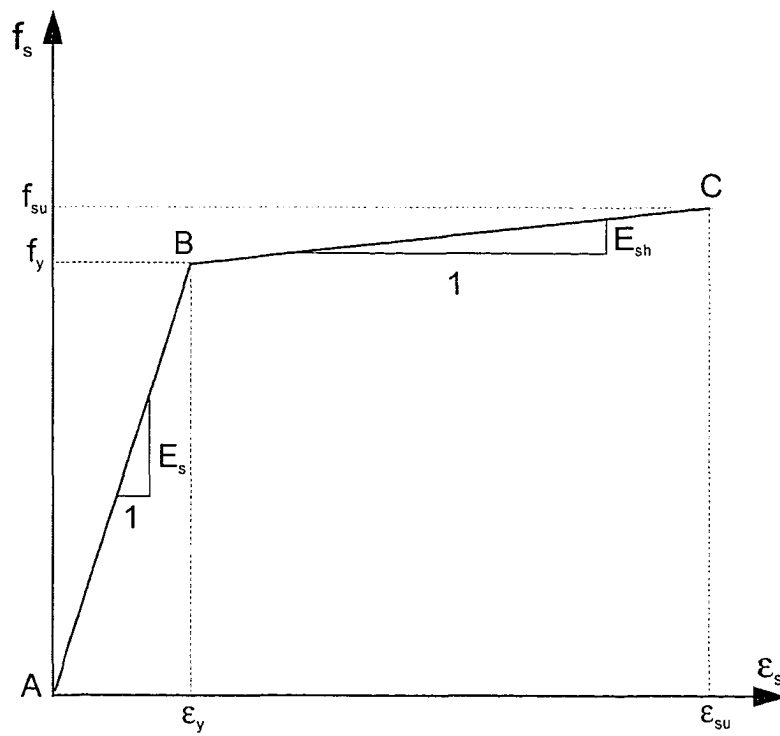Figure 4.5 Stress-strain relationship for concrete
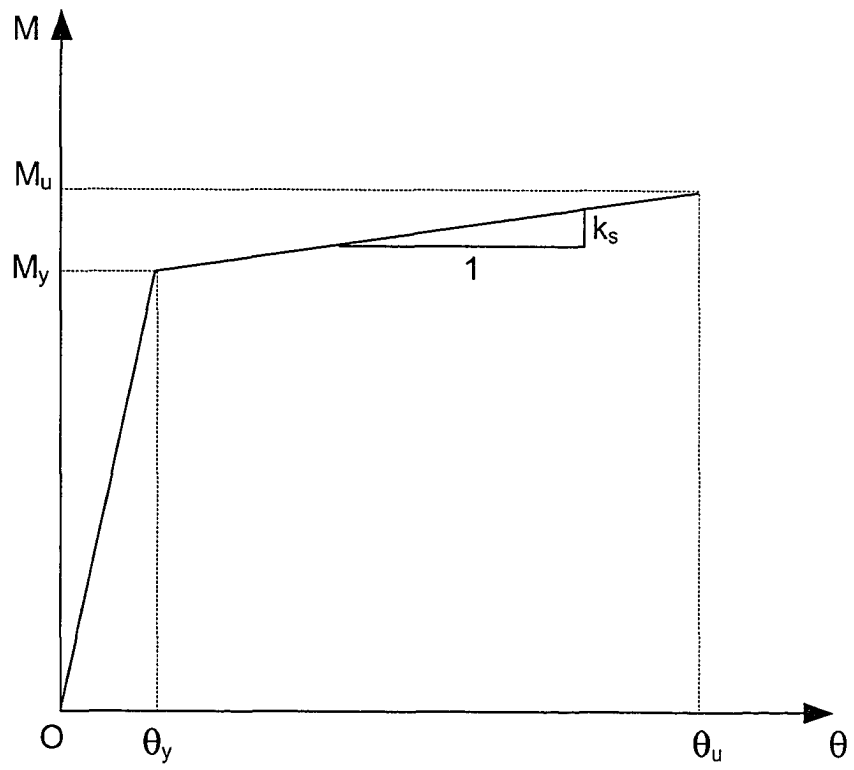(Park et al. 1982)

124

Figure 4.6 Stress-strain relationship for steel

125

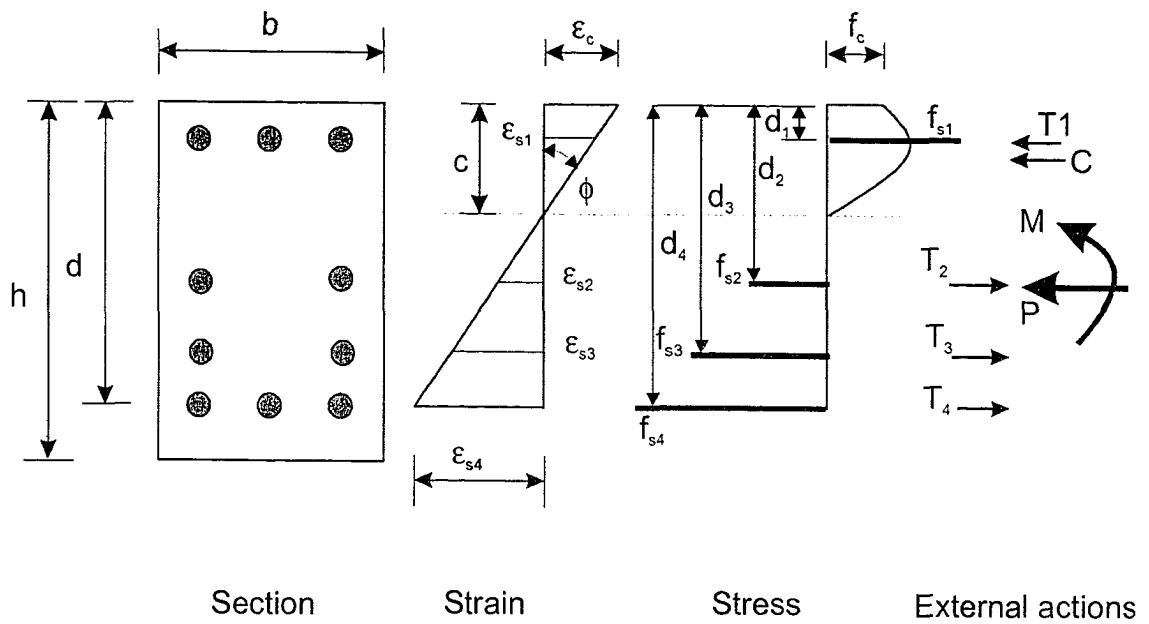Figure 4.7 Moment-rotation relationship at hinge

126

Section   Strain   Stress   External actions

Figure 4.8 Strain compatibility and equilibrium analysis of a section subjected to flexure and axial load
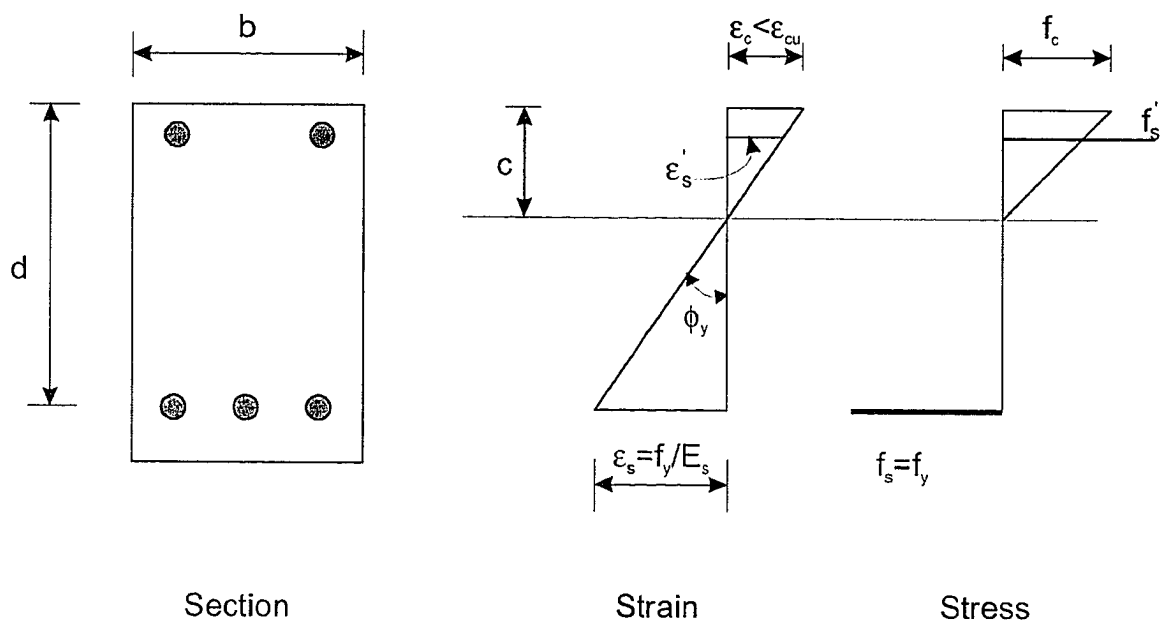
127

Section   Strain   Stress

Figure 4.9 Stress and strain distribution in flexure at first yield
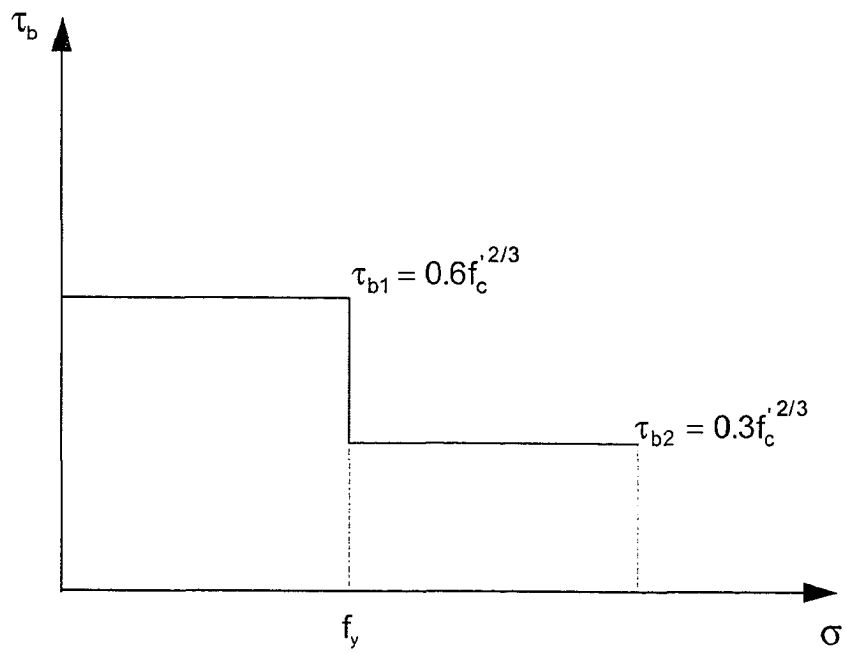
128

$$\tau_{b1} = 0.6f_c'^{2/3}$$

$$\tau_{b2} = 0.3f_c'^{2/3}$$

Figure 4.10 Bond Model (Marti et al. 1998)
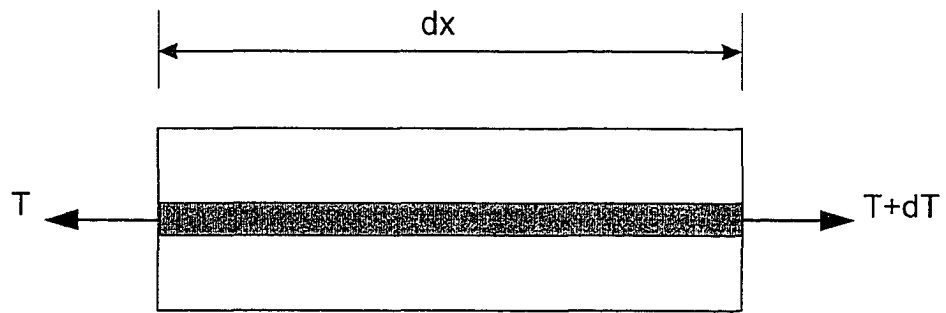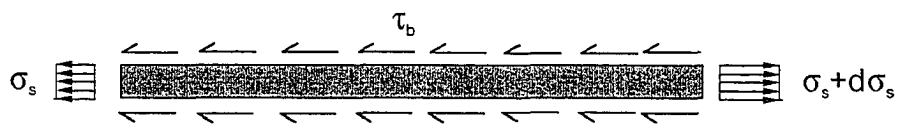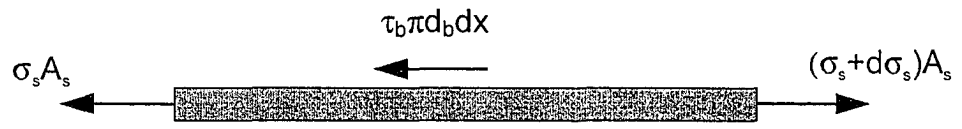
Figure 4.11 Equilibrium of a differential element of a bar: (a) bar element; (b) stress distribution; and (c) force equilibrium

130
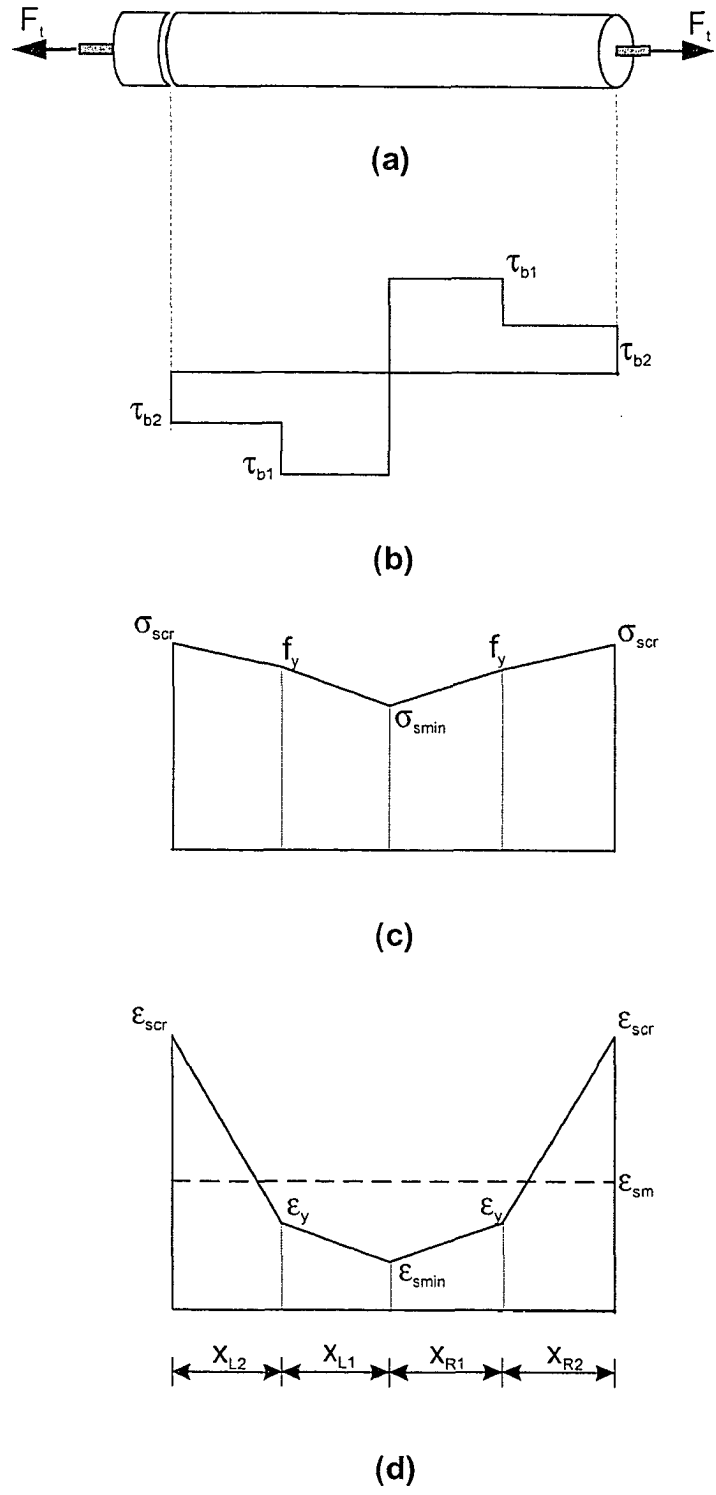
Figure 4.12 (a) Cracked element; (b) bond shear; (c) steel stress; and (d) steel strain

131
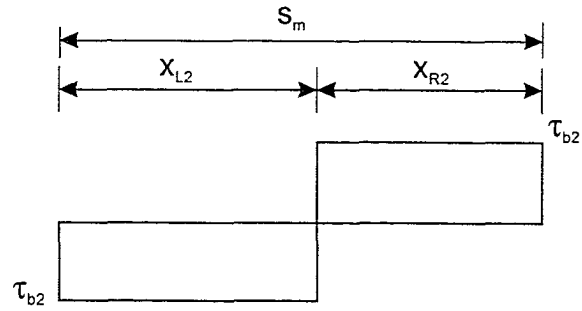
(a)
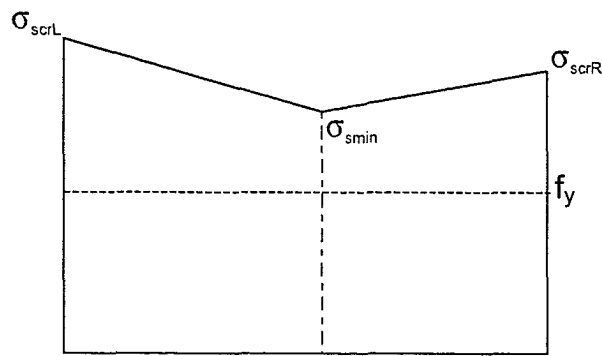
(b)
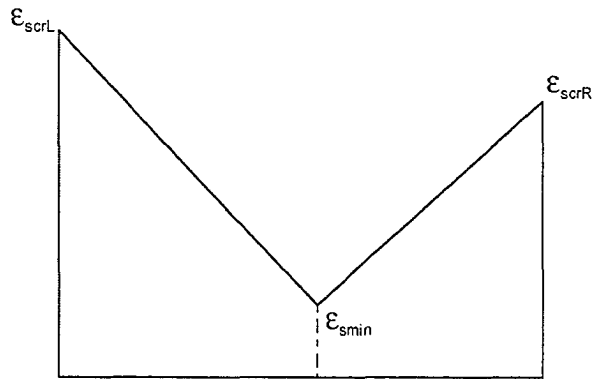
(c)

Figure 4.13 Case 1($\sigma_{scrL} > f_y$, $\sigma_{scrR} > f_y$, $\sigma_{smin} > f_y$): (a) bond shear; (b) steel stress; and (c) steel strain

132
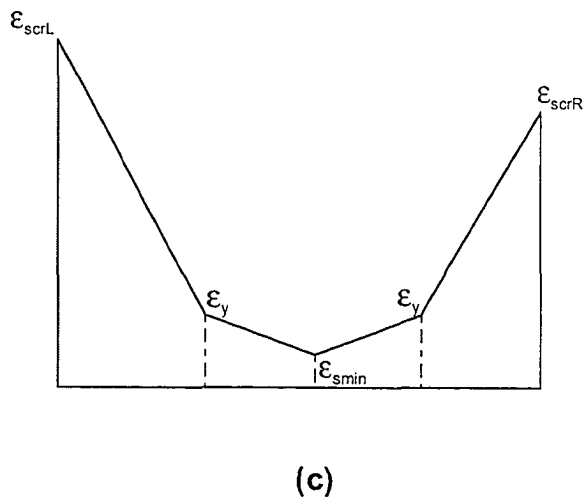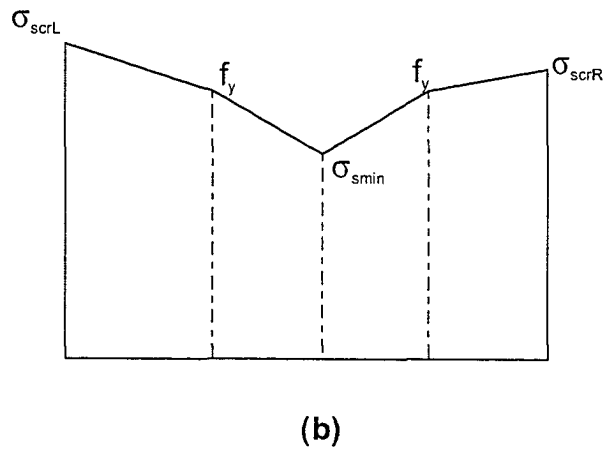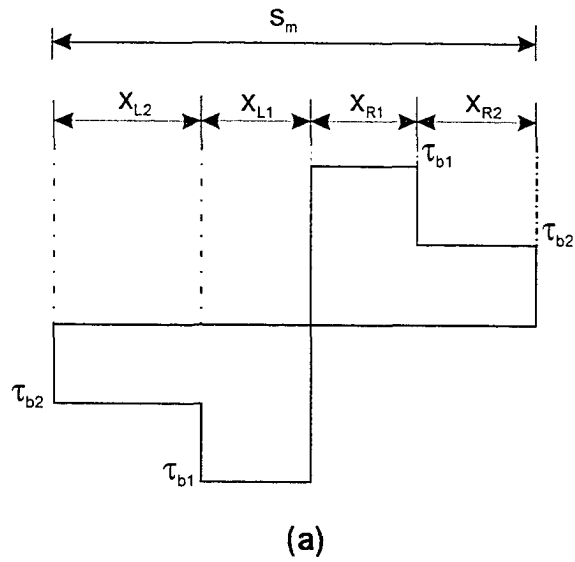
Figure 4.14   Case 2 ($\sigma_{scrL} > f_y$, $\sigma_{scrR} > f_y$, $\sigma_{smin} < f_y$): (a) bond shear; (b) steel stress; and (d) steel strain distribution

133
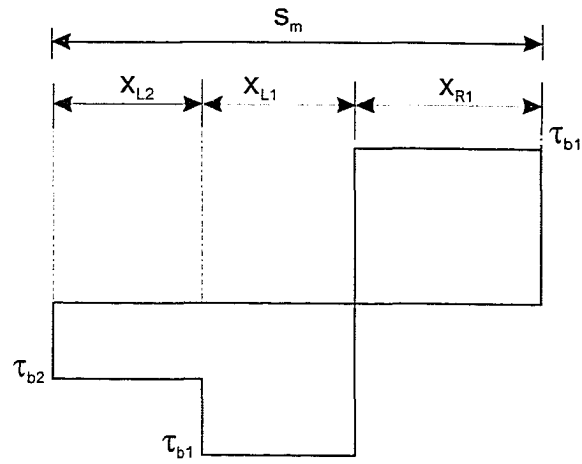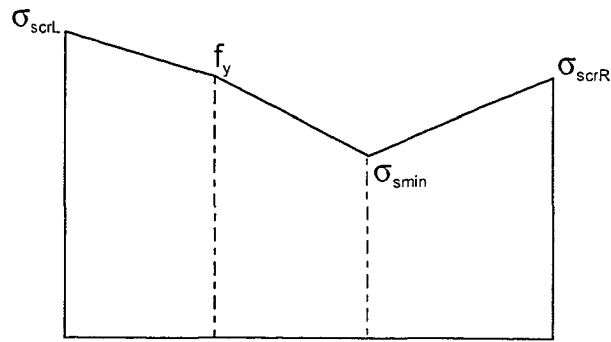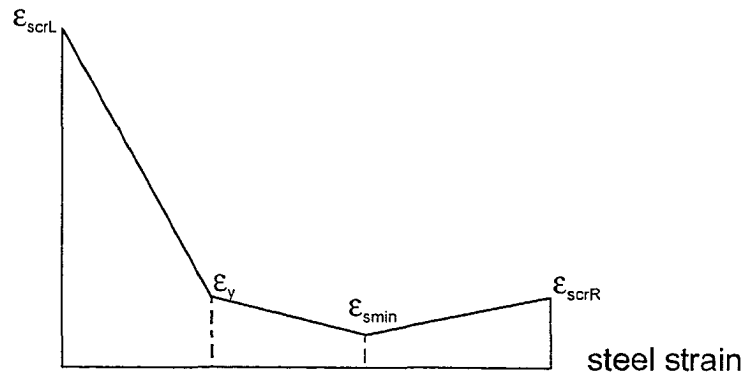
Figure 4.15 Case 3 ($\sigma_{scrL} > f_y$, $\sigma_{scrR} \leq f_y$, $\sigma_{smin} < f_y$): (a) bond shear; (b) steel stress; and (c) steel strain distribution

134
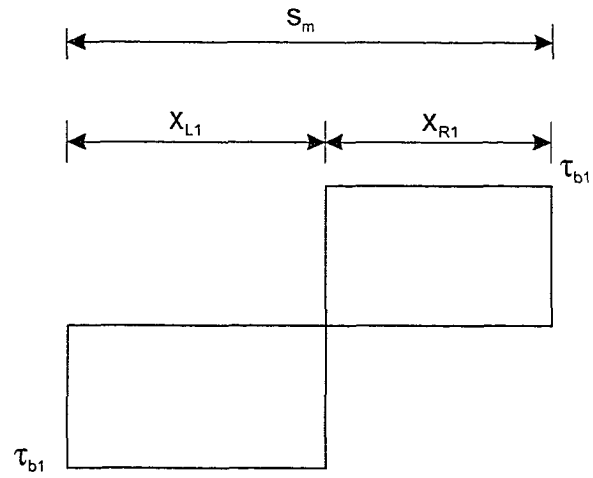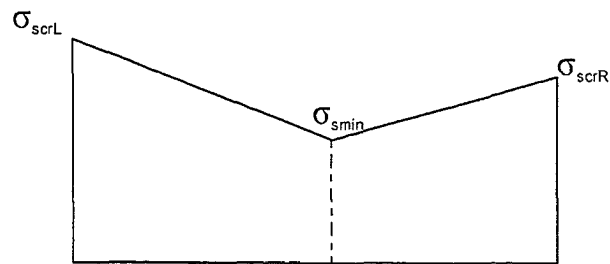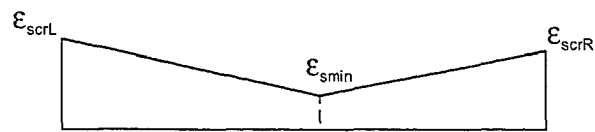
Figure 4.16 Case 4 ($\sigma_{scrL} < f_y$, $\sigma_{scrR} < f_y$, $\sigma_{smin} < f_y$): (a) bond shear; (b) steel stress; and (c) steel strain distribution

135
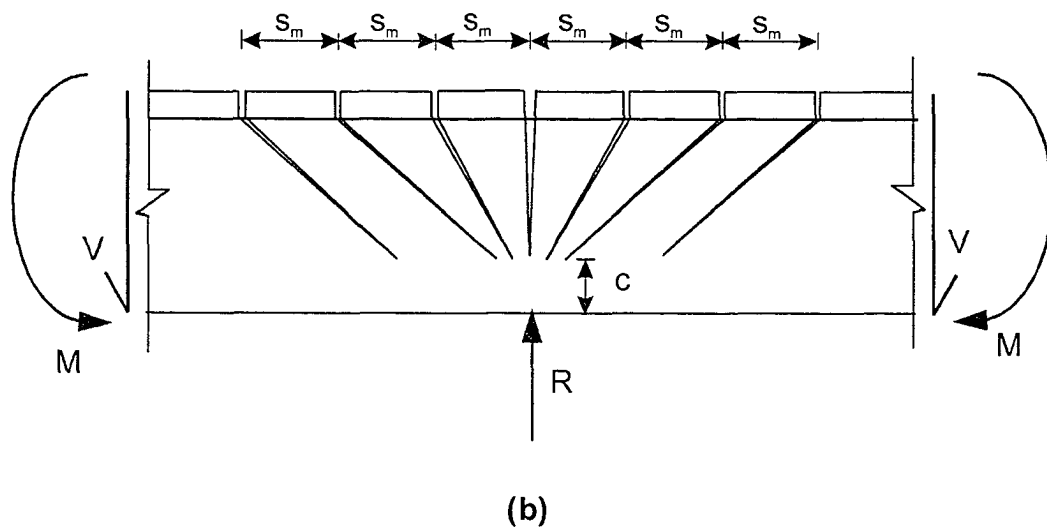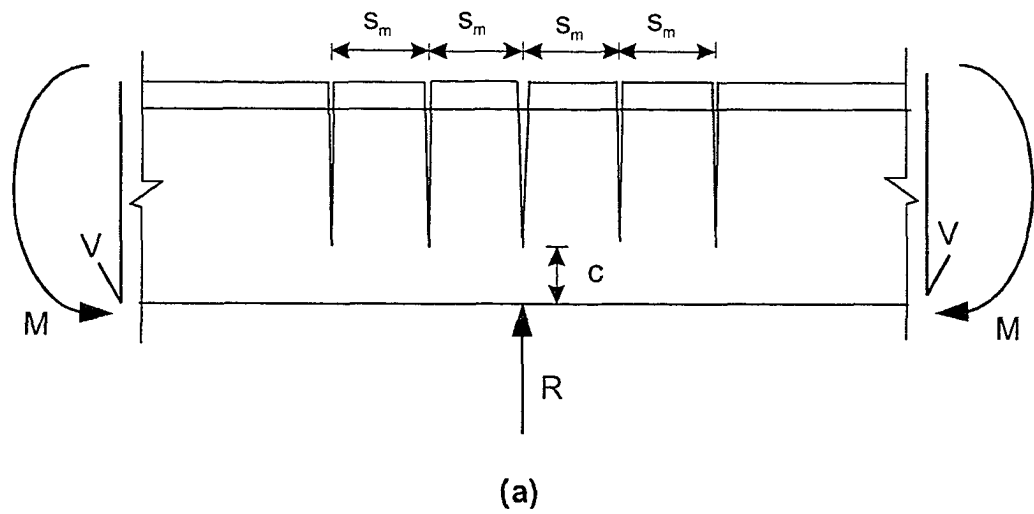
Figure 4.17 Plastic hinges at the interior support of a continuous beam: (a) flexural crack hinge; and (b) shear crack hinge

136
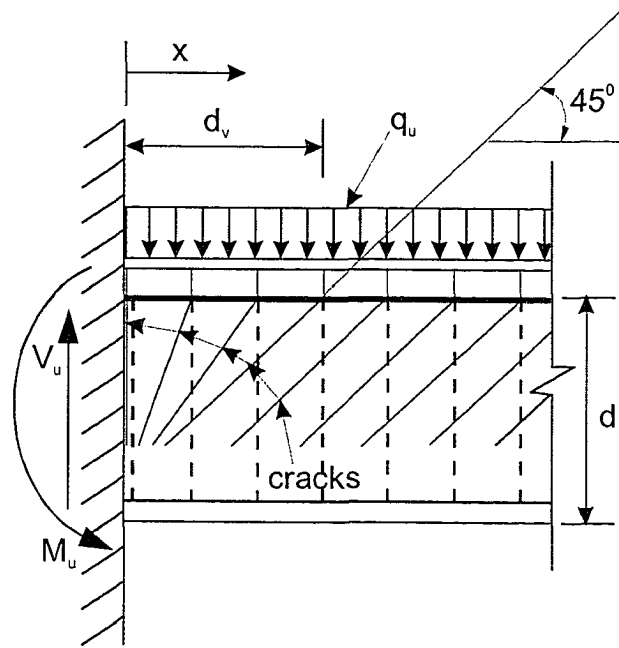
Figure 4.18 Cracking in the vicinity of plastic hinge

137
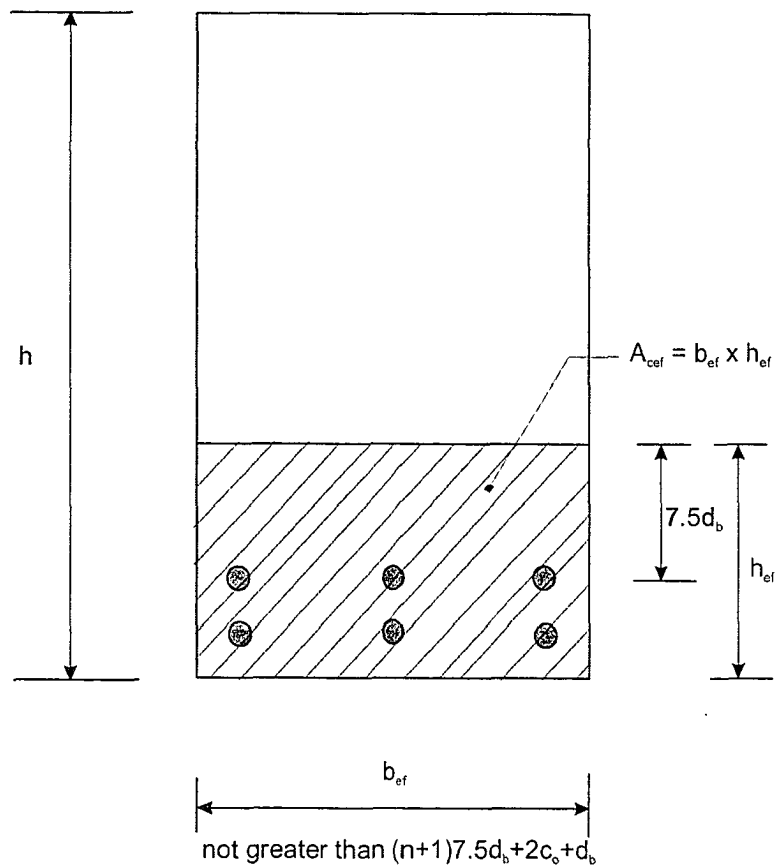
Figure 4.19 Effective area of concrete for computation of crack spacing

ε_{scrL}

ε_{scrR}

ε_{sm}

(c)

$\varepsilon_{sm} = \varepsilon_{cu}[(d/c)-1]$

S_m

steel

neutral axis

ε_{sm}

d-c

d

ϕ

c

M_1

M_2

ε_{cu}

(b)

R

ϕ

$$\frac{S_m}{R} = \frac{\Delta L_c}{c} = \frac{\Delta L_T}{d-c}$$

$$\frac{S_m}{R} = \frac{\varepsilon_{cu} S_m}{c} = \frac{\varepsilon_{sm} S_m}{d-c}$$

$$\frac{1}{R} = \frac{\varepsilon_{cu}}{c} = \frac{\varepsilon_{sm}}{d-c}$$

$$\varepsilon_{sm} = \varepsilon_{cu}\left(\frac{d}{c}-1\right)$$

ΔL_c=change in length of extreme compression fibre

ΔL_T=change in length of tension steel

(a)
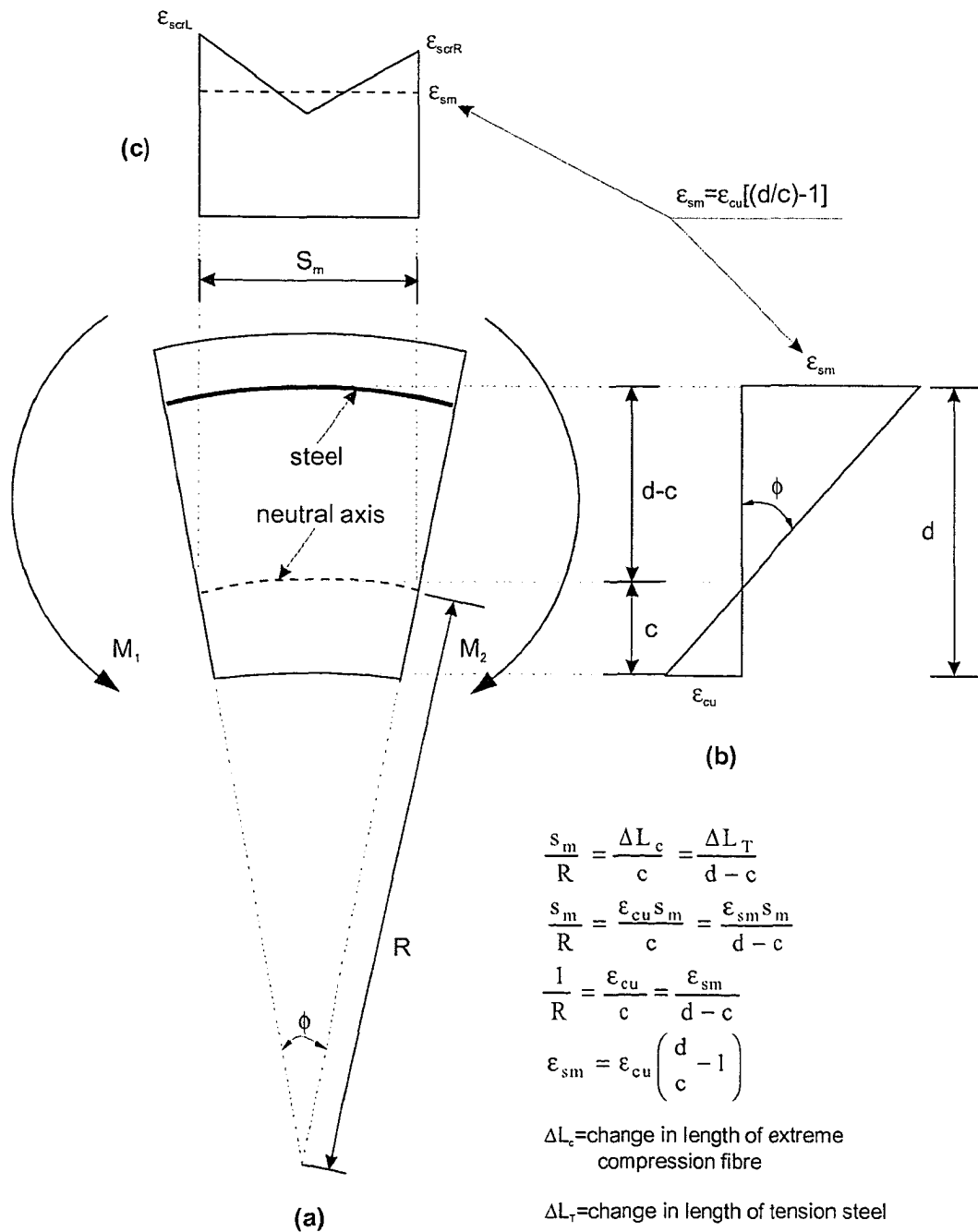
Figure 4.20 Average strain concept used in the model: (a) cracked element with curvature; (b) ε_{sm} from plane-section's analysis; and (c) ε_{sm} from bond model

139
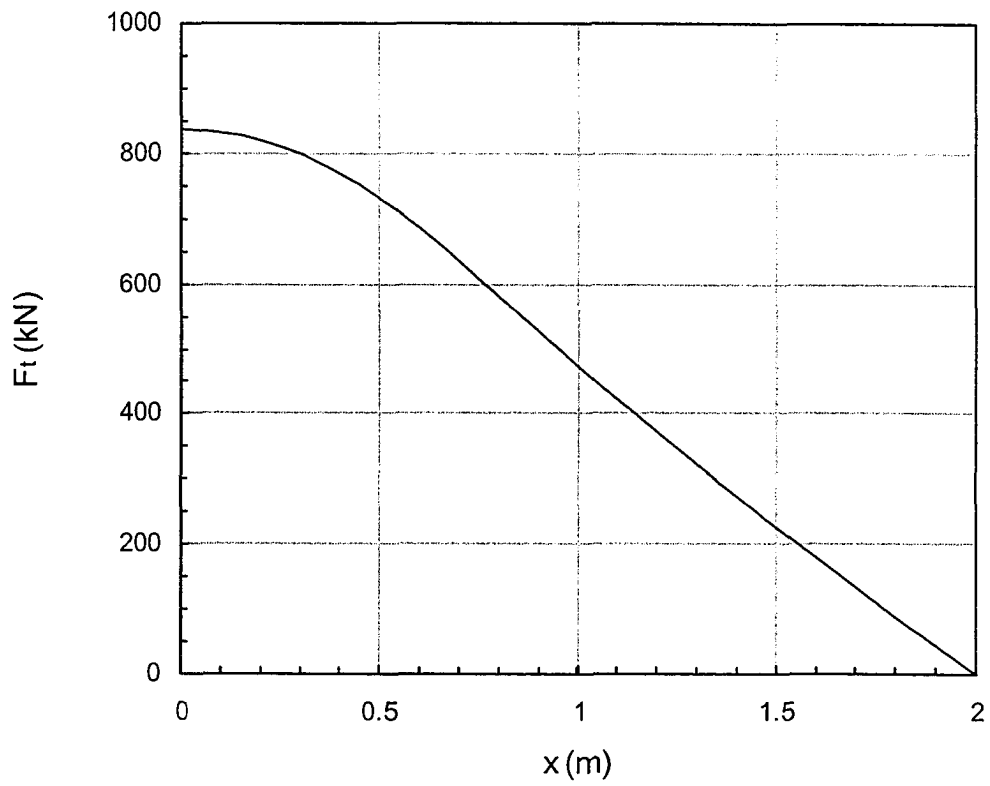
Figure 4.21 Variation of tension chord force
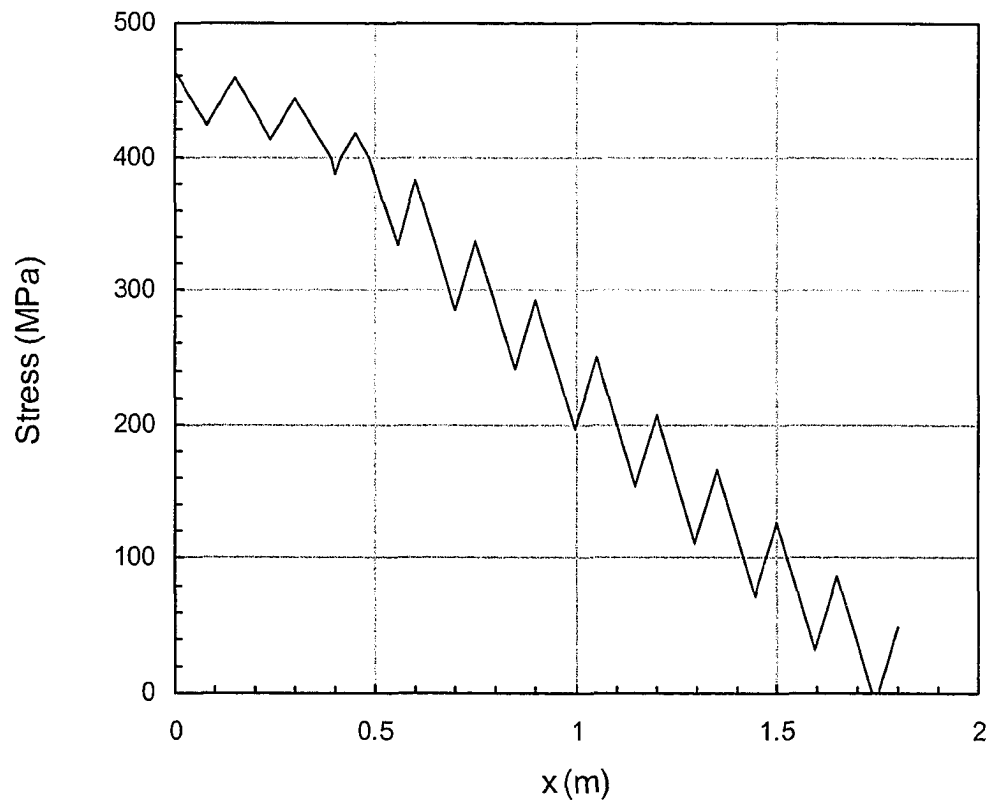
Figure 4.22 Variation of steel stress

140
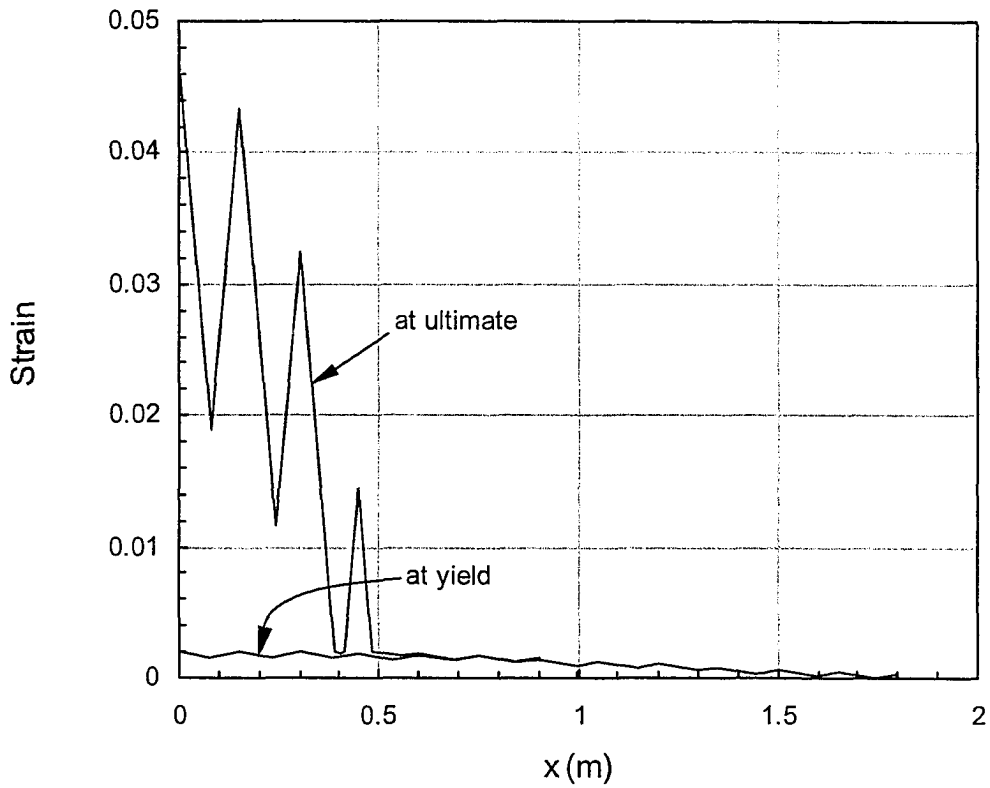
Figure 4.23 Variation of steel strain
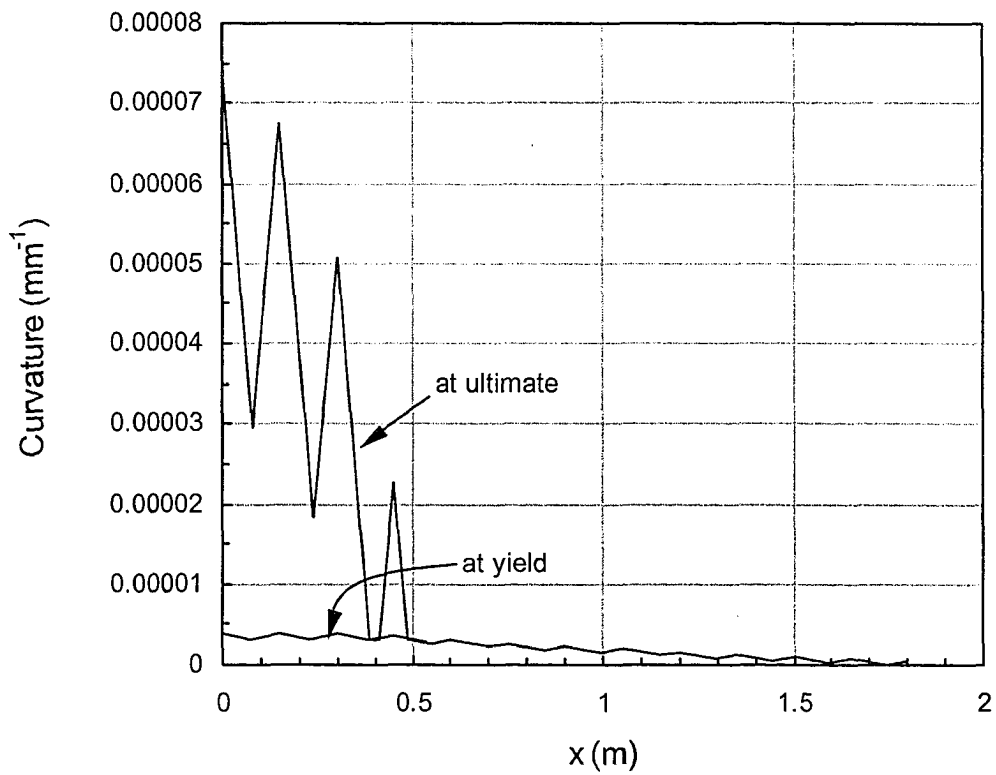
Figure 4.24 Variation of curvature

141
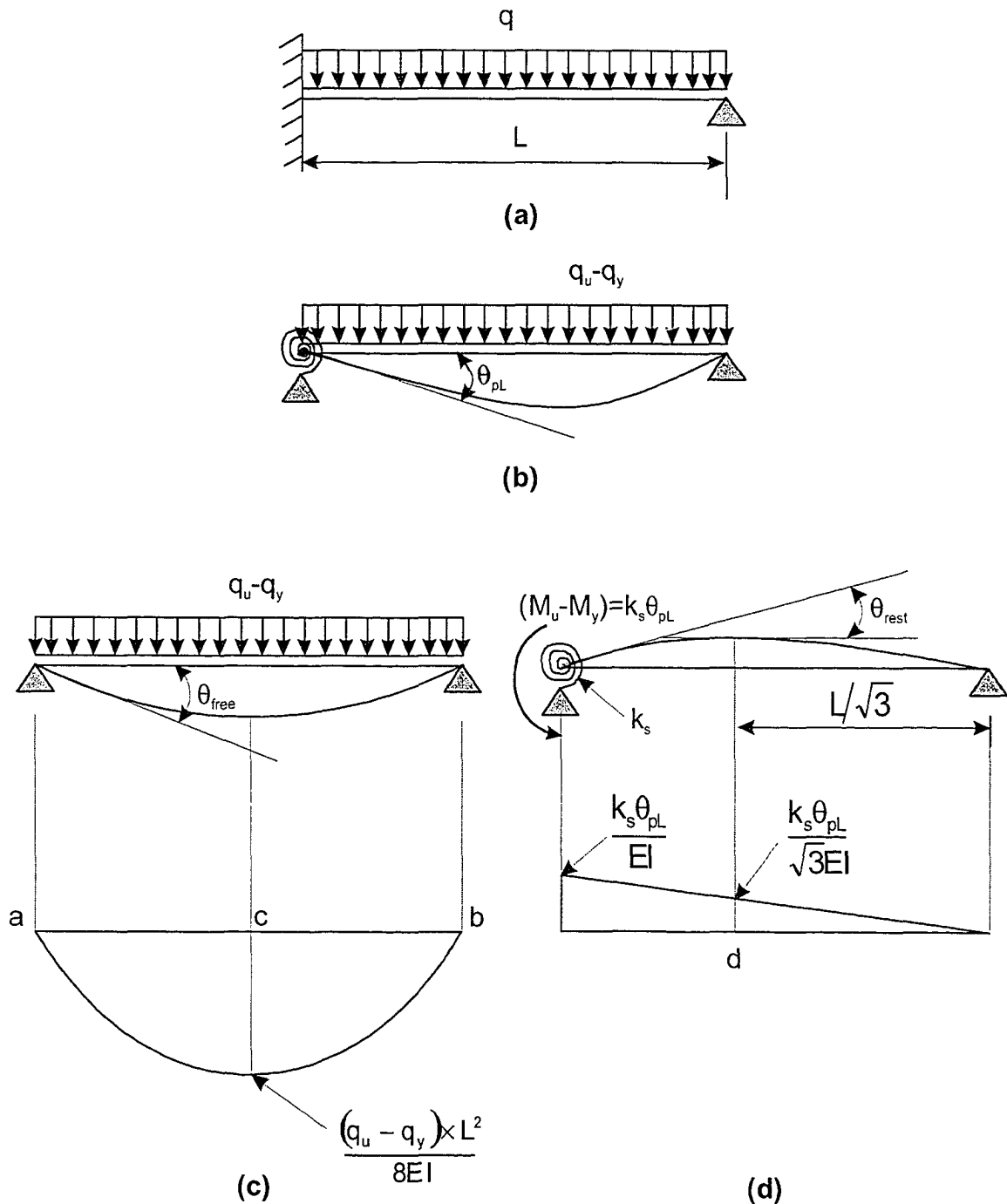
Figure 4.25 Computation of θ_p at support: (a) idealized single span beam; (b) beam and loading after formation of plastic hinge; (c) statical system, loading and M/EI diagram for computing free rotation; and (d) statical system, loading and M/EI diagram for computing restrained rotation due to spring
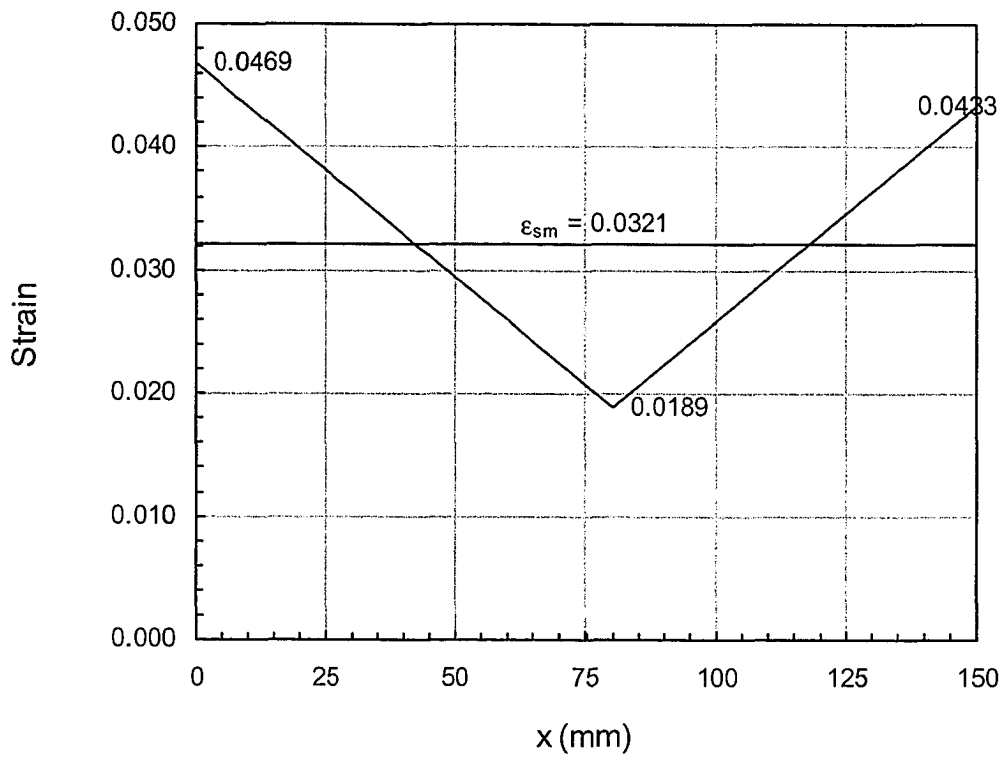
Figure 4.26 Strain variation in first cracked element

143
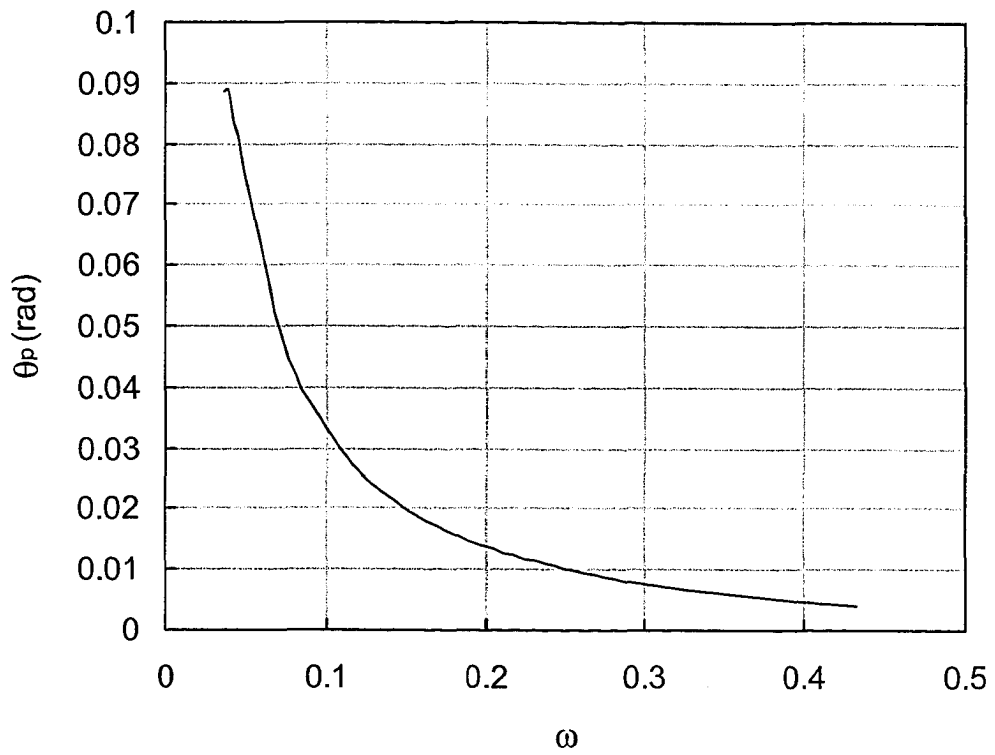
Figure 4.27 Variation of θ_p with mechanical reinforcement index
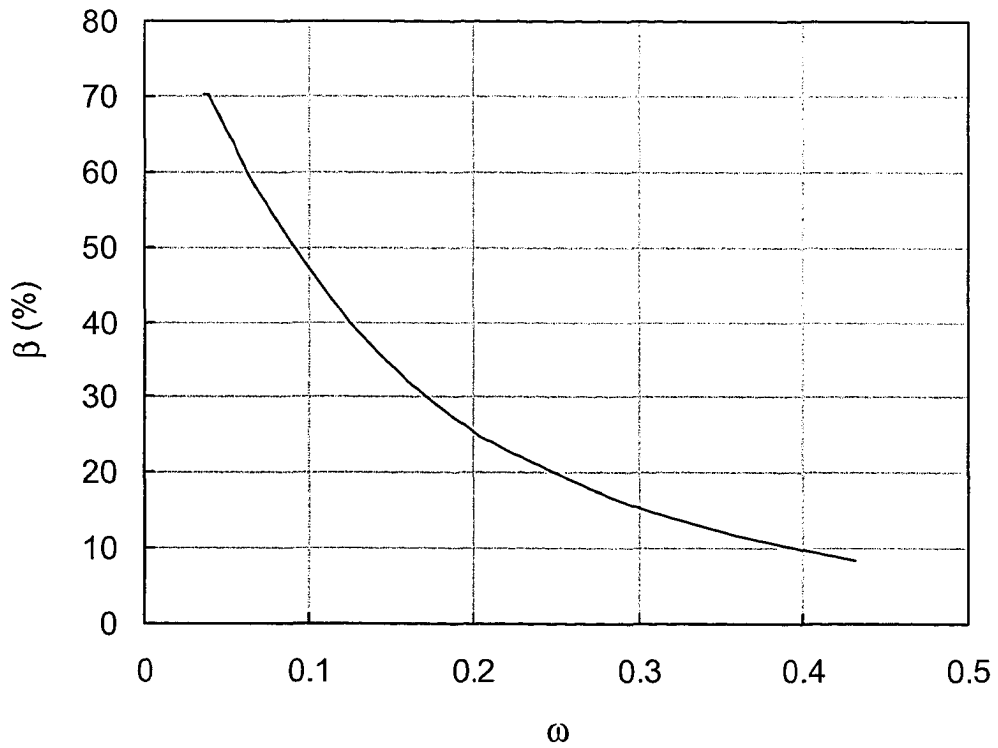
Figure 4.28 Variation of β with mechanical reinforcement index

144
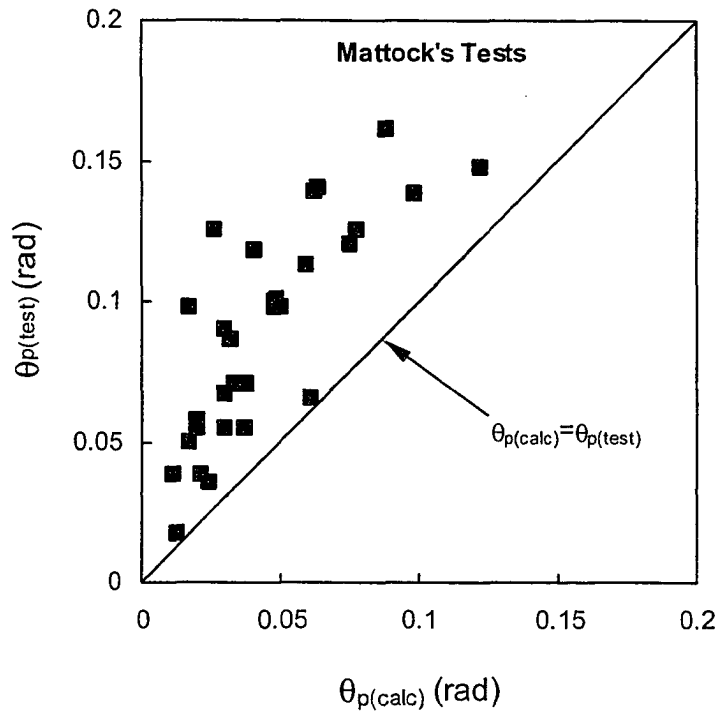
Figure 4.29 Comparison of calculated and measured plastic rotations
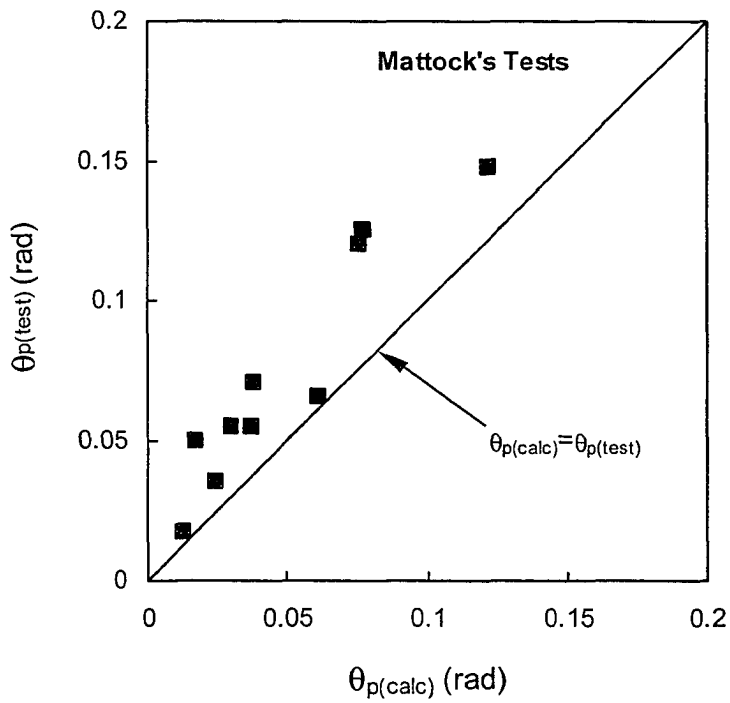
Figure 4.30 Comparison of calculated and measured rotations (Excluding beams With test $\varepsilon_{cu} > 0.01$)

145
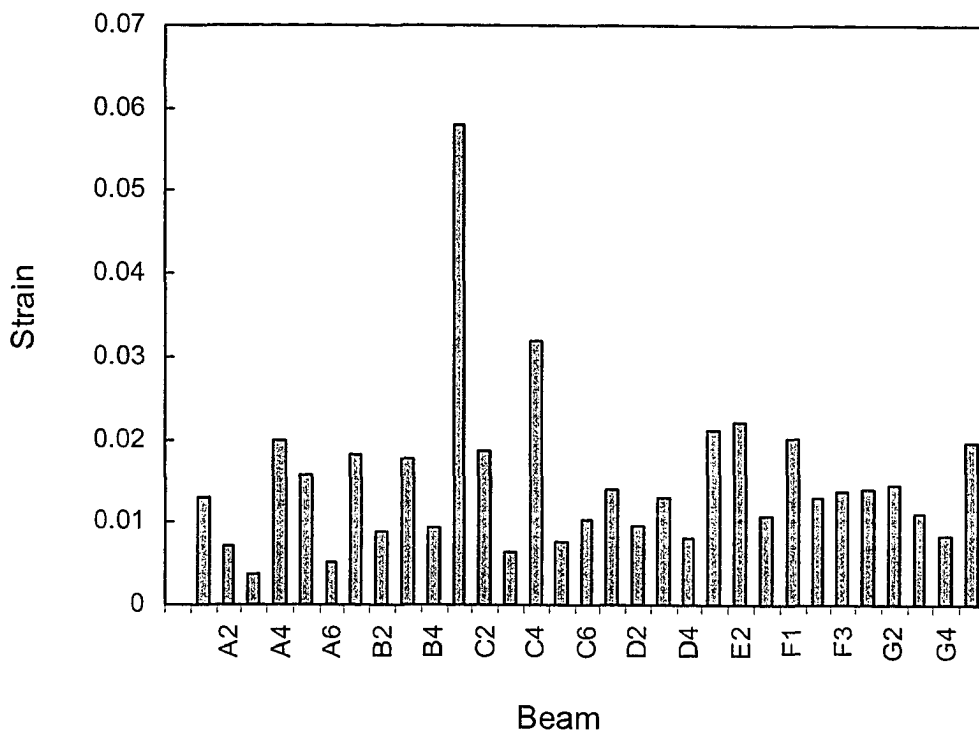
Figure 4.31 Variation of ultimate concrete strain in Mattock's tests

146
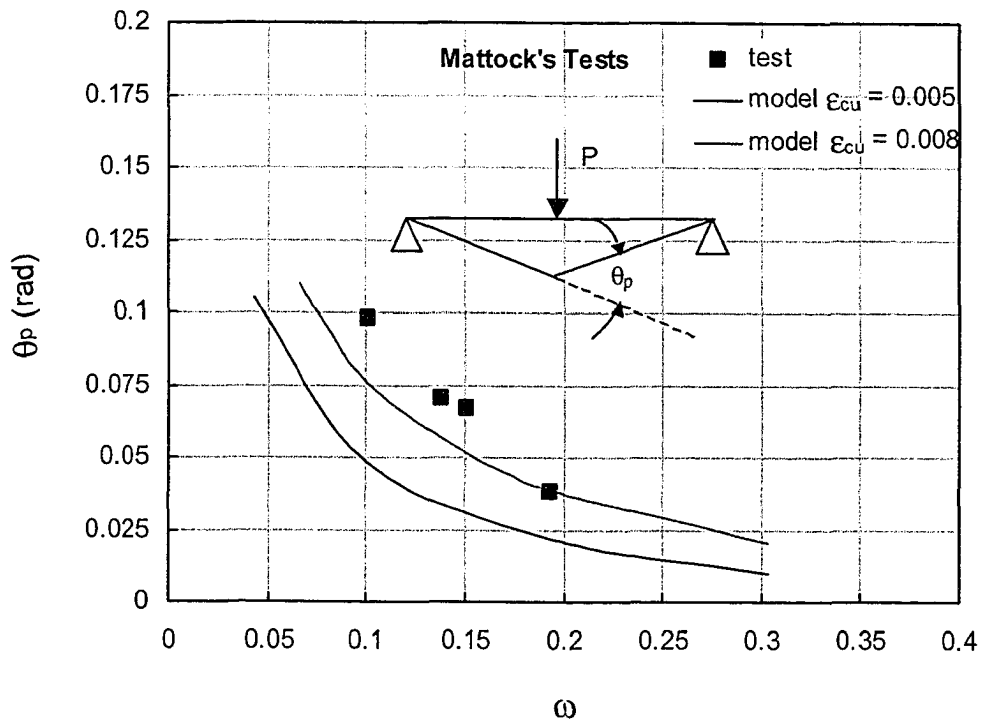
Figure 4.32 Effect of mechanical reinforcement index on
plastic rotation capacity (Group 1, L/d=5.5, ρ_s=0.01019)
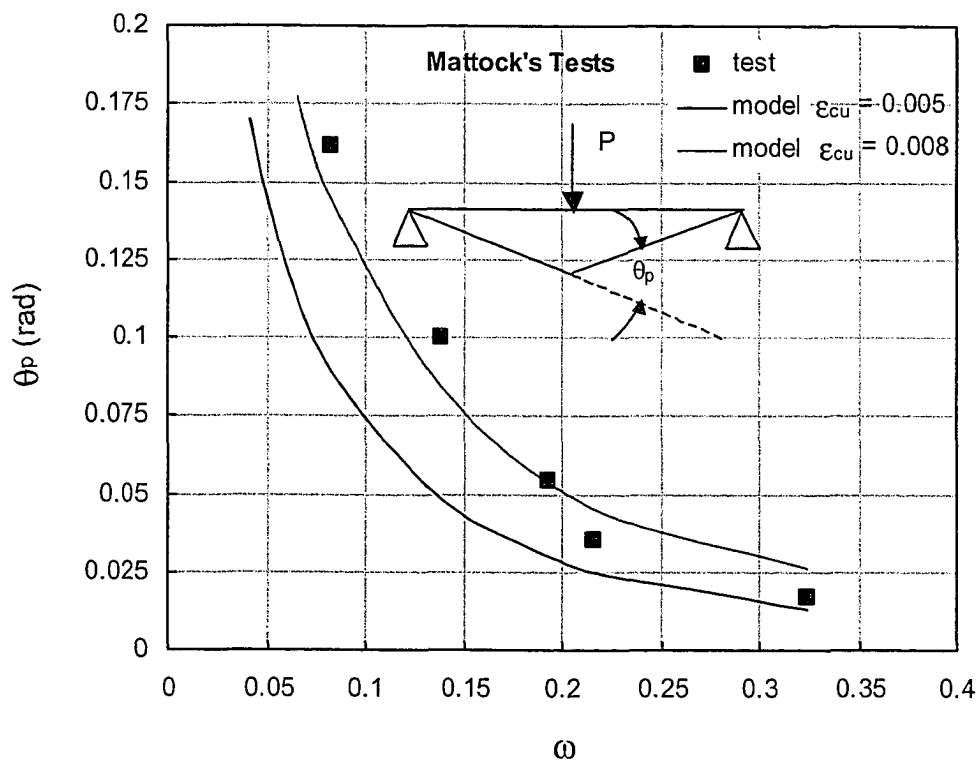
Figure 4.33 Effect of mechanical reinforcement index on
plastic rotation capacity (Group 2, L/d =11, ρ_s=0.01019)

147
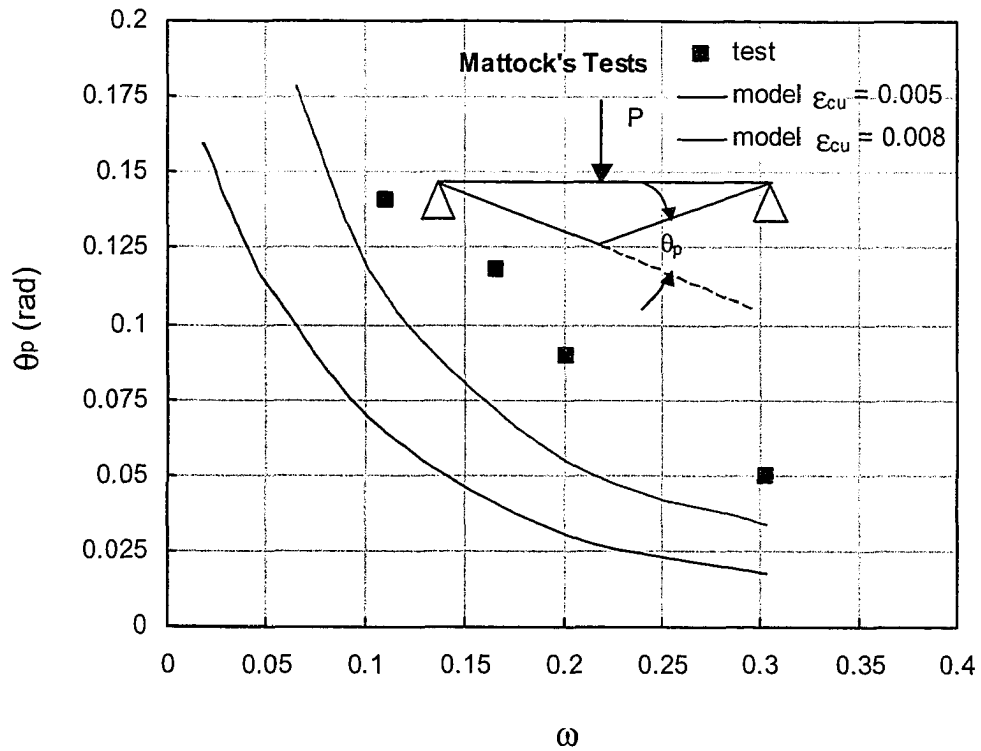
Figure 4.34 Effect of mechanical reinforcement index on
plastic rotation capacity (Group 3, L/d =11, ρ_s=0.01224)
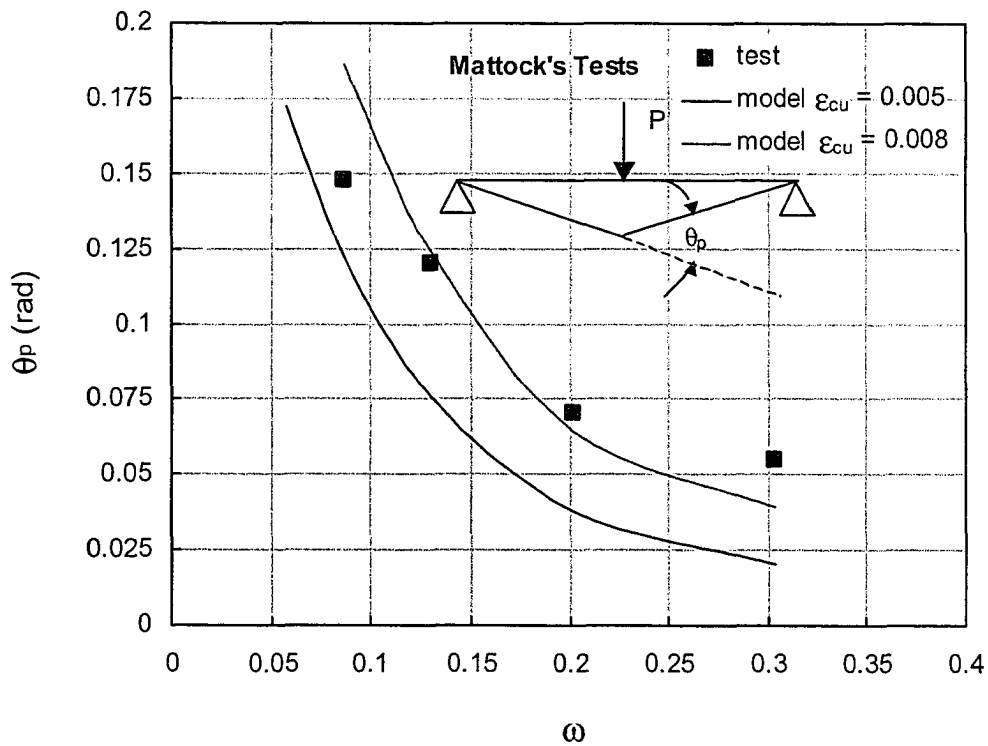
Figure 4.35 Effect of mechanical reinforcement index on
plastic rotation capacity (Group 4, L/d =22, ρ_s=0.005656)

148
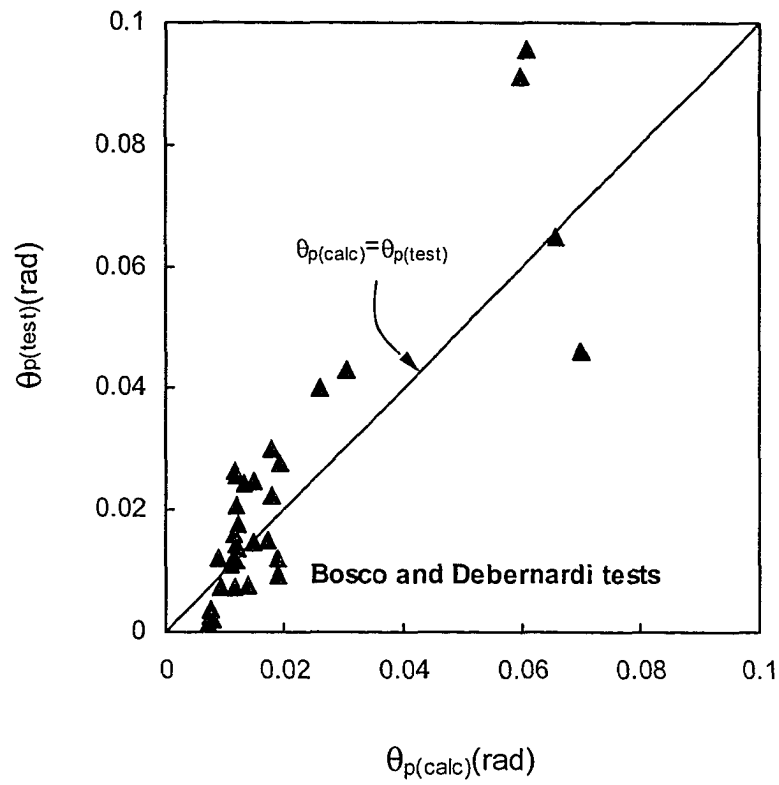
Figure 4.36 Comparison of calculated and measured plastic rotations

149
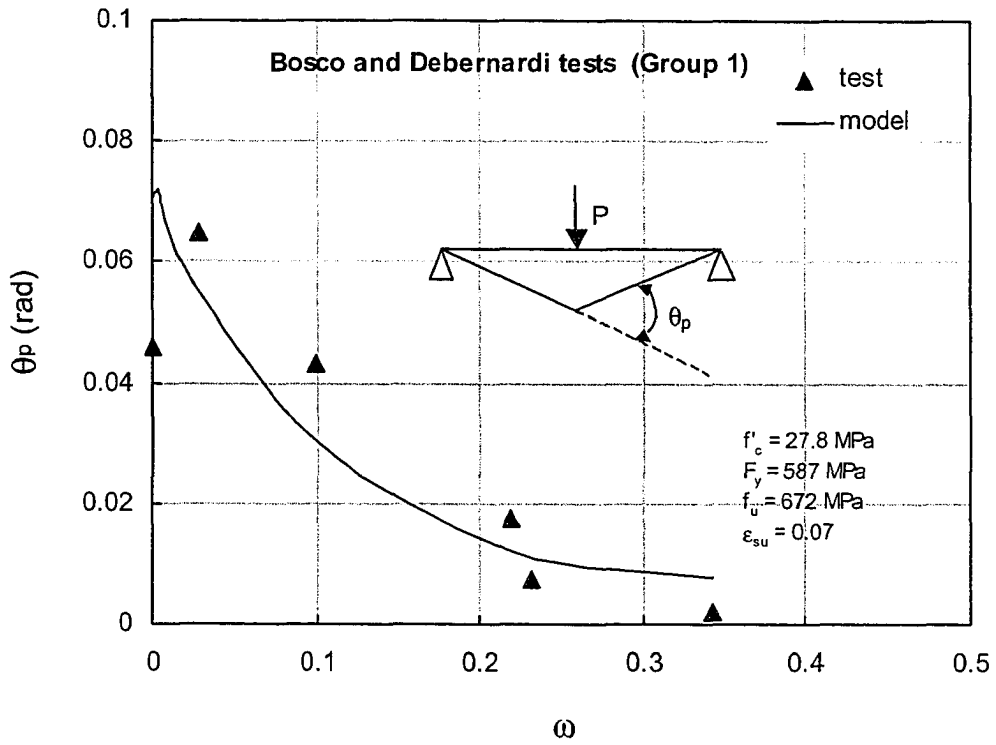
Figure 4.37 Comparison of calculated and measured plastic rotations (group 1)
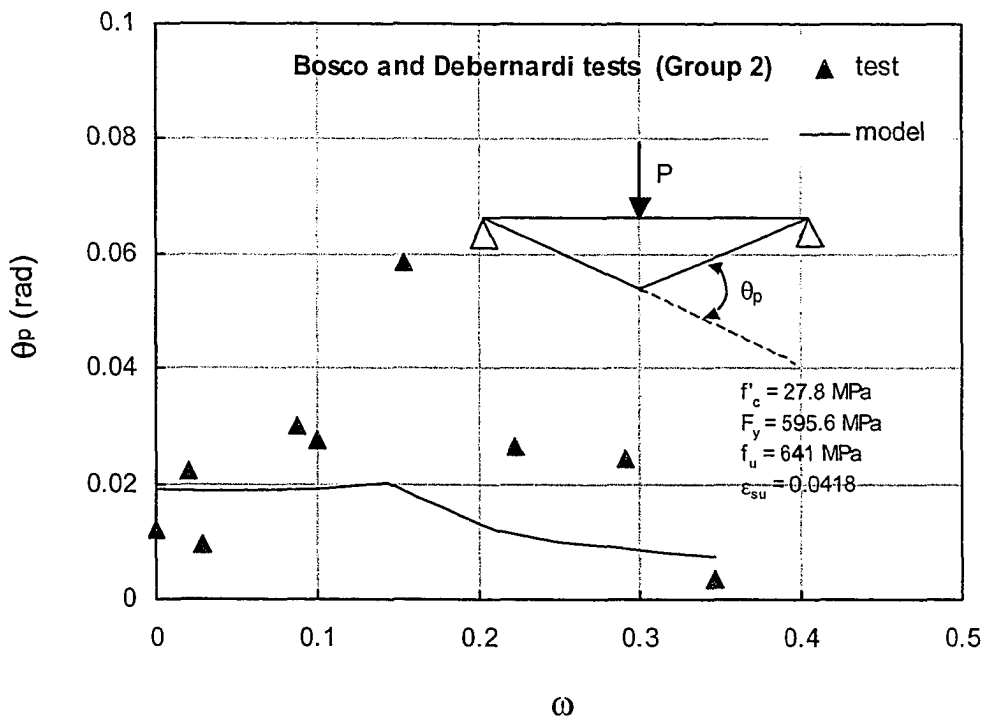
Figure 4.38 Comparison of calculated and measured plastic rotations (group 2)

150
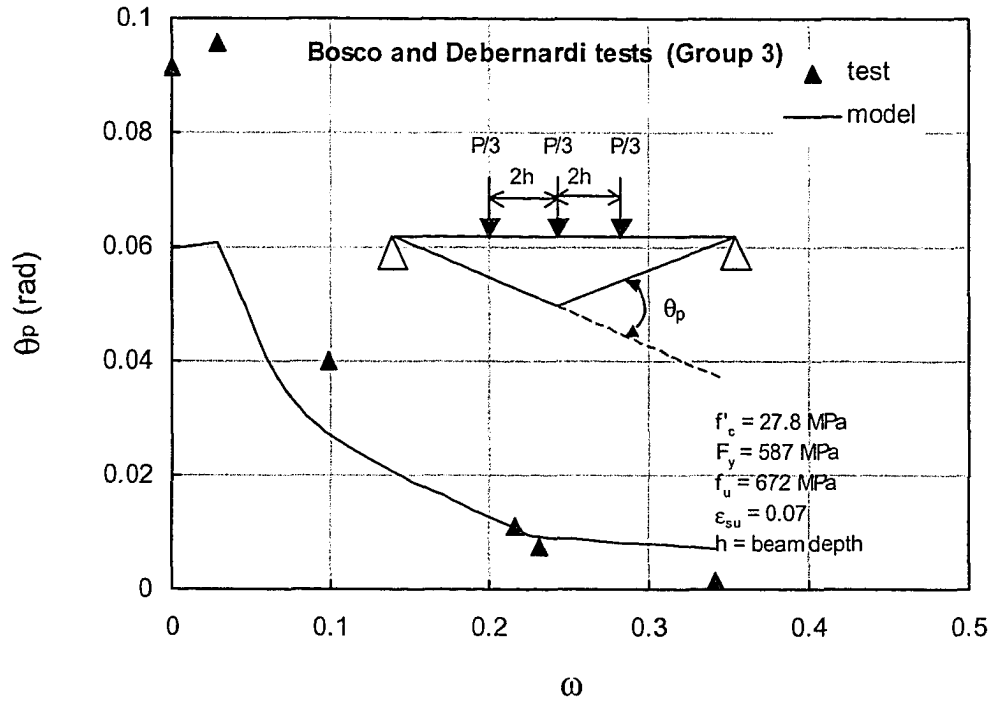
Figure 4.39 Comparison of calculated and measured plastic rotations (group 3)
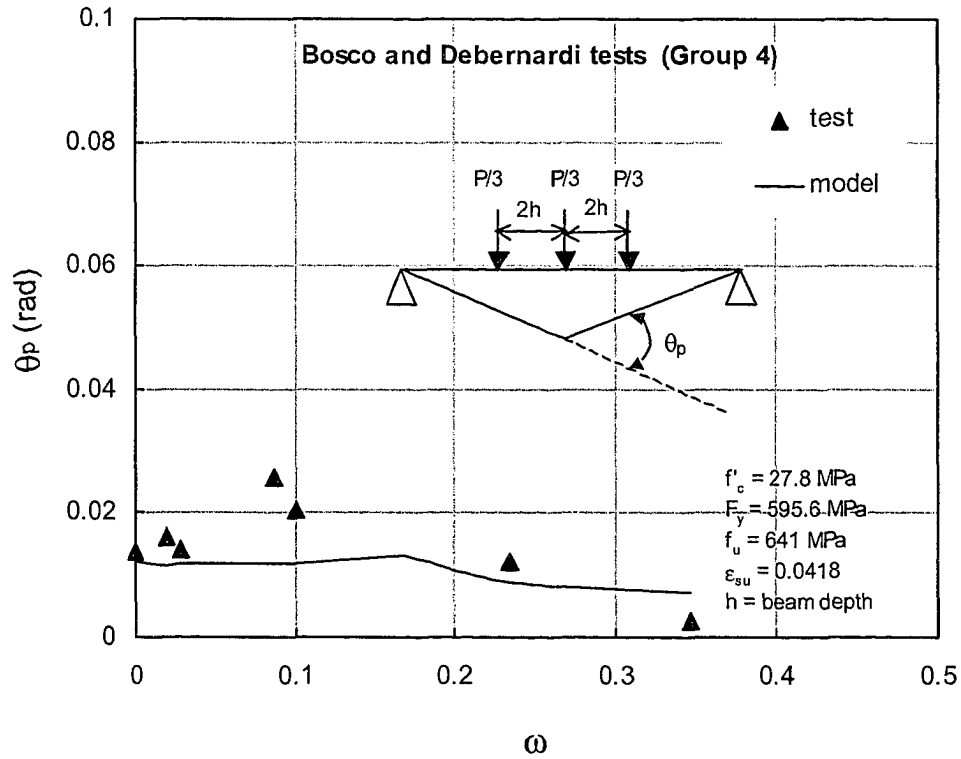
Figure 4.40 Comparison of calculated and measured plastic rotations (group 4)

151

5. PARAMETRIC STUDY[*]

5.1 Introduction

This chapter contains the parametric study of plastic rotation capacity, θ_p, and allowable moment redistribution, β, using the methodology developed in Chapter 4. The study was carried out to understand and quantify the influence of various parameters on θ_p and β. A better understanding of the influence of these parameters, on θ_p and β, will facilitate safe incorporation of moment redistribution in design practice.

Figure 5.1 gives a graphical representation of different standards formulae for allowable moment redistribution. The comparison shows that significant differences exist among various design standards, on the amount of allowable moment redistribution. These standard provisions consider moment redistribution as a section property and relate it to the relative depth of the compression zone at failure (c/d) or the reinforcement index ($\omega = A_s f_y / bd f_c'$) only. Although, c/d or ω can fairly well represent the combined effects of stress-strain characteristics of the materials, the geometry of the cross-section and the amount of tensile and compressive reinforcement, it is an oversimplification to relate moment redistribution to c/d or ω only.

Researchers have proposed empirical relations for computing the plastic rotation capacity and allowable moment redistribution. A summary of the expressions for available plastic rotation is given in Table 2.1.

It appears that none of the proposed formulations for θ_p can be considered completely satisfactory. Most of them are based on tests of simply supported beams with point loads, in which only a limited number of parameters governing the plastic rotation capacity of a member are considered. In particular, the formulations neglect the effects of loading

---

[*] Essentials of this chapter appear as a paper in the proceedings of the Annual Conference of the Canadian Society for Civil Engineering, held in London ON, 2000

152

distribution (uniformly distributed vs. concentrated) and structural configuration (continuous vs. simple spans).

The differences among the various design standards, and their deficiency in incorporating the main parameters, show the necessity for a detailed parametric study to quantify the influence of main parameters on allowable moment redistribution.

5.2 Parametric Study of θ_p and β

A two-span continuous beam is used for the parametric study. The loading on the beam may be either uniform or concentrated. The geometry, cross-section, loading, and material properties of the beam are shown in Fig. 5.2. Only uniformly distributed load case is considered for the study, except for the case where the effect of loading on θ_p and β is considered. Similarly, an ultimate concrete strain, ε_{cu}, of 0.005 is used for the study, except for the case where effect of ε_{cu} on θ_p and β is considered. The plastic rotation capacity and the allowable moment redistribution are evaluated for the interior support of the beam.

A shear crack hinge is assumed for the parametric study except for the case where effects of type of plastic hinge are considered. While most reinforced concrete beams exhibit shear cracking at the ultimate limit state, this may not be true for lightly reinforced concrete beams. For such beams an explicit shear capacity check may be required to confirm the presence of shear cracks. If shear cracks are not present, the recommendations and conclusions regarding allowable moment redistribution do not apply. However, the proposed model is general and can be used to determine the allowable moment redistribution with flexural hinges only.

The plastic rotation capacity and the allowable moment redistribution are expressed as a function of reinforcement index, ω. While not necessarily more correct, it is more convenient to express θ_p and β as a function of ω, rather than the c/d ratio, because ω remains constant for given amount of flexural reinforcement, material properties, and

153

section properties. On the other hand c/d ratio may be affected by other parameters, such as presence of compression and transverse reinforcement. The presence of axial load also influences the c/d ratio.

5.2.1 Effect of reinforcement index and ductility of steel

The reinforcement index and the c/d ratio are the most important parameters affecting plastic rotation capacity and moment redistribution. They incorporate within them the combined effects of material properties, section properties, and the amount of flexural reinforcement. Figure 5.3 and Fig. 5.4 show the effect of ω on θ_p, and β respectively. The curves are drawn for normal ductility steel ($\varepsilon_{su}=0.1$) and low ductility steel ($\varepsilon_{su}=0.04$). Two distinct regions can be identified on these curves: a linear portion, AB, and a hyperbolic portion (BC or DC). In region AB, the rupture of tension steel governs the failure of the section. In region BC or DC, the failure is governed by the crushing of concrete. For normal ductility steel the failure is almost always governed by the crushing of concrete unless the reinforcement provided is less than the minimum required reinforcement. For low ductility steel on the other hand, the failure is governed by the rupture of steel for low to moderate reinforcement ratios, while it is governed by the crushing of concrete in regions of higher reinforcement ratios.

For Canadian reinforcing steel the ultimate strain is high ($\varepsilon_{su} \geq 0.08$ for Grade 400R and $\varepsilon_{su} \geq 0.12$ for Grade 400W) and hence θ_p and β will be governed by the crushing of concrete rather than the rupture of steel.

When the failure is governed by the rupture of steel, θ_p increases slightly with an increase in the value of ω. When the failure is governed by the crushing of concrete, θ_p reduces hyperbolically with increasing ω. The highest point on the curve being the one where the steel ruptures simultaneously as the concrete crushes. The allowable moment redistribution, on the other hand, reduces with the increase in ω, for both steel rupture and concrete crushing failure.

154

The increase in θ_p with ω, in the regions of steel failure (AB), is attributed to the fact that for the same steel strain (strain at rupture), the depth of neutral axis increases with an increase in ω which results in an increase in curvature and hence plastic rotation capacity. In the concrete failure zone, however, the depth of neutral axis increases with an increase in ω while the concrete strain remains constant (ultimate concrete strain ε_{cu}). This results in a decrease in curvature and hence the plastic rotation capacity. The maximum steel strain values at beam failure load also decrease with increasing values of ω.

In the steel failure region AB, as ω increases, both moment capacity of the critical section, M_u, as well as the elastic value of the moment, M_e, increases. However, the increase in M_e is less than the increase in M_u. Since $\beta=(M_e-M_u/M_e)*100$, the net result is a reduction in the value of β.

It is clear from Fig. 5.3 and Fig. 5.4 that θ_p and β are very limited for low ductility steel, especially in the regions of low reinforcement ratios. For example for the particular example considered here, at $\omega=0.05$, θ_p is 0.021 radian for low ductility steel as opposed to 0.073 radian for normal ductility steel.

The Canadian standard (CSA A23.3-94) allows a maximum moment redistribution of 20% for c/d ratios of 0.2 or less. In the particular example considered here, moment redistribution as high as 66% can be allowed for low values of c/d. For c/d ratio of 0.2, more than 30% moment redistribution can be allowed in this particular example. It is to be noted, however, that the plastic rotation capacity and the allowable moment redistribution depends upon a number of other factors and hence could vary significantly for the same value of ω or c/d.

5.2.2 Effect of beam slenderness

Figure 5.5 and Fig. 5.6 show the influence of beam slenderness (L/d) on plastic rotation capacity and allowable moment redistribution respectively. The effective depth of the

155

beam is kept constant at 740 mm while the span length is varied from 4.5 m to 16 m (L/d = 6 to L/d = 21.6).

Figure 5.5 shows that the plastic rotation capacity increases, almost linearly, with increasing slenderness ratio. The effect is most significant at low values of ω and reduces as ω increases. This can be explained if we consider the deformations of the tension chord. For slender beams the yielding of steel is spread over a larger length as compared to the shorter beams. For example for ω=0.107, the plastic hinge length increases from 335 mm for L/d = 8 to 605 mm for L/d = 20. This increase in the plastic hinge length increases the plastic rotation capacity. The effect of beam slenderness on plastic hinge length, however, reduces with an increase in ω. Intuitively, most designers know that thin (slab like) lightly reinforced members can plastically deform a lot.

The effect of beam slenderness on allowable moment redistribution is counter-intuitive. Figure 5.6 shows that the allowable moment redistribution increases with a decrease in beam slenderness. This can be explained by the fact that for a given depth and reinforcement index, the nominal moment of resistance M_u remains almost constant. The beam failure load q_u reduces with the increase in L/d and although length of the beam increases the net result is a reduction in the elastic moment M_e.

It is well known that stiffer members (low L/d) experience larger changes in bending moments due to differential support settlements than do slender members. Similarly for stiff members small plastic hinge rotations produce large redistributions in moments. As one reduces L/d, the plastic rotation demand reduces faster than the plastic rotation capacity. Thus stiff (low L/d) members have higher allowable moment redistribution.

As an example of the influence of L/d on θ_p, for ω=0.144, θ_p increases from 0.0143 radian for L/d=6 to 0.0243 radian for L/d=21.6, an increase of 70%. Similarly for the same ω, β increases from 32% for L/d=21.6 to 50% for L/d=6, an increase of about 56%.

156

5.2.3 Effect of ultimate concrete strain

Experimental evidence (Mattock, 1964) has shown that the strain in concrete at ultimate, ε_{cu}, is an important parameter affecting plastic rotation capacity and allowable moment redistribution. This is shown in Fig. 5.7 and Fig. 5.8 by the slope of θ_p and β curves. Both θ_p and β increase almost proportionately with an increase in ε_{cu}.

As an example of the effect of ultimate concrete strain on θ_p and β, for $\omega=0.144$, θ_p increases from 0.013 radians for $\varepsilon_{cu}=0.0035$ to 0.035 radians for $\varepsilon_{cu}=0.008$, an increase of 169%. Similarly for the same ω, β increases from 26% for $\varepsilon_{cu}=0.0035$ to 47% for $\varepsilon_{cu}=0.008$, an increase of 74%.

The significant effect of ε_{cu} is due to the fact that an increase in ε_{cu} mobilises higher strains in tension steel, thereby increasing tension chord deformations and hence the plastic rotation capacity.

5.2.4 Effect of compression reinforcement

The effect of compression reinforcement on plastic rotation capacity and allowable moment redistribution is shown in Fig. 5.9 and Fig. 5.10. Both θ_p and β increase with an increase in the mechanical compression reinforcement index. The increase in compression reinforcement reduces the c/d ratio and mobilises greater strains in tension steel that leads to larger deformations of the tension chord and an increase in plastic rotation capacity and higher amounts of moment redistribution. Table 5.3 provide such details for $\omega=0.144$. For $\omega=0.144$, there is a 93% increase in plastic rotation capacity from $\omega_c=0$ to $\omega_c=0.1444$. Similarly there is about 39% increase in allowable moment redistribution from $\omega_c=0$ to $\omega_c=0.1444$.

For flexural members, the ductility of support sections is usually more critical than that of span sections, because span sections very often act as T-sections, so that their ductility is improved considerably by the inclusion of flange areas. The amount of positive moment steel in a typical flexural member is about 70 to 80% of the tension steel provided for

157

negative moments. If only half of this positive moment steel is continued through the support, that steel would provide enough compression reinforcement at the support to significantly increase the plastic rotation capacity and allowable moment redistribution.

5.2.5 Effect of concrete confinement

Transverse reinforcement in reinforced concrete beams provides confinement of the compression zone and increases the ductility of concrete in that region. Figure 5.11 and Fig. 5.12 illustrate the effect of confinement on θ_p and β respectively. The degree of confinement is expressed as a volumetric ratio of stirrups, $\rho_v=2(b_s+h_s)A_{vs}/b_{so}h_{so}s$, where b_s and h_s are the centre to centre width and height of the stirrup respectively, b_{so} and h_{so} are the width and height to the outside of stirrup respectively, A_{vs} is the area of one leg of stirrup, and s is the spacing of stirrups. The volumetric ratio of stirrups is varied from 0.003872 (No. 10-2 legged stirrups at 300 c/c) to 0.02954 (No. 15-2 legged stirrups at 75 c/c).

Both θ_p and β increase with an increase in the amount of transverse reinforcement. The plastic rotation capacity and allowable moment redistribution increase with increasing confinement

Figure 5.13 shows the effect of confinement on concrete stress-strain curve. The slope of the falling branch of the stress-strain curve of concrete reduces with increasing amounts of confinement. This leads to a reduction in the depth of the compression block, as shown in Fig. 5.14, and an increase in the steel strain and beam failure load. The net result is an increase in the plastic rotation capacity and allowable moment redistribution. Because the base case in this parametric study, limited ε_{cu} to 0.005 the beneficial effect of ρ_v on increasing ε_{cu} are not reflected in Figs 5.13 and 5.14.

As an example of the effect of confinement, at $\omega=0.144$, θ_p varies from 0.018 for $\rho_v=0.00387$ to 0.029 for $\rho_v=0.0295$, an increase of 61%. Similarly, for the same ω, β varies from 32.5% for $\rho_v=0.00387$ to 42% for $\rho_v=0.0295$, an increase of about 31%.

158

5.2.6 Effect of V_s/V_u

The effect of the ratio of shear carried by stirrups to the total shear, V_s/V_u, on the tension chord force, F_t, is shown in Fig. 5.15. The yielding is spread to a larger region for beams with small V_s/V_u ratio. Thus concrete beams that require little or no stirrups have more moment redistribution capacity than those requiring large amounts of shear reinforcement.

Figure 5.16 and Fig. 5.17 show the effect of V_s/V_u ratio on θ_p and β. Both θ_p and β increase with a decrease in the ratio V_s/V_u. As an example, for $\omega=0.144$, θ_p increases from 0.0212 radian for $V_s/V_u = 1$ to 0.035 radian for $V_s/V_u = 0.25$, a difference of 65%. Similarly, for the same ω, β increases from 36% for $V_s/V_u = 1$ to 48% for $V_s/V_u = 0.25$, a difference of about 33%. The plastic hinge length increases from 520 mm for $V_s/V_u = 1$ to 725 mm for $V_s/V_u = 0.25$.

5.2.7 Effect of type of hinge

Two types of plastic hinges can form at a critical section, the flexure crack hinge, and the shear crack hinge. The shear crack hinge contains inclined cracks that increase the length over which the steel has yielded and thus increase the plastic hinge length. In some cases, the shear might not be enough to cause cracking of concrete. In this case only flexure crack hinge is formed. The flexure crack hinge extends only over one or two cracks and the corresponding rotation capacity is quite low as compared to the shear crack hinge.

Figure 5.18 shows the effect of the type of hinge on the distribution of tension chord force. It is clear that the tension chord force is increased and the yielding is spread over a much larger region, in case of shear crack hinge.

Figure 5.19 and Fig. 5.20 show the effect of the type of hinge on plastic rotation capacity and allowable moment redistribution respectively. As expected, θ_p and β are much larger in the case of a shear crack hinge than in case of a flexure crack hinge. For example, for $\omega=0.144$, θ_p is 0.0212 radian for shear crack hinge as opposed to 0.0077 radian for

159

flexure crack hinge, a difference of 175%. Similarly, for the same ω, β is 36% for the shear crack hinge as opposed to 17% for the flexure crack hinge, a difference of 112%. The plastic hinge length for the shear crack hinge is 520 mm as opposed to 250 mm for the flexure crack hinge, in this particular example (ω=0.144).

5.2.8 Effect of axial load

Figure 5.21 and Fig. 5.22 show the effect of axial load on plastic rotation capacity and allowable moment redistribution respectively. Since, in general, flexural members carry small axial loads, the ratio P_u/A_g is varied between -1 MPa (tension) to $+1$ MPa (compression) only. A plastic hinge is usually avoided in compression members and as such these are not considered in the study.

A compressive axial load reduces θ_p and β while a tensile axial load increases θ_p and β. This is because θ_p and β benefit from the steel elongation. The compressive load reduces the steel strains and hence θ_p and β, while the tensile load increases the steel strains and hence θ_p and β.

5.2.9 Effect of load type

Figure 5.23 and Fig. 5.24 show the effect of the type of loading on plastic rotation capacity and allowable moment redistribution respectively. Three load cases were investigated, as shown in Fig. 5.2. These include, a uniformly distributed load on each span, a concentrated load at the centre of each span, and concentrated loads at third points of each span. It is found that the type of loading has no significant effect on θ_p or β. This is attributed to the fact that the shape of the moment diagram in the vicinity of the plastic hinge does not change much from one load case to the other, while the other parameters remain unchanged.

5.3 Comparison of Model Limits with Code Limits

Figure 5.25 and Fig. 5.26 show the upper and lower limits of θ_p and β respectively, obtained from the theoretical model. For θ_p, the lower limit is obtained for a beam with a

160

slenderness ratio of 6 and a volumetric ratio of stirrups of 0.0038, while the upper limit is obtained for a slenderness ratio of 21 and volumetric ratio of stirrups of 0.0295. For β, the lower limit is obtained for a beam with a slenderness ratio of 21, and a volumetric ratio of stirrups of 0.0038, while the upper limit is obtained for a slenderness ratio of 6, and a volumetric ratio of stirrups of 0.0295. The ultimate concrete strain is taken as 0.005 for both cases. A shear hinge is assumed in the analysis and the ratio V_s/V_u is taken as 1. The effect of axial load is not taken into account. The ω considered is the net ω and hence takes into account, the effect of any compression reinforcement. Figure 5.26 shows that there is a significant difference in the minimum and maximum allowable limits of moment redistribution. For example for $\omega = 0.2$, the lower limit of β is 20% while the upper limit is 45%.

Figure 5.27 provides a comparison of different code limits for β with the model limits. Compared to the model limits, the British standard (BS8110-85) can be unconservative for moderate to high values of ω. Similarly, German standard (DIN 1045-78) is unconservative for values of ω greater than 0.25. The CEB Model Code limit is slightly higher than the model lower limit for the middle range of ω. The American standard (ACI 318-95) limit is highly conservative.

Figure 5.28 provides an exclusive comparison of CSA A23.3-94 limits for β with the model limits. The code limit is conservative compared to the lower limit of the model and extremely conservative compared to the upper limit of the model. For smaller values of ω (less than 0.15), the code is very conservative even for the lower limit of the model. For example, the code restricts the allowable moment redistribution to 20% at $c/d = 0.2$ ($\omega = 0.106$). For the same value of c/d, the lower limit of the model would allow almost 40% moment redistribution. In general even the lower limit of the model allows almost twice as much moment redistribution as that allowed by the code.

161

5.4 Empirical Equations for β Based on Ductility

Due to interaction of all the influencing parameters, determination of β is a complex problem. While a complex ductility model is more appropriate for use as an analytical research tool, it may not be entirely suitable for routine applications where one needs a quick estimate of allowable moment redistribution. A set of β curves or empirical equations, encompassing the influence of major parameters provide an alternative to the ductility model. The data from the parametric study is used to obtain empirical expressions for the allowable moment redistribution. Although nine independent variables were considered in the parametric study, including all these parameters in the regression analysis will lead to a complex formulation not suitable for practical use. The strategy used considers the influence of a few important variables while assuming conservative values for the rest. In the following paragraphs, each variable is looked upon, on case-by-case bases, to decide which variables to include as independent variables and which variables to assign conservative constant values.

1. The reinforcement index is the most important parameters affecting moment redistribution. It incorporates the combined effects of material properties, section properties, and the amount of flexural reinforcement. It must be included as an independent variable in regression analysis.

2. Beam slenderness (L/d) is another major factor that considers the effects of structure geometry on allowable moment redistribution. It will be included as independent variable in regression analysis.

3. Concrete ultimate strain value can be kept constant at 0.005, in line with the assumptions used in this thesis.

4. Compression reinforcement is very effective in increasing the plastic rotation capacity and allowable moment redistribution. Its effect can be included within ω by using ω_{eff} as $\left(A_s - A_s'\right)f_y/bdf_c'$; where A_s' is the compression reinforcement.

162

5. The confinement of concrete by transverse reinforcement improves the ductility of concrete. Using a lower bound value of volumetric ratio of stirrups, as 0.0038, will provide a conservative estimate of β.

6. The ratio of the shear stress carried by the stirrups to the total shear stress V_s/V_u can be assumed as unity. This will provide a conservative estimate of β.

7. The type of plastic hinge has a major influence on the plastic rotation capacity and allowable moment redistribution. Usually the magnitude of shear at the support is high enough to form diagonal cracks (ie $V_f \geq V_c$) and hence a shear plastic hinge can be assumed for all practical purposes.

8. The effects of axial load can be neglected for flexural members.

9. The type of loading has insignificant influence on the allowable moment redistribution and hence its effects are not included.

From above, it is concluded that ω and L/d are the two most important variables that must be included in any expression for allowable moment redistribution. The rest can be included as constants with values that provide conservative estimate of allowable moment redistribution.

There are two options that one can look at to determine the relationship between β and the two independent variables ω and L/d. Option one would be to perform non-linear regression analysis to obtain a single equation, using both ω and L/d as independent variables. Option 2 would be to obtain a set of equations, relating β to ω for different values of L/d. The second option is adopted here as it will provide a simple relationship for calculating β and will always err on the conservative side.

163

Based on the above discussion, β vs ω curves are generated for a range of L/d values from 6 to 21 as shown in Fig. 5.29. The graph shows that β reduces with increasing L/d, the rate of reduction being more pronounced in the lower range of L/d. For example, reduction in the value of β from L/d = 6 to L/d = 12.5 is more than twice as much as that from L/d = 12.5 to L/d = 21. Having noted that, following five values of L/d are selected for providing a set of β curves and equations; 6, 8.5, 12.5, 16 and 21. For obvious reasons, a tighter spread of values is considered in the lower range of L/d than the upper range. Figures 5.30 through 5.34 show the model data points and the regression curves for each individual value of L/d. The curves are second-degree polynomial and provide excellent fit to the model data. The following equations are obtained for the allowable moment redistribution:

Case 1: L/d $\leq$ 6 (Fig. 5.30)

$$\beta = 528\omega^2 - 382\omega + 92 \tag{5.1}$$

Case 2: 6 < L/d $\leq$ 8.5 (Fig. 5.31)

$$\beta = 622\omega^2 - 417\omega + 89 \tag{5.2}$$

Case3: 8.5 < L/d $\leq$ 12.5 (Fig. 5.32)

$$\beta = 651\omega^2 - 425\omega + 84 \tag{5.3}$$

Case 4: 12.5 < L/d $\leq$ 16 (Fig. 5.33)

$$\beta = 700\omega^2 - 439\omega + 82 \tag{5.4}$$

164

Case 5: 16 < L/d ≤ 21 (Fig. 5.34)

$$\beta = 715\omega^2 - 439\omega + 78 \qquad\qquad [5.5]$$

The above equations or the β curves in Figures 5.30 to 5.34 can be used to establish the limits of moment redistribution, based on the ultimate limit-state. These equations can be useful in the strength evaluation of existing structures when the structural collapse, rather than serviceability, is a prime concern. For design of new structures, the serviceability limit must be evaluated before using these equations. Serviceability limit-state is a topic of the next Chapter.

5.5 Summary and Conclusions

A parametric study is done to understand the influence of various parameters on plastic rotation capacity, θ_p, and allowable moment redistribution, β. The study reveals that in addition to ω, θ_p and β depend upon several other parameters. The most important among these are the type of plastic hinge, ultimate concrete strain, beam slenderness, amount of compression reinforcement, amount of transverse reinforcement, and the ratio of the shear carried by the stirrups to the total shear. The ductility of steel and the presence of axial load also influence the plastic rotation capacity and allowable moment redistribution. For low ductility steel θ_p and β are very small compared to those for normal ductility steel, at low to moderate reinforcement ratios. The following observations are made with regard to the influencing parameters:

1. The reinforcement index ω and the c/d ratio are the most important parameters affecting plastic rotation capacity and moment redistribution. For low ductility steel ($\varepsilon_{su} \leq 0.04$), the failure is governed by the rupture of steel, while for normal ductility steel ($\varepsilon_{su} \geq 0.08$), the failure is governed by the crushing of concrete. For low ductility steel, θ_p and β are significantly reduce at lower values of ω (< 0.15).

165

2. Beam slenderness (L/d) affects both θ_p and β. The plastic rotation capacity increases as the beam slenderness increases, while the allowable moment redistribution decreases as the slenderness increases.

3. Concrete ultimate strain has significant effect on θ_p and β. Both θ_p and β increase with an increase in the concrete ultimate strain.

4. Compression reinforcement is effective in increasing the plastic rotation capacity and allowable moment redistribution.

5. The confinement of concrete by transverse reinforcement improves the ductility of concrete.

6. The ratio of the shear stress carried by the stirrups to the total shear stress affects the distribution of tension steel force and hence θ_p and β. The smaller the ratio V_s/V_u the larger is the tension steel force and the extent of yielding and hence larger is the plastic rotation capacity and allowable moment redistribution.

7. The type of plastic hinge has a major influence on the plastic rotation capacity and allowable moment redistribution. The available rotation capacity and moment redistribution could be twice as large for the case of a shear crack hinge as compared to a flexural crack hinge.

8. The presence of a tensile axial load increases θ_p and β, while the presence of compressive axial load reduces θ_p and β.

9. The type of loading, uniform or concentrated, has insignificant influence on plastic rotation capacity and allowable moment redistribution.

10. In general, most design standards are conservative. Moment redistribution much greater than 20% can be achieved, especially for low reinforcement ratios. Even for

166

20% moment redistribution, the code allowable limits of c/d are very conservative and would not allow taking advantage of moment redistribution under practical situations.

A set of empirical equations and β curves are produced to evaluate the allowable moment redistribution in continuous reinforced concrete beams. These equations provide explicit relationship between β and ω for different values of L/d. The effects of compression reinforcement are implicit in ω. For the rest of the parameters, constant values are assumed that provide conservative estimates of β. It is to be noted that these equations provide moment redistribution limits based on ductility criteria. The equations can be particularly useful in strength evaluation of existing structures when structural collapse, rather than serviceability, is a matter of concern. For new design, the serviceability criteria must be evaluated before using these equations.
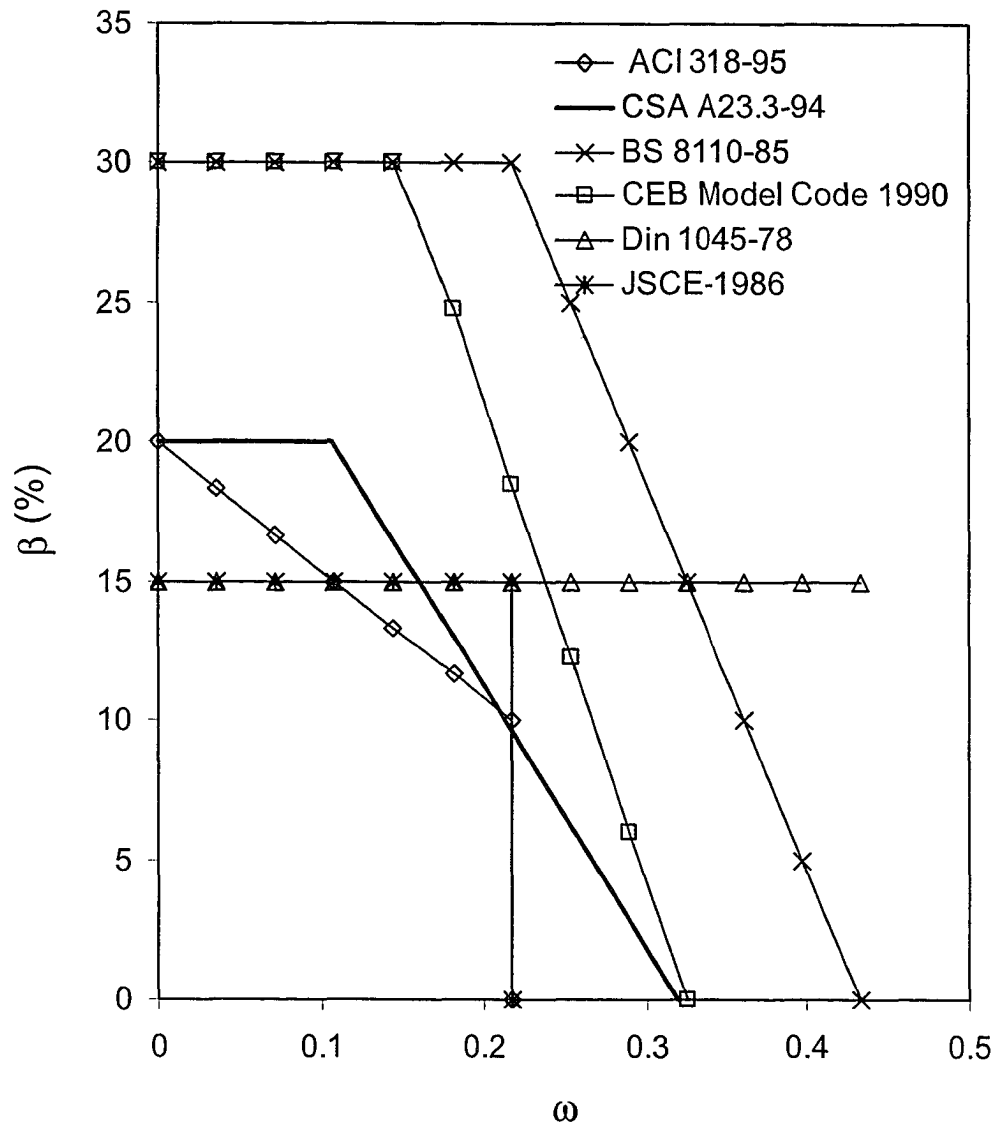
Figure 5.1 Comparison of provisions for allowable moment redistribution from various design standards

168
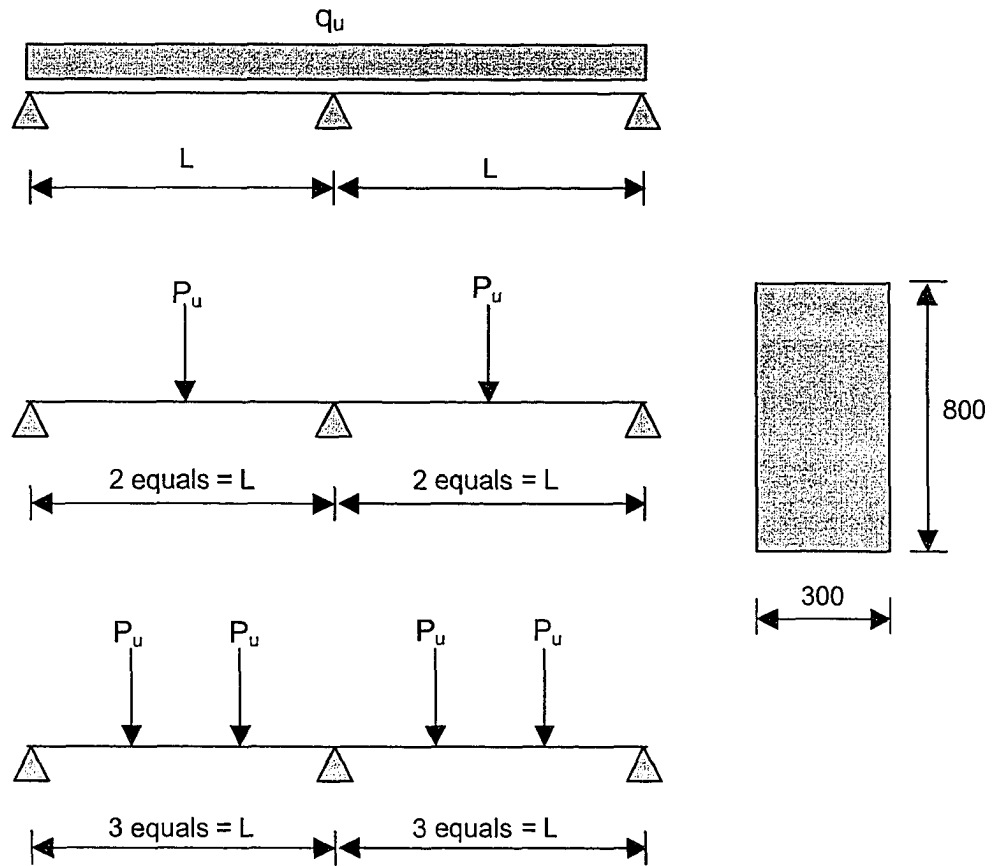
Material Properties:

Concrete

$f'_c = 30$ MPa
$\varepsilon_{cu} = 0.005$

Steel

$f_y = 400$ MPa
$\varepsilon_{su} = 0.1$ | For normal steel
$f_{su} = 540$ MPa |

$\varepsilon_{su} = 0.04$ | For low ductility steel
$f_{su} = 454$ MPa |

Figure 5.2. Beam geometry, cross-section, loading, and material properties

169
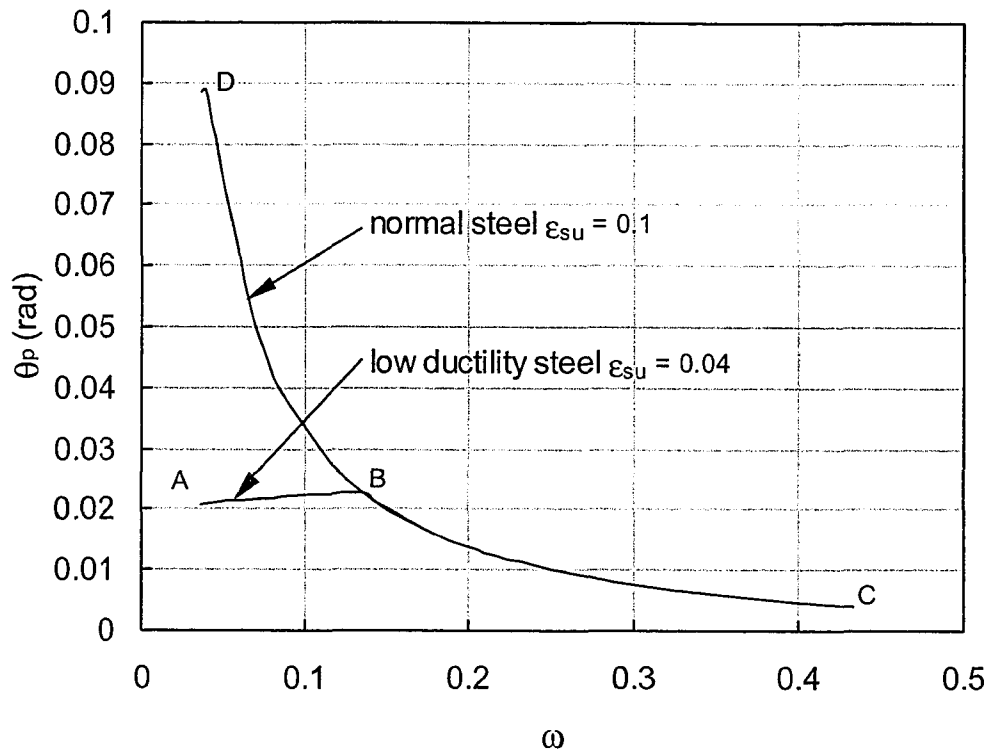
Figure 5.3 Effect of mechanical reinforcement index on θ_p
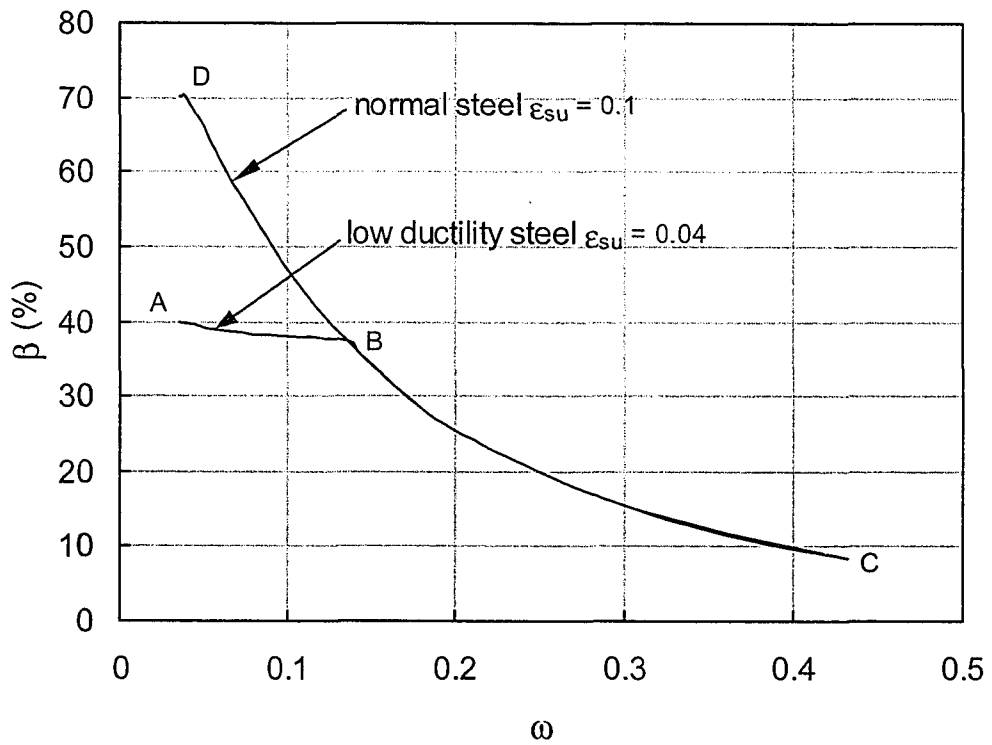
Figure 5.4 Effect of mechanical reinforcement index on β

170
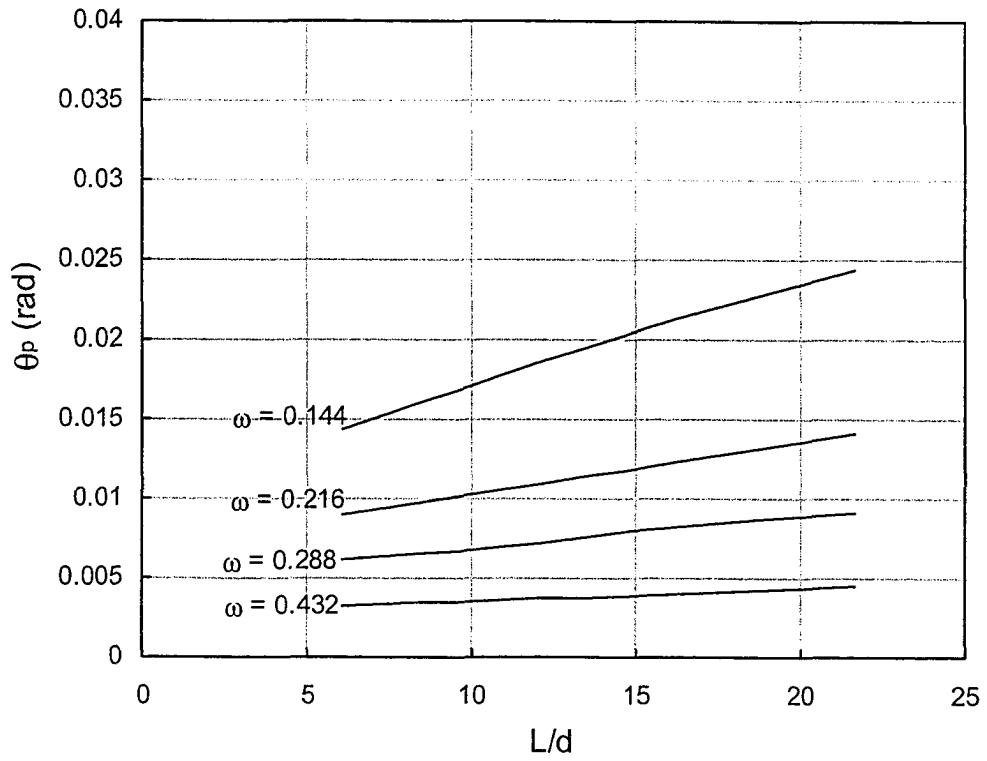
Figure 5.5 Effect of beam slenderness on θ_p
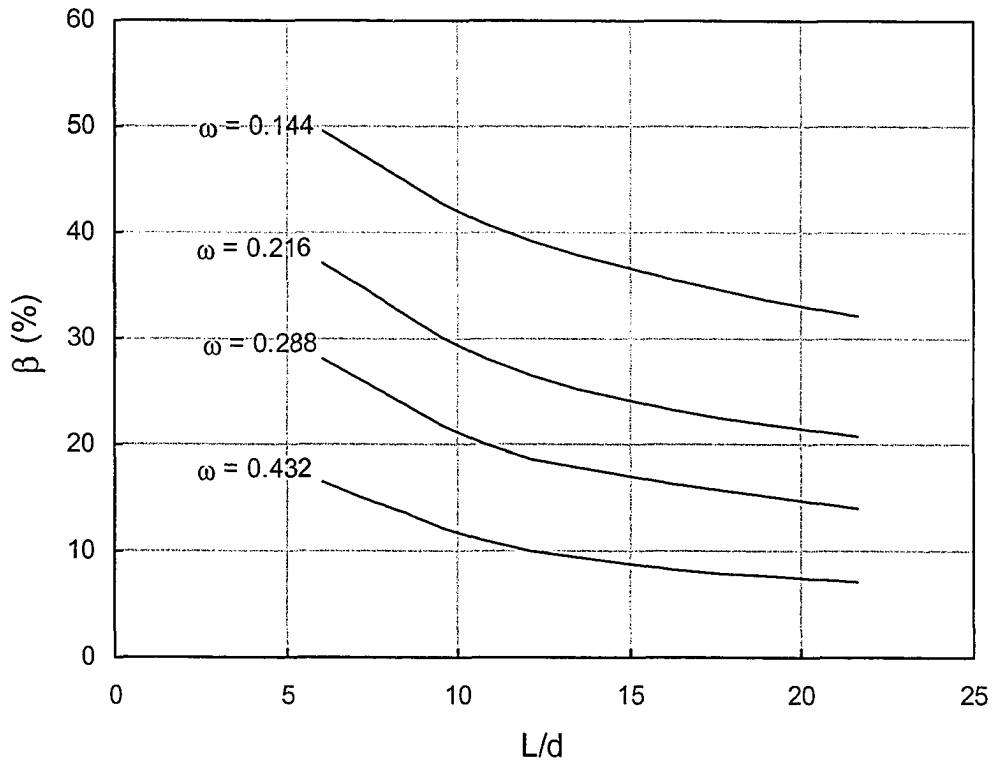
Figure 5.6 Effect of beam slenderness on β

171
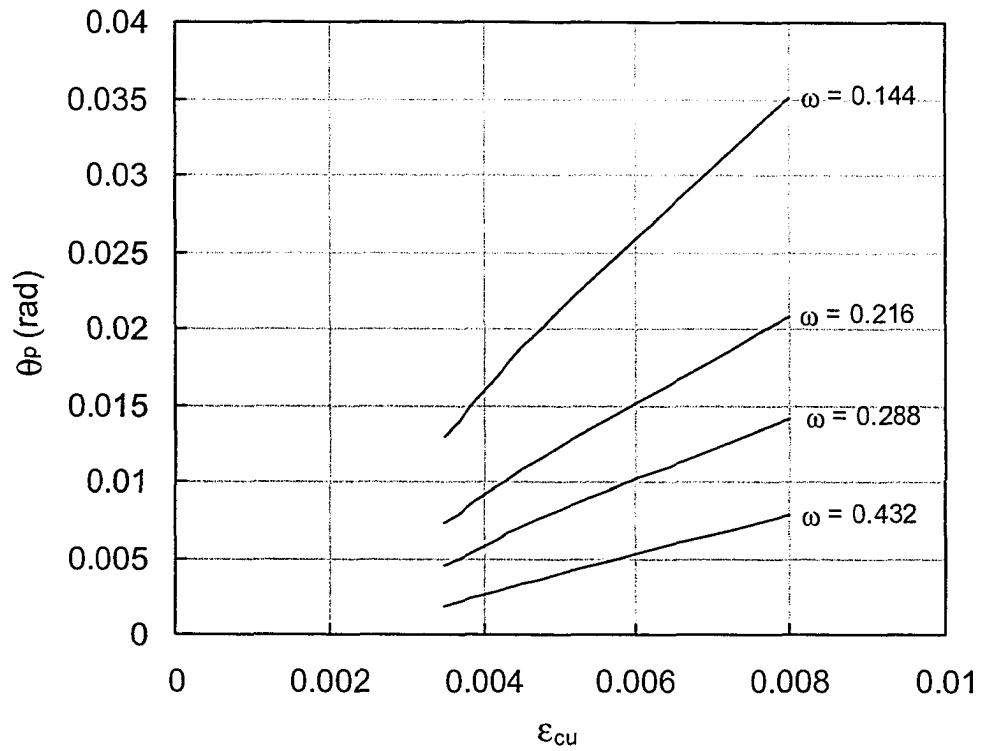
Figure 5.7 Effect of concrete ultimate strain on θ_p
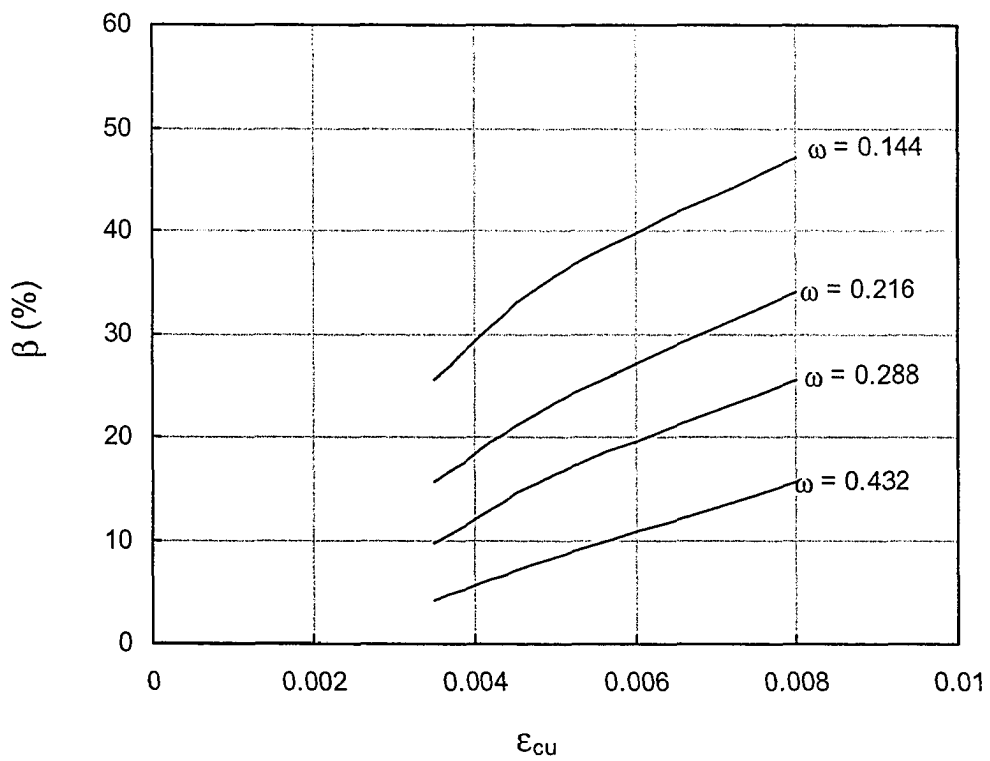
Figure 5.8 Effect of concrete ultimate strain on β

172
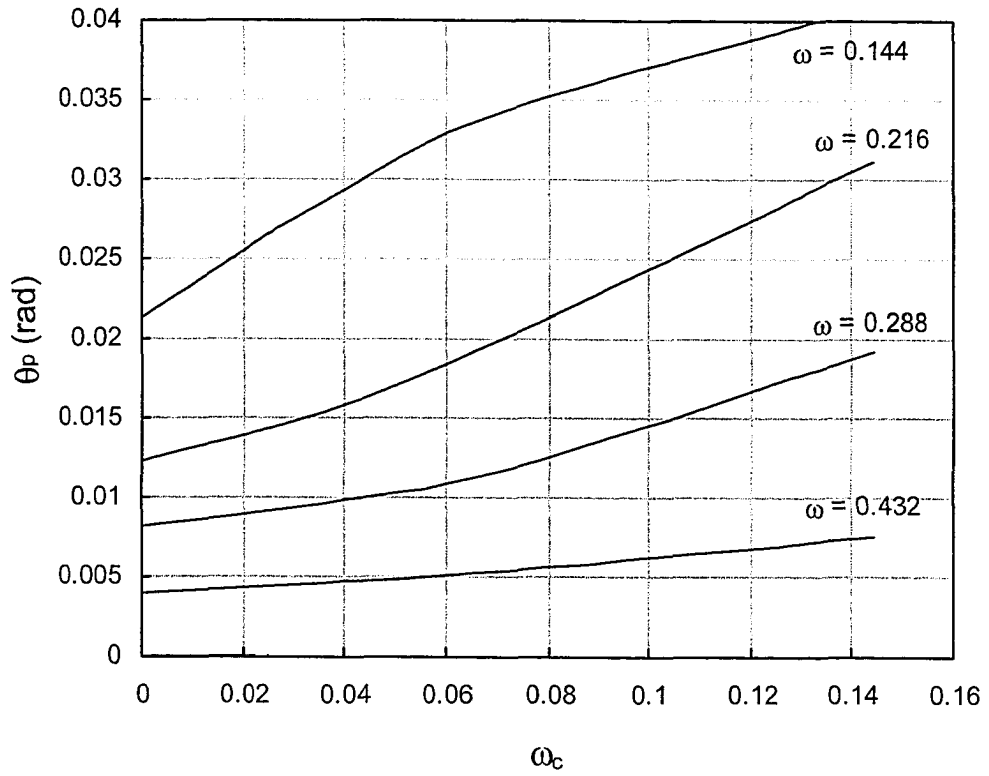
Figure 5.9 Effect of compression reinforcement on θ_p
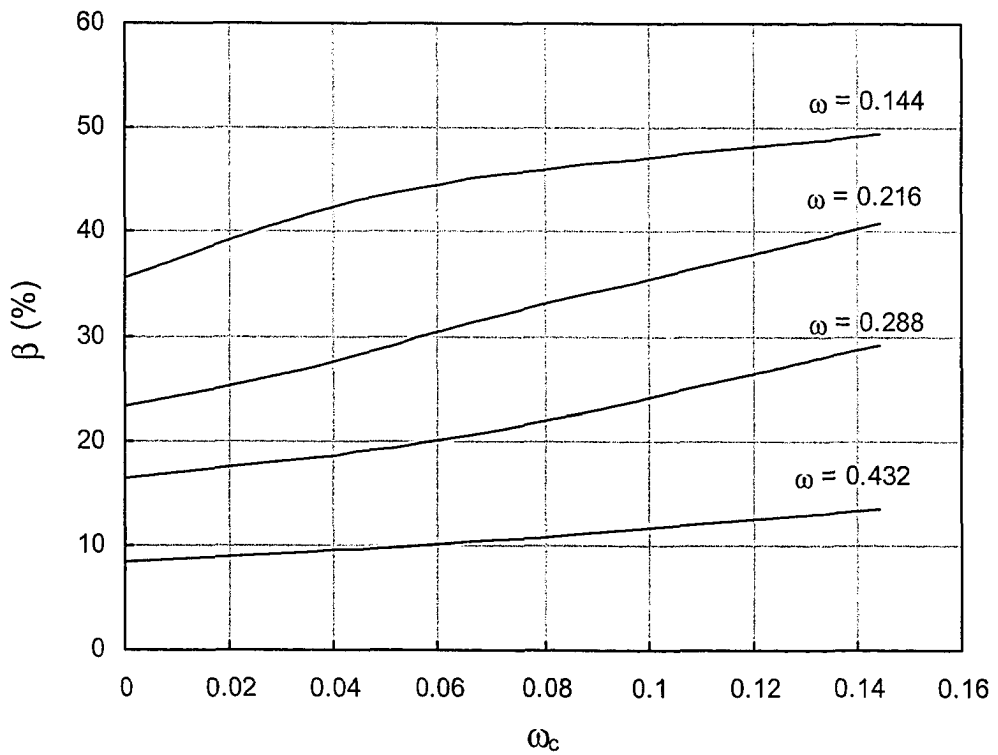
Figure 5.10 Effect of compression reinforcement on β

173
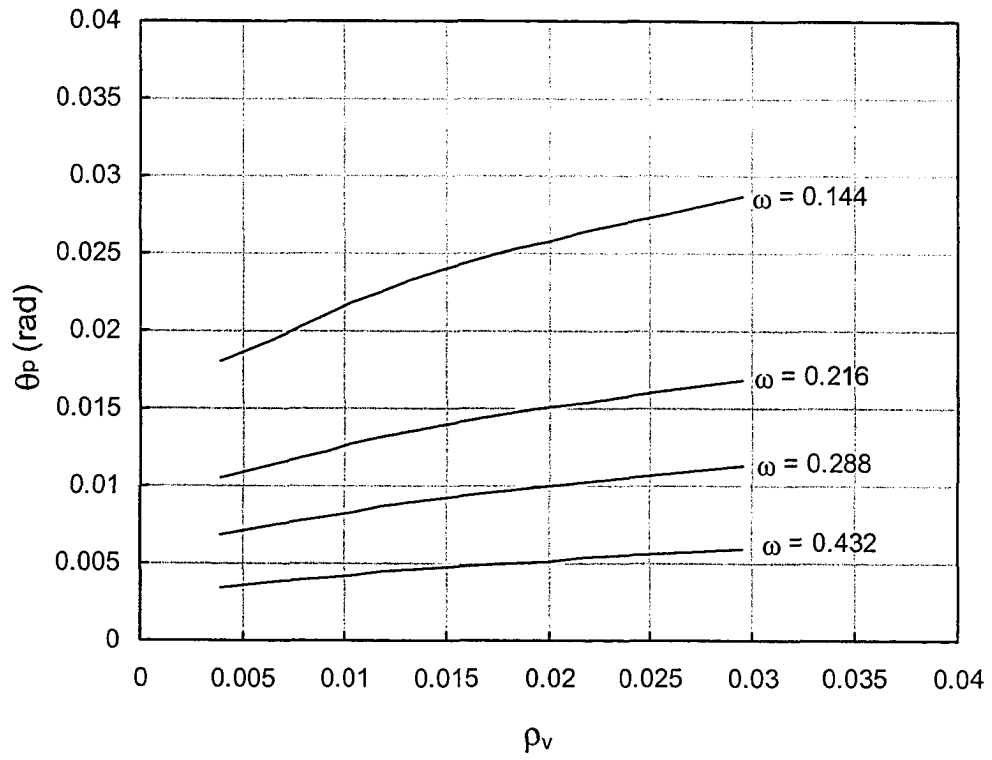
Figure 5.11 Effect of confinement on θ_p
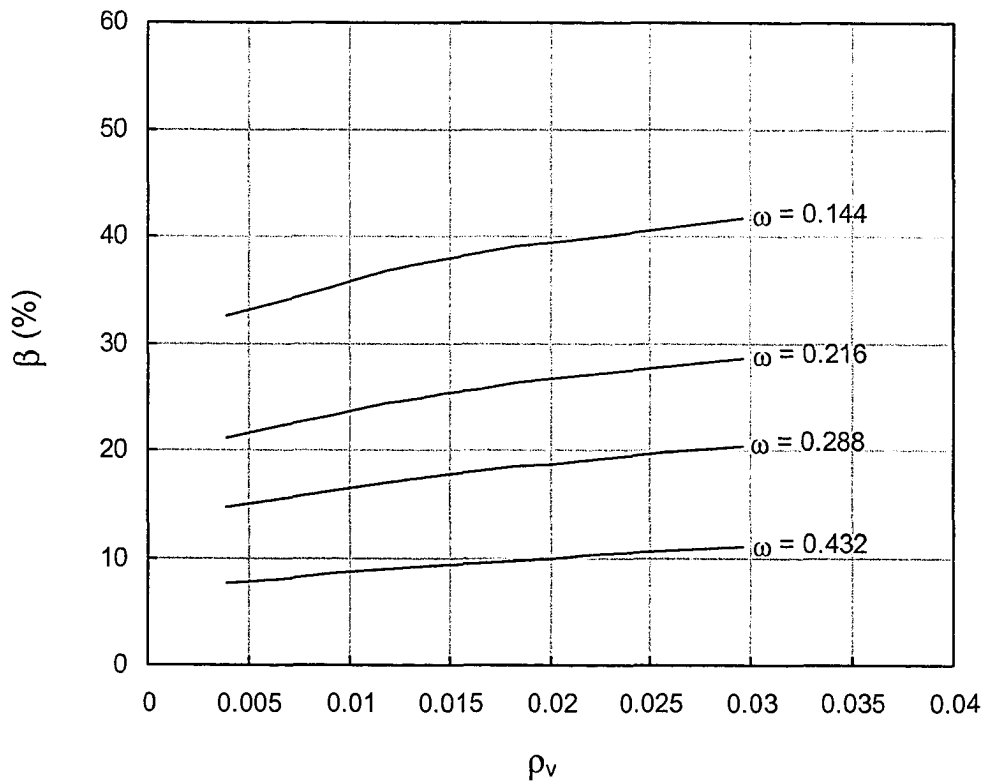
Figure 5.12 Effect of confinement on β

174
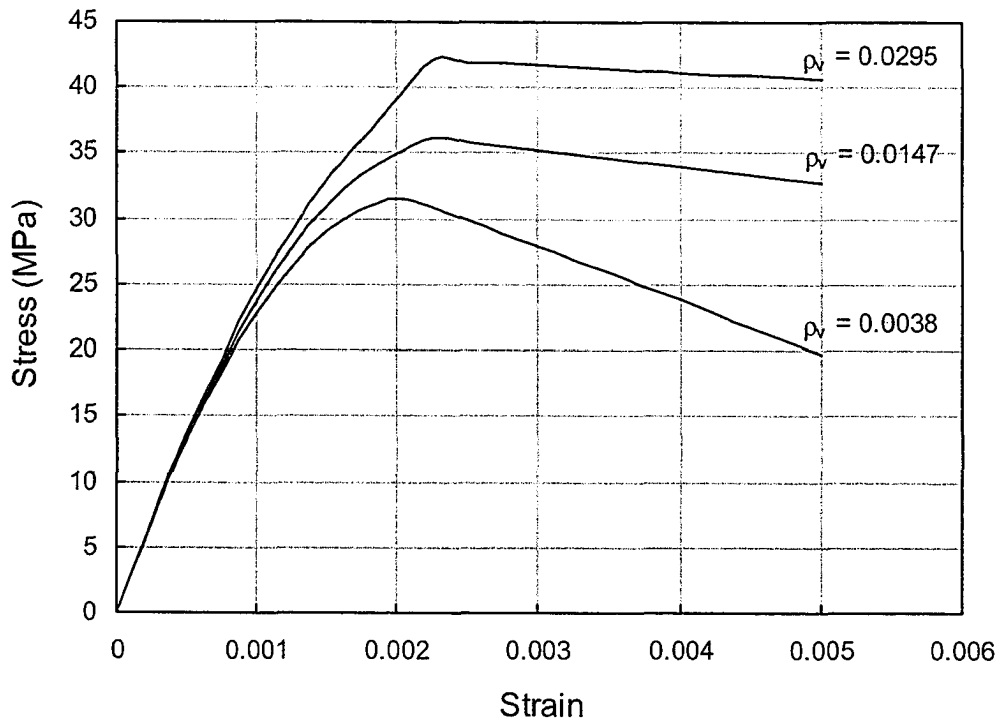
Figure 5.13 Effect of confinement on concrete stress-strain curve
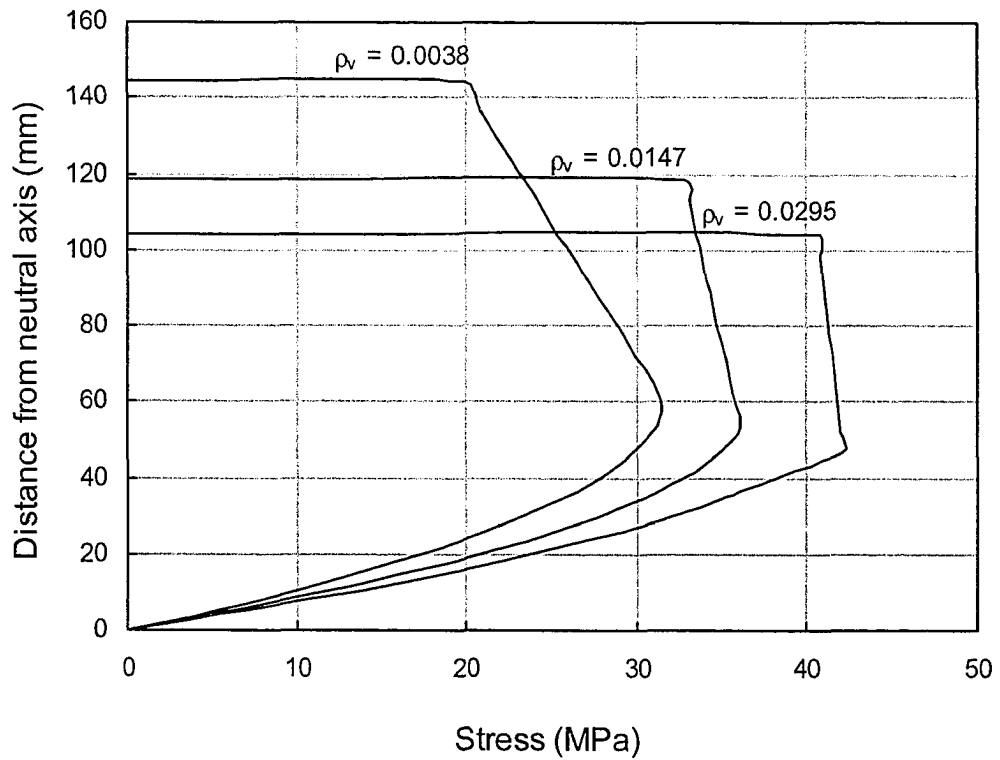
Figure 5.14 Effect of confinement on concrete stress-block

175
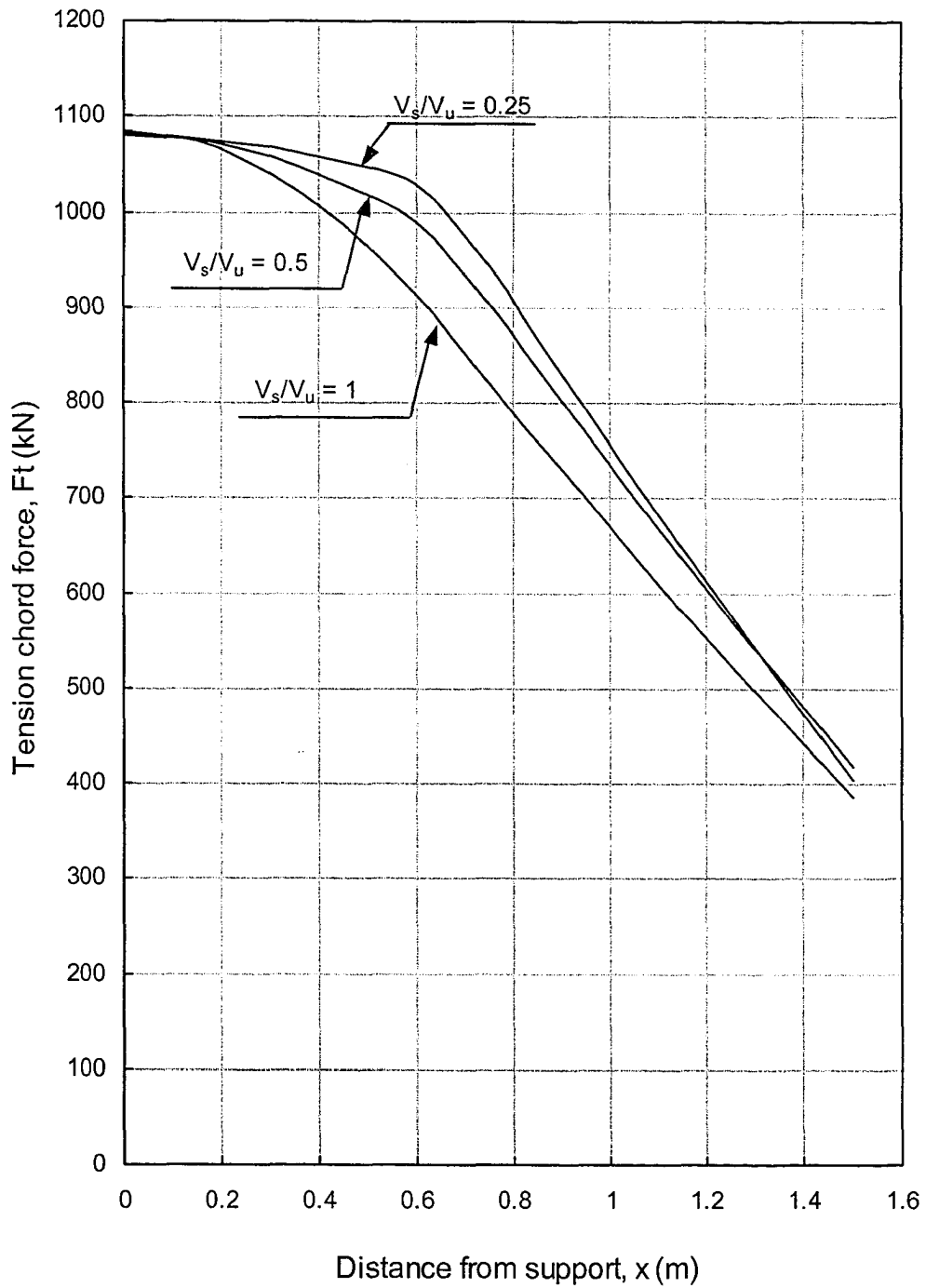
Figure 5.15 Effect of V_s/V_u on tension chord force

176
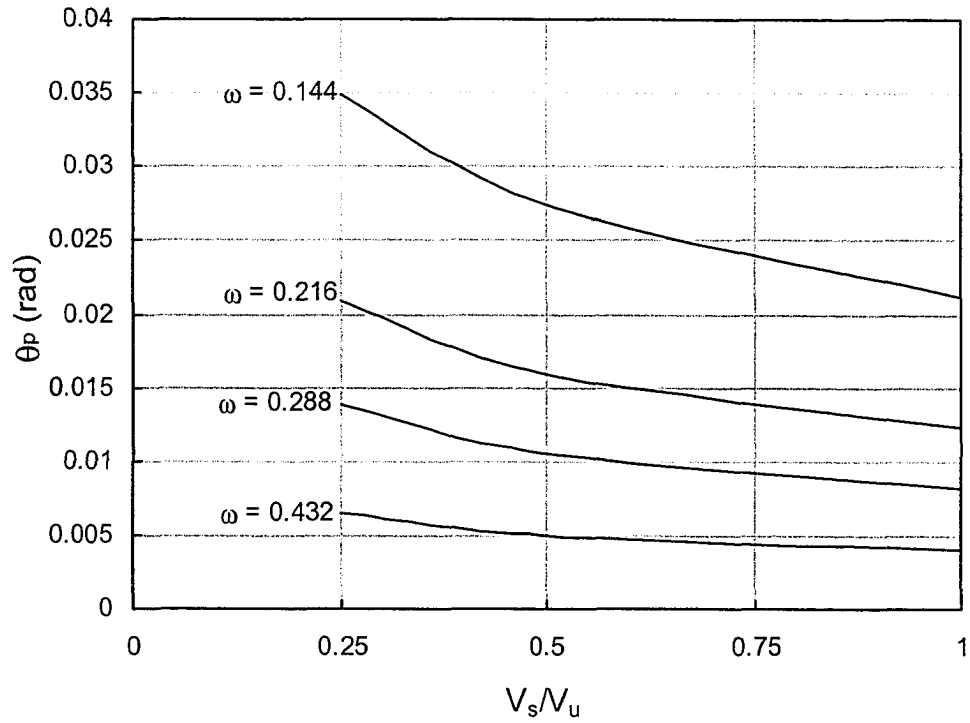
Figure 5.16 Effect of V_s/V_u on θ_p
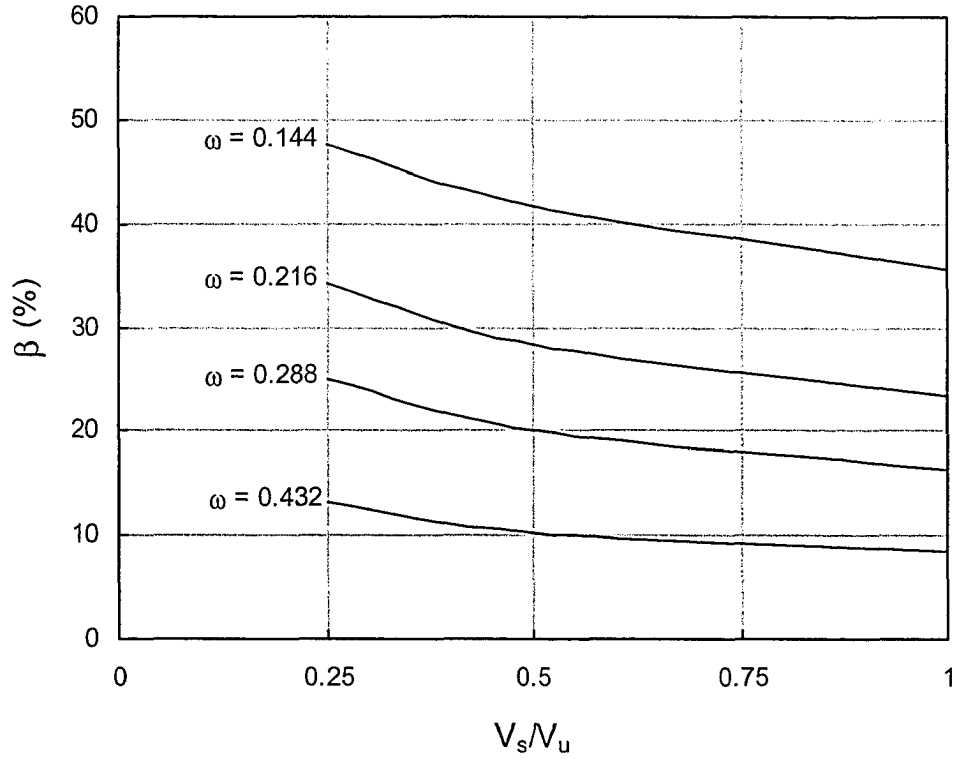
Figure 5.17 Effect of V_s/V_u on β

177
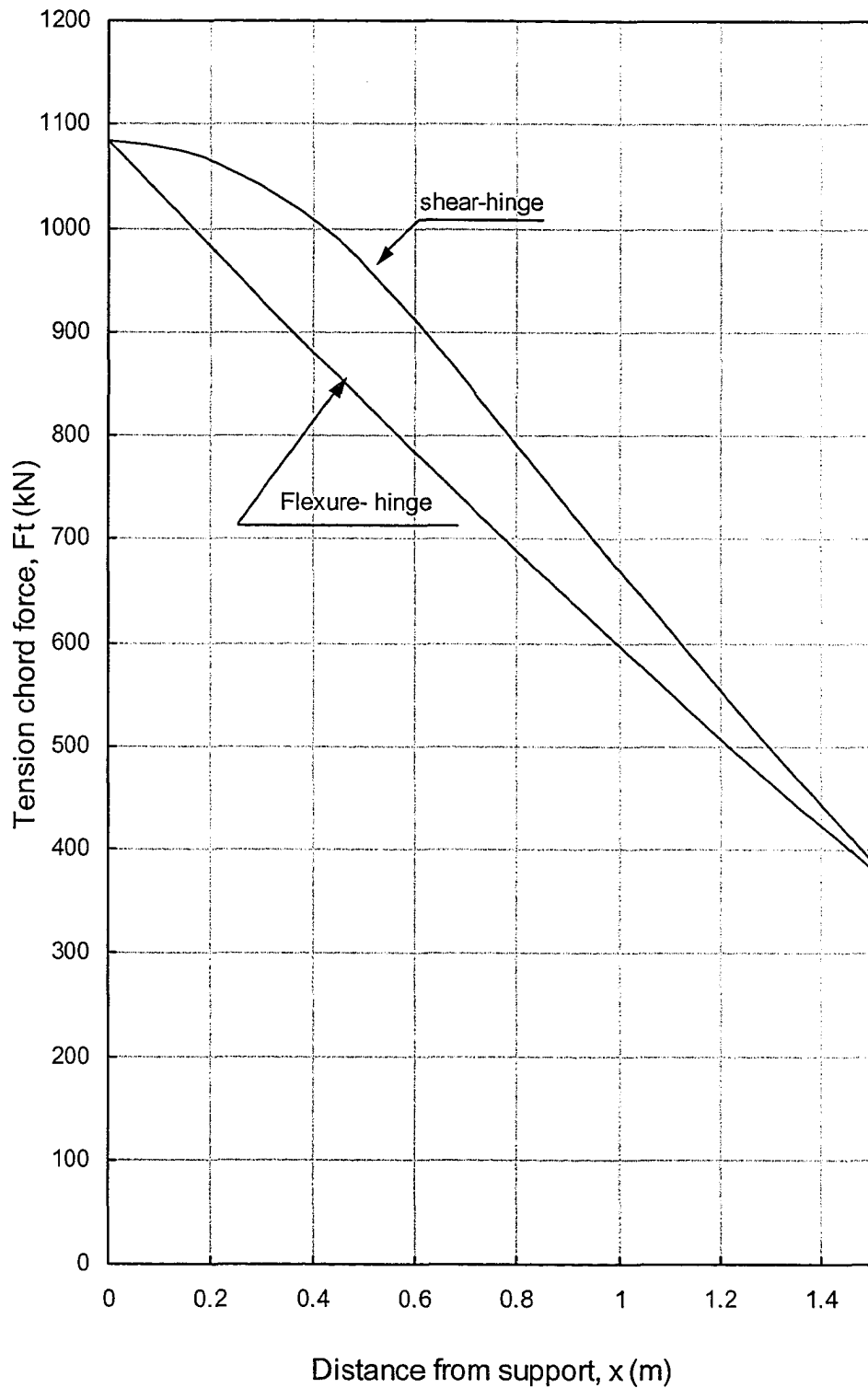
Figure 5.18 Effect of type of plastic-hinge on tension chord force

178
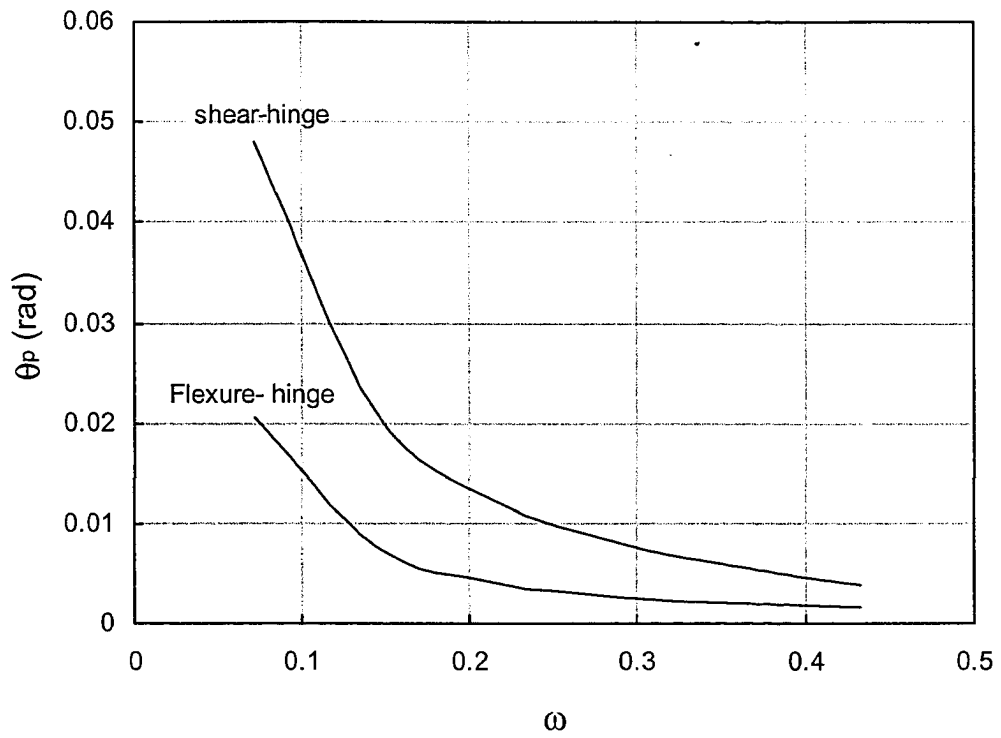
Figure 5.19 Effect of type of plastic-hinge on θ_p
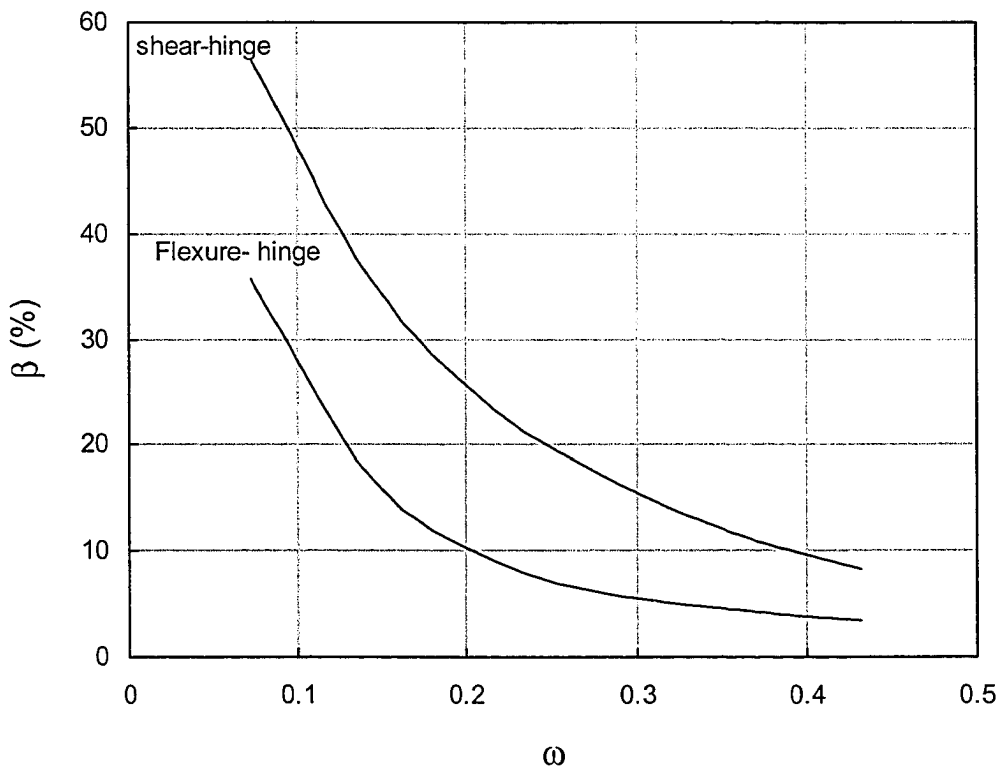
Figure 5.20 Effect of type of plastic-hinge on β

179
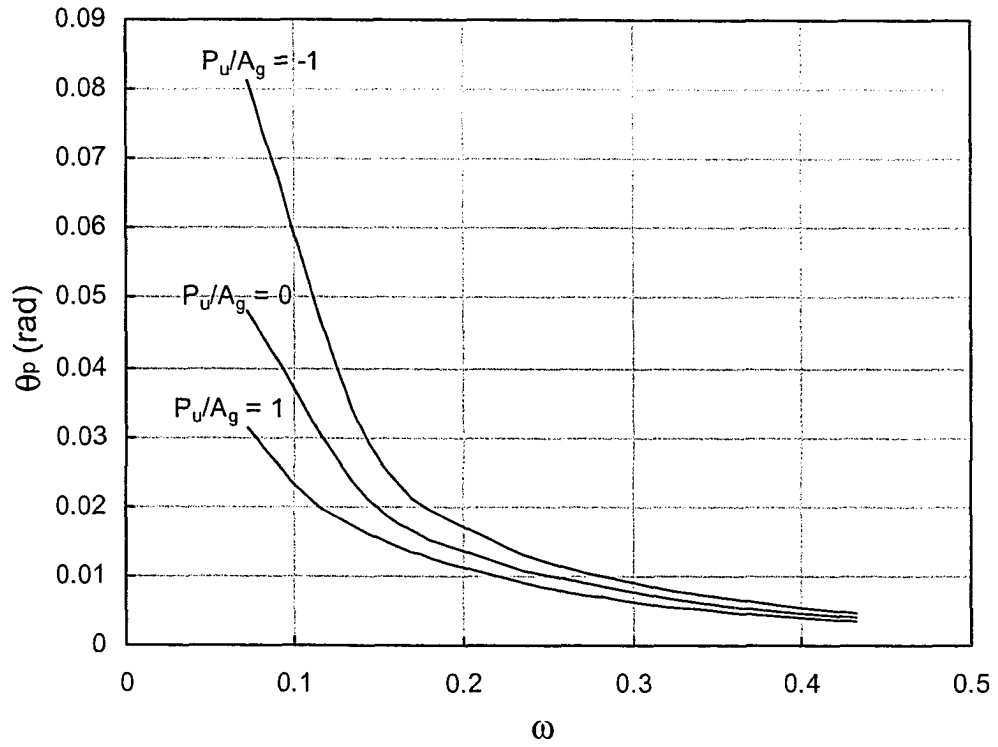
Figure 5.21 Effect of axial load on θ_p
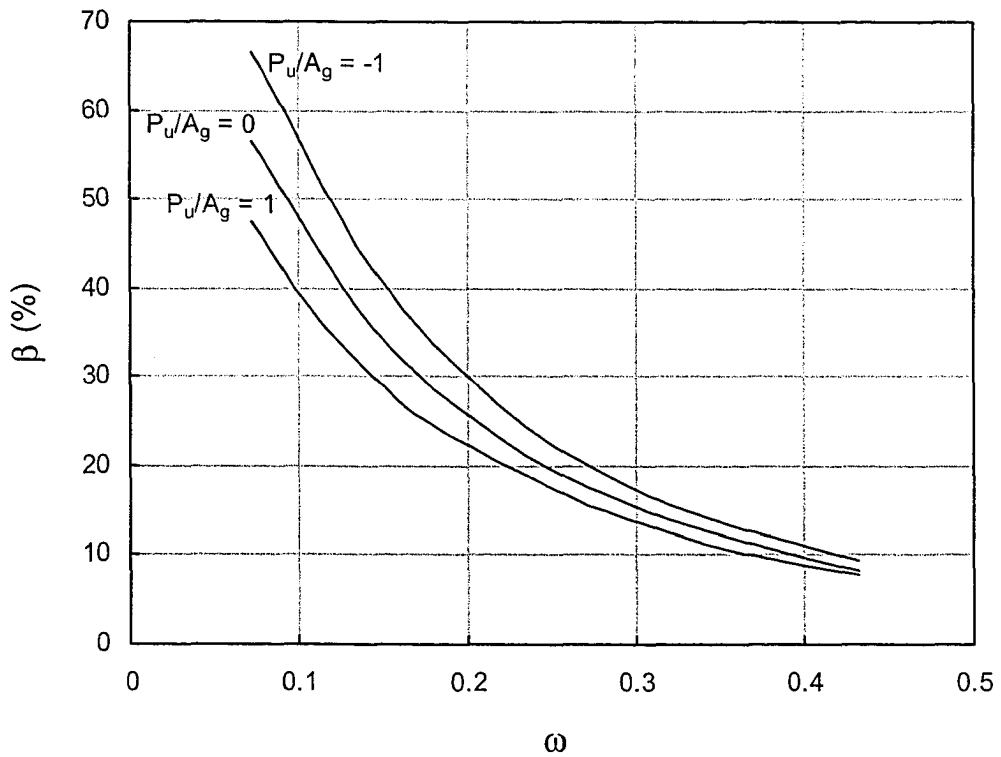
Figure 5.22 Effect of axial load on β

180
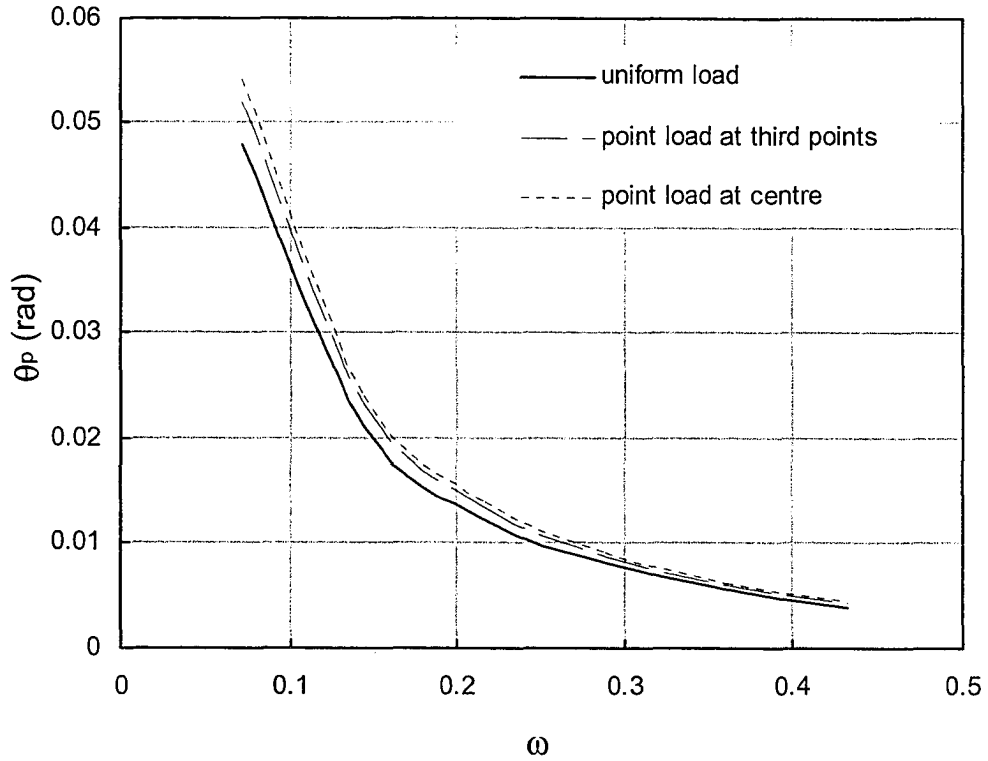
Figure 5.23 Effect of type of loading on θ_p
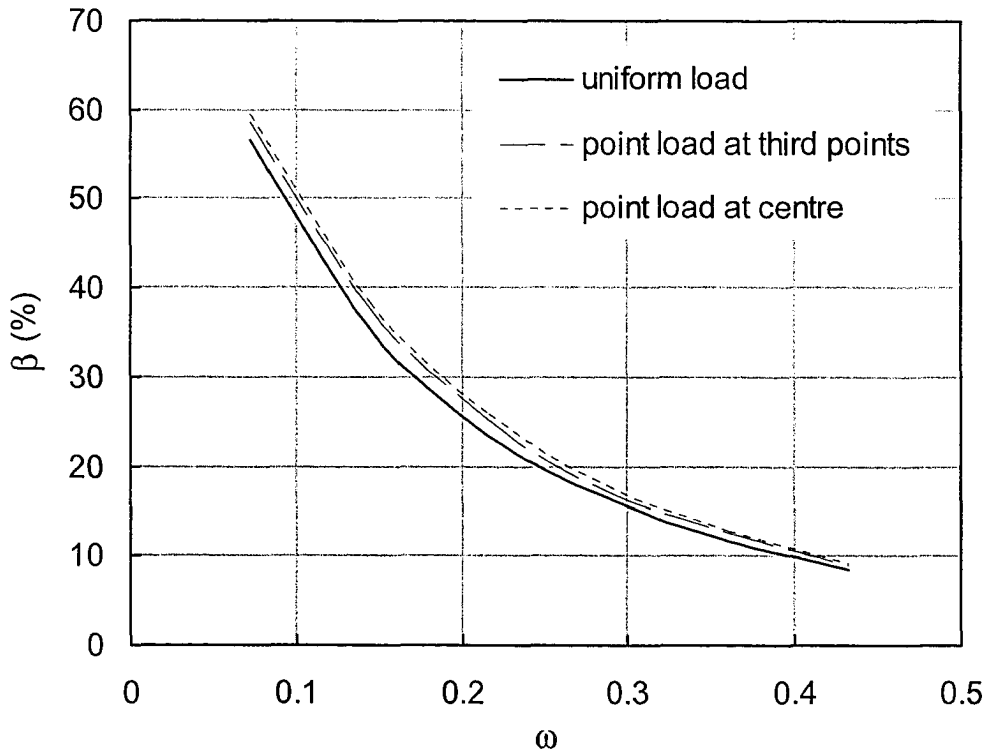
Figure 5.24 Effect of type of loading on β

181
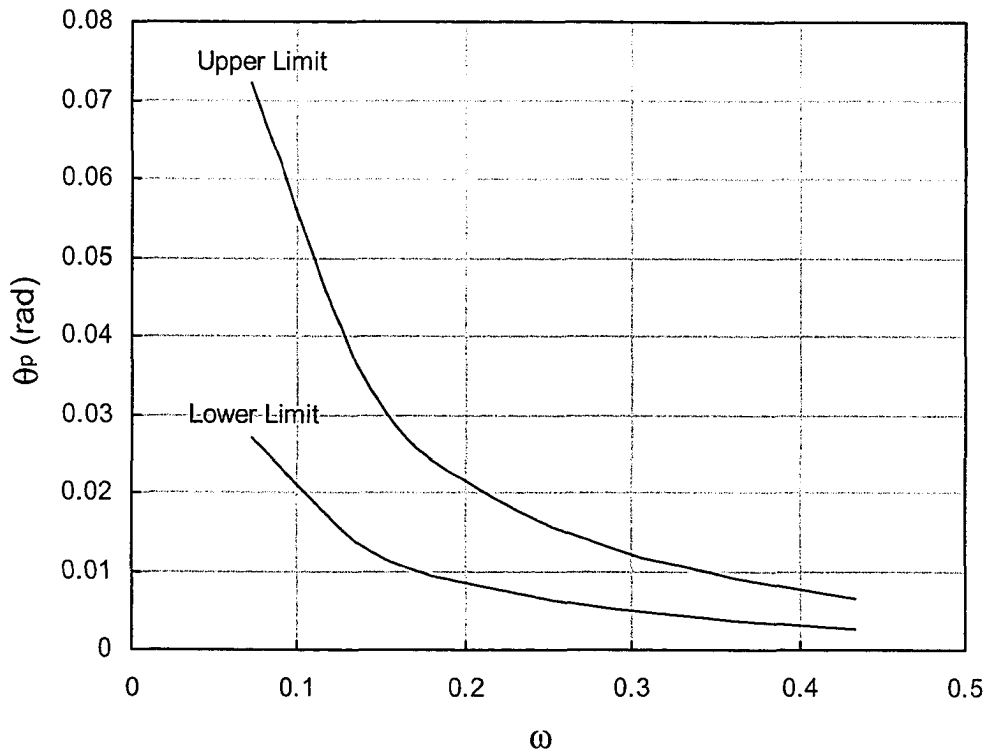
Figure 5.25 Upper and lower theoretical limits of θ_p
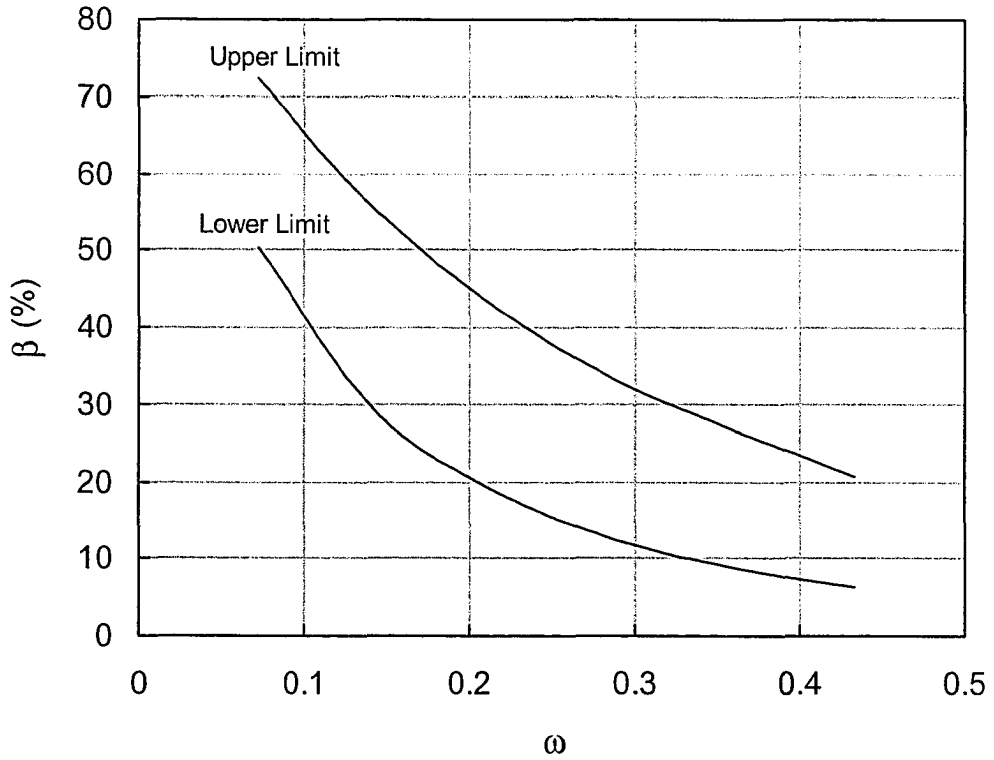
Figure 5.26 Upper and lower theoretical limits of β

182
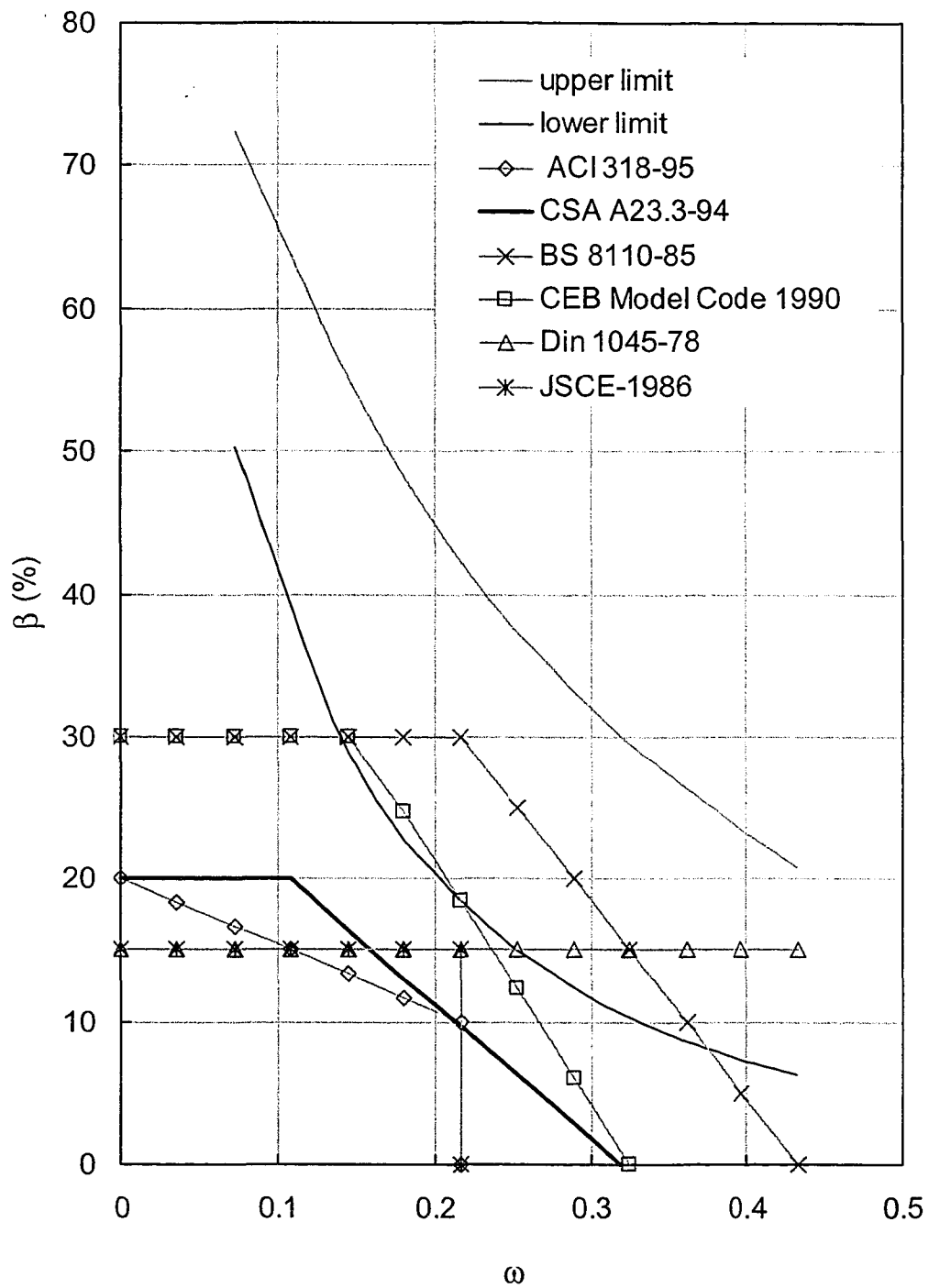
Figure 5.27 Comparison of model limits and various standards limits for β

183
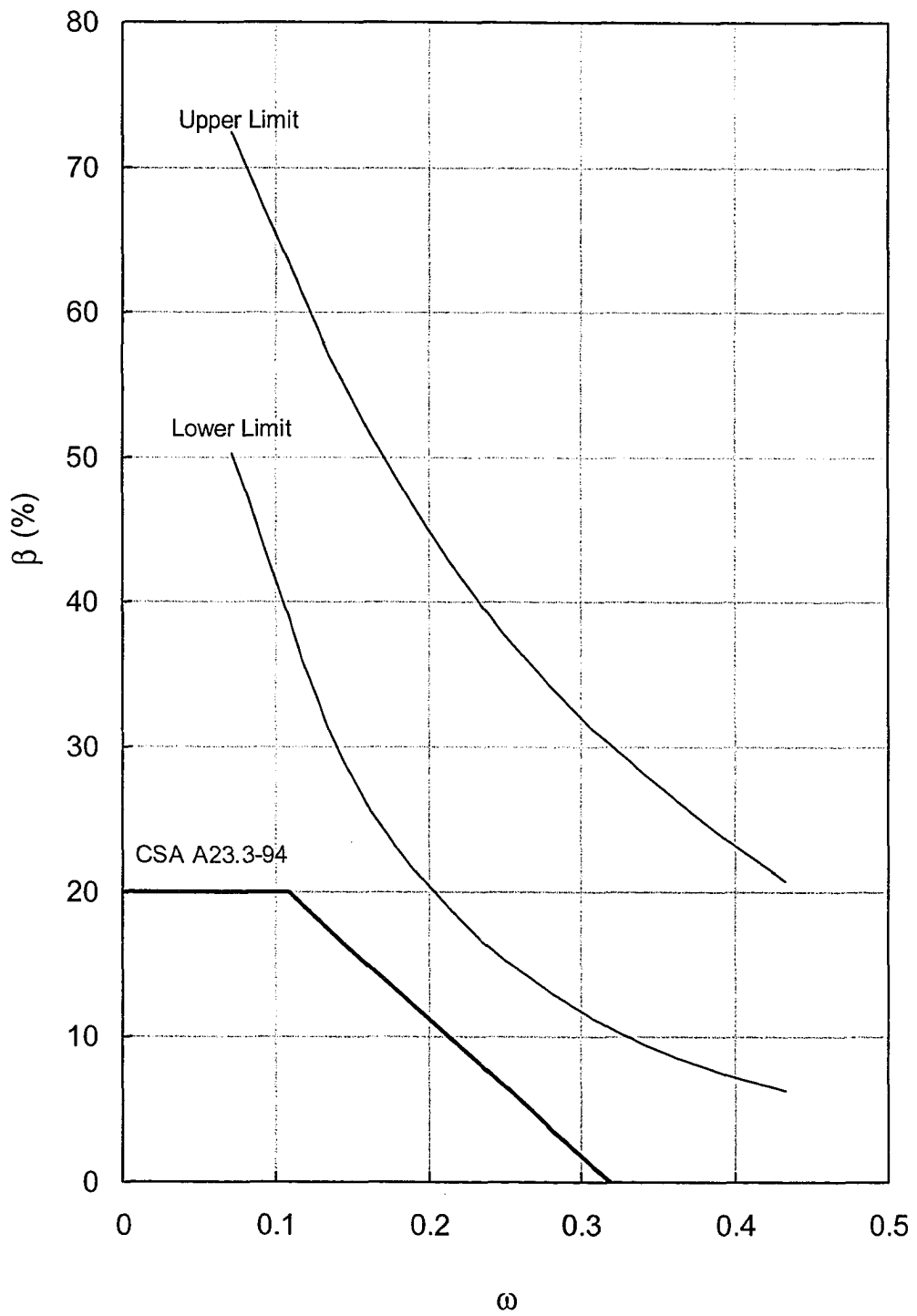
Figure 5.28 Comparison of model limits and CSA-A23.3-94 limits for β
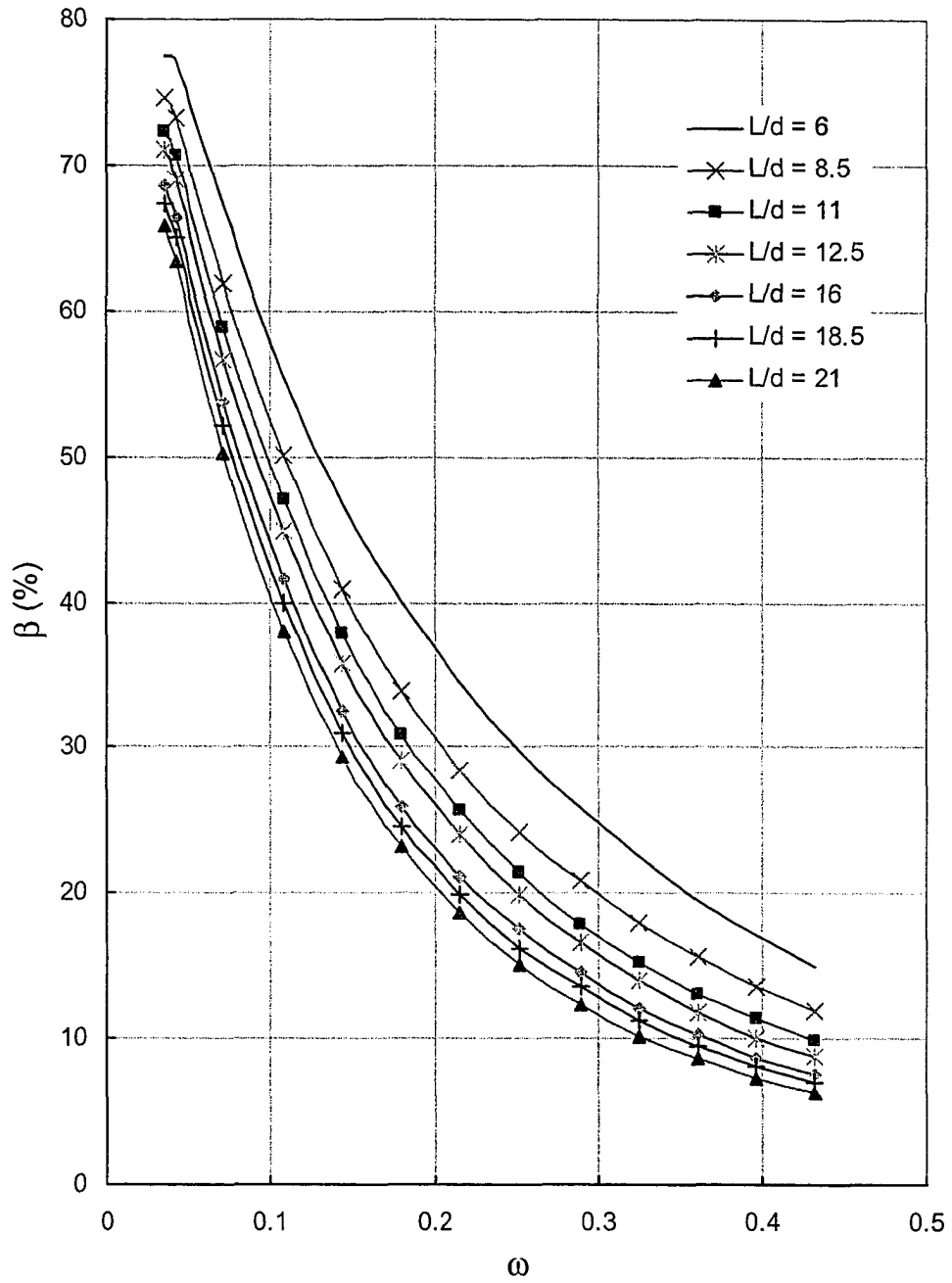
Figure 5.29 Range of Allowable moment redistribution for L/d
= 6 to 21

185
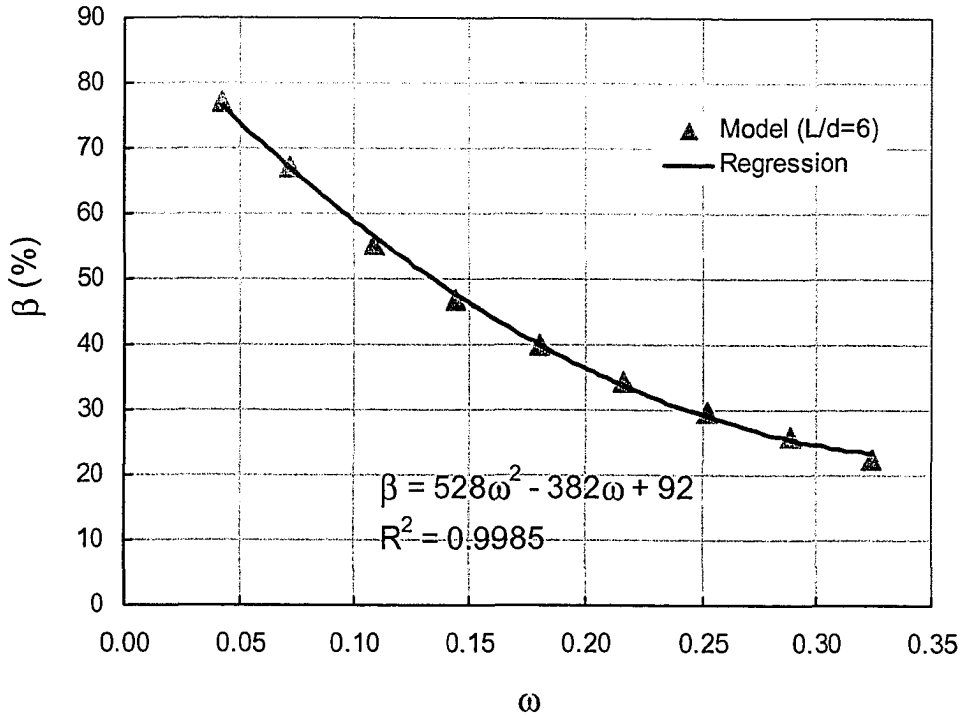
Figure 5.30 Allowable moment redistribution for L/d ≤ 6
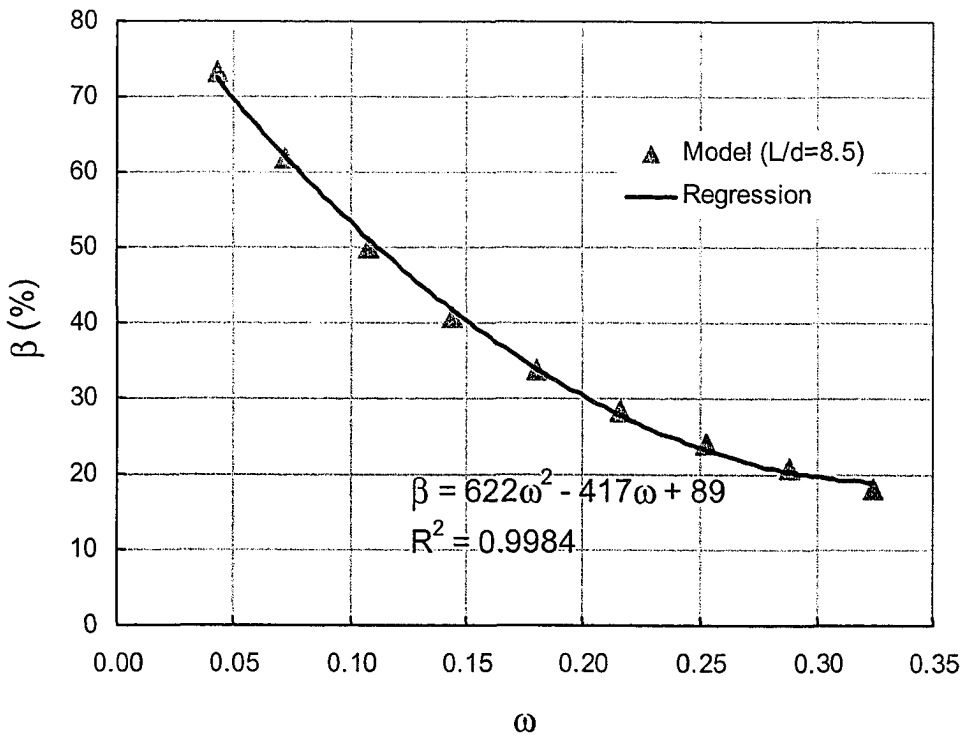
Figure 5.31 Allowable moment redistribution, 6 < L/d ≤ 8.5

186
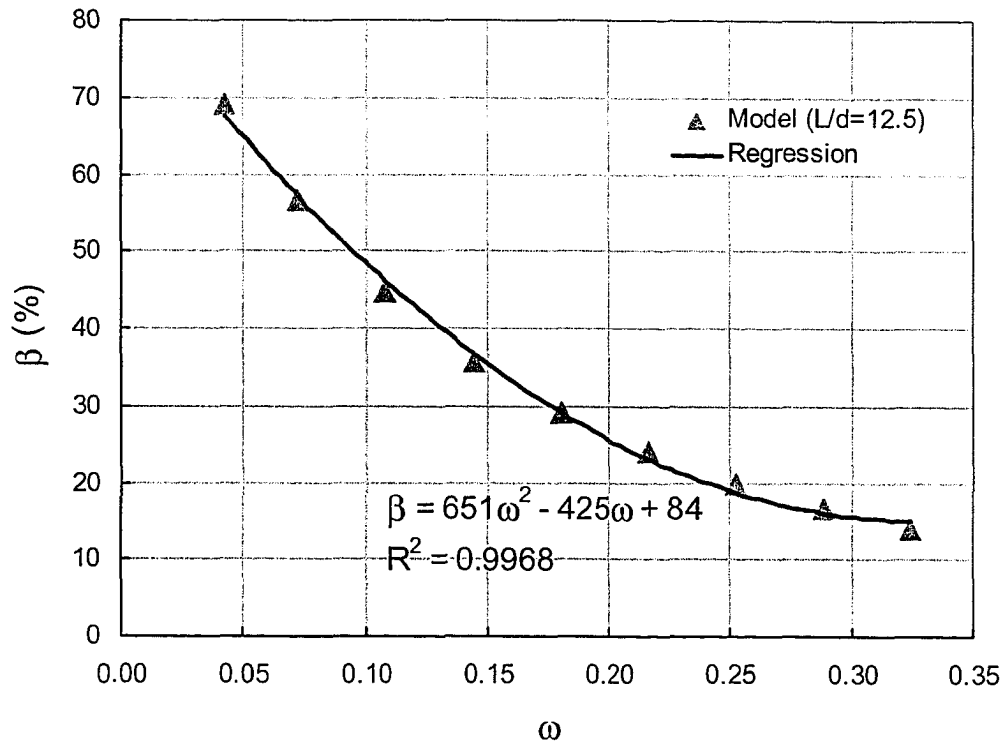
Figure 5.32 Allowable moment redistribution, 8.5<L/d≤12.5

Equation on figure 5.32:

$$\beta = 651\omega^2 - 425\omega + 84$$
$$R^2 = 0.9968$$
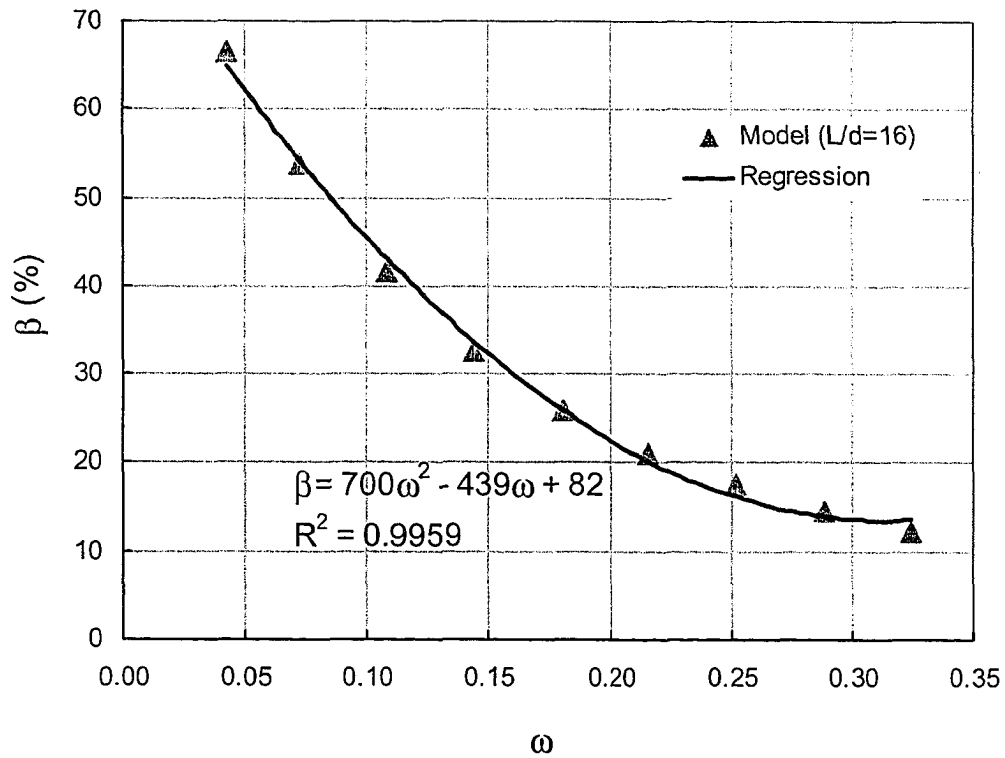
Figure 5.33 Allowable moment redistribution, 12.5<L/d≤16

Equation on figure 5.33:

$$\beta = 700\omega^2 - 439\omega + 82$$
$$R^2 = 0.9959$$

187
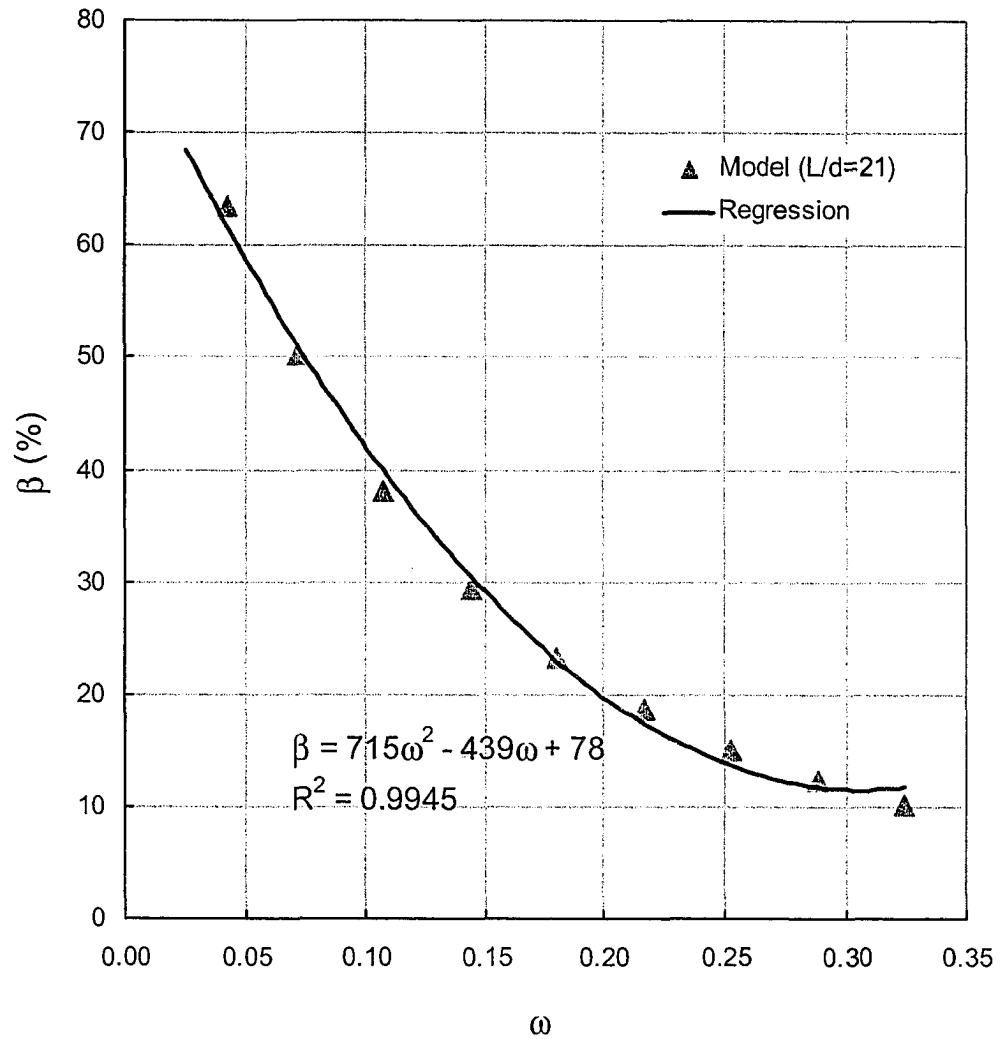
Figure 5.34 Allowable moment redistribution, $16.5 < L/d \leq 21$

The plotted data and regression relationship shown:

$$\beta = 715\omega^2 - 439\omega + 78$$
$$R^2 = 0.9945$$

With axes β (%) on the vertical and ω on the horizontal, legend entries: Model (L/d=21) and Regression.

188

6. MOMENT REDISTRIBUTION AND SERVICEABILITY

6.1 Introduction

This chapter evaluates the allowable limits for moment redistribution, in continuous reinforced concrete beams, with respect to the serviceability limit state. Ductility model developed earlier in Chapter 4 shows that the allowable moment redistribution can be very high under favourable conditions. Moment redistribution implies yielding of the reinforcement. This chapter examines limits on moment redistribution to avoid the adverse effects of concrete cracking and yielding of reinforcement at service load levels.

6.2 Serviceability Requirement

Serviceability requires that crack widths and deflections are not excessive at service load level. Crack widths and deflection checks should be done in accordance with standard practice. Such checks are outside the scope of this thesis. To satisfy the serviceability criteria, it is a virtual certainty that one must avoid yielding of reinforcement at service load level. If M_s is the maximum service moment at a critical section, to avoid yielding of reinforcement at that section at service load level, the minimum design moment M_{des} must be at least:

$$M_{des} = M_s / \lambda \qquad [6.1]$$

Where λ is the limiting yield moment coefficient defined as (Furlong and Carlos, 1979) :

$$\lambda = M_y / M_r \qquad [6.2]$$

If M_f is the maximum factored elastic moment and M_s is the maximum unfactored service elastic moment, the allowable moment redistribution β to satisfy the no yielding criteria is given as:

189

$$\beta = \frac{M_f - (M_s / \lambda)}{M_f} \times 100 \qquad\qquad [6.3]$$

The above equation can be normalized by dividing the numerator and denominator by $w_f L^2$.

$$\beta = \frac{\mu_f - \mu_s}{\mu_f} \times 100 \qquad\qquad [6.4]$$

where

$$\mu_s = \frac{M_s}{\lambda w_f L^2} \qquad\qquad [6.5]$$

$$\mu_f = \frac{M_f}{w_f L^2} \qquad\qquad [6.6]$$

To determine the allowable moment redistribution for the serviceability limit state, one needs to determine the maximum elastic moment coefficients, μ_s and μ_f, at all critical sections and the limiting yield moment coefficient λ. It is to be noted here that while the reinforced concrete members can be proportioned based on Eq. 6.4, an explicit check of crack widths and deflections may be required to ensure that serviceability requirements are met as per applicable standard.

6.2.1 Limiting yield moment coefficient λ

The limiting yield moment coefficient can be obtained by determining M_y and M_r from plane-sections analysis. Considering linear stress-strain relation at yield, as shown in Fig. 6.1a, one can write an expression for M_y as:

$$M_y = A_s f_y \left(d - \frac{c_y}{3} \right) = A_s f_y d \left(1 - 0.33 \frac{c_y}{d} \right) \qquad\qquad [6.7]$$

190

Similarly, considering equivalent stress block at ultimate, as shown in Fig. 6.1b, one can write an expression for M_r as:

$$M_r = A_s f_y \left(d - \frac{a}{2} \right) = A_s f_y d \left(1 - 0.5\beta_1 \frac{c}{d} \right)$$ [6.8]

Substituting M_y and M_r into Eq. 6.2 yields:

$$\lambda = \frac{M_y}{M_r} = \frac{1 - 0.33\dfrac{c_y}{d}}{1 - 0.5\beta_1\dfrac{c}{d}}$$ [6.9]

where c_y/d is the relative depth of neutral axis at yield and c/d is the relative depth of neutral axis at ultimate. β_1 is the ratio of the depth of stress block, a, to the depth of neutral axis at ultimate, given as: $\beta_1 = 0.97 - 0.0025 f_c'$ (CSA A23.3-94). c_y/d was derived in Chapter 3, Eq. 3.5 as:

$$\frac{c_y}{d} = \sqrt{\rho^2 n^2 + 2\rho n} - \rho n$$ [6.10]

Since there is a unique relationship between ρ and c/d at ultimate, Eq. 6.10 can be rewritten in terms of c/d as:

$$\frac{c_y}{d} = \sqrt{n^2 n_1^2 \left(\frac{c}{d} \right)^2 + 2 n n_1 \frac{c}{d}} - n n_1 \frac{c}{d}$$ (6.11)

where $n = E_s/E_c$ and n_1 is given as:

191

$$n_1 = \frac{\alpha_1 \beta_1 f_c'}{f_y}$$ [6.12]

where α_1 is the ratio of average stress in the rectangular compression block to the specified concrete strength = $0.85 - 0.0015 f_c'$ but not less than 0.67 (CSA A23.3-94).

Fig. 6.2 shows the plot of Eq. 6.9 for commonly used grades of steel and concrete. No combination gives value of λ lower than 0.949. It can be concluded that yield moments are at least as large as 95% of the computed ultimate moments.

6.2.2 Derivation of elastic moment coefficients μ_s and μ_f

The procedure used for determining moment coefficients is based on the general principles of structural analysis and limit design methods (Furlong and Carlos, 1979). The coefficients for maximum elastic moments at critical sections are derived using "three moment equation" method of elastic analysis. Different load patterns and span variations, providing maximum load effects, are considered for each critical section. The maximum effect of load placement and span length variation occurs when a continuous beam is supported on knife-edge supports without any rotational restraint. The results can be applied as upper limits for beams with rotationally restrained supports. The spans used are clear spans to account for the reduction of moment at the face of supports. It is assumed that the structure and the loading met the following six conditions:

(1)   There are two or more spans

(2)   Adjacent spans do not differ by more than 50% of the shorter span.

(3)   The loads are uniformly distributed.

(4)   The service live load does not exceed 3 times the service dead load

192

(5)   The members are prismatic

(6)   The beam is in a braced frame without significant moments due to lateral loads.

The main parameters used to derive moment coefficients are the service live load to dead load ratio α and the adjacent span ratio γ. Variations of these parameters are considered to produce the upper bound values of moment coefficients. A minimum value of $\alpha=0.5$ is used to avoid moment redistribution under permanent loads.

6.2.2.1 Serviceability moment coefficients μ_s

The loading and span configurations for maximum moments at critical sections are shown in Fig. 6.3 to 6.8. Table 6.1 lists the expressions for service load moment M_s at the critical sections. Substituting the expressions for M_s in Eq. 6.5 and applying CSA A23.3-94 load factors ($w_f =1.25w_d + 1.5w_L$) gives the expressions for μ_s at critical sections. The expressions for μ_s are also listed in Table 6.1 and are plotted in Fig. 6.3 to 6.8.

6.2.2.2 Factored moment coefficients μ_f

The factored elastic moment coefficients are determined in exactly the same fashion as the serviceability moment coefficients. The governing loadings and span configurations for each critical section are shown in Figs. 6.9 to 6.14. Table 6.2 lists the expressions for factored load moment M_f and factored moment coefficient μ_f at the critical sections. The expressions for μ_f are plotted in Fig. 6.9 to 6.14.

6.2.3 Allowable Moment Redistribution for Serviceability Limit State

The allowable moment redistribution limits for serviceability limit-state are determined using Eq. 6.4. Equation 6.4 is plotted for all critical sections in Fig. 6.15 to Fig. 6.21. The plots show that the allowable moment redistribution increases with increasing values of load ratio and adjacent span ratio. Table 6.3 provides the minimum and maximum values of allowable moment redistribution for each critical section.

193

Table 6.1 Expressions for service moments and serviceability moment coefficients

Location	Expression for M_s	Expression for μ_s
Interior support negative moment	$M_s = \dfrac{w_d L^2}{8}\left[\dfrac{\left(2+7\gamma+3\gamma^2\right)(1+\alpha)-(2+\gamma)\gamma^3}{3+7\gamma+3\gamma^2}\right]$	$\mu_s = \dfrac{\left(2+7\gamma+3\gamma^2\right)(1+\alpha)-(2+\gamma)\gamma^3}{8\lambda(1.25+1.5\alpha)\left(3+7\gamma+3\gamma^2\right)}$
First interior support negative moment	$M_s = \dfrac{w_d L^2}{16}\left[\dfrac{\left(5\gamma^4+6\gamma^3+8\gamma+8\right)(1+\alpha)-(2+\gamma)\gamma^3}{4+7\gamma+3\gamma^2}\right]$	$\mu_s = \dfrac{\left(2+7\gamma+3\gamma^2\right)(1+\alpha)-(2+\gamma)\gamma^3}{8\lambda(1.25+1.5\alpha)\left(3+7\gamma+3\gamma^2\right)}$
Interior span positive moment	$M_s = \dfrac{w_d L^2}{8}\left[\dfrac{\left(2+8\gamma+3\gamma^2\right)(1+\alpha)-2(2+\gamma)\gamma^3}{6+10\gamma+3\gamma^2}\right]$	$\mu_s = \dfrac{\left(2+8\gamma+3\gamma^2\right)(1+\alpha)-2(2+\gamma)\gamma^3}{8\lambda(1.25+1.5\alpha)\left(6+10\gamma+3\gamma^2\right)}$
Exterior span positive moment	$M_s = \dfrac{w_d L^2}{32(1+\alpha)}\left[\dfrac{\left(9+19\gamma+6\gamma^2\right)(1+\alpha)-\gamma^3(3+\gamma)}{6+10\gamma+3\gamma^2}\right]^2$	$\mu_s = \dfrac{1}{32\lambda(1.25+1.5\alpha)(1+\alpha)}\left[\dfrac{\left(9+19\gamma+6\gamma^2\right)(1+\alpha)-(3+\gamma)\gamma^3}{\left(6+10\gamma+3\gamma^2\right)}\right]^2$
Two span beam negative moment at interior support	$M_s = \dfrac{w_d L^2}{8}\left[\dfrac{(1+\alpha)\left(1+\gamma^3\right)}{1+\gamma}\right]$	$\mu_s = \dfrac{(1+\alpha)\left(1+\gamma^3\right)}{8\lambda(1.25+1.5\alpha)(1+\gamma)}$
Two span beam positive moment	$M_s = \dfrac{w_d L^2}{8(1+\alpha)}\left[\dfrac{(1+\alpha)(3+4\gamma)-\gamma^3}{4(1+\gamma)}\right]^2$	$\mu_s = \dfrac{1}{8\lambda(1+\alpha)(1.25+1.5\alpha)}\left[\dfrac{(1+\alpha)(3+4\gamma)-\gamma^3}{4(1+\gamma)}\right]^2$

Table 6.2 Expressions for factored moments and factored moment coefficients

Location	Expression for M_f	Expression for μ_f
Interior support negative moment	$M_f = \dfrac{w_d L^2}{8}\left[\dfrac{\left(2+7\gamma+3\gamma^2\right)\left(1.25+1.5\alpha\right)-1.25\left(2+\gamma\right)\gamma^3}{3+7\gamma+3\gamma^2}\right]$	$\mu_f = \dfrac{\left(2+7\gamma+3\gamma^2\right)\left(1.25+1.5\alpha\right)-1.25\left(2+\gamma\right)\gamma^3}{8\left(1.25+1.5\alpha\right)\left(3+7\gamma+3\gamma^2\right)}$
First interior support negative moment	$M_f = \dfrac{w_d L^2}{16}\left[\dfrac{\left(5\gamma^4+6\gamma^3+8\gamma+8\right)\left(1.25+1.5\alpha\right)-1.25\left(2+\gamma\right)\gamma^3}{4+7\gamma+3\gamma^2}\right]$	$\mu_f = \dfrac{\left(5\gamma^4+6\gamma^3+8\gamma+8\right)\left(1.25+1.5\alpha\right)-1.25\left(2+\gamma\right)\gamma^3}{8\left(1.25+1.5\alpha\right)\left(8+14\gamma+6\gamma^2\right)}$
Interior span positive moment	$M_f = \dfrac{w_d L^2}{8}\left[\dfrac{\left(2+8\gamma+3\gamma^2\right)\left(1.25+1.5\alpha\right)-2.5\left(2+\gamma\right)\gamma^3}{6+10\gamma+3\gamma^2}\right]$	$\mu_f = \dfrac{\left(2+8\gamma+3\gamma^2\right)\left(1.25+1.5\alpha\right)-2.5\left(2+\gamma\right)\gamma^3}{8\left(1.25+1.5\alpha\right)\left(6+10\gamma+3\gamma^2\right)}$
Exterior span positive moment	$M_f = \dfrac{w_d L^2}{32\left(1.25+1.5\alpha\right)}\left[\dfrac{\left(9+19\gamma+6\gamma^2\right)\left(1.25+1.5\alpha\right)-1.25\left(3+\gamma\right)\gamma^3}{6+10\gamma+3\gamma^2}\right]^2$	$\mu_f = \dfrac{1}{32}\left[\dfrac{\left(9+19\gamma+6\gamma^2\right)\left(1.25+1.5\alpha\right)-1.25\left(3+\gamma\right)\gamma^3}{\left(1.25+1.5\alpha\right)\left(6+10\gamma+3\gamma^2\right)}\right]^2$
Two span beam negative moment at interior support	$M_f = \dfrac{w_d L^2}{8}\left[\dfrac{\left(1.25+1.5\alpha\right)\left(1+\gamma^3\right)}{1+\gamma}\right]$	$\mu_f = \dfrac{\left(1+\gamma^3\right)}{8\left(1+\gamma\right)}$
Two span beam positive moment	$M_f = \dfrac{w_d L^2}{8\left(1.25+1.5\alpha\right)}\left[\dfrac{\left(1.25+1.5\alpha\right)\left(3+4\gamma\right)-1.25\gamma^3}{4\left(1+\gamma\right)}\right]^2$	$\mu_f = \dfrac{1}{8}\left[\dfrac{\left(1.25+1.5\alpha\right)\left(3+4\gamma\right)-1.25\gamma^3}{4\left(1+\gamma\right)\left(1.25+1.5\alpha\right)}\right]^2$

Table 6.3 Moment Redistribution Limits for Serviceability

Location	Minimum β %	Maximum β %
Interior Support	21.3	28.4
First Interior Support	21	27.1
Interior Span	21.7	34
Exterior Span	21.3	28.2
Two Span - Int. Support	21	26.7
Two Span - Span	21.3	28.6

The allowable moment redistribution for critical sections ranges from 21% to 34%. The lower limit of β for all critical sections is about 21% and occurs for the case when the load ratio and adjacent span ratio are at their lowest value (α=0.5, γ=0.67). The upper limit for β varies between 27% and 34% and occurs for the case when the load ratio and adjacent span ratio are at their maximum value (α=3, γ=1.5).

6.3 Comparison Between Serviceability and Ductility

For serviceability limit-state the moment redistribution limit varies from 21% to 34%, depending upon the location of critical section, the adjacent span ratio and the service live load to dead load ratio. Within given ranges of parameters, the lower limit for allowable moment redistribution is 21%. Ductility model developed in Chapter 4 provides allowable moment redistribution for variations of different parameters. The lower and upper limits of the model were given in Fig. 6.21. Assuming a reinforcement index of 0.2 (ω=$A_s f_y$/bdf_c') for most practical cases, the ductility model gives a minimum allowable moment redistribution of 20% and a maximum value of 45%. For values of reinforcement index below 0.2, the ductility model allows much higher redistribution than that allowed by serviceability. Thus for beams with reinforcement index below 0.2, the serviceability limit state dictates the allowable limit of moment redistribution. For beams with reinforcement index greater than 0.2, either serviceability or ductility may govern depending upon the influencing parameters. For reinforcement index values of 0.2

196

or less, 20% moment redistribution can be used without explicit check of ductility and serviceability.

6.4 Empirical Equations For β based on Serviceability

It was noted in previous chapters that ductility limit-state could allow moment redistribution in excess of 50% for favourable combinations of parameters. Detailed evaluation of serviceability requirements in this chapter reveals that serviceability can restrict the allowable moment redistribution to as low as 21%, depending upon the live load to dead load ratio and the ratio of adjacent spans. Considering the lower limit of serviceability as the basis for allowable moment redistribution, one can develop a set of empirical equations by putting serviceability limits on the ductility curves, produced in Chapter 5. These ductility curves of β vs ω are shown in Fig. 6.22 to Fig. 6.26 for different values of L/d. The range of L/d values is the same as that used in the previous Chapter. The maximum value of ω used is 0.318, which corresponds to the maximum value of c/d=0.6 allowed by the code. Superimposing the requirements of serviceability on ductility curves, gives the allowable limits of β as shown in Fig. 6.22 to Fig. 6.26. The corresponding empirical equations for β are:

Case 1: L/d ≤ 8.5, ω ≤ 0.318 (Fig. 6.22 and 6.23)

$$\beta = 20\%$$

Case 2: 8.5 <L/d ≤ 12.5, ω ≤ 0.318 (Fig. 6.24)

$$\beta = 42 - 88\omega \le 20\% \qquad [6.13]$$

Case 3: 12.5 <L/d ≤ 16, ω ≤ 0.318 (Fig. 6.25)

$$\beta = 38 - 82\omega \le 20\% \qquad [6.14]$$

197

Case 4: 16 <L/d ≤ 21, ω ≤ 0.318 (Fig. 6.26)

$$\beta = 38.6 - 93\omega \le 20\%$$ [6.15]

CSA A23.3-94 limits for moment redistribution are also superimposed in Figures 6.22 through 6.26. Table 6.4 shows the comparison between the code limits and the proposed limits of ω for 20% moment redistribution. The comparison shows that the code limits for ω are very restrictive. The code allowable limit of ω for 20% moment redistribution is only 0.106 (c/d = 0.2). The proposed equations would allow ω as high as 0.318 (c/d = 0.6) for 20% moment redistribution, depending upon the slenderness ratio. On the contrary code would allow 0% moment redistribution for ω = 0.318. Even for the highest slenderness ratio of 21, the proposed equations would allow ω = 0.2 (c/d=0.38) for 20% moment redistribution.

Table 6.4 Comparison of allowable ω for 20% moment redistribution

Slenderness ratio (L/d)	ω (Code Equation)	ω (Proposed Equations)
6	0.106	0.318
8.5	0.106	0.318
12.5	0.106	0.25
16	0.106	0.22
21	0.106	0.2

Moment redistribution is often required to reduce the congestion of reinforcement at a heavily reinforced section. Such a section would have a value of ω typically in excess of 0.1. The code limit of ω is very conservative and will not allow taking advantage of moment redistribution in such situations.

The proposed equations for moment redistribution take into account both the ductility and the serviceability limit states. Theses consider the effects of various parameters both

explicitly and implicitly. These equations are simple, yet not overly conservative, and hence can be used in place of code equation for moment redistribution. For real simplicity, one could use Eq. 6.15, which is the most conservative of the governing equations. Equation 6.15 can be rewritten in terms of c/d as:

$$\beta = 38.6 - 49.3 \frac{c}{d}$$

[6.16]

6.5 Summary and Conclusions

Moment redistribution limits are evaluated for the condition of no yielding under service loads, for continuous reinforced concrete beams. For practical limits of service live load to dead load ratio, the allowable moment redistribution ranges from 21% to 34%. While ductility criteria allow moment redistribution in excess of 50% under favourable conditions, the maximum limit from serviceability criteria is in the range of 28% for most cases. Unless one allows for yielding of steel and cracking of concrete at service load level, serviceability rather than ductility would dictate the allowable limit of moment redistribution for values of reinforcement index below 0.2. For beams with a reinforcement index greater than 0.2, either serviceability or ductility may govern depending upon the values of influencing parameters. For mechanical reinforcement index values of 0.2 or less, 20% moment redistribution can be used without explicit check of ductility and yielding under service loads.

Empirical equations for allowable moment redistribution are derived considering both serviceability and ductility requirements. These consider the effects of various parameters both explicitly and implicitly. The allowable values of ω (or c/d) using these equations are much more liberal than the code allowable values. These equations are simple, yet not overly conservative, and hence can be used in place of code equation for moment redistribution. For real simplicity, one could use Eq. 6.16, which is the most conservative of the governing equations.

199

Section   Strain   Stress

(a)

Section   Strain   Stress
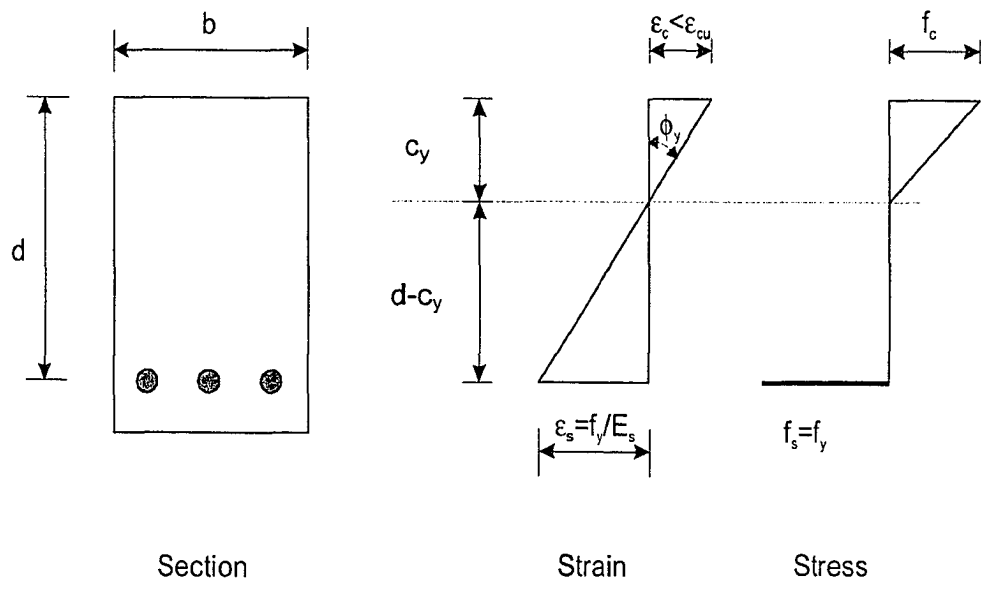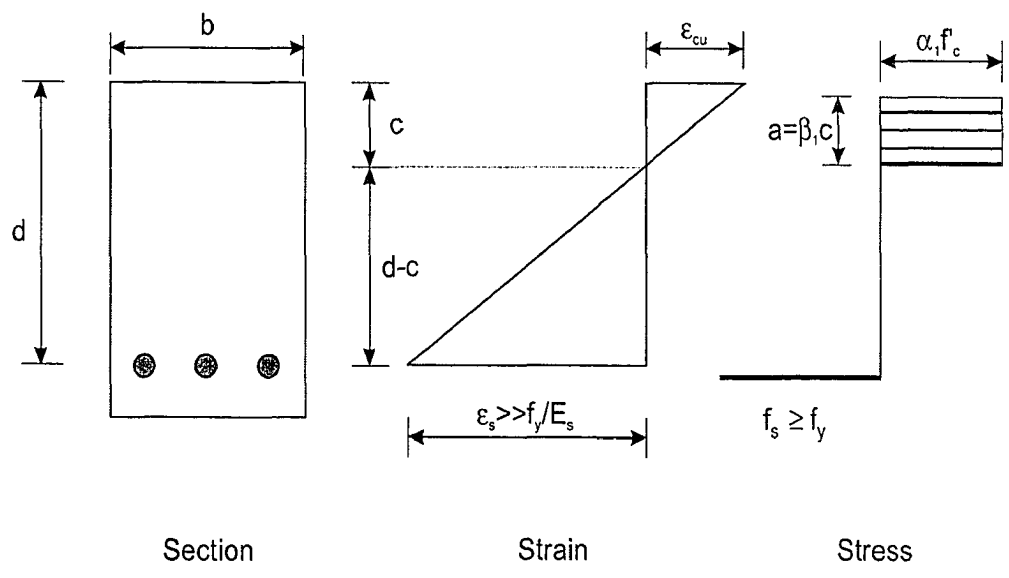
(b)

Figure 6.1 Stress and strain distribution in flexure (a) at first yield (b) at ultimate

200
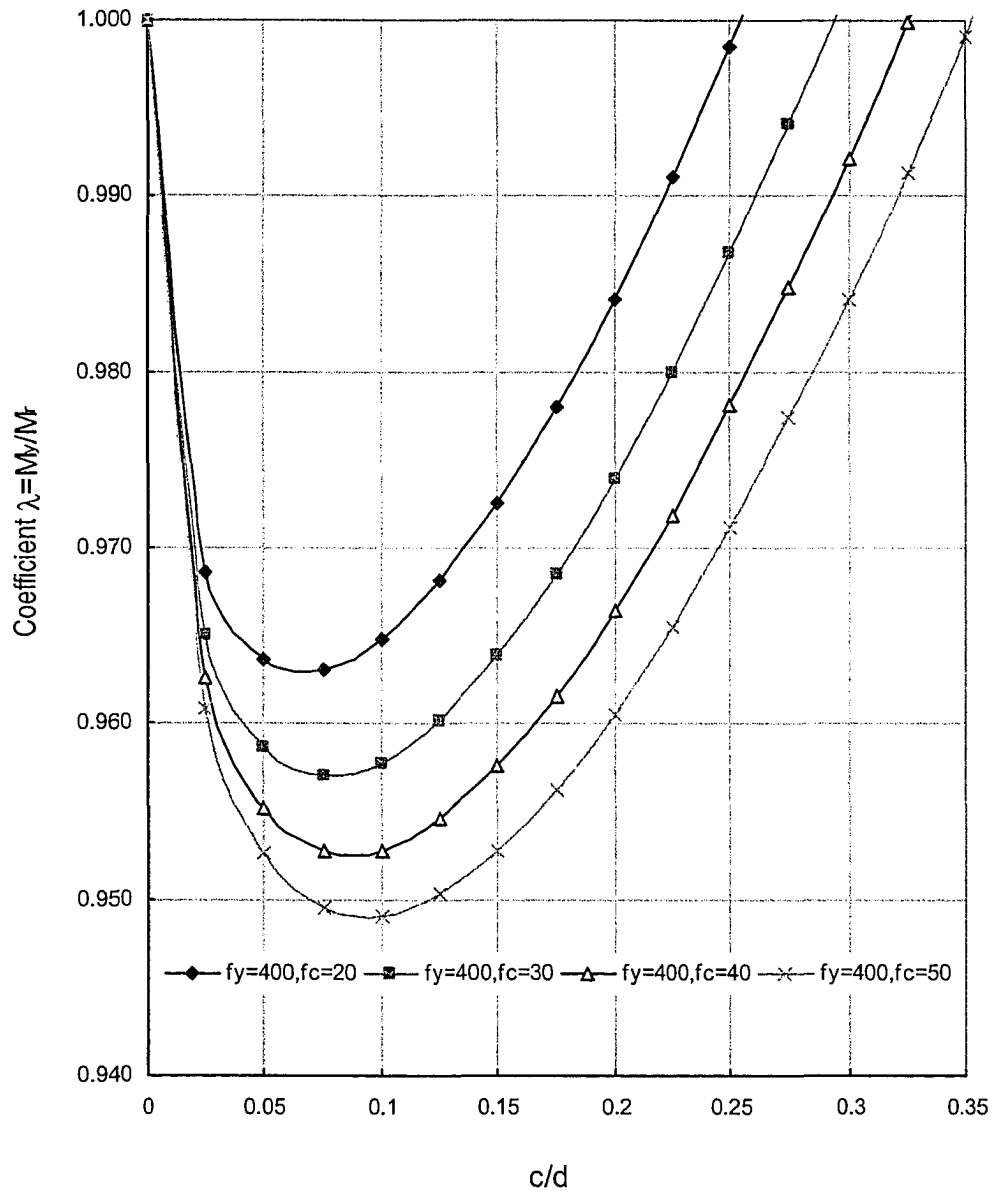
Figure 6.2 Limiting yield moment coefficient vs c/d

201
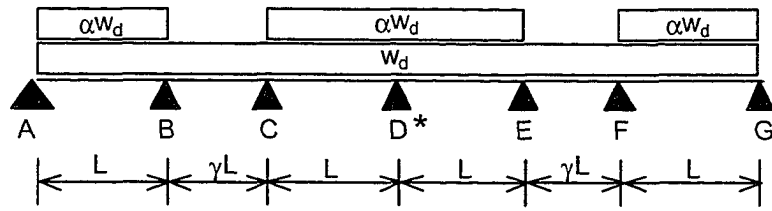
$$* \quad \mu_s = \frac{\left(2 + 7\gamma + 3\gamma^2\right)\left(1 + \alpha\right) - \left(2 + \gamma\right)\gamma^3}{8\lambda\left(1.25 + 1.5\alpha\right)\left(3 + 7\gamma + 3\gamma^2\right)}$$
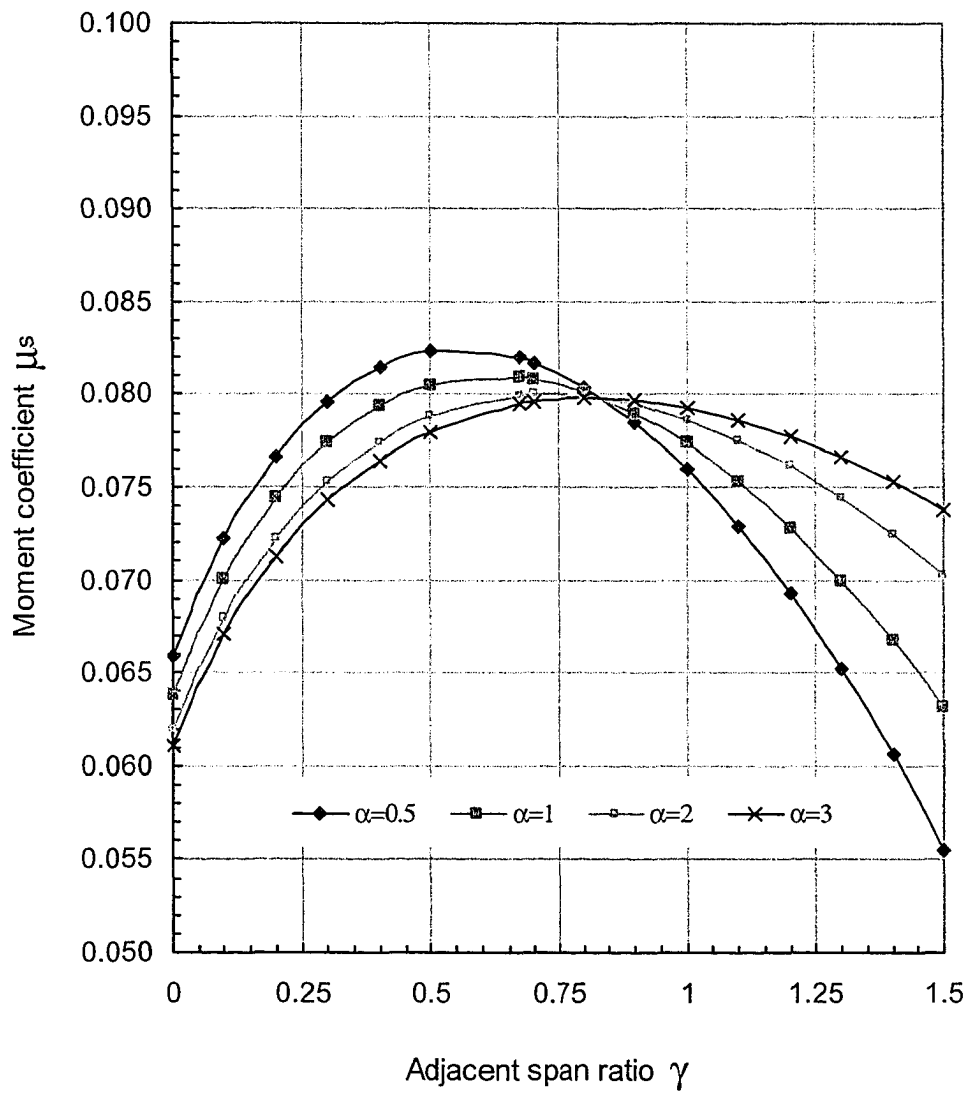
Figure 6.3 Serviceability moment coefficient for negative moment at interior support of a continuous beam

202
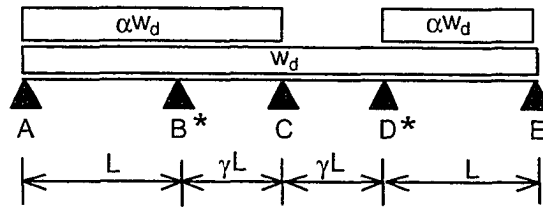
$$\ast \quad \mu_s = \frac{\left(5\gamma^4 + 6\gamma^3 + 8\gamma + 8\right)\left(1 + \alpha\right) - \left(2 + \gamma\right)\gamma^3}{8\lambda\left(1.25 + 1.5\alpha\right)\left(8 + 14\gamma + 6\gamma^2\right)\gamma^2} \xleftarrow{} \text{omit } \gamma^2 \text{ if } \gamma < 1$$
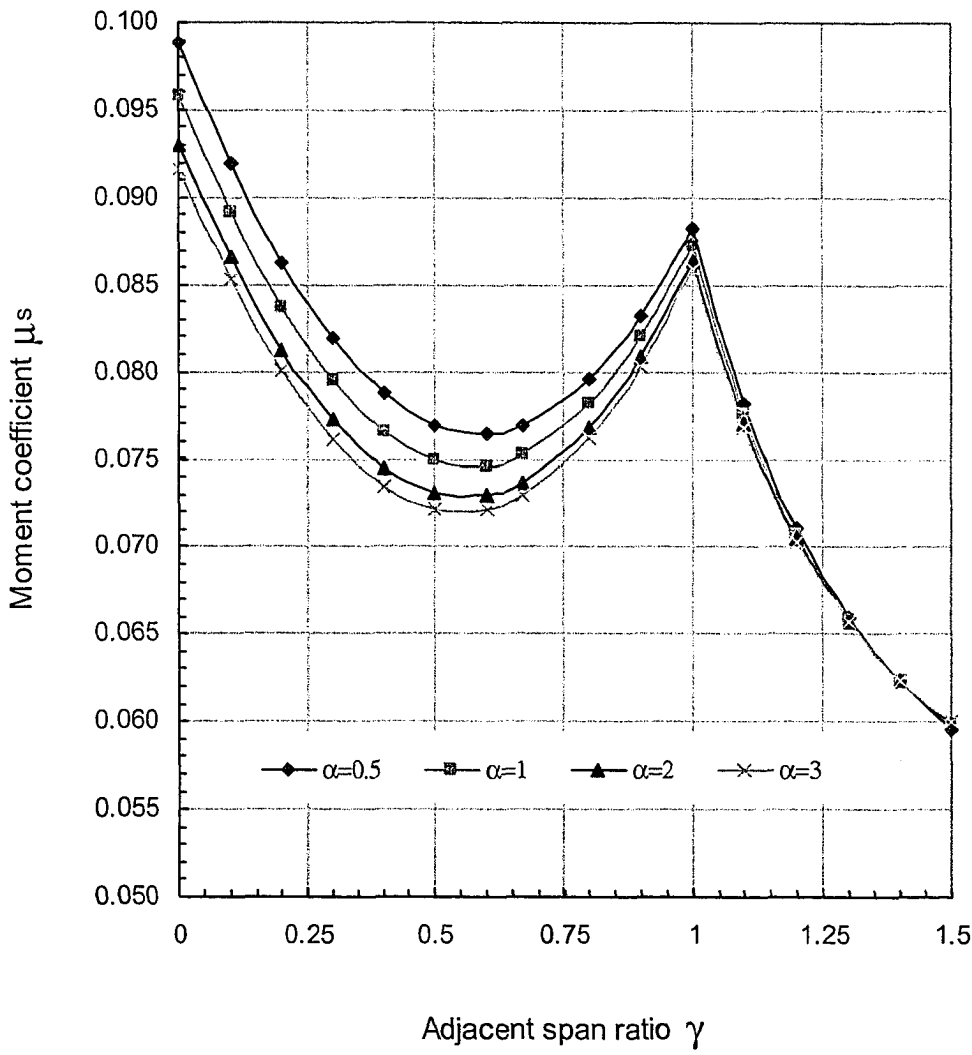
Figure 6.4 Serviceability moment coefficient for negative moment at first interior support of a continuous beam

203
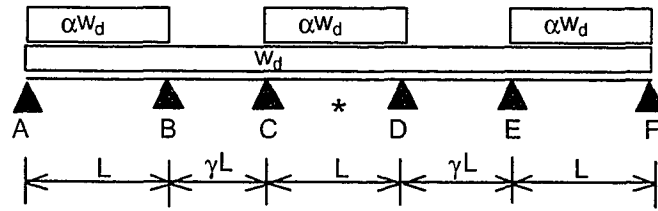
$$* \quad \mu_s = \frac{(2+8\gamma+3\gamma^2)(1+\alpha)-2\gamma^3(2+\gamma)}{8\lambda(1.25+1.5\alpha)(6+10\gamma+3\gamma^2)}$$
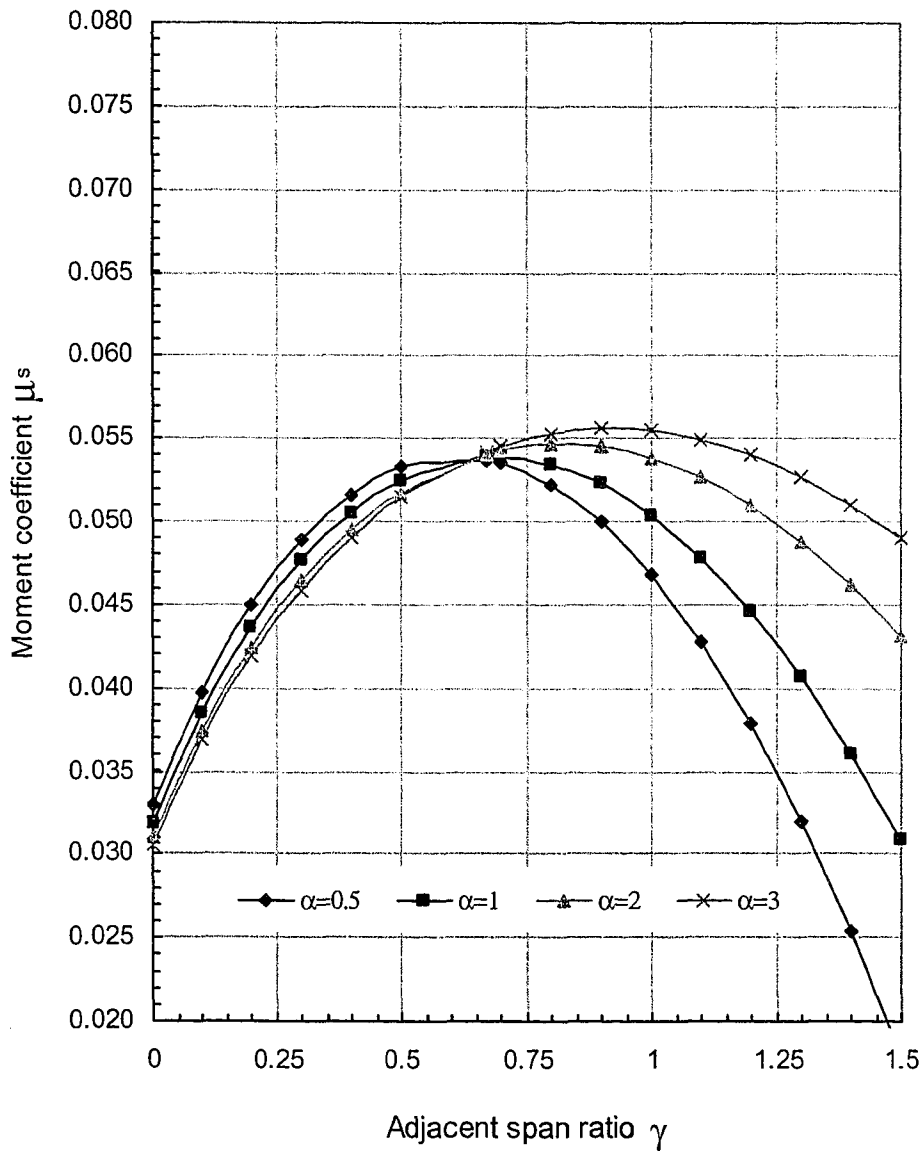
Figure 6.5 Serviceability moment coefficient for positive moment in interior span of a continuous beam

204
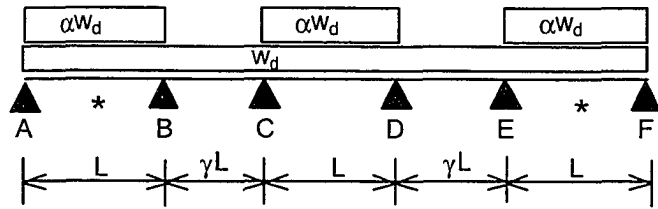
$$\mu_s = \frac{1}{32\lambda(1.25+1.5\alpha)(1+\alpha)}\left[\frac{(9+19\gamma+6\gamma^2)(1+\alpha)-(3+\gamma)\gamma^3}{(6+10\gamma+3\gamma^2)}\right]^2$$
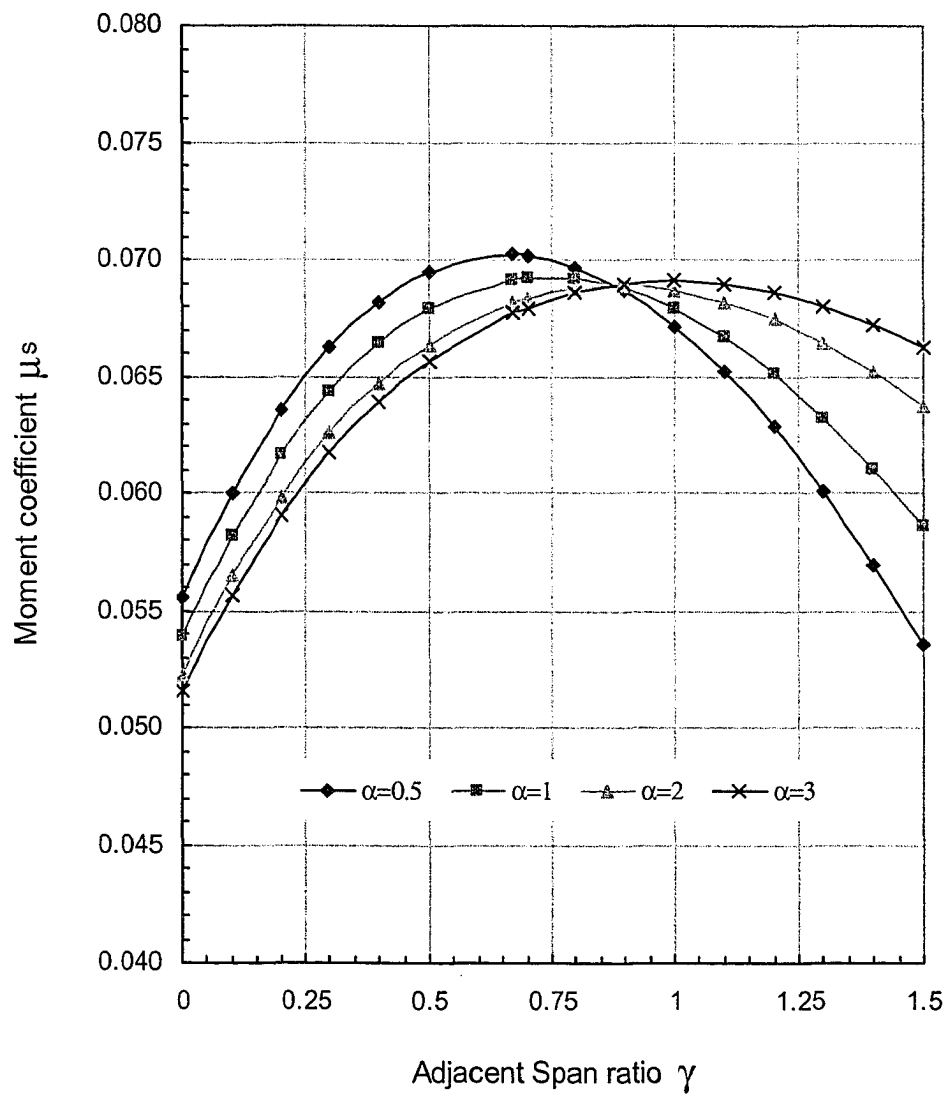
Figure 6.6 Serviceability moment coefficient for positive moment in exterior span of a continuous beam

205

$$* \quad \mu_s = \frac{(1+\alpha)(1+\gamma^3)}{8\lambda(1.25+1.5\alpha)(1+\gamma)}$$

Adjacent span ratio γ
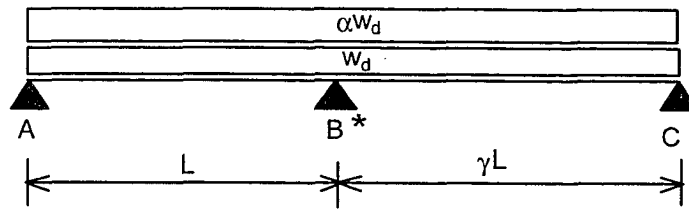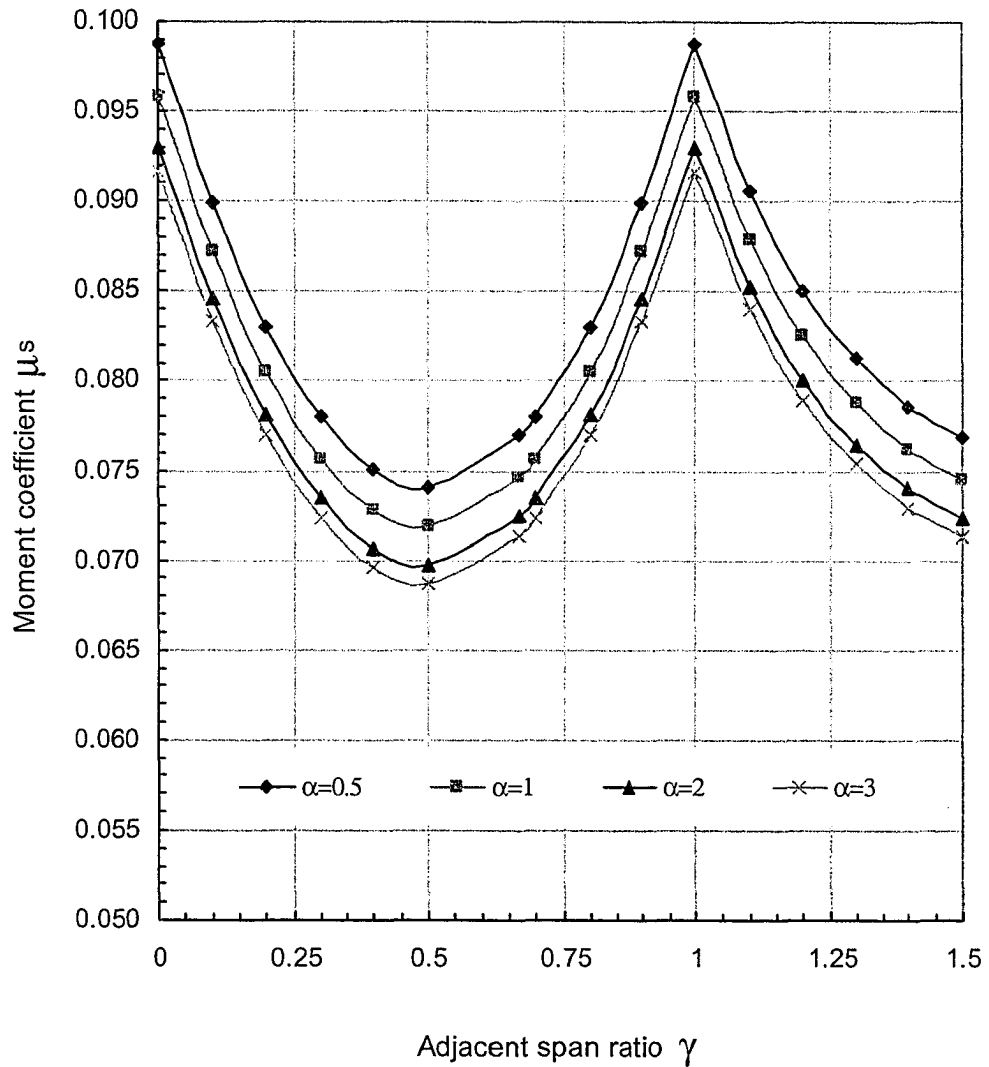
Figure 6.7   Serviceability moment coefficient for negative moment at interior support of a two-span beam
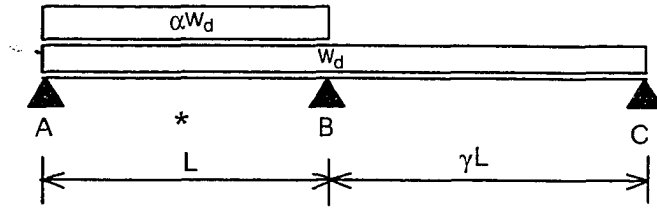
$$* \quad \mu_s = \frac{1}{8\lambda(1+\alpha)(1.25+1.5\alpha)}\left[\frac{(1+\alpha)(3+4\gamma)-\gamma^3}{4(1+\gamma)}\right]^2$$
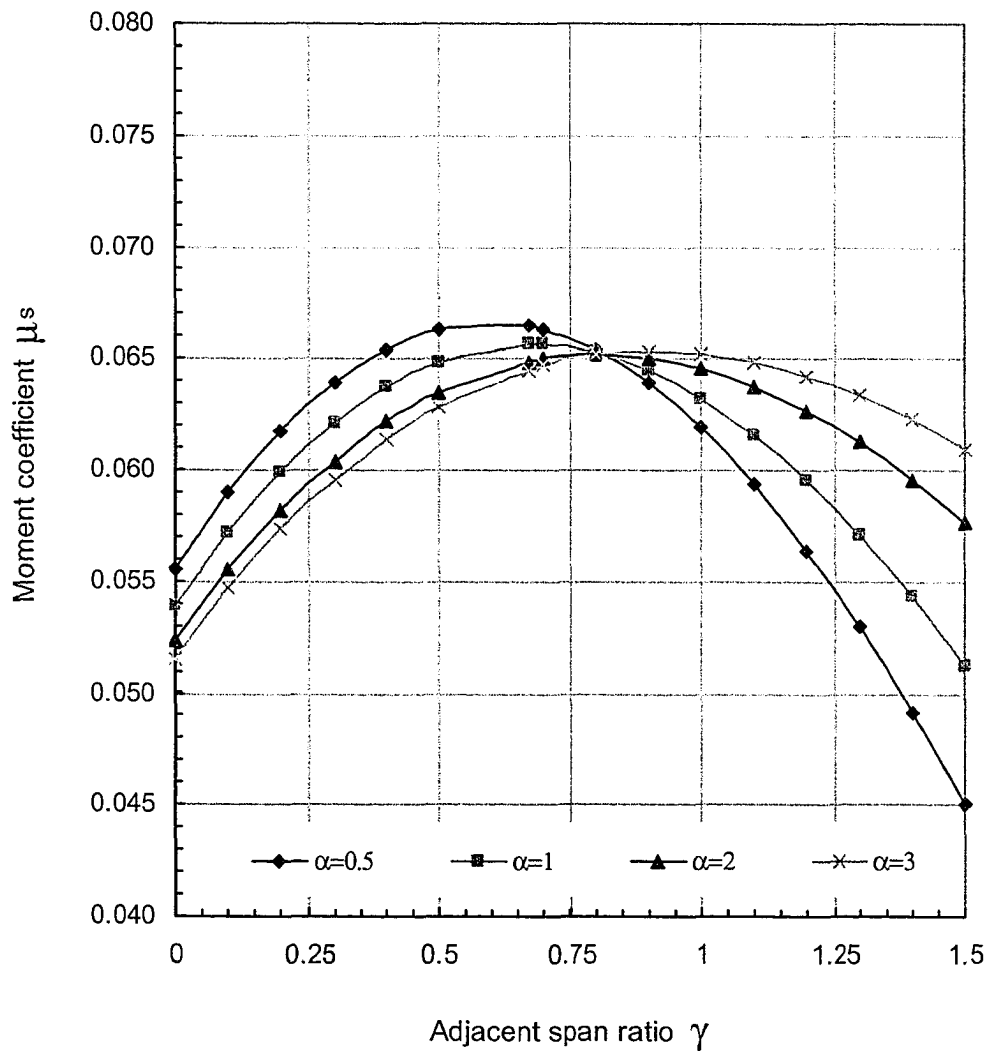
Figure 6.8 Serviceability moment coefficient for positive span moment in a two-span beam

207
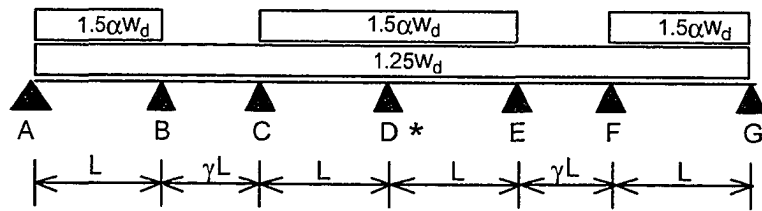
$$\mu_f = \frac{(2+7\gamma+3\gamma^2)(1.25+1.5\alpha)-1.25(2+\gamma)\gamma^3}{8(1.25+1.5\alpha)(3+7\gamma+3\gamma^2)}$$
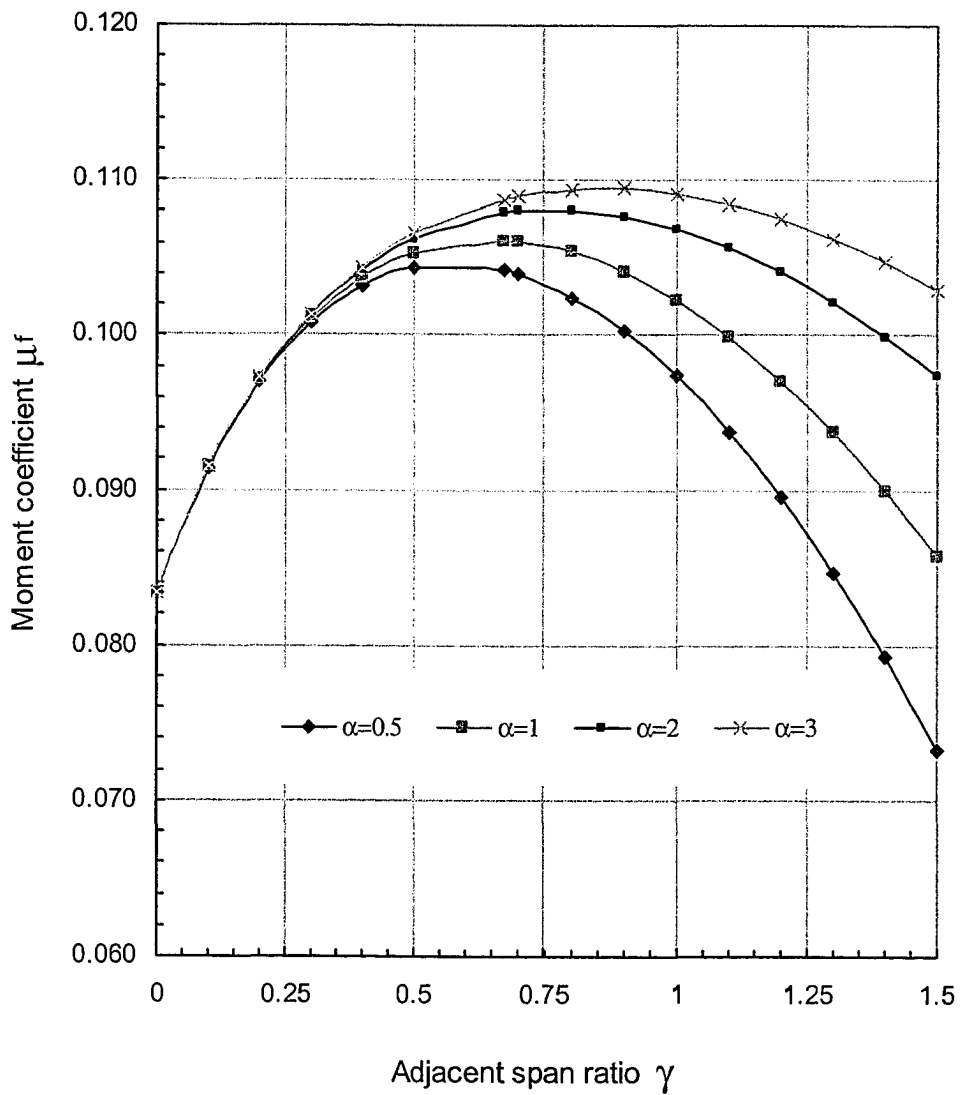
Figure 6.9 Factored moment coefficient for negative moment at interior support of a continuous beam

208
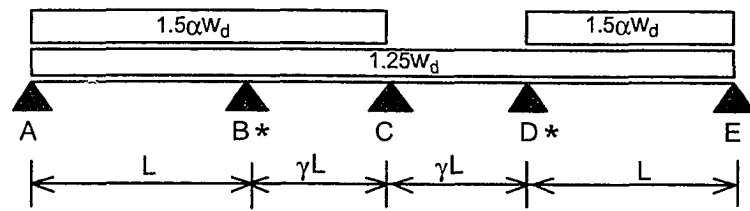
$$\mu_f = \frac{\left(5\gamma^4 + 6\gamma^3 + 8\gamma + 8\right)\left(1.25 + 1.5\alpha\right) - 1.25\left(2 + \gamma\right)\gamma^3}{8\left(1.25 + 1.5\alpha\right)\left(8 + 14\gamma + 6\gamma^2\right)\gamma^2} \quad \longleftarrow \text{omit } \gamma^2 \text{ if } \gamma < 1$$
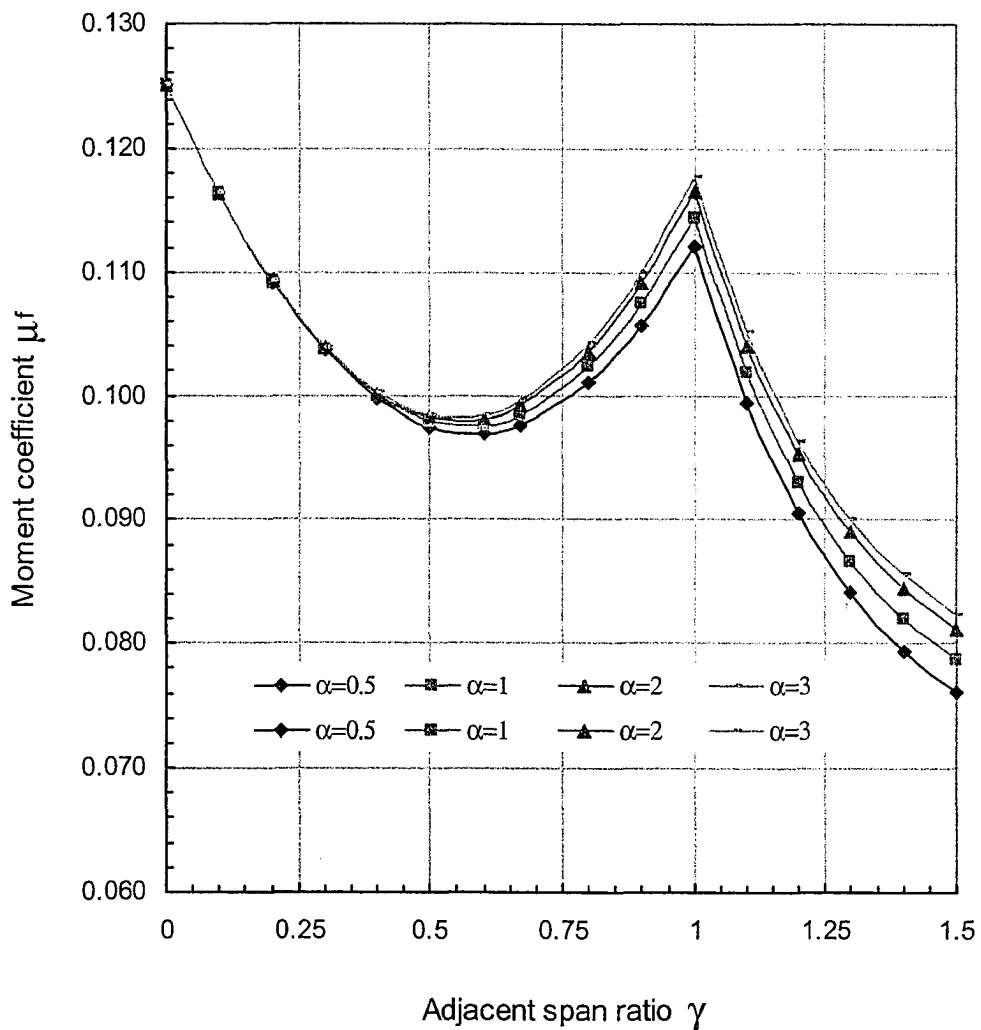
Figure 6.10 Factored moment coefficients for negative moment at first interior support of a continuous beam

209
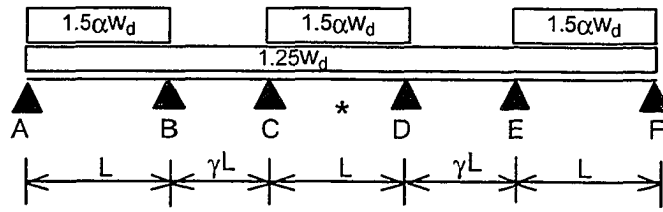
$$* \quad \mu_f = \frac{\left(2 + 8\gamma + 3\gamma^2\right)\left(1.25 + 1.5\alpha\right) - 1.25\left(2 + \gamma\right)2\gamma^3}{8 \quad \left(1.25 + 1.5\alpha\right)\left(6 + 10\gamma + 3\gamma^2\right)}$$
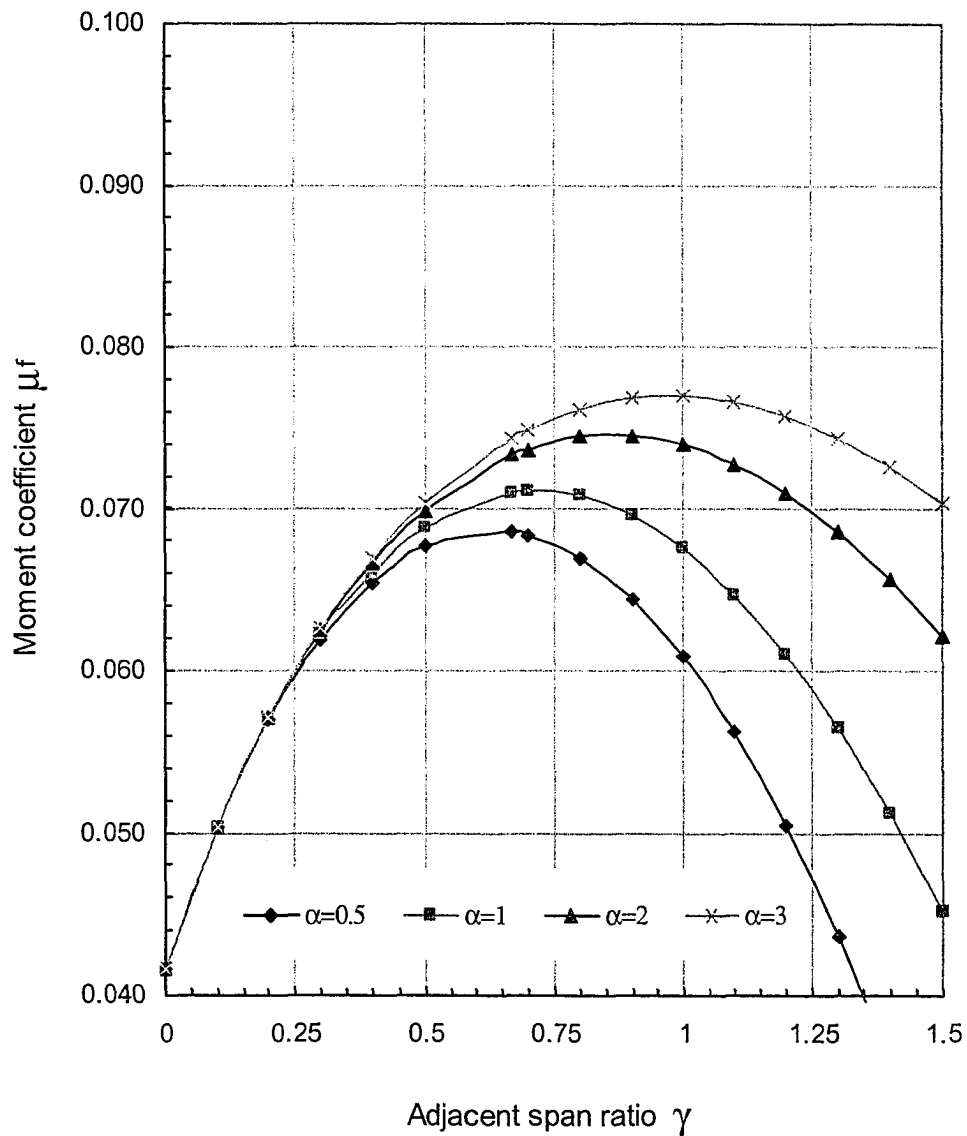
Figure 6.11 Factored elastic moment coefficient for positive moment in interior span of a continuous beam

210
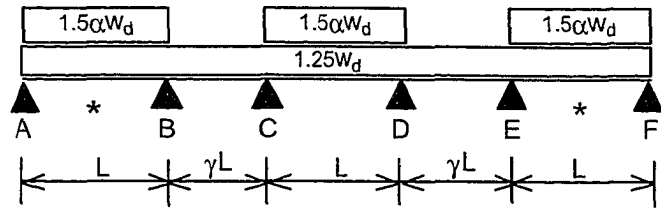
$$* \quad \mu_f = \frac{1}{32}\left[\frac{(9+19\gamma+6\gamma^2)(1.25+1.5\alpha)-1.25(3+\gamma)\gamma^3}{(1.25+1.5\alpha)(6+10\gamma+3\gamma^2)}\right]^2$$
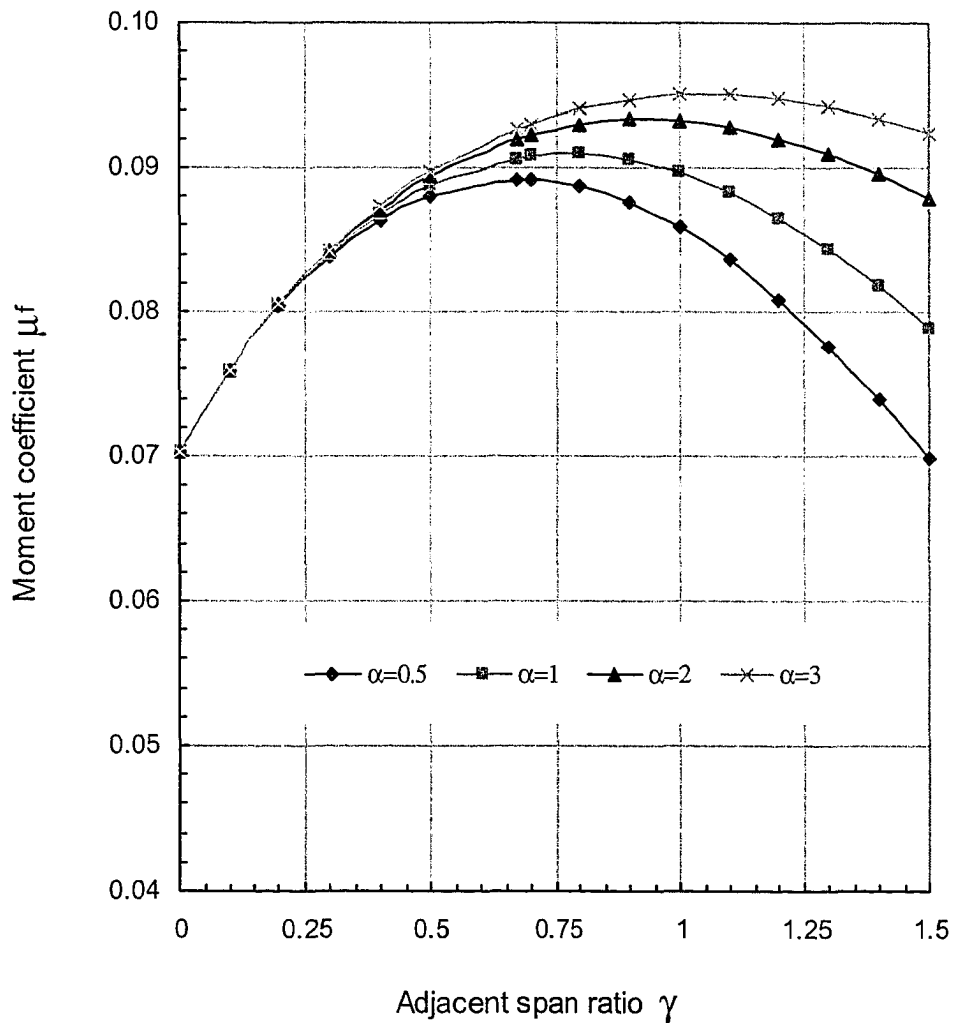
Figure 6.12 Factored elastic moment coefficient For positive moment in exterior span of a continuous beam

211

$$* \quad \mu_f = \frac{\left(1+\gamma^3\right)}{8(1+\gamma)}$$

Adjacent span ratio γ
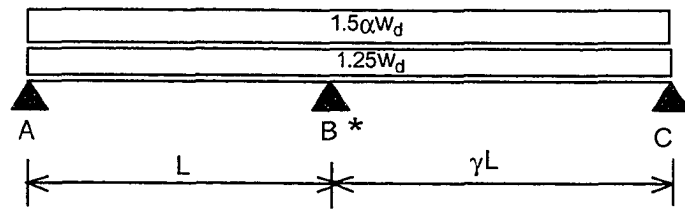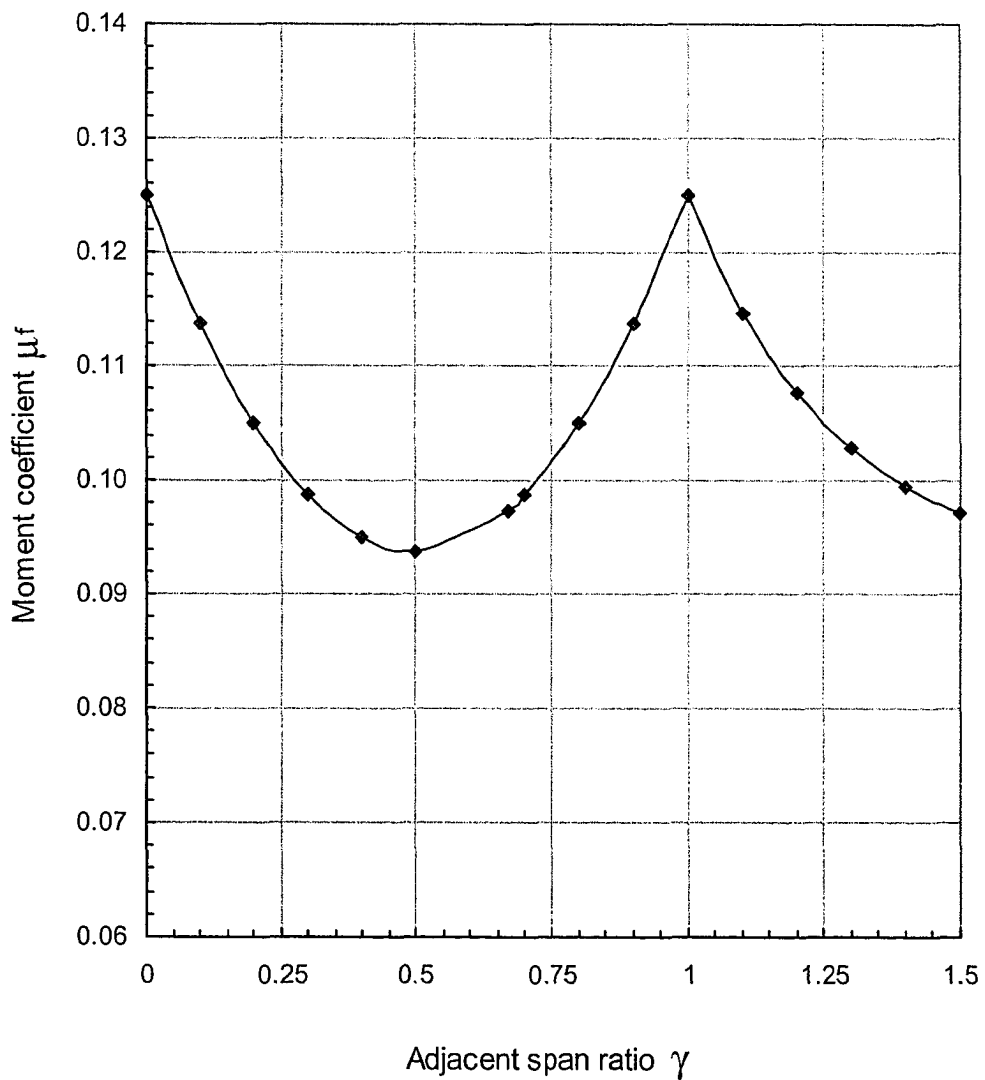
Figure 6.13 Factored elastic moment coefficient for negative moment at interior support of a two span beam

212
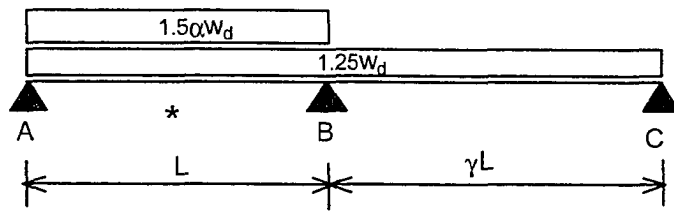
$$* \quad \mu_f = \frac{1}{8} \left[\frac{(1.25 + 1.5\alpha)(3 + 4\gamma) - 1.25\gamma^3}{4(1 + \gamma)(1.25 + 1.5\alpha)} \right]^2$$
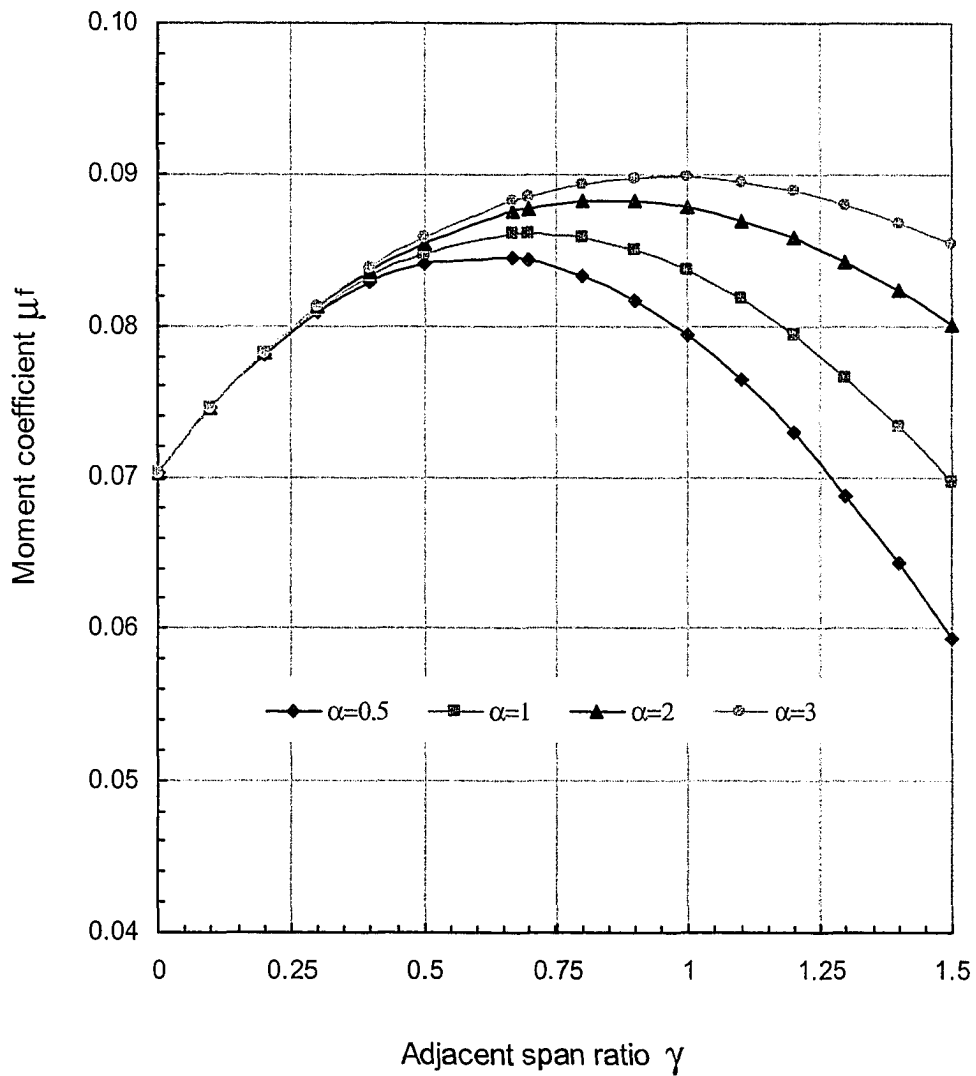
Figure 6.14 Factored elastic moment coefficient for positive span moment in a two span beam

213
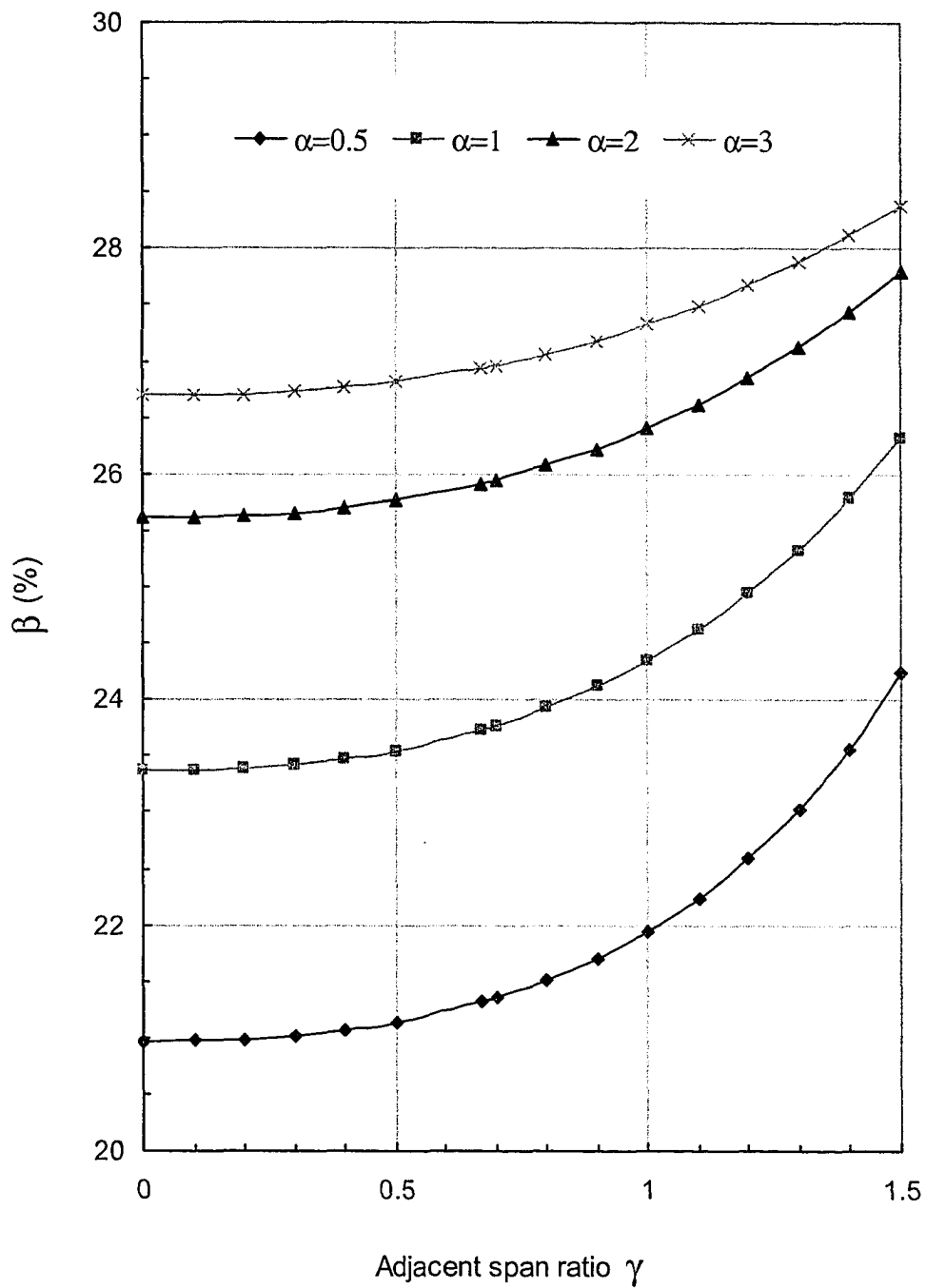
Figure 6.15 Allowable moment redistribution for negative moment at interior support of a continuous beam

214
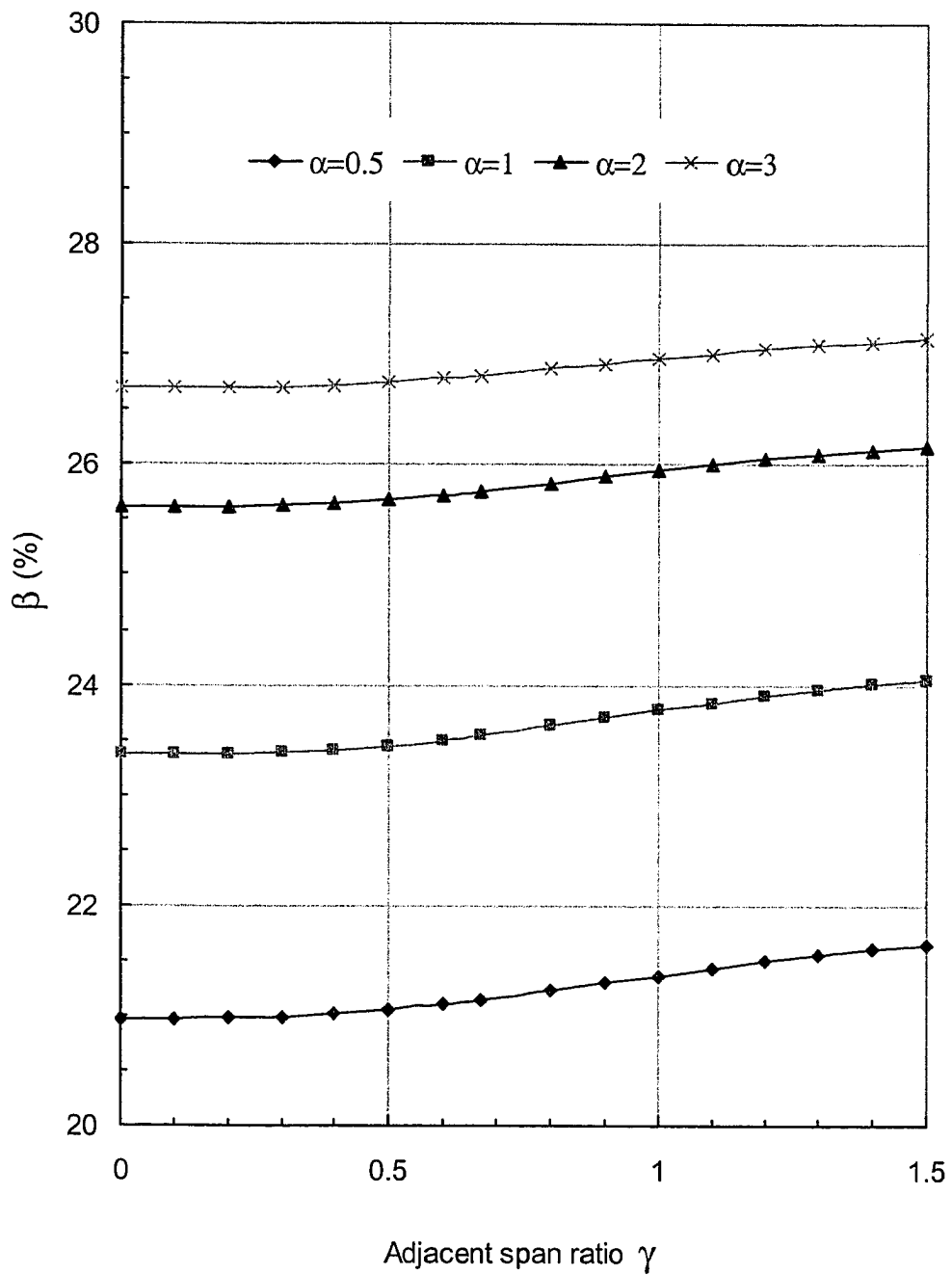
Figure 6.16 Allowable moment redistribution for negative
moment at first interior support of a continuous beam

215
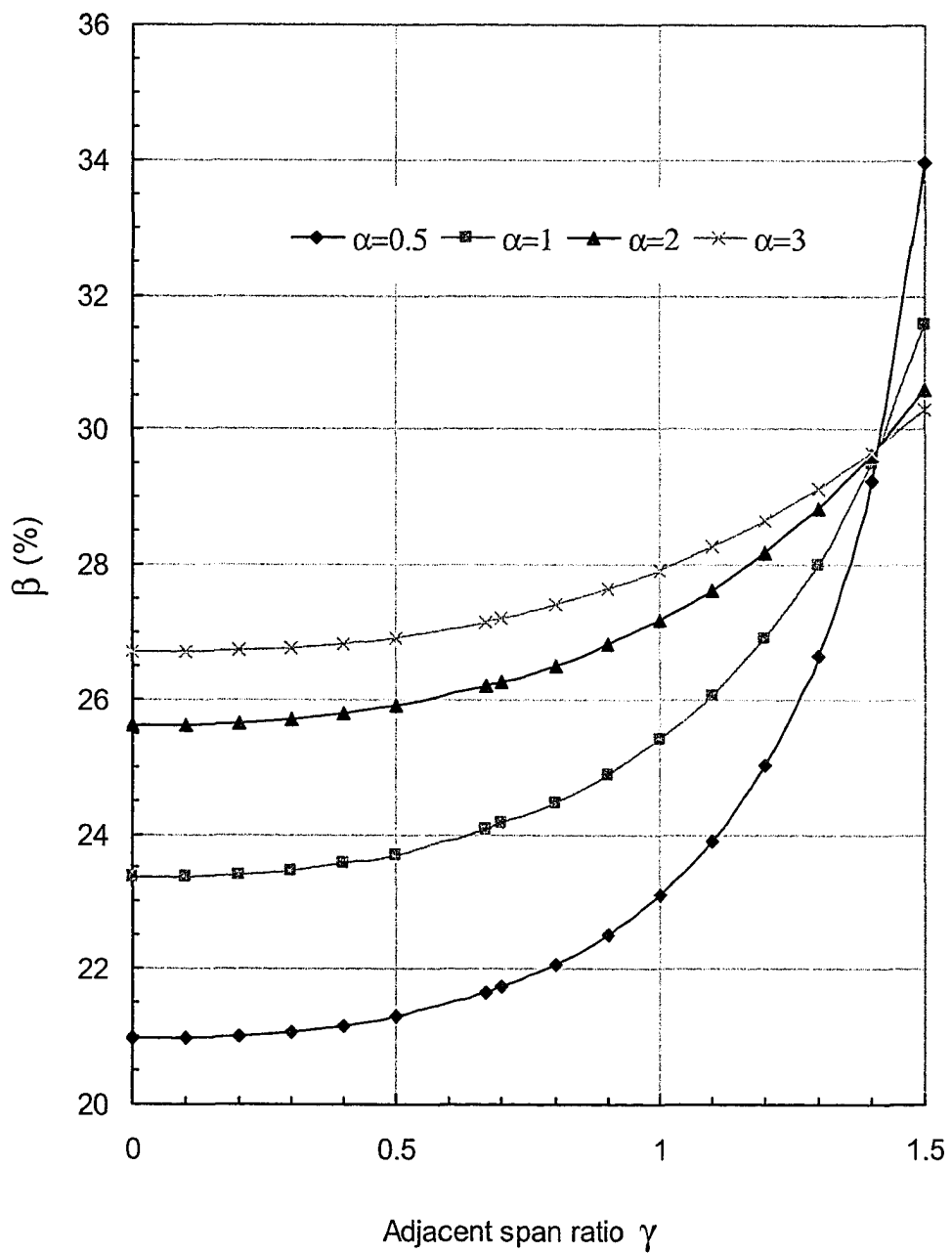
Figure 6.17 Allowable moment redistribution for positive
moment in interior span of a continuous beam

216
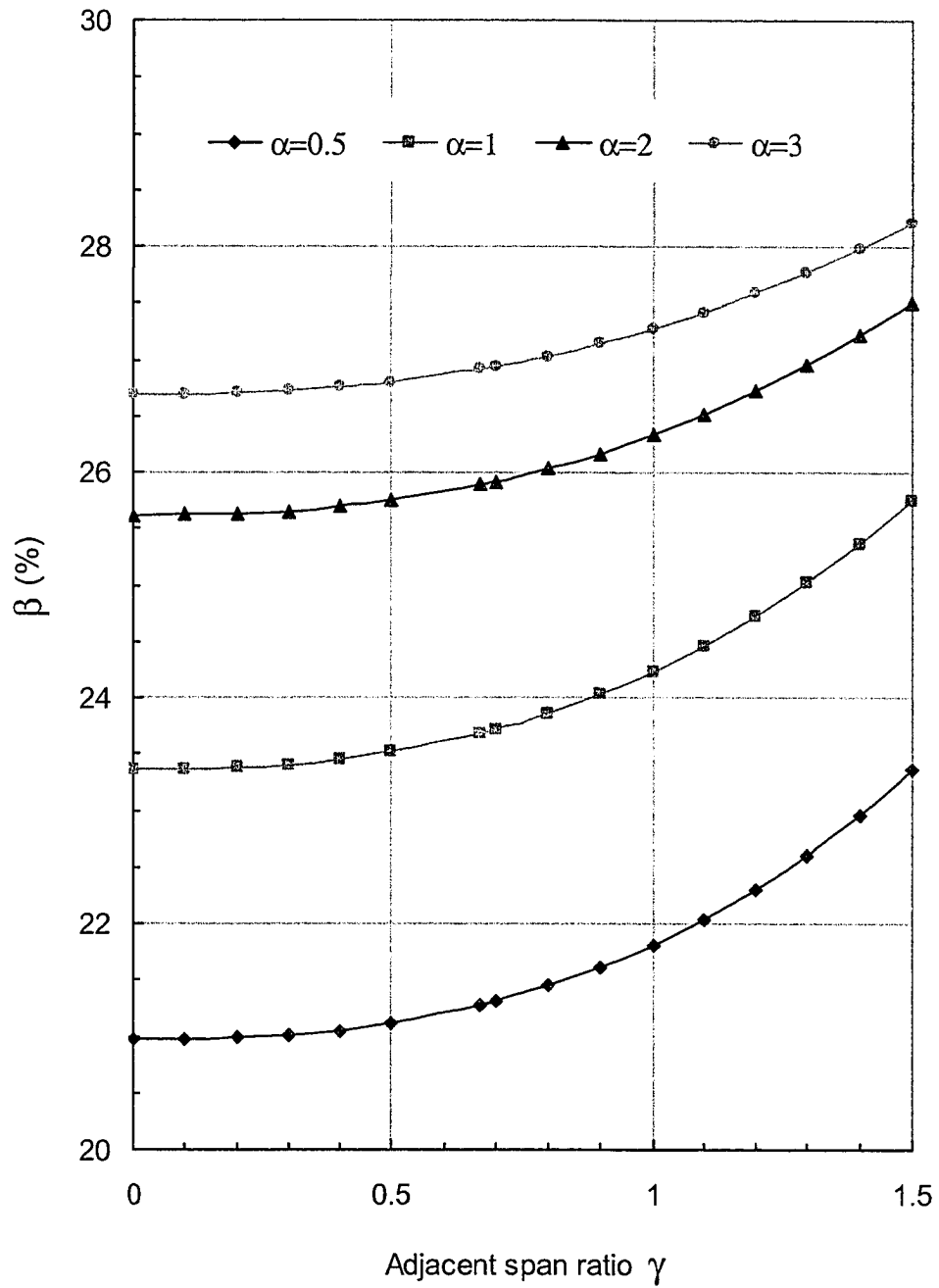
Figure 6.18 Allowable moment redistribution for positive
moment in exterior span of a continuous beam

217
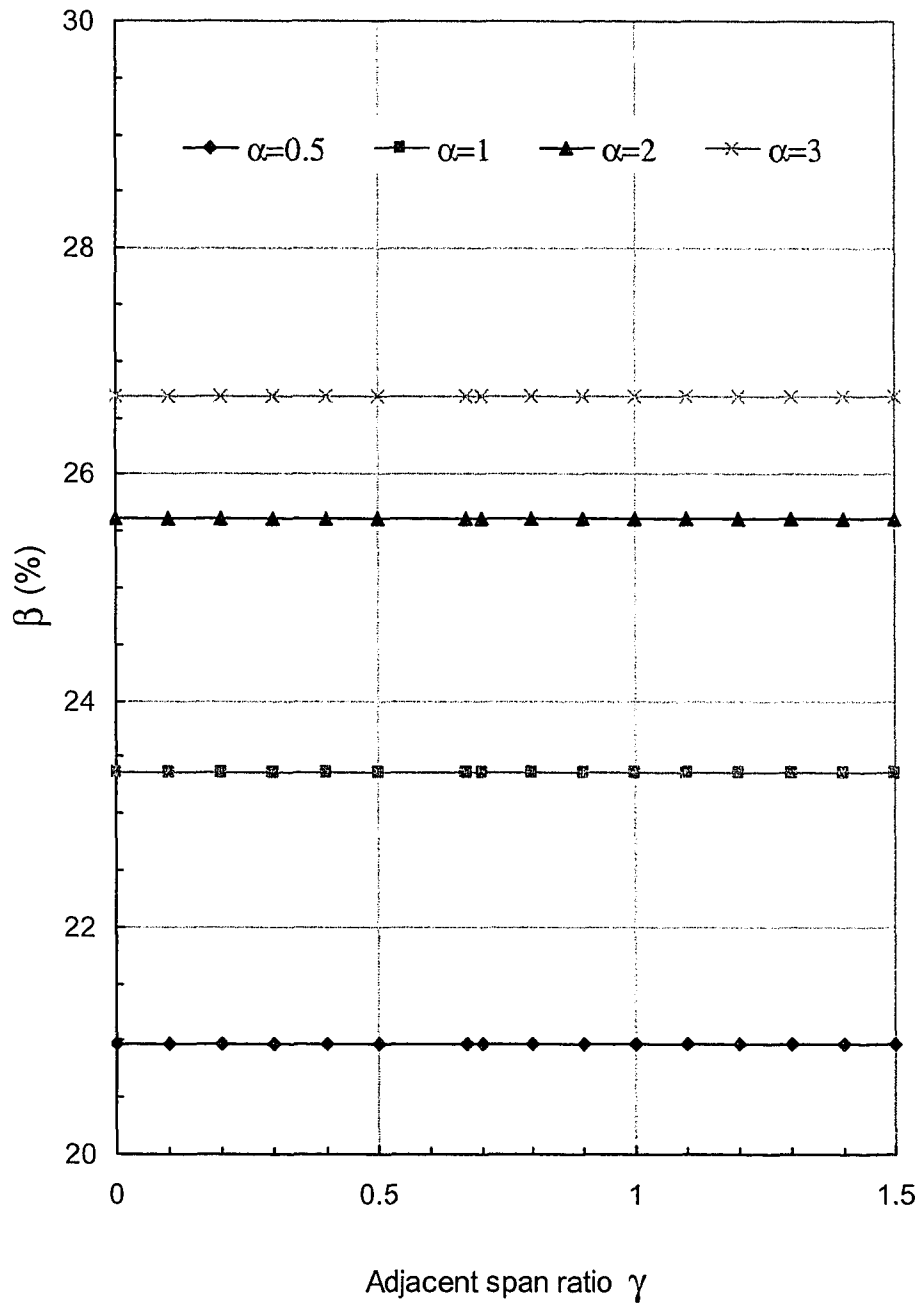
Figure 6.19 Allowable moment redistribution for negative
moment at interior support of a two-span beam

218
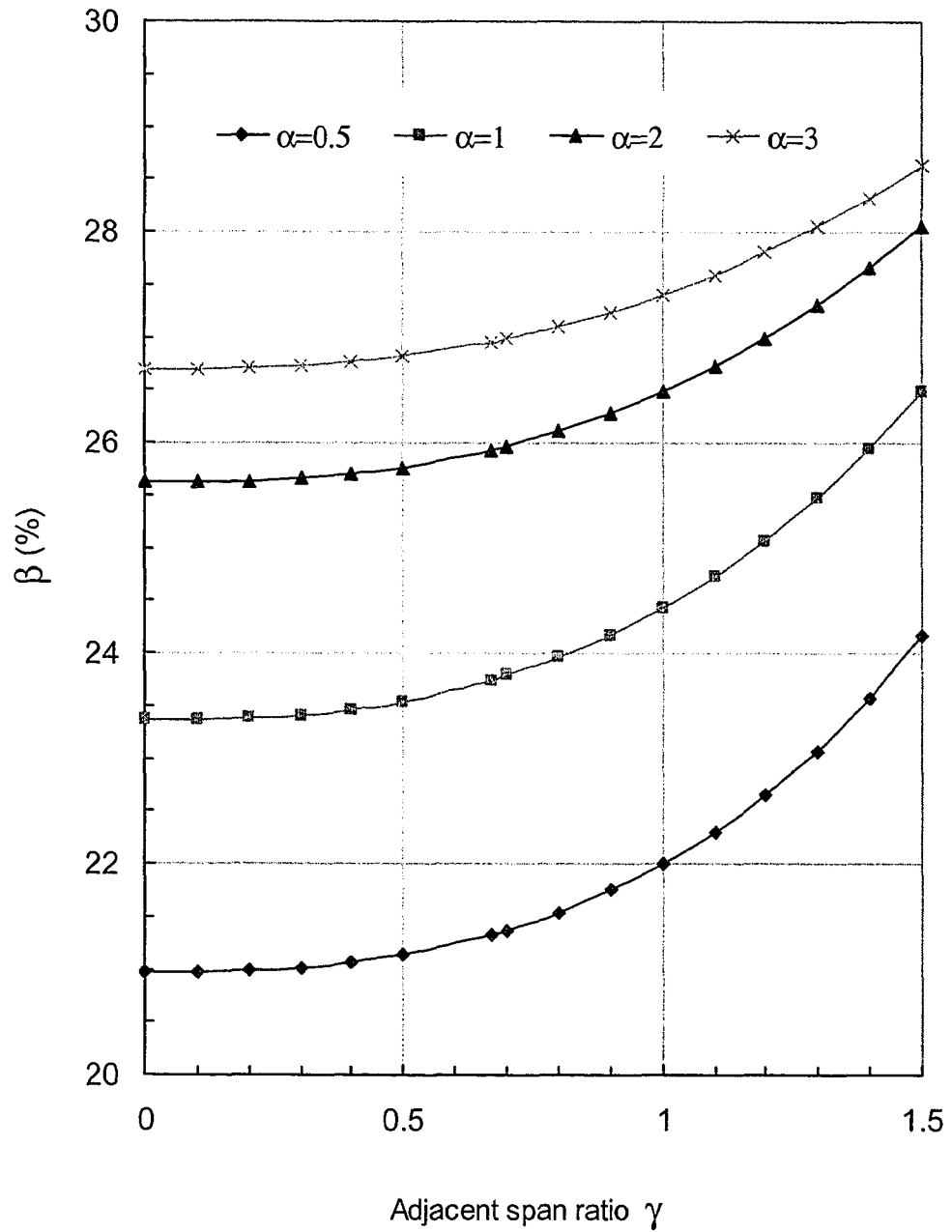
Fiure 6.20 Allowable moment redistribution for positive span
moment in a two-span beam

219
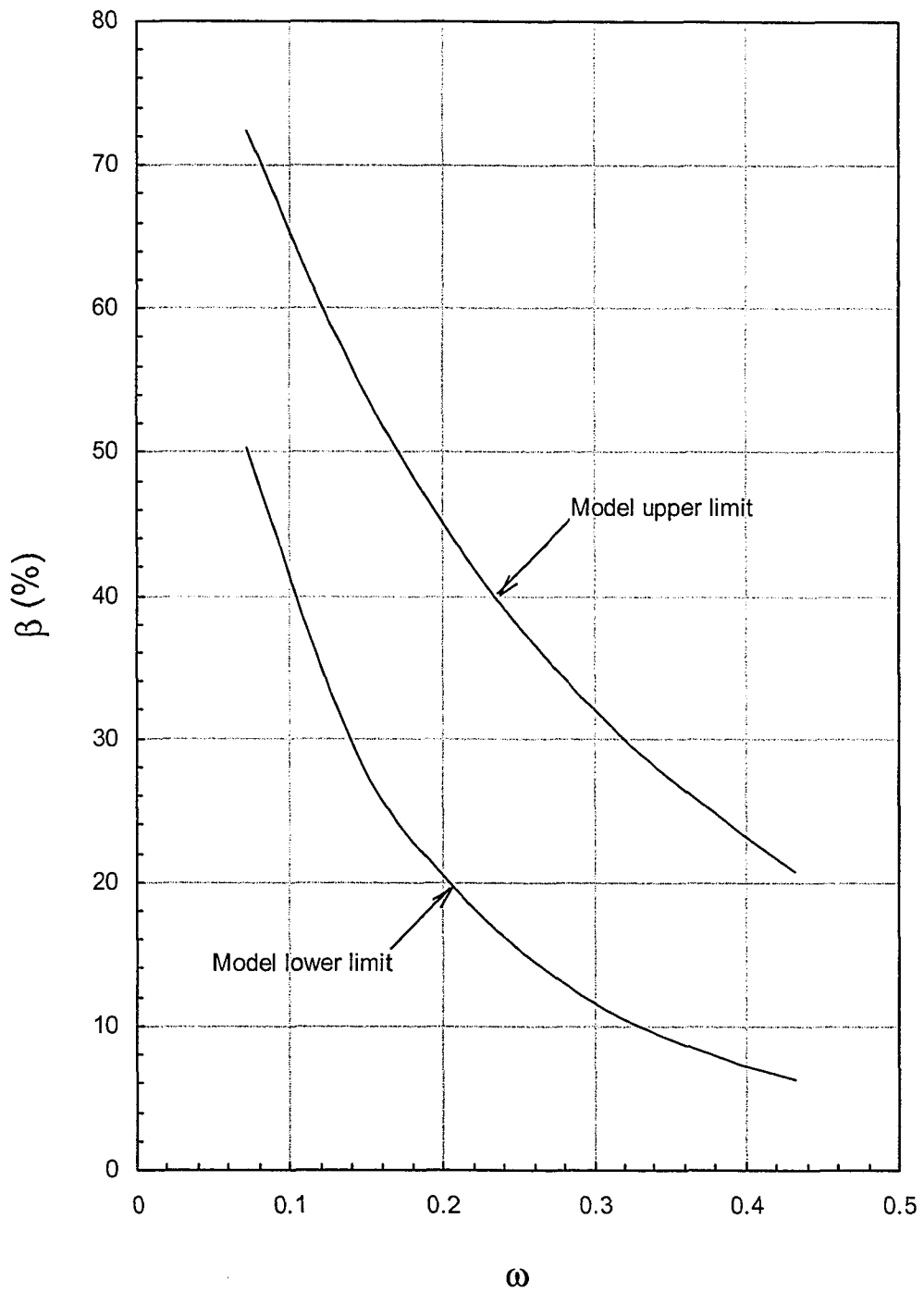
Figure 6.21 Ductility model limits for moment redistribution

220
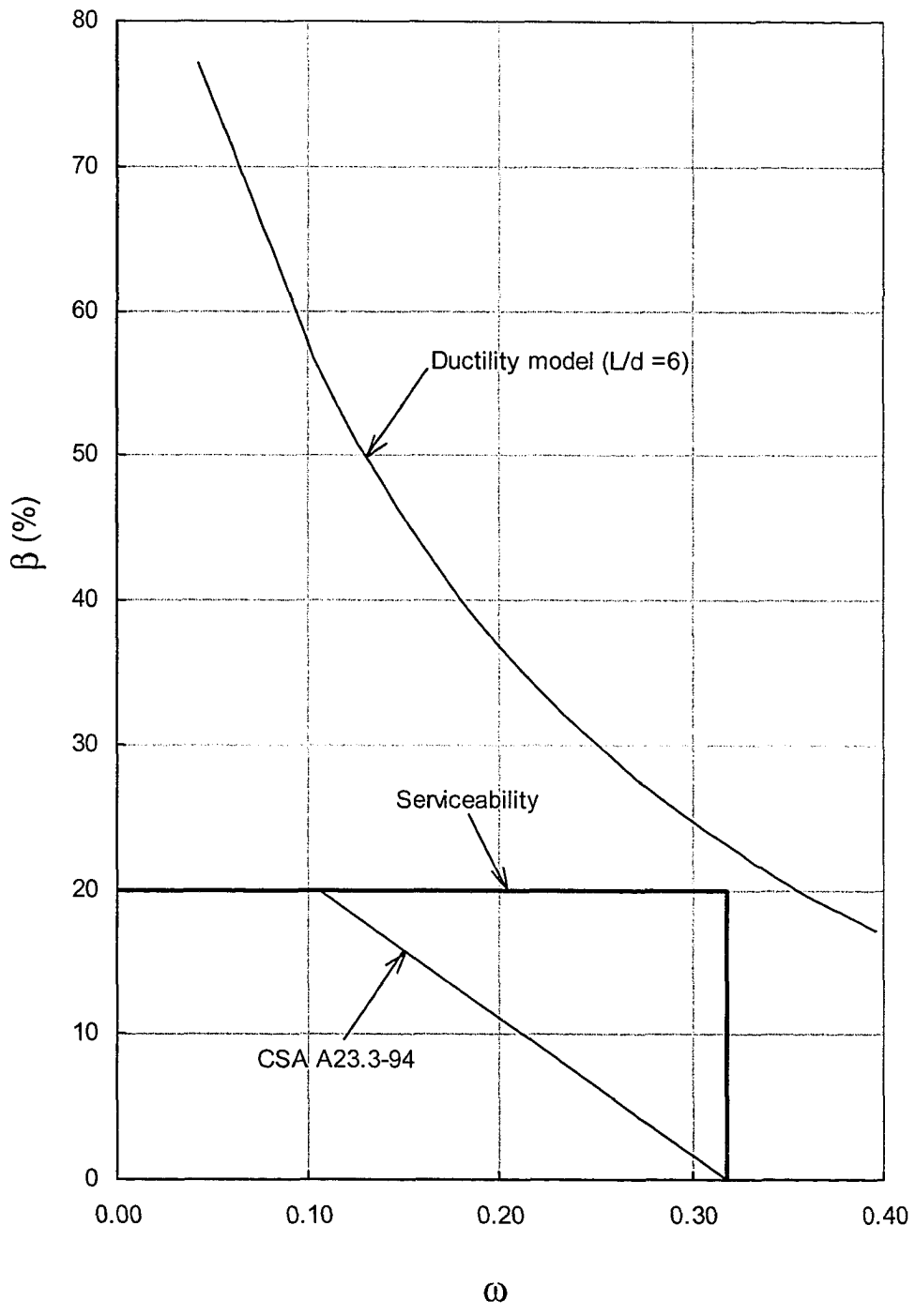
Figure 6.22 Allowable moment redistribution for L/d ≤ 6

221
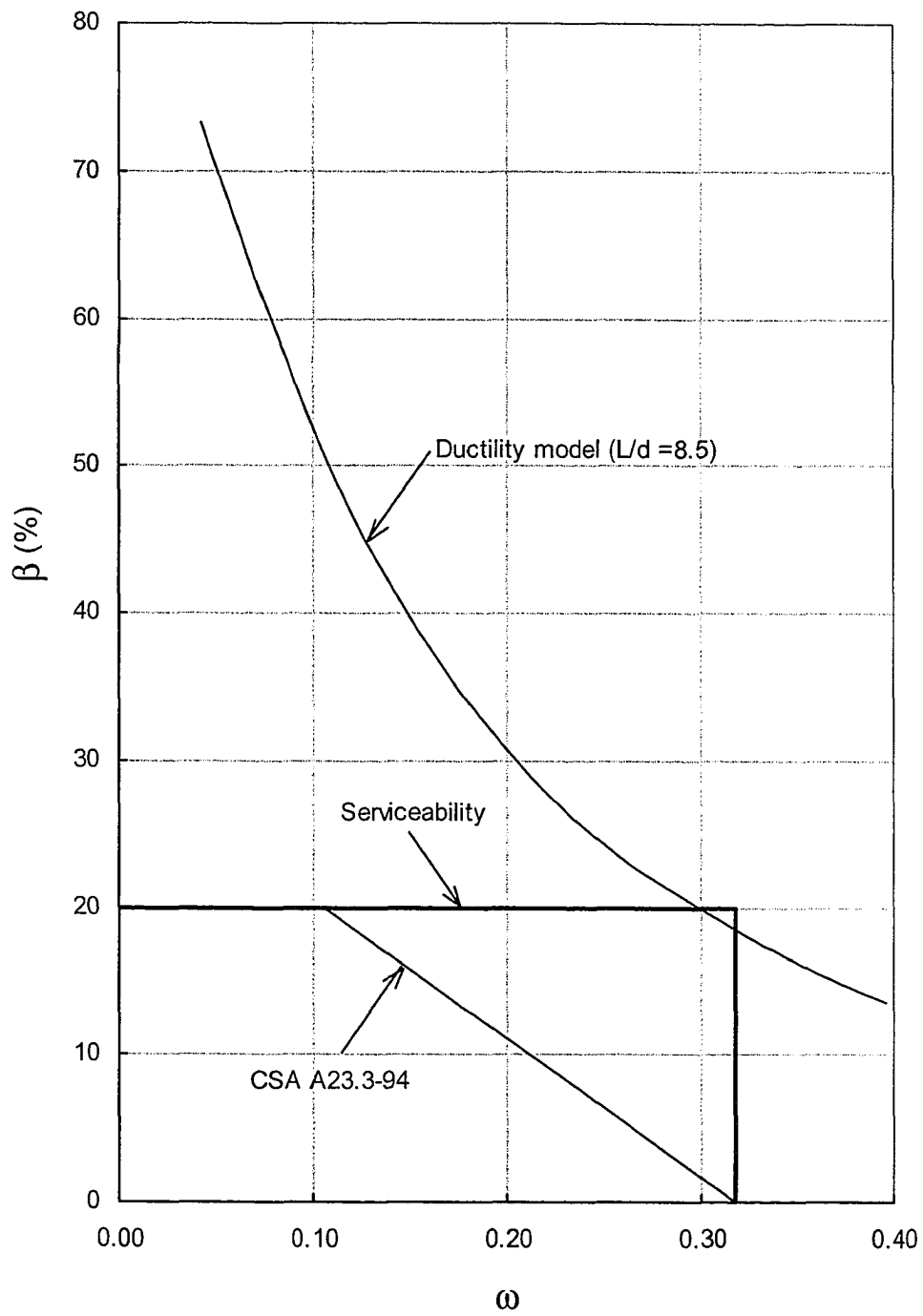
Figure 6.23 Allowable moment redistribution for 6<L/d≤8.5

222
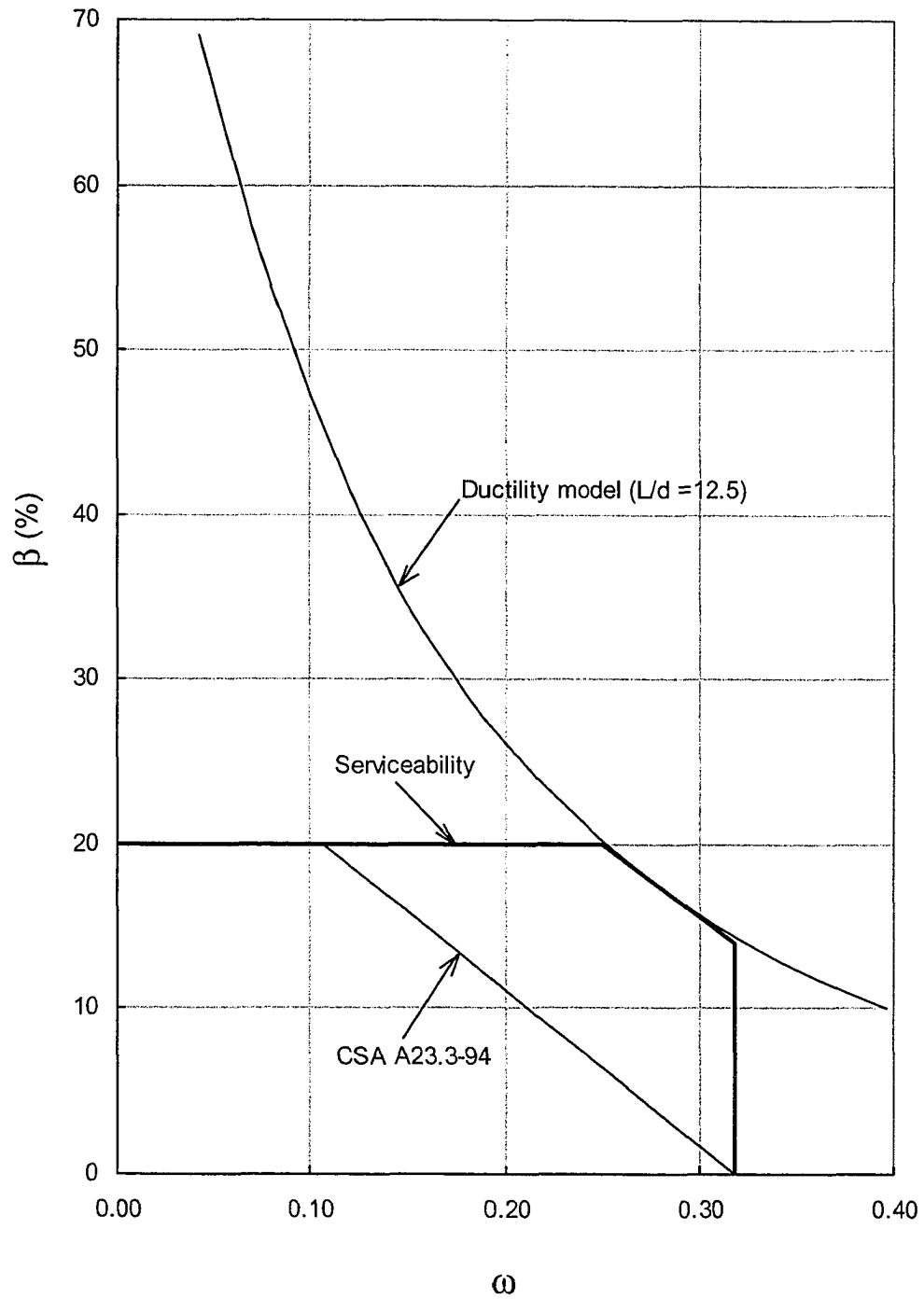
Figure 6.24 Allowable moment redistribution for 8.5<L/d≤12.5

223
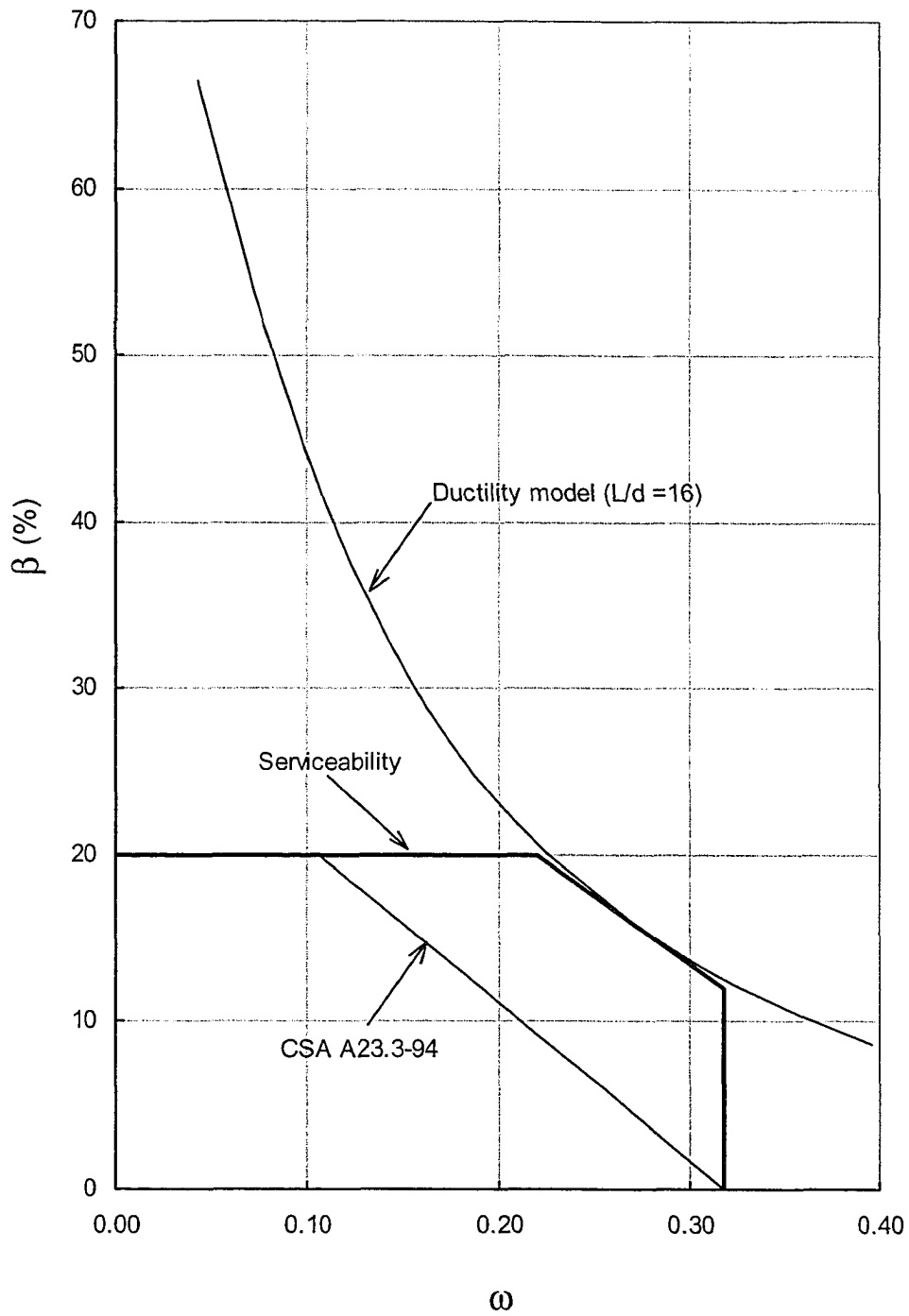
Figure 6.25 Allowable moment redistribution for 12.5<L/d≤16

224
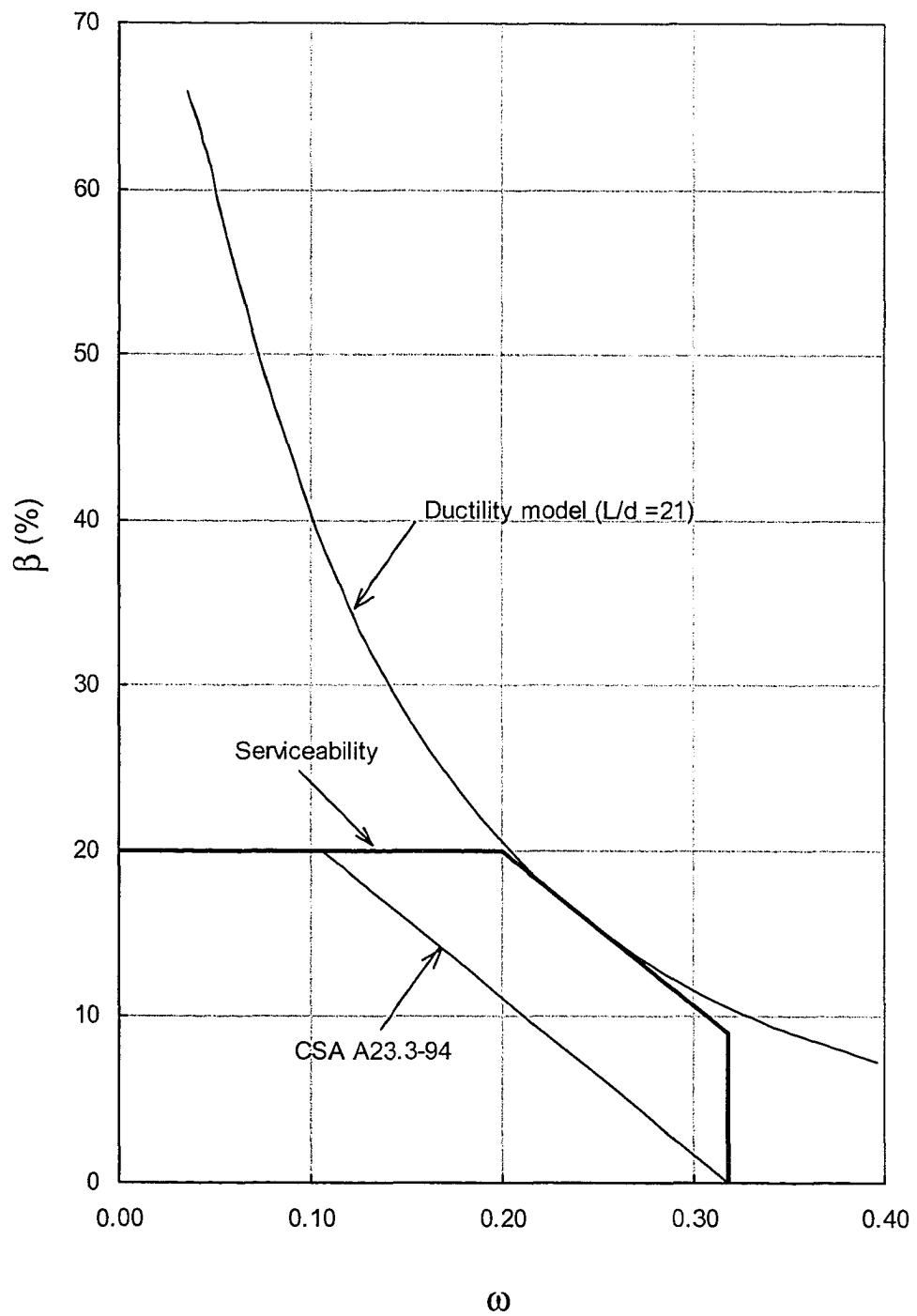
Figure 6.26 Allowable moment redistribution for 16.5<L/d≤21

7. MOMENT REDISTRIBUTION AND ANALYSIS OF CONTINUOUS REINFORCED CONCRETE BEAMS

7.1 Introduction

Continuous beams are typically analysed for a number of pattern load cases to obtain the design moment envelope. Since maximum values of design moment do not occur simultaneously, at all critical sections, the beams reinforced on the basis of such elastic analysis are typically over-designed. Moment redistribution is a tool that can be used to obtain design moments without being overly conservative. However pattern load analysis followed by an analysis with plastic hinges to obtain design moments becomes too cumbersome even for simple structures like continuous beams. The purpose of this chapter is:

1. To develop design moment coefficients, for continuous reinforced concrete beams, by taking into account the allowable moment redistribution.

2. To compare derived moment coefficients with the CSA A23.3-94 design moment coefficients.

3. To examine the need for pattern load analysis in the design of continuous reinforced concrete beams and determine if continuous beams can be designed for a single load case without performing the pattern load analysis.

7.2 Derivation of Design Moment Coefficients

The moment coefficients are derived for each critical section with the moment redistribution allowed based on ductility criteria at the ultimate limit state, and with the moment redistribution allowed to avoid any yielding at service load level. The largest coefficient from the two conditions provides the design moment coefficient. These coefficients may need to be adjusted to satisfy the limit strength criteria.

226

The strategy adopted for determination of design moment coefficients is the same as that used in the previous chapter. Different load patterns and span variations, providing maximum load effects, are considered for each critical section. The maximum effect of load placement and span length variation occurs when a continuous beam is supported on knife-edge supports without any rotational restraint. Results from analysis of beams supported on knife-edges can be applied as upper limits for beams with rotationally restrained supports. The spans used are clear spans to account for the reduction of moment at the face of supports. For the derivation of the design moment, it is assumed that the structure and the loading met the same five conditions as required for the use of CSA A23.3-94 moment coefficients. These conditions are:

1. There are two or more spans

2. The spans are approximately equal, with the longer of two adjacent spans not greater than the shorter by more than 20%

3. The loads are uniformly distributed

4. The factored live load does not exceed 2 times the factored dead load

5. The members are prismatic

In addition there is a sixth condition that is not stated in CSA A23.3-94 but is necessary for the use of approximate moment coefficients. This condition states; "the beams must be in a braced frame without significant moments due to lateral loads."

In addition to pattern loading, the main parameters used to derive moment coefficients are the adjacent span ratio γ and service live load to dead load ratio α. For the purpose of this exercise the relevant range of γ is 0.833 to 1.2 and the maximum value of α is 1.67, to meet the code limitations stated in 2 and 4 above. A minimum value of $\alpha=0.5$ is used to avoid moment redistribution under permanent loads.

7.2.1 Serviceability moment coefficients

The expressions for serviceability coefficients μ_s were developed in Chapter 6. These expressions are plotted for the relevant range of α and γ in Figs. 7.1 to 7.6. The maximum values of μ_s for each critical section are tabulated in Table 7.1.

Table 7.1 Serviceability moment coefficients

Location	Maximum serviceability coefficient μ_s	LL to DL ratio α	Adjacent span ratio γ
Interior support negative moment	0.0798	1.67	0.833
First interior support negative moment	0.0882	0.5	1
Interior span positive moment	0.0543	1.67	0.833
Exterior span positive moment	0.0694	0.5	0.833
Two span beam negative moment at interior support	0.0988	0.5	1
Two span beam positive moment	0.0652	1.67	0.833

7.2.2 Ductility moment coefficients

Ductility requirements are evaluated to ensure that the moments can redistribute without exhausting the ductility of the plastic hinges. When a critical section yields, it undergoes inelastic rotation and redistributes the moment to other critical sections. The amount of moment redistribution depends upon the plastic rotation capacity of the critical section.

228

Given enough rotation capacity, the member continues to carry increasing load until all three critical sections of the member reach their moment capacity. The section that yields first is the most critical because it undergoes the most plastic rotation. For a member to develop its full flexural capacity, the available rotation capacity of this critical section must be greater than the required plastic rotation at that section.

Maximum ductility demand typically occurs at support regions, especially when the tangents at the ends must retain a slope of zero. The ductility model developed in Chapter 4 for this condition provides the allowable moment redistribution values. The upper and lower limit of the model is given in Fig. 5.28 and is reproduced here in Fig. 7.7. Using lower limit of the ductility model, the allowable moment redistribution for the range of ω from 0.15 to 0.25 is:

For $\omega = 0.15$, $\beta = 28.5\%$

For $\omega = 0.2$, $\beta = 20\%$

For $\omega = 0.25$, $\beta = 15\%$

For most practical cases the value of ω rarely exceeds 0.2. The ductility moment coefficients can be obtained by applying the allowable moment redistribution (β) to the elastic factored moment coefficients at critical sections. The factored elastic moment coefficient is given as:

$$\mu_f = \frac{M_f}{w_f L^2} \qquad [7.1]$$

The corresponding ductility moment coefficient is given as:

$$\mu_d = \left(1 - \frac{\beta}{100}\right) \times \mu_f \qquad [7.2]$$

229

The factored elastic moment coefficients are determined in exactly the same fashion as the service limit moment coefficients were determined in the previous section. The limits for α and γ are the same as considered for the serviceability moment coefficients. The expressions for μ_f are plotted in Figs. 7.8 to 7.13 and the maximum values of μ_f are tabulated in Table 7.2.

Table 7.2 Factored elastic moment coefficients

Location	μ_f	α	γ
Interior Support	0.1073	1.67	0.833
First Interior Support	0.1161	1.67	1
Interior Span	0.0735	1.67	0.833
Exterior Span	0.0926	1.67	0.833
Two-Span Int. Support	0.125	n/a	1
Two-Span Span	0.0876	1.67	0.833

The corresponding ductility moment coefficients μ_d are tabulated in Table 7.3.

Table 7.3 Ductility moment coefficients

Location	μ_d $\omega = 0.15$	μ_d $\omega = 0.20$	μ_d $\omega = 0.25$
Interior Support	0.0767	0.0858	0.0912
First Interior Support	0.083	0.0929	0.0987
Interior Span	0.0525	0.0588	0.0625
Exterior Span	0.0662	0.0741	0.0787
Two-Span Int. Support	0.0894	0.10	0.106
Two-Span Span	0.0626	0.0701	0.0745

230

7.2.3 Design moment coefficients

The design moment coefficients will be the maximum of the serviceability and ductility moment coefficients given in Tables 7.1 and 7.3 respectively, provided they satisfy the limit strength requirement for each span as given by Eq. 3.12. The interior span moment coefficients do not need any adjustment, however the exterior span positive moments are increased where required to satisfy this requirement. The factor for the increment of positive moment is evaluated as follows:

$$k_m = \frac{0.125 - \dfrac{\mu_{eL} + \mu_{eR}}{2}}{\mu_{mid}} \tag{7.3}$$

The final adjusted design moment coefficients are given in Table 7.4. The exterior span positive moments that are adjusted to satisfy Eq. 3.12 are highlighted in the table.

Table 7.4 Design moment coefficients

Location	μ_{des} $\omega = 0.15$	μ_{des} $\omega = 0.20$	μ_{des} $\omega = 0.25$
Interior Support	0.0798	0.0858	0.0912
First Interior Support	0.0882	0.0929	0.0987
Interior Span	0.0543	0.0588	0.0625
Exterior Span	**0.081**	**0.0785**	0.0787
Two-Span Int. Support	0.0988	0.10	0.106
Two-Span Span	**0.0756**	**0.075**	0.0745

For low to moderate values of ω ($\omega \leq 0.15$), serviceability governs the allowable moment redistribution limit and hence the design moment coefficients. For higher values of ω ($\omega = 0.2$ to 0.25), ductility governs the allowable moment redistribution limit and hence the design moment coefficients.

231

7.2.4 Comparison with CSA A23.3-94 moment coefficients

Tables 7.5 to 7.7 show comparison of derived moment coefficients with CSA A23.3-94 moment coefficients.

Table 7.5 Comparison between derived moment coefficients and CSA A23.3-94 moment coefficients ($\omega = 0.15$)

Location	μ_{des} $\omega = 0.15$	CSA A23.3-94	Ratio
Interior Support	0.0798	0.091	0.87
First Interior Support	0.0882	0.1	0.88
Interior Span	0.0543	0.0625	0.87
Exterior Span	**0.081**	0.091	0.89
Two-Span Int. Support	0.0988	0.111	0.89
Two-Span Span	**0.0756**	**0.091**	0.83

Table 7.6 Comparison between derived moment coefficients and CSA A23.3-94 moment coefficients ($\omega = 0.20$)

Location	μ_{des} $\omega = 0.20$	CSA A23.3-94	Ratio
Interior Support	0.0858	0.091	0.94
First Interior Support	0.0929	0.1	0.93
Interior Span	0.0588	0.0625	0.94
Exterior Span	**0.0785**	0.091	0.86
Two-Span Int. Support	0.10	0.111	0.9
Two-Span Span	**0.075**	0.091	0.82

232

Table 7.7 Comparison between derived moment coefficients and CSA A23.3-94 moment coefficients ($\omega = 0.25$)

Location	μ_{des} $\omega = 0.25$	CSA A23.3-94	Ratio
Interior Support	0.0912	0.091	1
First Interior Support	0.0987	0.1	0.99
Interior Span	0.0625	0.0625	1
Exterior Span	0.0787	0.091	0.86
Two-Span Int. Support	0.106	0.111	0.95
Two-Span Span	0.0745	0.091	0.82

The code design moment coefficients are conservative. For $\omega = 0.15$, the derived coefficients are smaller than the code coefficients by 18% to 11%, depending upon the location of critical section. For $\omega = 0.20$, the derived coefficients are smaller than the code coefficients by 18% to 6%. For $\omega = 0.25$, the derived coefficients are comparable to code coefficients at most locations, yet smaller than 18% -14% at other locations. For most practical cases the maximum values of ω are between 0.15 and 0.2 and hence savings can be achieved by using the derived moment coefficients.

7.3 Moment Redistribution and Pattern Loading

Continuous beams are typically analysed for pattern load cases to obtain the design moment envelope. This is tedious and time consuming, as a variety of load cases need to be considered for the analysis of the beam. Since maximum values of design moment do not occur simultaneously at all critical sections, the beams reinforced on the basis of such elastic analysis are typically over designed. Moment redistribution can be used to determine if one really needs to perform pattern load analysis to obtain design moments.

The procedure for assessing the need for pattern load analysis would be as follows:

1. Determine the design moment coefficients at critical sections based on pattern loading and moment redistribution. This has already been done in previous sections.

2. Next calculate the moment coefficients at critical sections due to a single case of non-pattern loading. This would be the case where full factored load is applied uniformly on all spans of the continuous beam.

3. Compare the non-pattern load moment coefficients with the redistributed design moment coefficients. If the non-pattern load moment coefficients are greater than the redistributed design moment coefficients, there is no need to perform pattern load analysis.

The expressions for the non-pattern load moment coefficients are derived by considering different variations of adjacent span ratios. The range of γ considered is the same as that used for deriving the redistributed design moment coefficients in this chapter. Redistributed design moment coefficients for $\omega = 0.2$ are used as this would be the case for most practical situations. The loading and span configurations for maximum moments at critical sections are given in Figs. 7.14 to 7.19. The moment coefficient expressions are obtained by dividing the maximum moment by $W_f L^2$ and are given in Table 7.8. These moment coefficient expressions for non-pattern load moment are plotted in Figs. 7.14 to 7.19. The maximum values of the moment coefficients are tabulated in Table 7.9.

Table 7.10 shows comparison between the non-pattern load moment coefficients and the pattern load redistributed moment coefficients. The non-pattern load moment coefficients are greater than the redistributed moment coefficients for all critical sections except for the positive moment in the interior span. The difference between the two for the interior span positive moment is only 3% and hence for all practical purposes non-pattern load moment coefficients govern the flexural design of reinforced concrete beams. Consequently it can be concluded that, within given range of parameters, there is no need for performing pattern load analysis to obtain the design moment coefficients. The

234

continuous reinforced concrete beams can be safely designed for a single case of uniformly distributed load.

Table 7.8 Expressions for non-pattern load moment coefficients

Location	Expression for moment coefficient μ
Interior support negative moment	$\mu = \dfrac{(2 + 7\gamma + 3\gamma^2) - (2 + \gamma)\gamma^3}{8(3 + 7\gamma + 3\gamma^2)}$
First interior support negative moment	$\mu = \dfrac{(5\gamma^4 + 6\gamma^3 + 8\gamma + 8) - (2 + \gamma)\gamma^3}{8(8 + 14\gamma + 6\gamma^2)}$
Interior span positive moment	$\mu = \dfrac{(2 + 8\gamma + 3\gamma^2) - 2(2 + \gamma)\gamma^3}{8(6 + 10\gamma + 3\gamma^2)}$
Exterior span positive moment	$\mu = \dfrac{1}{32}\left[\dfrac{(9 + 19\gamma + 6\gamma^2)(1 + \alpha) - (3 + \gamma)\gamma^3}{(6 + 10\gamma + 3\gamma^2)}\right]^2$
Two span beam negative moment at interior support	$\mu = \dfrac{(1 + \gamma^3)}{8(1 + \gamma)}$
Two span beam positive moment	$\mu = \dfrac{1}{8}\left[\dfrac{(3 + 4\gamma) - \gamma^3}{4(1 + \gamma)}\right]^2$

Table 7.9 Maximum non-pattern load moment coefficients

Location	μ	γ
Interior support negative moment	0.0948	0.833
First interior support negative moment	0.1071	1
Interior span positive moment	0.0569	0.833
Exterior span positive moment	0.0832	0.833
Two span beam negative moment at interior support	0.125	1
Two span beam positive moment	0.077	0.833

235

Table 7.10 Comparison between non-pattern load moment coefficients and redistributed moment coefficients

Location	μ	μ_{red}	Ratio $\mu/(\mu_{red})$
Interior Support	0.0948	0.0858	1.1
First Interior Support	0.1071	0.0929	1.15
Interior Span	0.0569	0.0588	0.97
Exterior Span	0.0832	0.0785	1.06
Two-Span Int. Support	0.125	0.10	1.25
Two-Span Span	0.077	0.075	1.03

7.4 Summary and Conclusions

Moment coefficients were determined for the design of continuous reinforced concrete beams. The coefficients use moment redistribution limits that ensure that the plastic hinge ductility is not exhausted at the ultimate limit state and that yielding does not occur at service load level. The conditions for the use of these coefficients are the same as those specified for the use of CSA A23.3-94 moment coefficients. Three sets of moment coefficients were determined, one each for $\omega = 0.15$, $\omega = 0.2$ and $\omega = 0.25$. For lower value of ω ($\omega = 0.15$), serviceability (avoiding yielding at service load) governs the design moment coefficients, while for higher value of ω ($\omega = 0.2$ and 0.25) hinge ductility governs the design moment coefficients. Comparison between the CSA A23.3-94 coefficients and the derived coefficients show that the code moment coefficients are conservative especially for lower values of ω. For $\omega = 0.15$ the derived coefficients are smaller than the code coefficients by 11% to 18%. For $\omega = 0.20$, the derived coefficients are less than the CSA A23.3-94 coefficients by 6% to 18%. For $\omega = 0.25$, the derived coefficients are comparable to code coefficients at most locations. For most practical cases beams are designed with ω between 0.15 and 0.2 and hence savings can be achieved by using the derived moment coefficients.

236

The need for pattern load analysis is assessed for the design of continuous reinforced concrete beams. It is assumed that the factored live load to dead load ratio is not greater than 2 and the adjacent longer span is not greater than the shorter span by 20%. These limits are the same as specified by CSA A23.3-94. The maximum elastic moments from a non-pattern single load analysis without moment redistribution are evaluated and compared with the redistributed design moments from pattern load analysis. The elastic moments from non-pattern load analysis are found to be greater than the redistributed moments from the pattern load analysis and hence govern the flexural design. The work of running multiple pattern load cases and then applying moment redistribution to reduce the extreme moments can be avoided. Within given range of parameters, continuous reinforced concrete beams can be analysed and designed on the basis of a single load case without considering pattern load analysis.
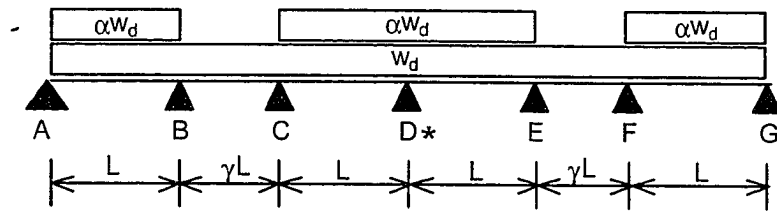
$$\ast \quad \mu_s = \frac{(2+7\gamma+3\gamma^2)(1+\alpha)-(2+\gamma)\gamma^3}{8\lambda(1.25+1.5\alpha)(3+7\gamma+3\gamma^2)}$$
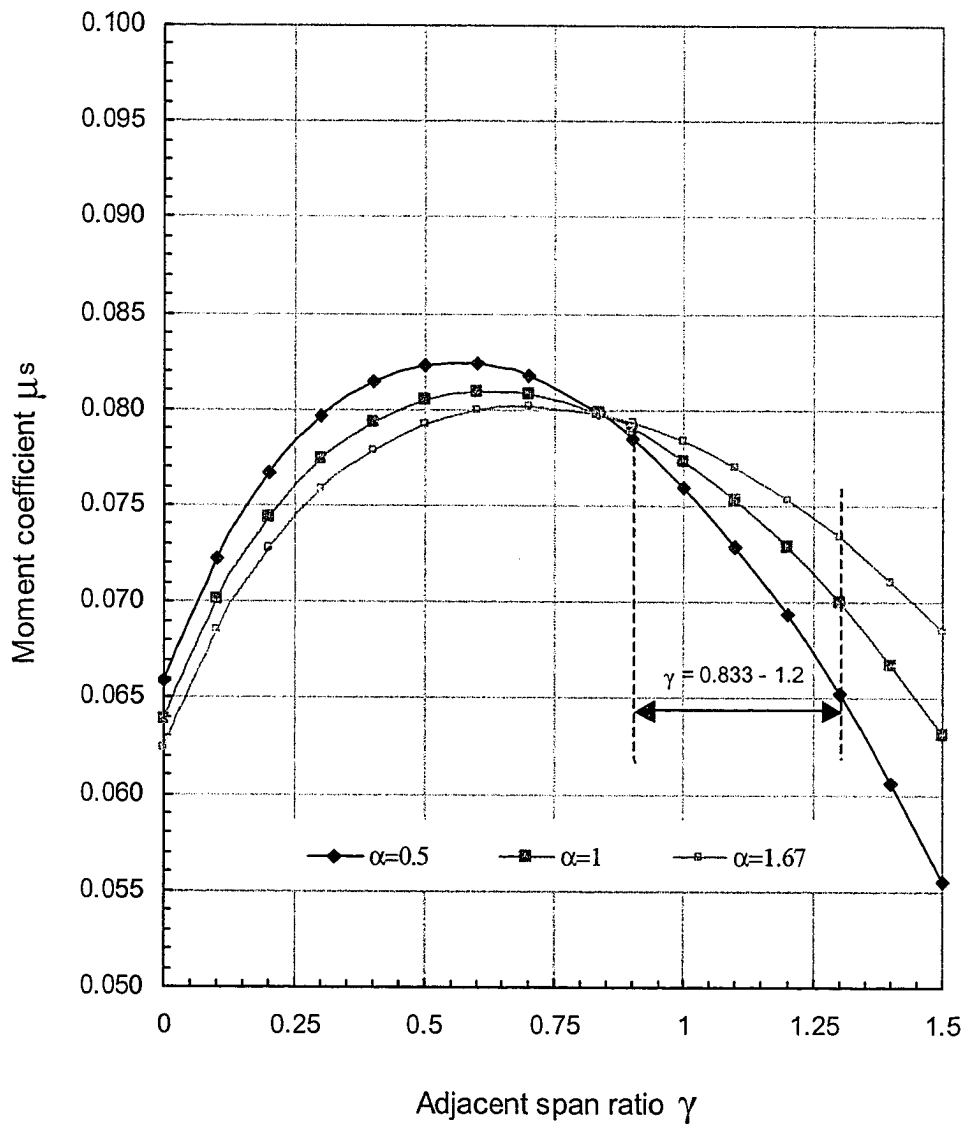
Figure 7.1 Serviceability moment coefficient for negative moment at interior support of a continuous beam

238
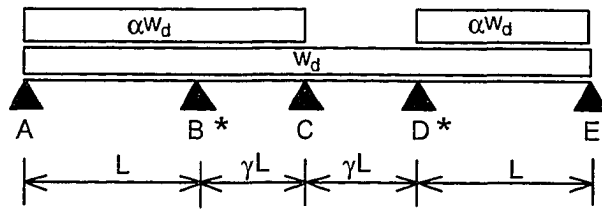
$$* \quad \mu_s = \frac{(5\gamma^4 + 6\gamma^3 + 8\gamma + 8)(1+\alpha) - (2+\gamma)\gamma^3}{8\lambda(1.25+1.5\alpha)(8+14\gamma+6\gamma^2)\gamma^2} \quad \longleftarrow \quad \text{omit } \gamma^2 \text{ if } \gamma < 1$$
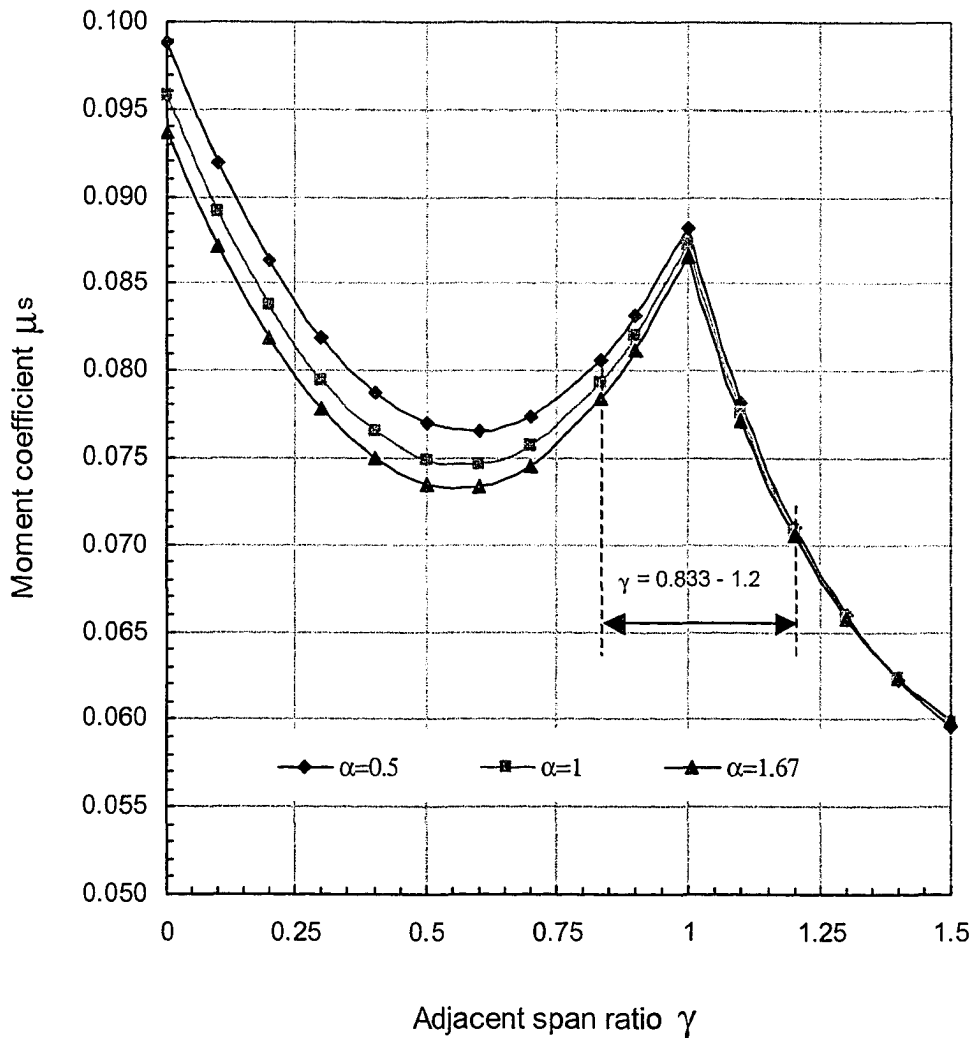
Figure 7.2 Serviceability moment coefficient for negative
moment at first interior support of a continuous beam

239
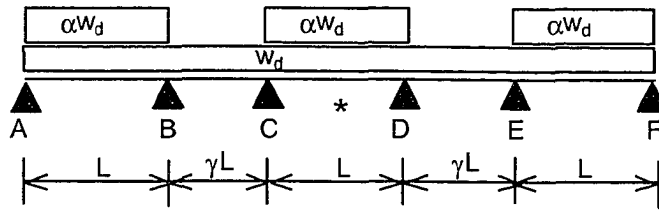
$$* \quad \mu_s = \frac{(2+8\gamma+3\gamma^2)(1+\alpha)-2\gamma^3(2+\gamma)}{8\lambda(1.25+1.5\alpha)(6+10\gamma+3\gamma^2)}$$
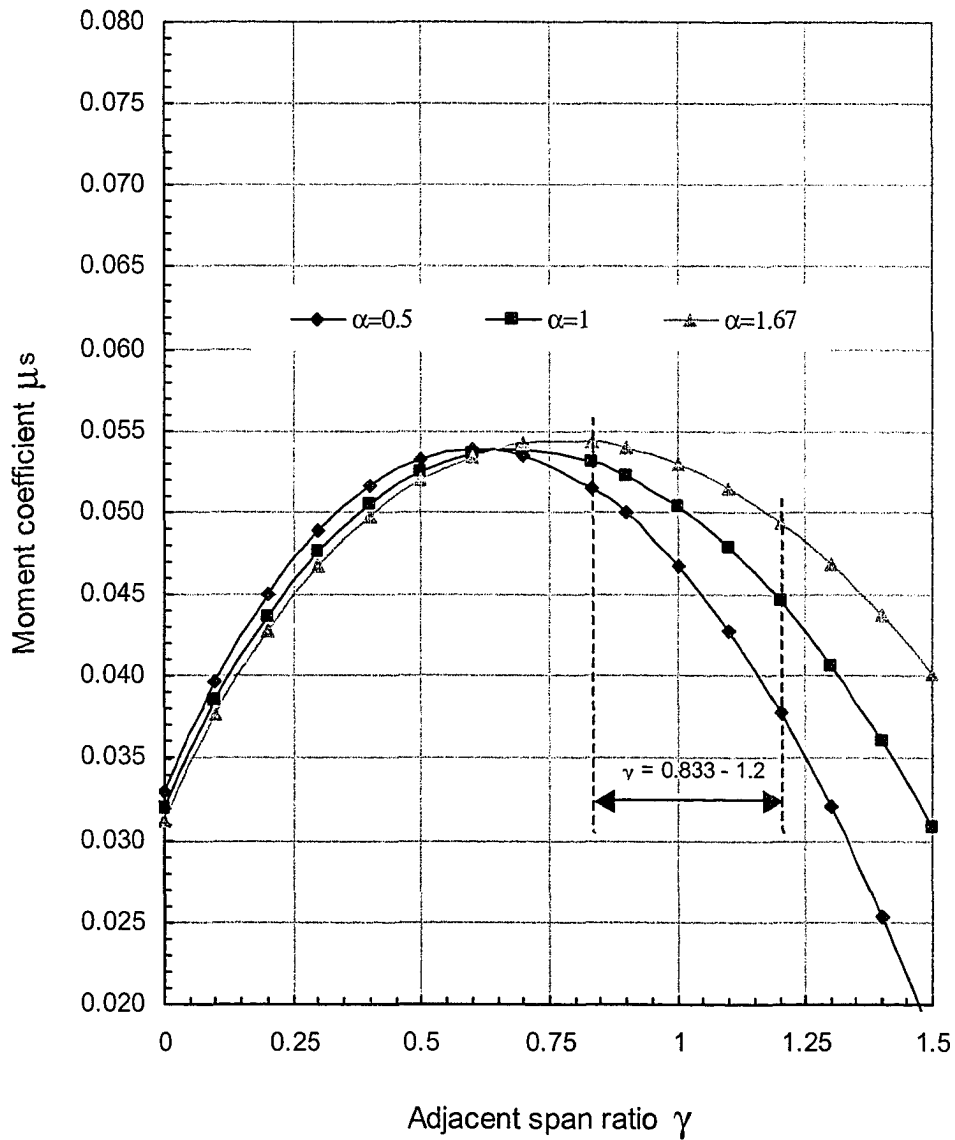
Figure 7.3 Serviceability moment coefficient for positive moment in interior span of a continuous beam

240

αw_d αw_d αw_d

w_d

A   *   B   C   D   E   *

L γL   L γL   L

$$* \quad \mu_s = \frac{1}{32(1.25+1.5\alpha)(1+\alpha)}\left[\frac{(9+19\gamma+6\gamma^2)(1+\alpha)-(3+\gamma)\gamma^3}{(6+10\gamma+3\gamma^2)}\right]^2$$

Moment coefficient μ_s

$\gamma = 0.833 - 1.2$

— α=0.5   — α=1   — α=1.67

Adjacent span ratio γ
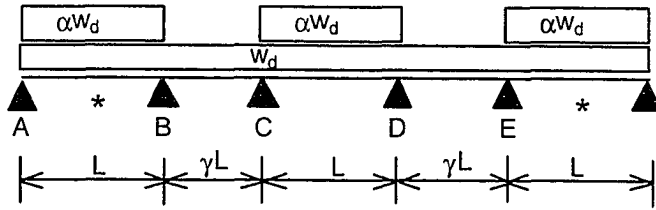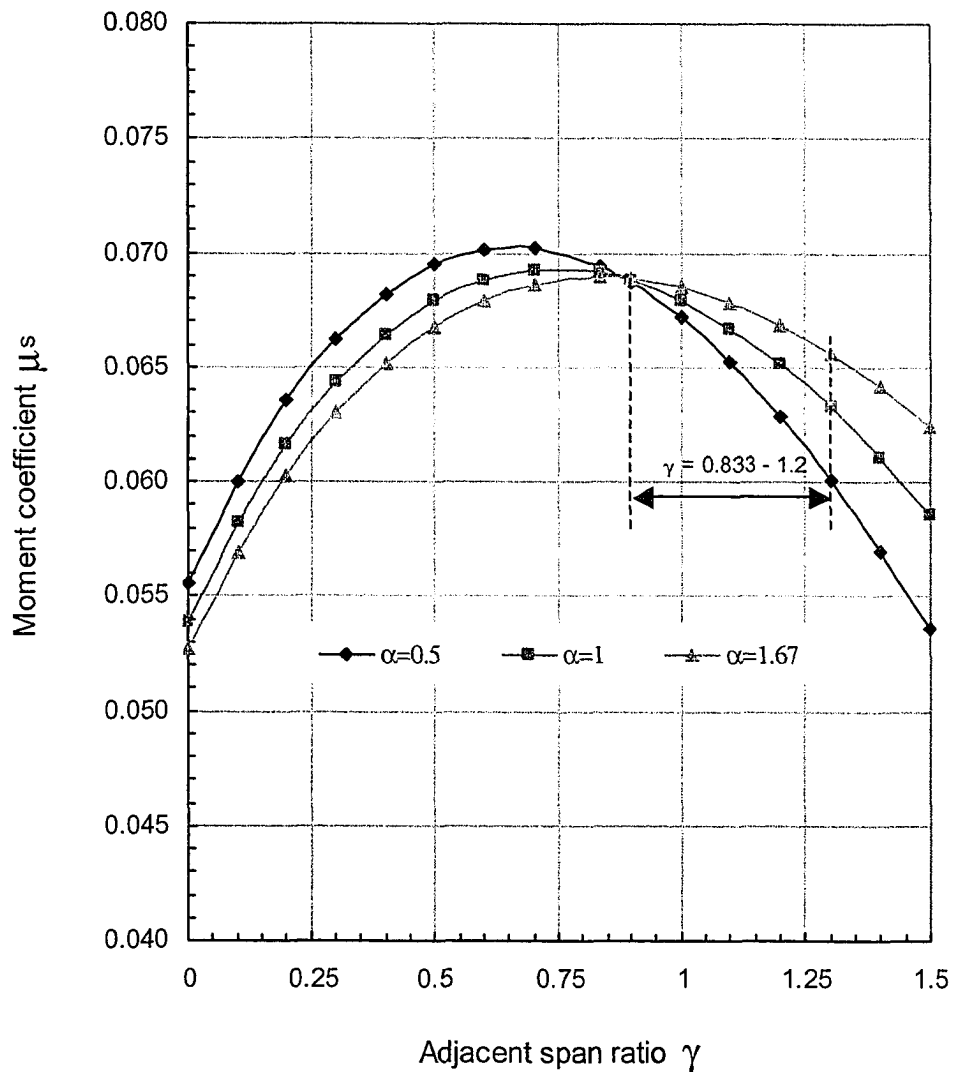
Figure 7.4 Serviceability moment coefficient for positive moment in exterior span of a continuous beam

241
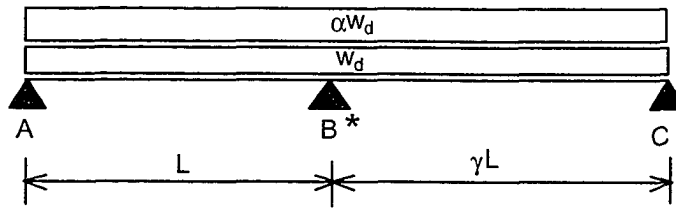
$$* \quad \mu_s = \frac{(1+\alpha)(1+\gamma^3)}{8\lambda(1.25+1.5\alpha)(1+\gamma)}$$
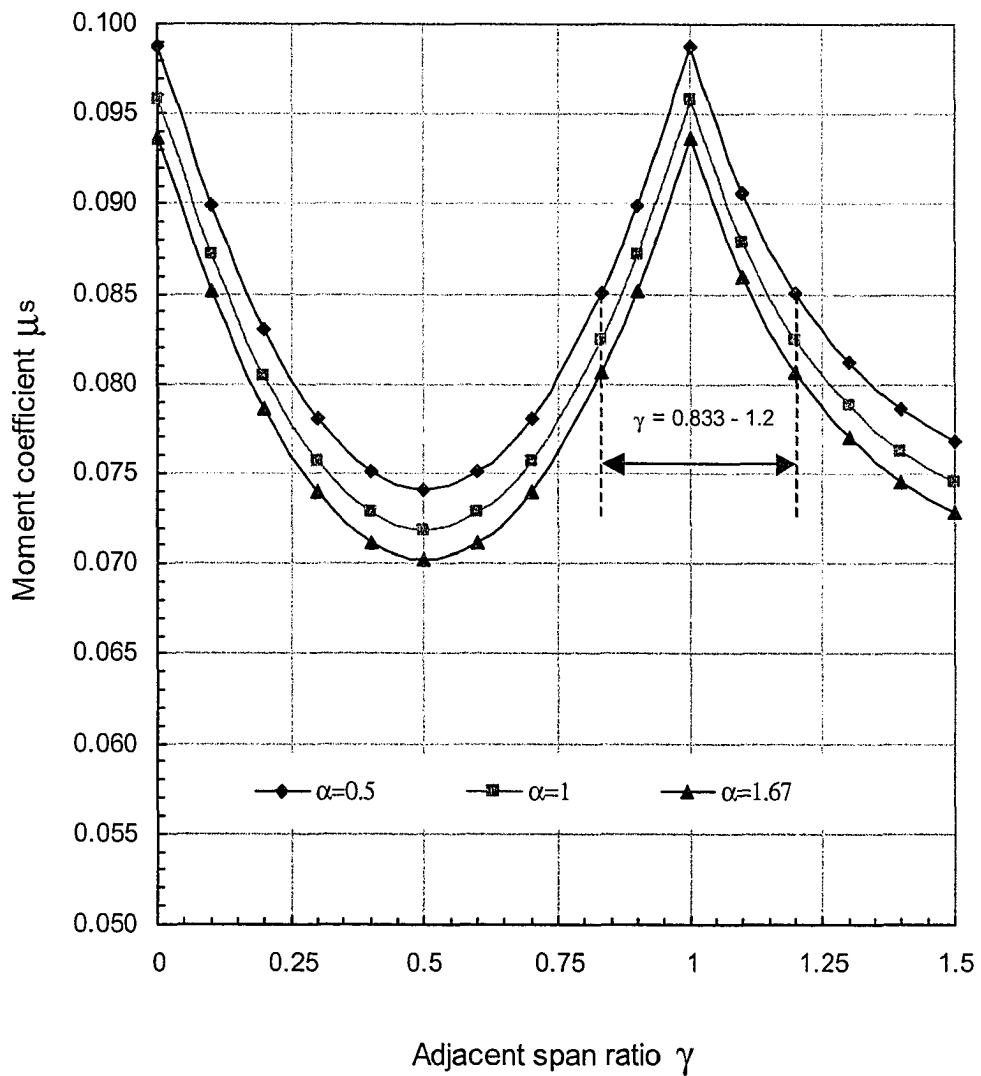
Figure 7.5 Serviceability moment coefficient for negative
moment at interior support of a two-span beam

242
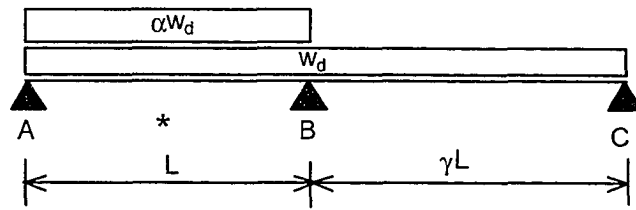
$$* \quad \mu_s = \frac{1}{8\lambda(1+\alpha)(1.25+1.5\alpha)}\left[\frac{(1+\alpha)(3+4\gamma)-\gamma^3}{4(1+\gamma)}\right]^2$$
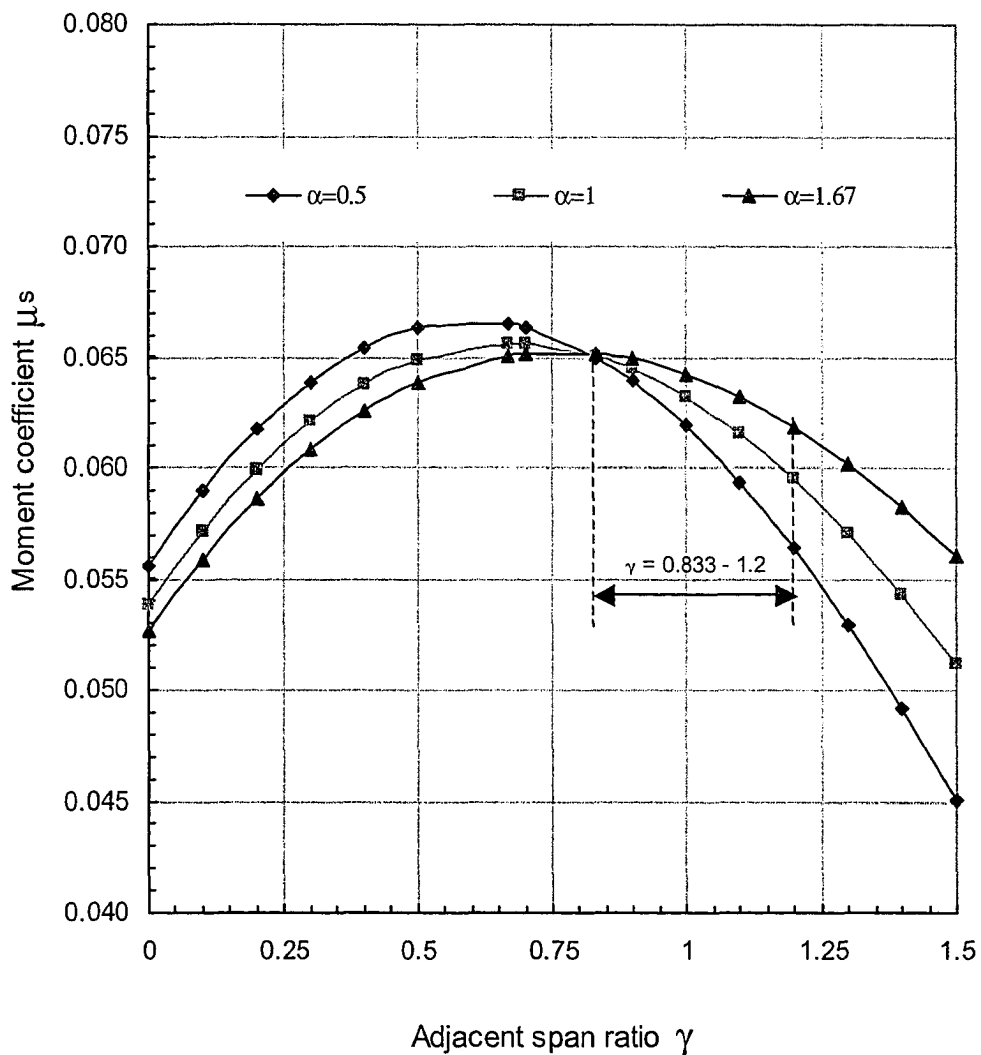
Figure 7.6 Serviceability moment coefficient for positive span moment in a two-span beam

243
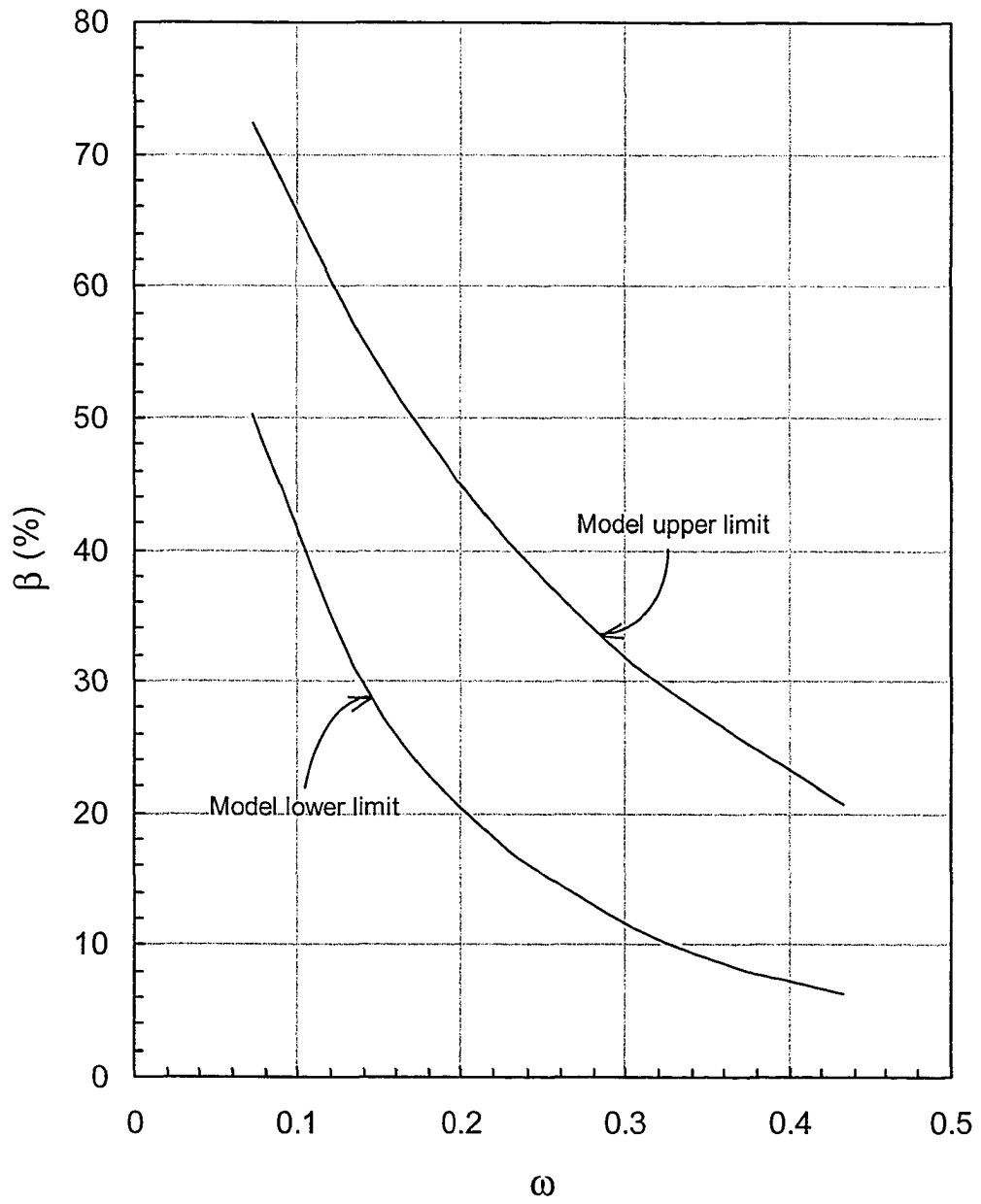
Figure 7.7. Ductility model limits for moment redistribution

$$* \quad \mu_f = \frac{(2 + 7\gamma + 3\gamma^2)(1.25 + 1.5\alpha) - 1.25(2 + \gamma)\gamma^3}{8(1.25 + 1.5\alpha)(3 + 7\gamma + 3\gamma^2)}$$

Adjacent span ratio γ
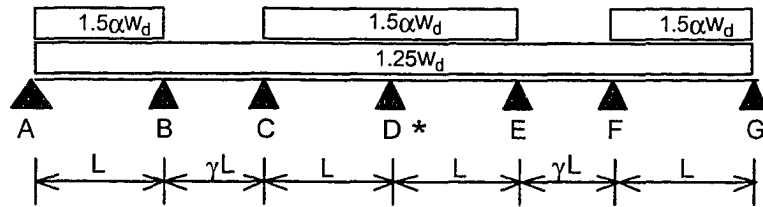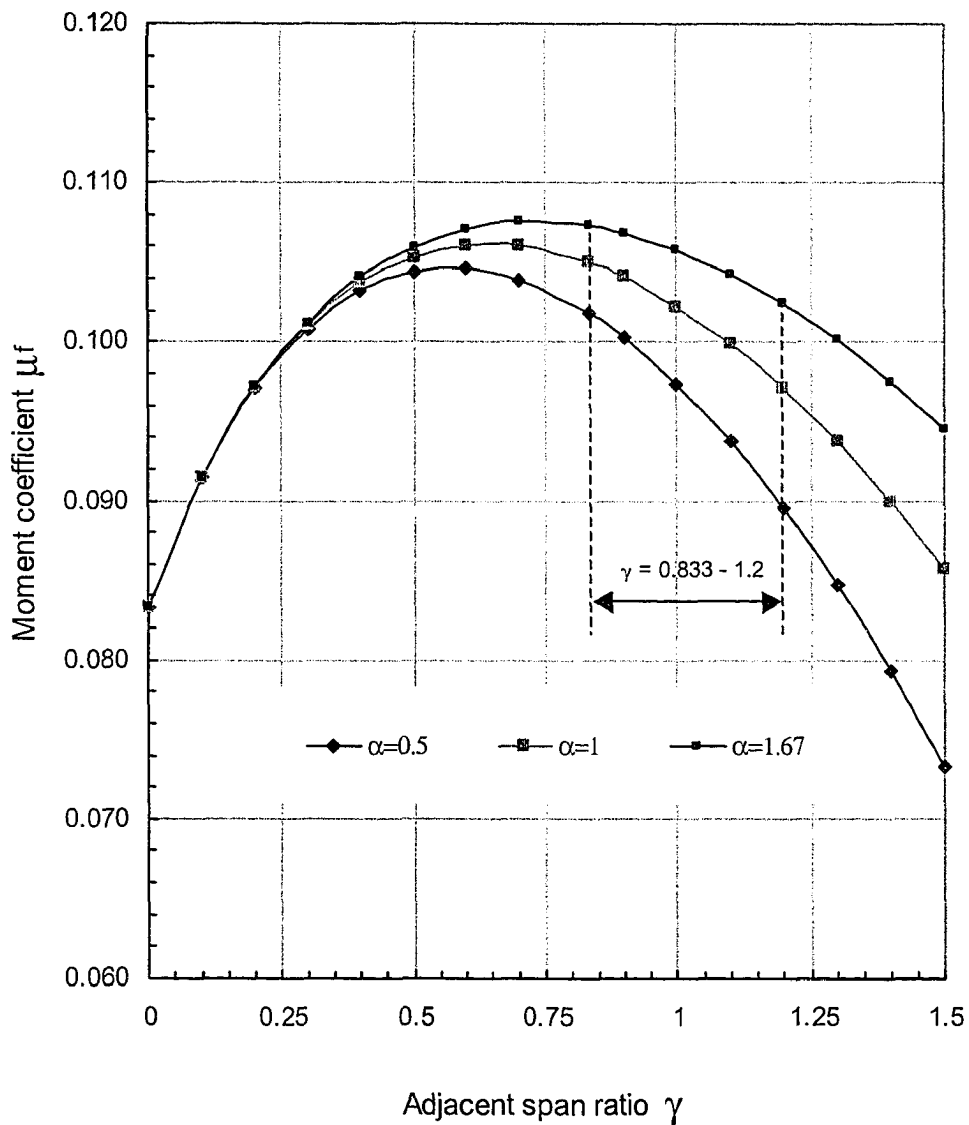
Figure 7.8 Factored moment coefficient for negative
moment at interior support of a continuous beam

245
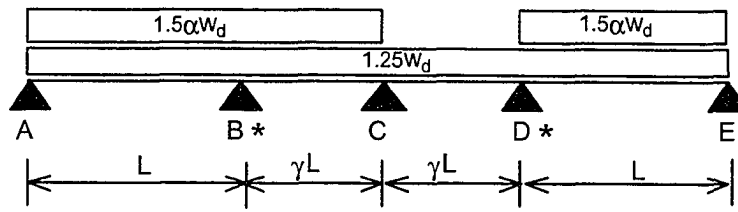
$$* \quad \mu_f = \frac{(5\gamma^4 + 6\gamma^3 + 8\gamma + 8)(1+\alpha) - (2+\gamma)\gamma^3}{8\lambda(1.25 + 1.5\alpha)(8 + 14\gamma + 6\gamma^2)\gamma^2} \longleftarrow \text{omit } \gamma^2 \text{ if } \gamma < 1$$
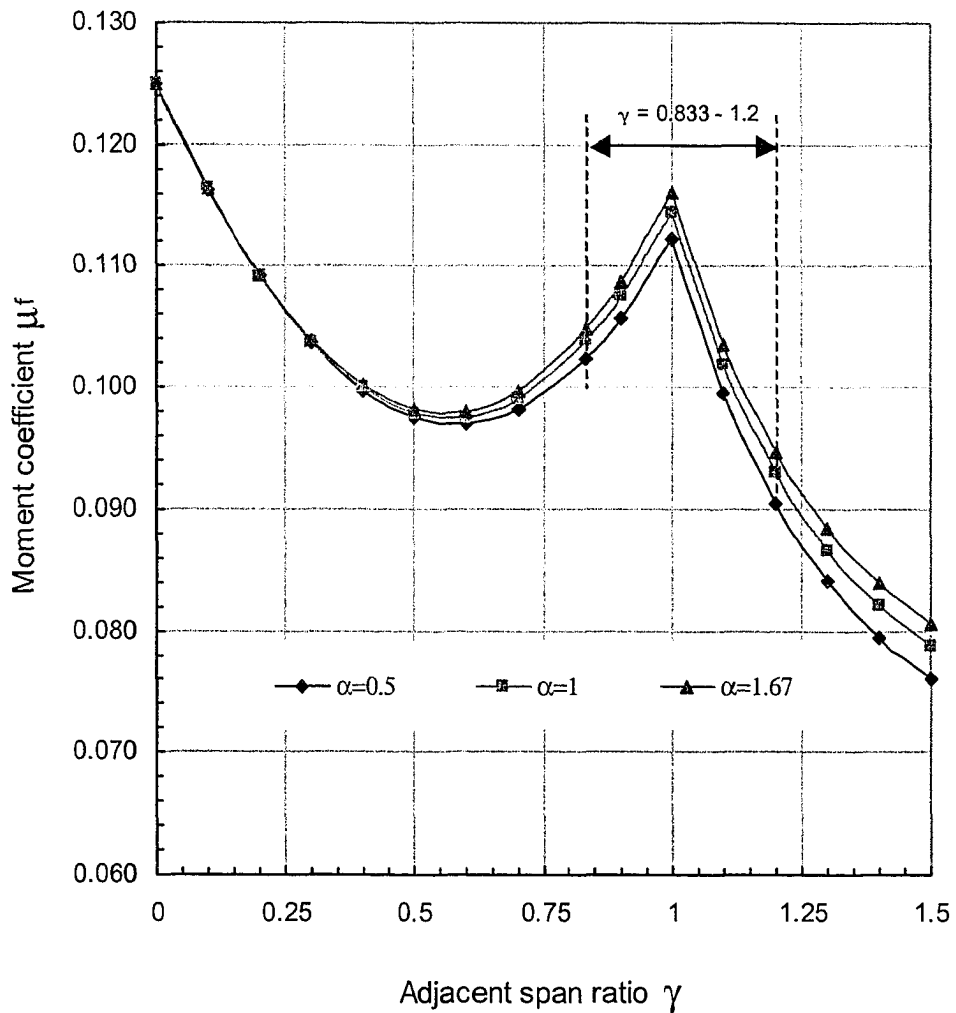
Figure 7.9 Factored moment coefficients for negative moment at first interior support of a continuous beam

246
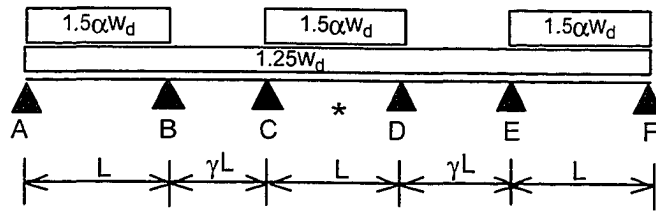
$$\ast \quad \mu_f = \frac{(2+8\gamma+3\gamma^2)(1.25+1.5\alpha)-1.25^*(2+\gamma)2\gamma^3}{8\lambda(1.25+1.5\alpha)(6+10\gamma+3\gamma^2)}$$
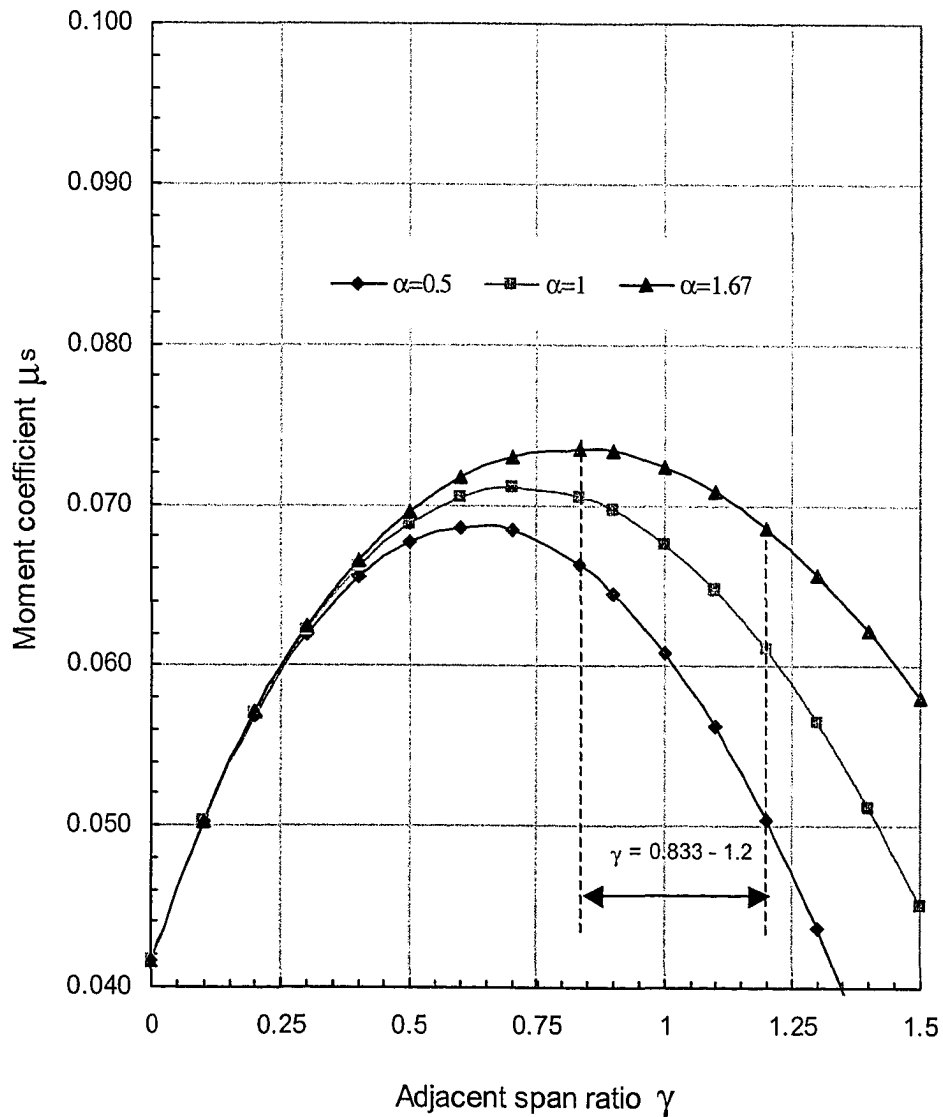
Figure 7.10 Factored elastic moment coefficient for positive moment in interior span of a continuous beam

247
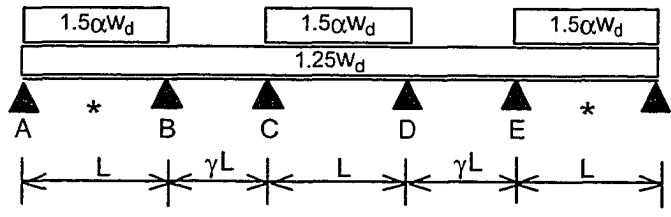
$$* \quad \mu_f = \frac{1}{32}\left[\frac{(9+19\gamma+6\gamma^2)(1.25+1.5\alpha)-1.25(3+\gamma)\gamma^3}{(1.25+1.5\alpha)(6+10\gamma+3\gamma^2)}\right]^2$$
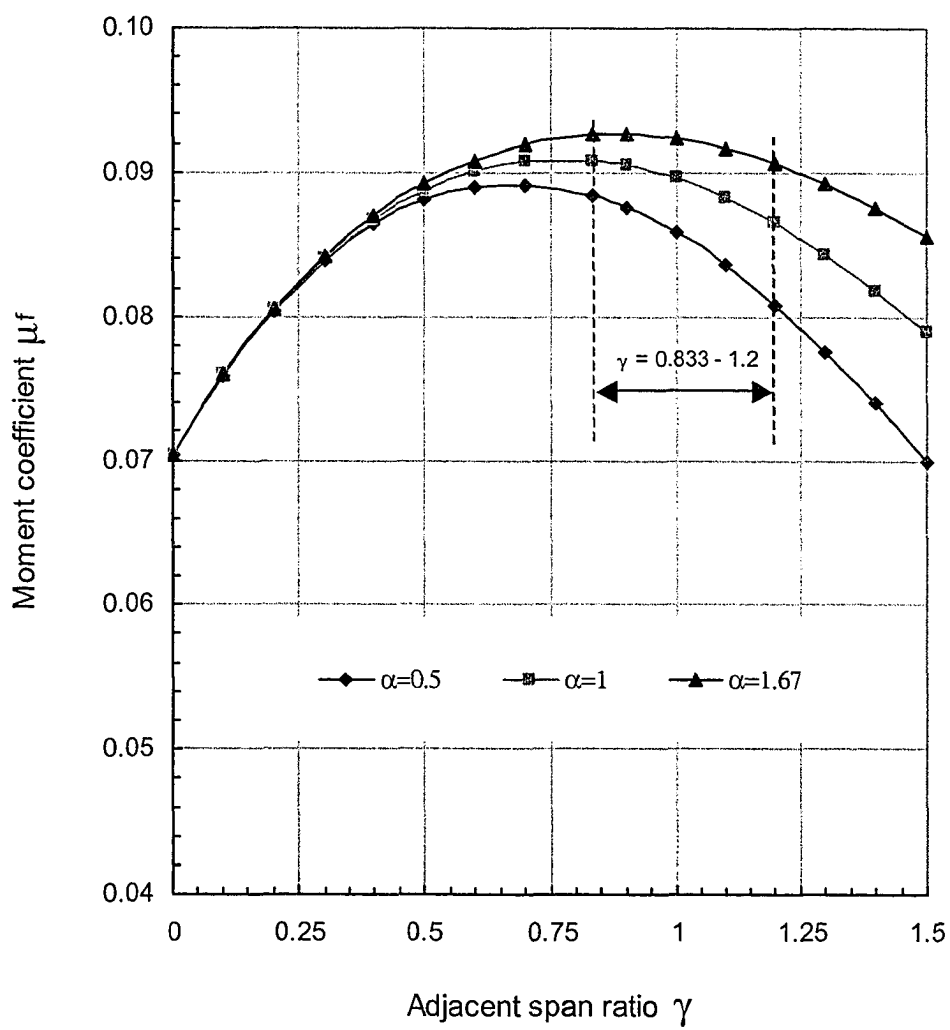
Figure 7.11 Factored elastic moment coefficient for positive
moment in exterior span of a continuous beam

248
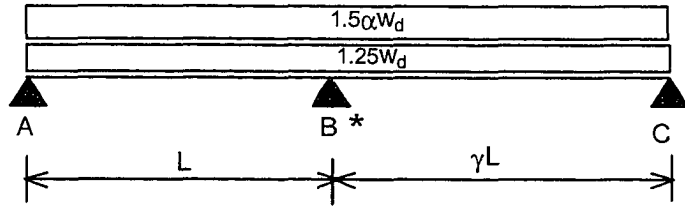
$$* \quad \mu_f = \frac{\left(1+\gamma^3\right)}{8(1+\gamma)}$$
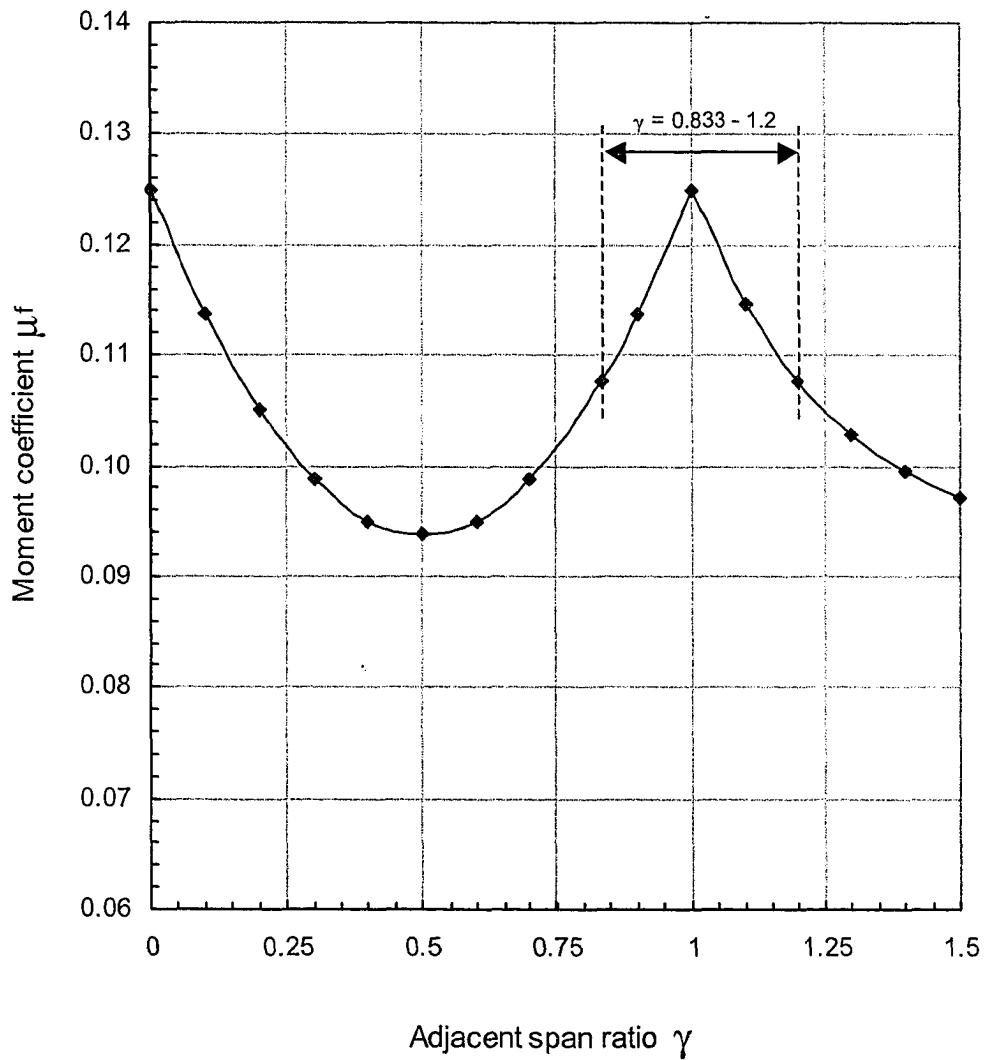
Figure 7.12 Factored elastic moment coefficient for negative moment at interior support of a two span beam

249
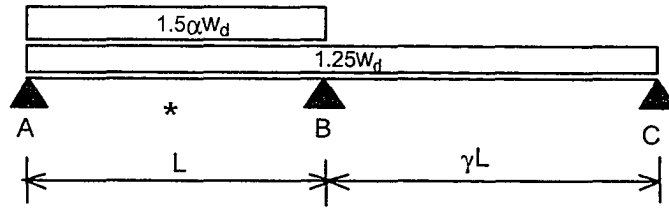
$$* \quad \mu_f = \frac{1}{8}\left[\frac{(1.25 + 1.5\alpha)(3 + 4\gamma) - 1.25\gamma^3}{4(1 + \gamma)(1.25 + 1.5\alpha)}\right]^2$$
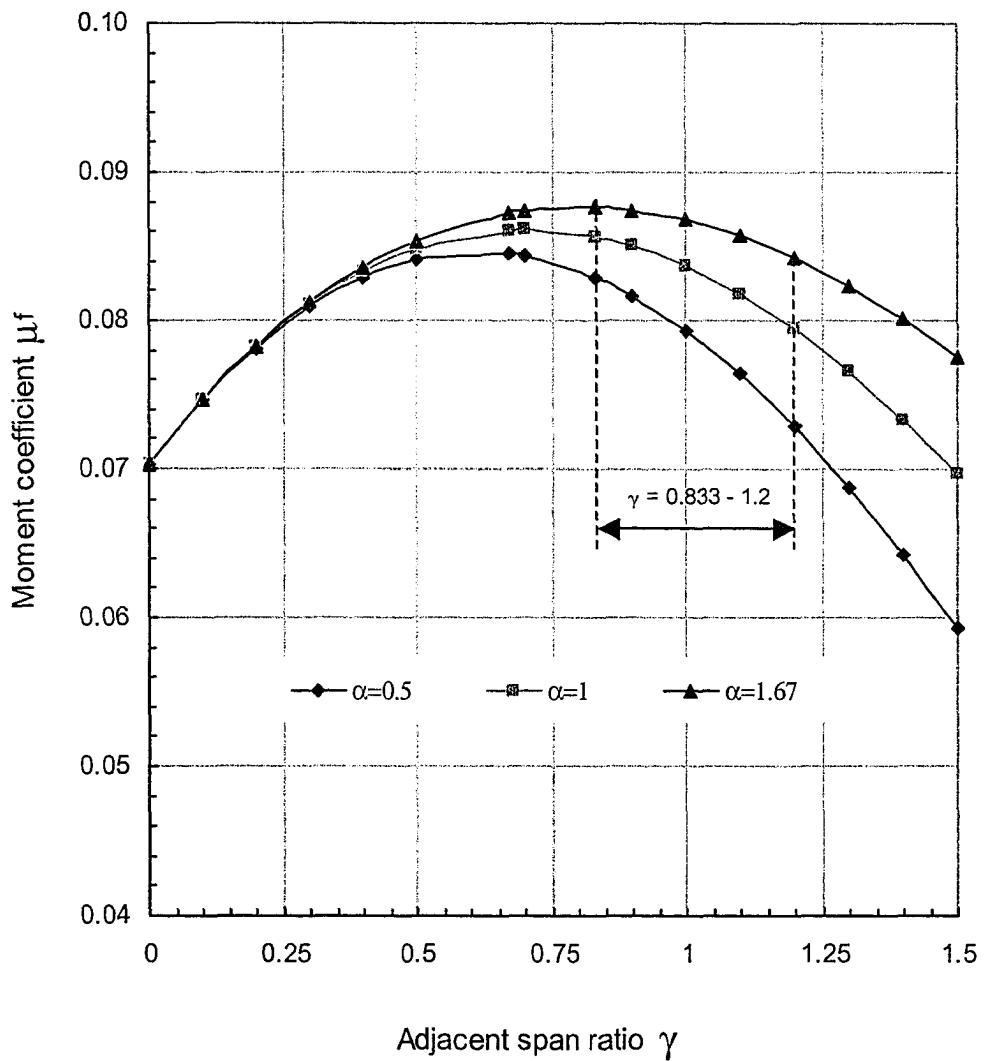
Figure 7.13 Factored elastic moment coefficient for positive span moment in a two span beam

250
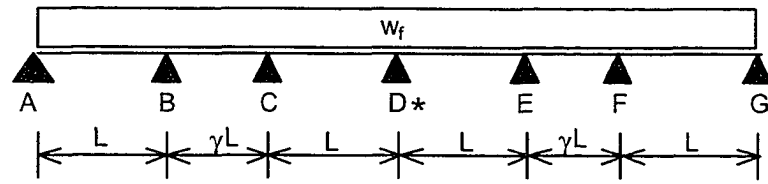
$$* \quad \mu = \frac{\left(2 + 7\gamma + 3\gamma^2\right) - \left(2 + \gamma\right)\gamma^3}{8\left(3 + 7\gamma + 3\gamma^2\right)}$$
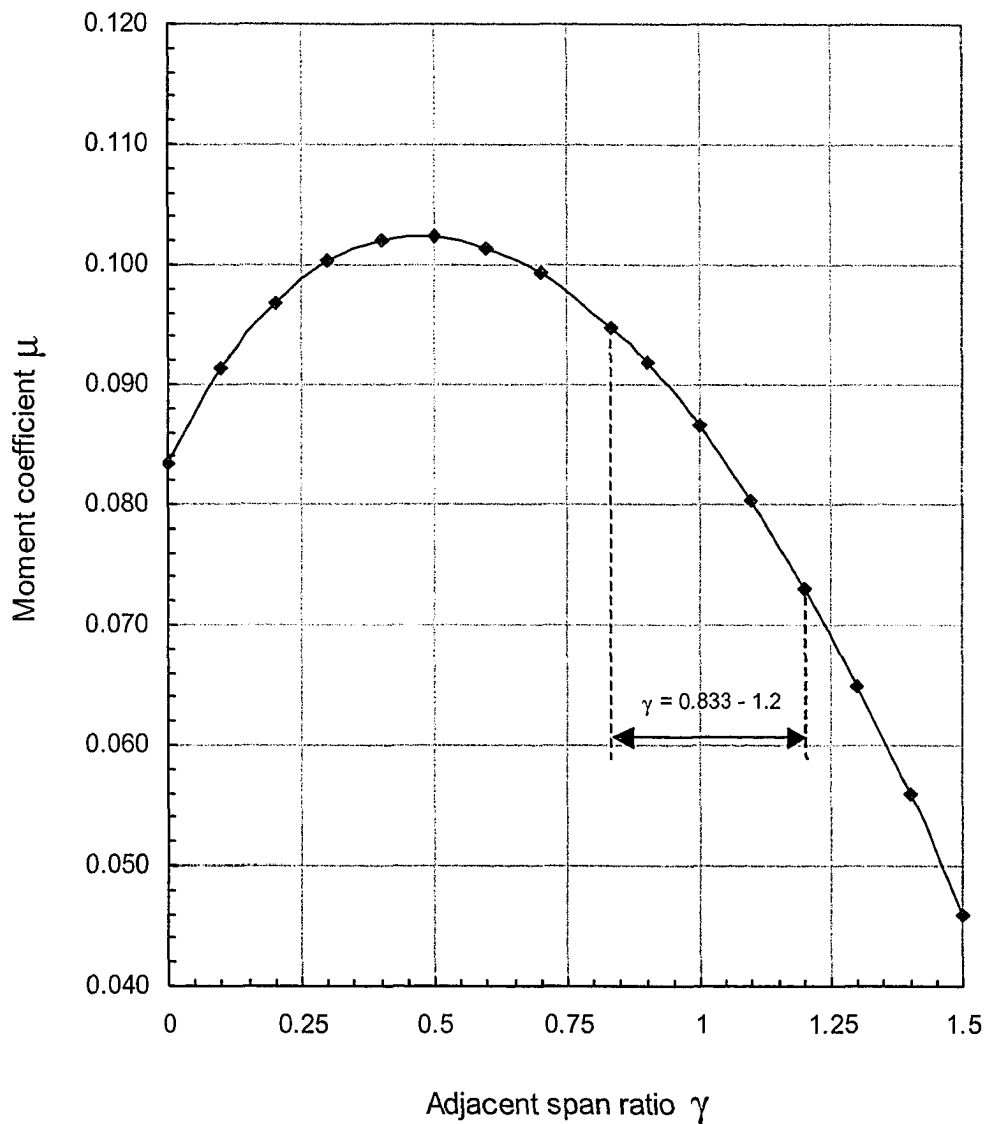
Figure 7.14 Non-pattern load moment coefficient for negative moment at interior support of a continuous beam

251
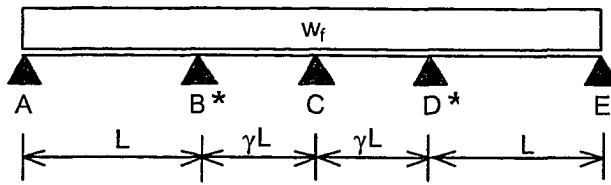
$$* \quad \mu = \frac{\left(5\gamma^4 + 6\gamma^3 + 8\gamma + 8\right) - \left(2 + \gamma\right)\gamma^3}{8\left(8 + 14\gamma + 6\gamma^2\right)\gamma^2} \longleftarrow \text{omit } \gamma^2 \text{ if } \gamma < 1$$
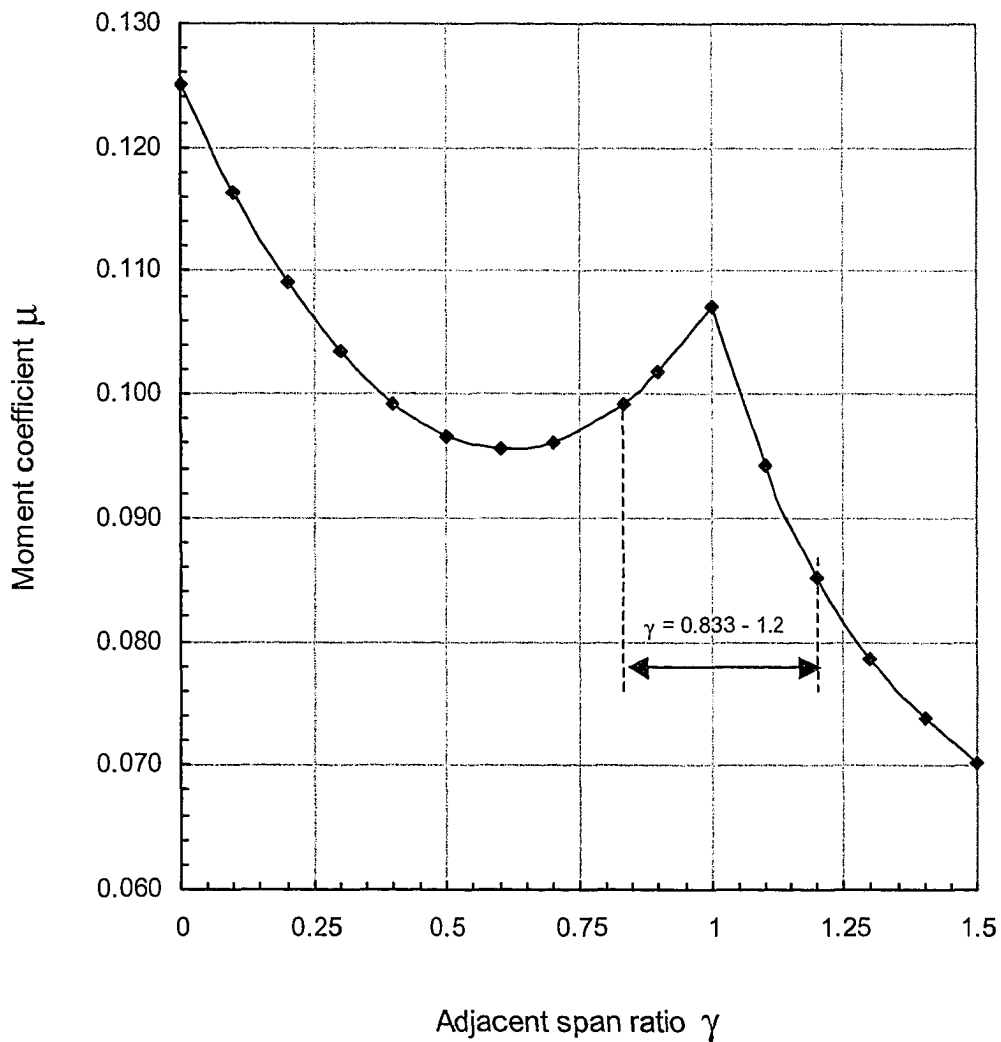
Figure 7.15 Non-pattern load moment coefficient for negative moment at first interior support of a continuous beam

252

$$\mu = \frac{(2+8\gamma+3\gamma^2)-2\gamma^3(2+\gamma)}{8(6+10\gamma+3\gamma^2)}$$

$\gamma = 0.833 - 1.2$

Adjacent span ratio γ
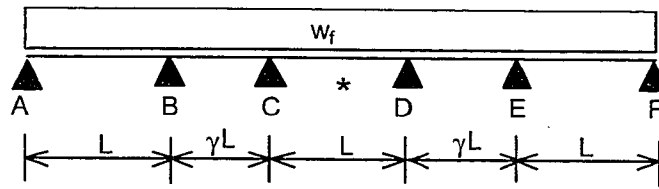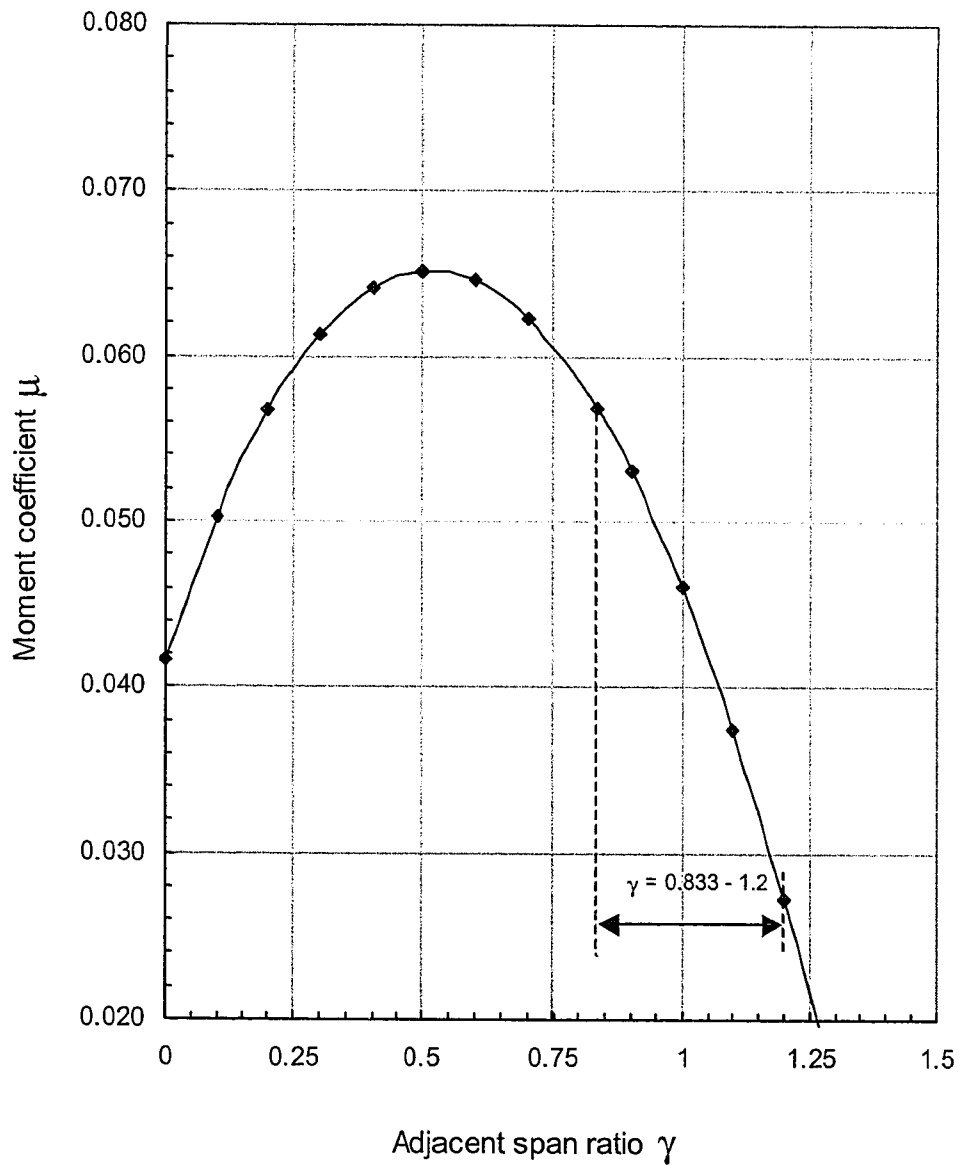
Figure 7.16 Non-pattern load moment coefficient for positive moment in interior span of a continuous beam

253
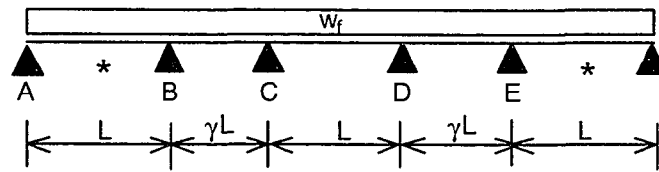
$$* \quad \mu = \frac{1}{32}\left[\frac{(9+19\gamma+6\gamma^2)-(3+\gamma)\gamma^3}{(6+10\gamma+3\gamma^2)}\right]^2$$
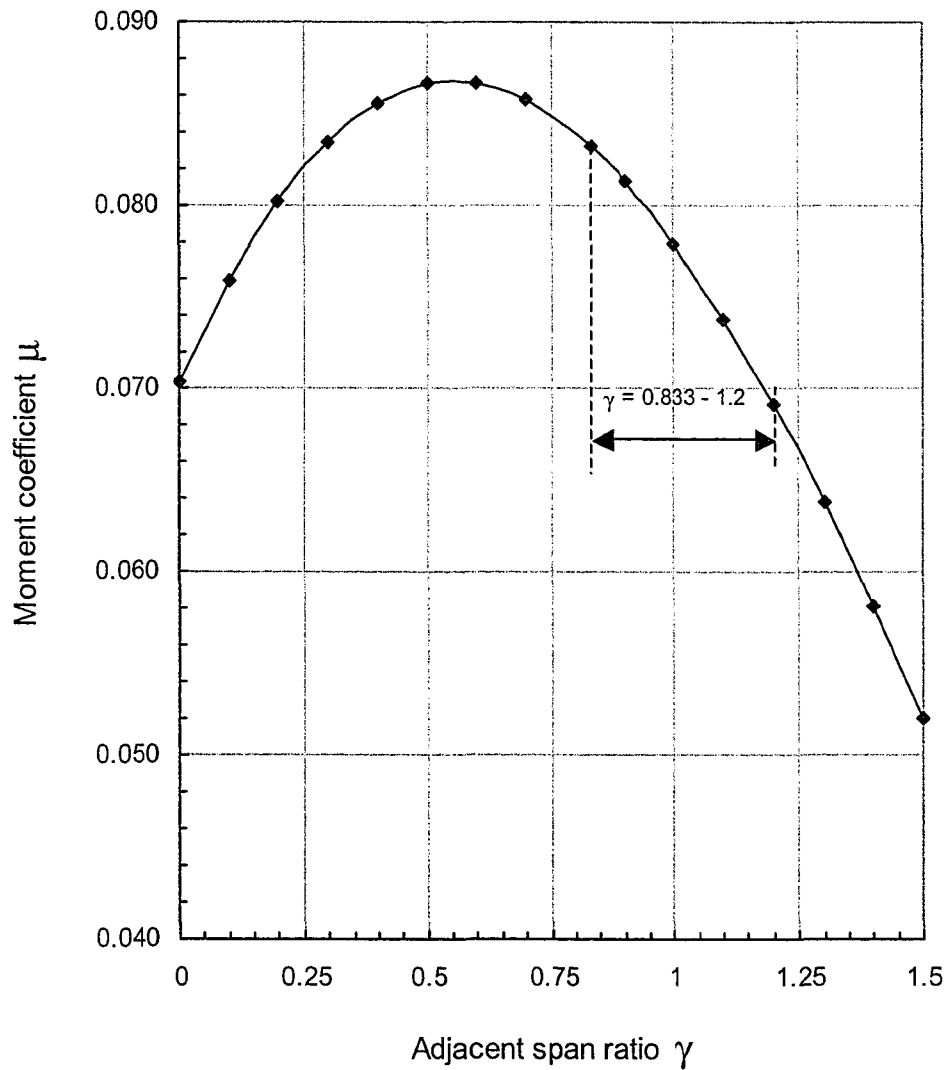
Figure 7.17 Non-pattern load moment coefficient for positive moment in exterior span of a continuous beam

254
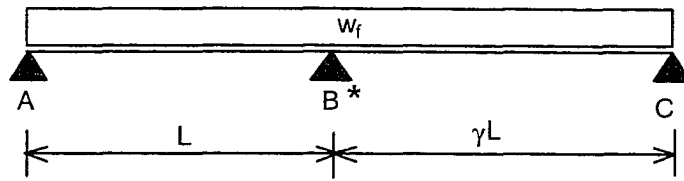
$$\mu = \frac{\left(1 + \gamma^3\right)}{8(1 + \gamma)}$$
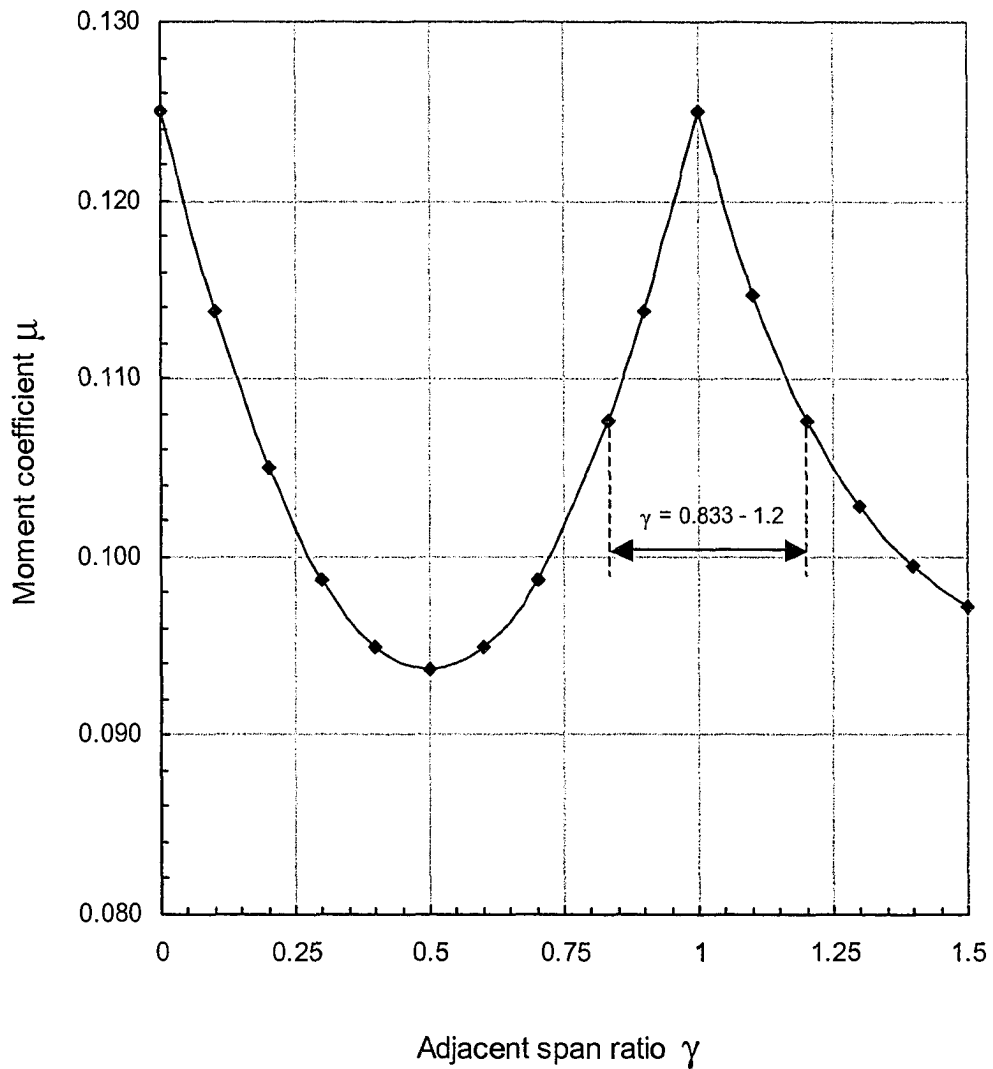
Figure 7.18 Non-pattern load moment coefficient for negative moment at interior support of a two-span beam

255
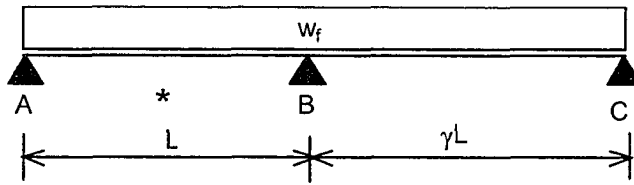
$$* \quad \mu = \frac{1}{8}\left[\frac{(3+4\gamma)-\gamma^3}{4(1+\gamma)}\right]^2$$
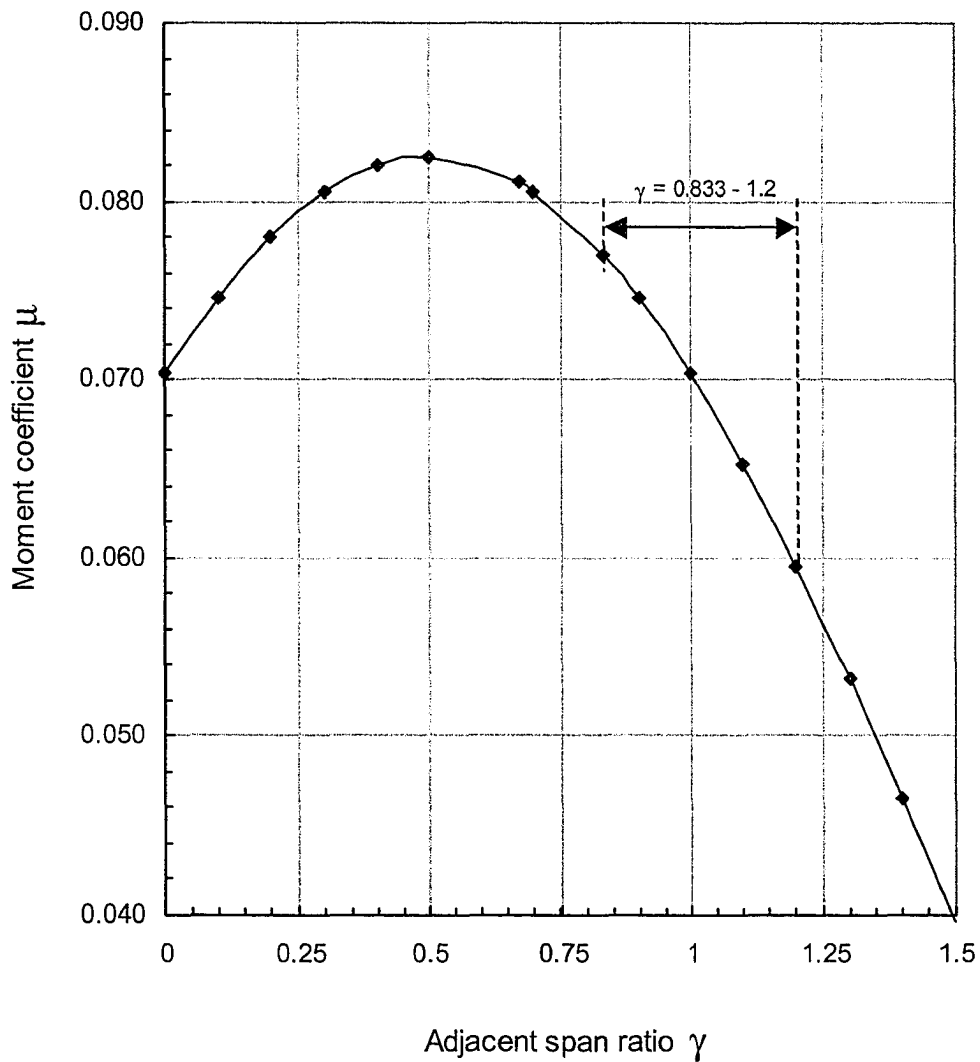
Figure 7.19 Non-pattern load moment coefficient for positive span moment in a two-span beam

256

8. SUMMARY, CONCLUSIONS AND RECOMMENDATIONS

8.1 Summary

Moment redistribution can be used as a tool to reduce the design moment envelope of indeterminate reinforced concrete structures. This, however, requires a realistic estimate of allowable moment redistribution. Significant differences exist among various design standards on the amount of allowable moment redistribution. While the Canadian standard (A23.3-94) and the American standard (ACI 318-95) allow a maximum of 20% moment redistribution, other standards allow much higher moment redistribution. The Danish standard (DS 411-1986) allows moment redistribution as high as 66%. Furthermore, the code (CSA A23.3-94) considers c/d to be the only parameter affecting allowable moment redistribution. The literature review reveals that there are many other parameters that affect the allowable moment redistribution. This points to the need for a more thorough examination of the code (A23.3-94) limit for moment redistribution.

Code (CSA A23.3-94) provisions for allowable moment redistribution are examined in Chapter 3 to assess the need for a rational ductility model. Ductility equations from plane-section analysis, combined with classical equilibrium method of analysis and subsequent hinge moment analysis, are used to establish the c/d limit for given amounts of moment redistribution. Comparison with code c/d limit shows that the code limit is very conservative and does not account for the influence of other important parameters.

An analytical model is developed in Chapter 4 to predict the plastic rotation capacity, θ_p, and allowable moment redistribution, β, in reinforced concrete sections. The model is developed by considering the mechanics of reinforced concrete, concrete and steel constitutive laws and a bond-slip law that allows computation of stresses and strains within the cracked elements. The material constitutive relationships, used, allow the inclusion of the effect of concrete confinement and steel strain hardening. The bond-slip relationship used allows including the effects of tension stiffening. A linear moment – rotation (M-θ_p) relationship allows accounting for the finite stiffness of hinge. Effects of shear cracking on θ_p and β are taken into account by considering the shift of the tension

257

force in the steel. An effort is made to incorporate the important variables identified in literature review, especially beam slenderness, concrete confinement, ultimate concrete strain, steel ductility, shear cracking, and the type of loading.

The model considers the tension region of the beam to be composed of individual cracked elements. The analysis to determine θ_p and β consists of two parts. In the first part θ_p is computed by summing up the individual rotations of each cracked element. The steel strain distribution within each cracked element is determined, using the bond-slip law. The steel strain distribution leads to the curvature distribution, which is integrated over the plastic hinge length to provide the plastic hinge rotation. In the second part, θ_p is computed using the stiffness, geometry and loading on the structure. The correct solution requires iteration in which the values of loading and the steel strain at failure are adjusted to give same value of θ_p from the two approaches. It gives the maximum load that the member can carry without exhausting the ductility of the plastic hinges in the collapse mechanism.

A parametric study is done to understand and quantify the effects of various parameters on plastic rotation capacity and allowable moment redistribution. The study is carried out using the model developed in Chapter 4. The study reveals that although ω is the most important parameter, there are several other parameters that affect plastic rotation capacity and allowable moment redistribution. The most important among these are the type of plastic hinge, ultimate concrete strain, beam slenderness, amount of compression reinforcement, amount of transverse reinforcement, and the ratio of the shear carried by the stirrups to the total shear. The ductility of steel and the presence of axial load also influence the plastic rotation capacity and allowable moment redistribution. For low ductility steel θ_p and β are small compared to those for normal ductility steel, at low to moderate reinforcement ratios. The following observations are made with regard to the influencing parameters:

1. The reinforcement index and/or the c/d ratio are the most important parameters affecting plastic rotation capacity and moment redistribution. They incorporate

258

within them the combined effects of material properties, section properties, and the amount of flexural reinforcement. For normal ductility steel, such as that used in Canadian design, the failure is almost always governed by the crushing of concrete unless the reinforcement provided is less than the minimum required reinforcement. For low ductility steel (ε_{su}=0.04) on the other hand, the failure is governed by the rupture of steel for low to moderate reinforcement ratios, while it is governed by the crushing of concrete in regions of higher reinforcement ratios.

2. The beam slenderness (L/d) affects both θ_p and β. The plastic rotation capacity increases as the beam slenderness increases, while the allowable moment redistribution decreases as the slenderness increases. Thus relatively deep beams (smaller L/d) allow more redistribution of moment provided that premature shear failure is prevented.

3. Concrete ultimate strain has significant effect on θ_p and β. Both θ_p and β increase with an increase in the concrete ultimate strain.

4. Compression reinforcement is effective in increasing the plastic rotation capacity and allowable moment redistribution.

5. The confinement of concrete by transverse reinforcement improves θ_p and β. While confinement increases the effective strength of the concrete, it is the increase in ultimate concrete strain that is mostly responsible for increasing θ_p and β.

6. The ratio of the shear stress carried by the stirrups to the total shear stress affects the distribution of tension steel force and hence θ_p and β. A smaller V_s/V_u gives greater θ_p and β and vice versa.

7. The type of plastic hinge has a major influence on the plastic rotation capacity and allowable moment redistribution. The available rotation capacity and moment

259

redistribution for the case of a shear crack hinge is possibly twice as great as a hinge that only contains flexural cracks.

8. The presence of a tensile axial load increases θ_p and β, while the presence of a compressive axial load reduces θ_p and β.

9. The type of loading, uniform or concentrated, has insignificant influence on plastic rotation capacity and allowable moment redistribution.

It is realized that although a complex ductility model is more appropriate for use as an analytical tool, it may not be entirely suitable for routine applications where one needs a quick estimate of allowable moment redistribution. Empirical equation seems to be a better alternative to rigorous analysis. With this in mind, a set of empirical equations and curves are produced to determine the allowable moment redistribution in continuous reinforced concrete beams. These equations provide an explicit relationship between β and ω for a range of L/d values. The effects of compression reinforcement are implicit in ω while for the rest of the parameters, constant values are assumed that provide conservative estimates of β. These equations can be used to determine the allowable moment redistribution based on ductility criteria. These can particularly be useful in the strength evaluation of existing structures when the structural collapse, rather than serviceability, is a prime concern.

Although ductility considerations may allow very high amounts of moment redistribution under favourable conditions, the serviceability must be considered when establishing an upper limit on allowable moment redistribution. In Chapter 6, allowable moment redistribution limits are established to prevent steel yielding at service load levels. These can govern the moment redistribution limits that only consider the ultimate limit state.

Empirical equations for the allowable moment redistribution are developed. Comparison with the code equation shows that the code is conservative if one is considering the

260

ultimate limit state and moderately conservative if one wants to prevent yielding at service load level.

CSA A23.3-94 Clause 9.3 gives approximate moment coefficients for frame analysis. In Chapter 7 an alternative set of coefficients that utilize moment redistribution is developed. They allow a reduction in design moments of about 10% for beams with ω less than 0.2.

Moment redistribution is used to assess the need for pattern load analysis, for continuous reinforced concrete beams. The factored live load to dead load ratio is assumed not to be greater than 2 and the adjacent longer span is assumed not to be greater than the shorter span by 20%. These limits are the same as specified by CSA A23.3-94 for the use of approximate coefficients. The maximum elastic moments from non-pattern load analysis are evaluated and compared with the redistributed design moments from pattern load analysis. The elastic moments from non-pattern load analysis are found to be greater than the redistributed moments from the pattern load analysis and hence govern the flexural design. Thus allowing for moment redistribution can eliminate the need for pattern load analysis and the reinforced concrete beams can be analysed and designed on the basis of a single load case.

8.2 Conclusions

The following conclusions are made:

1. A ductility model is developed and validated against test results from the literature. A set of empirical equations derived from the ductility model allows one to assess the allowable moment redistribution in reinforced concrete beams.

2. The standard (CSA A23.3-94) limits for allowable moment redistribution are very conservative relative to the ultimate limit-state. Under favourable conditions moment redistribution in excess of 50% is possible, provided that the serviceability is not an issue.

261

3. Serviceability consideration can and generally will limit the allowable moment redistribution. With respect to avoiding yielding at service load level, the code limits on moment redistribution are conservative.

4. For low ductility steel (ε_{su} less than 0.04) the plastic rotation capacity and the allowable moment redistribution is significantly reduced in regions of low ω (ω less than 0.15), where the failure is governed by the rupture of steel.

5. Higher ultimate strain in concrete allows higher moment redistribution. While the 0.0035 code limit is adequate for computing moment resistance, it is too conservative for computing hinge rotation capacity.

6. Non-slender beams with shear reinforcement provide much higher moment redistribution capacity than slender beams or slabs with little or no shear reinforcement.

7. Compression reinforcement can be effective in increasing the allowable moment redistribution by reducing the c/d ratio.

8. The presence of shear cracking in a plastic hinge has a major impact on the allowable moment redistribution. Shear cracks substantially increase the plastic rotation capacity and allowable moment redistribution.

9. Use of redistributed moment coefficients instead of the code coefficients can provide potential savings in the amount of flexural reinforcement.

10. Considering moment redistribution can eliminate the need for a pattern load analysis, for the design of continuous reinforced concrete beams.

262

8.3 Recommendations for Future Research

The following research needs are identified:

1. Ultimate strain in concrete has a major influence on the allowable moment redistribution. The standard (CSA A23.3-94) uses 0.0035 as the ultimate strain in concrete at failure. Experimental work done earlier has reported much higher strains at failure. There is a need to re-evaluate the limit for ε_{cu} through experimental research.

2. Experimental and analytical studies need to be done to evaluate the effects of moment redistribution on the shear capacity of reinforced concrete beams.

3. Serviceability criteria need to be examined through analytical and experimental research to determine if more relaxed limits can be adopted to allow taking full advantage of moment redistribution.

4. A knife-edge support is assumed in the development of the model and the analysis of continuous beams. In reality, supports such as columns have finite width that contributes to the plastic hinge length and improves ductility. The benefits of finite width of support on rotation capacity and moment redistribution warrant further study.

References

Abele, G. 1974. Initial and time dependent shear deformation of reinforced concrete T-beams. Deflections of Concrete Structures, ACI SP 43-20, 1974, pp. 487-513.

Ahner, C., and Kliver, J. 1999. Development of a new concept for the rotation capacity in Din 1045, Part 1. Leipzig Annual Civil Engineering Report, N0. 4 1999.

Alca, N., Alexander, S. D. B., and MacGregor, J. G. 1997. Effect of size on flexural behaviour of high-strength concrete beams. ACI Journal, Vol. 94, No. 1, January-February 1997, pp 59-67.

Alvarez, M., Koppel, S., and Marti, P. 2000. Rotation capacity of reinforced concrete slabs. ACI Journal, Vol. 97, No. 2, March-April 2000, pp 235-242.

Al-Haddad, M. S. 1995. Curvature ductility of reinforced concrete beams under low and high strain rates. ACI Journal, Vol. 92, No. 5, September-October 1995, pp 526-534.

ACI 318-95. Building Code for Reinforced Concrete, American Concrete Institute, Detroit, 1995.

Bachmann, H. 1970. Influence of shear and bond on rotation capacity of reinforced concrete beams. IABSE Publications, vol. 30-II, Zurich, pp. 28.

Baker, A. L. L., 1956. Ultimate Load Theory Applied to the Design of Reinforced and Prestressed Concrete Frames. Concrete Publications, London, England.

Baker, A. L. L. 1971. Limit State Design of Reinforced Concrete. Cement and Concrete Association, London.

264

Baker, A. L. L., and Amarakone, A. M. N. 1964. Inelastic hyperstatic frame analysis. Proc. Int. Symp. on Flexural Mechanics of Reinforced Concrete, ACI SP-12, pp. 85-142.

Bosco, C., and Debernardi, P. G. 1993. Influence of some basic parameters on the plastic rotation capacity of reinforced concrete elements. CEB Bulletin d'Information, No. 218, pp. 25-44

BS 8110-85. Structural Use of Concrete. Handbook to British Standards, Viewpoint Publications, London, England, 1987.

CEB-FIP 1990. Model Code 1990 for Concrete Structures. Comite Euro-International du Beton, Bulletin d'Information n. 213/214, Lausanne, May 1993.

CEB. 1985. CEB design manual on cracking and deformations. Ecole Polytechnique Federale de Lausanne, Switzerland, pp. 2.30-2.32

Chan, W. W. L. 1955. The ultimate strength and deformation of plastic hinges in reinforced concrete frameworks. Magazine of Concrete Research (London), V. 7, No. 21, Nov. 1955, pp. 121-132.

Cohn, M. Z. 1964. Rotation compatibility in the limit design of reinforced concrete continuous beams. Proceedings of the International Symposium on Flexural Mechanics of Reinforced Concrete, ACI SP-12, pp. 359-381.

Cohn, M. Z. 1967. Limit design solutions for reinforced concrete structures. ASCE Journal of the Structural Division, Vol. 93, No. ST1, February 1967, pp. 37-58.

Cohn, M. Z. 1968. Limit design of reinforced concrete frames. ASCE Journal of the Structural Division, Vol. 94, No. ST10, October 1968, pp. 2467-2483.

265

Cohn, M. Z. 1979. Nonlinear design of concrete structures: Problems and prospects. Proceedings of the CSCE-ASCE-ACI-CEB International symposium on "Non-linear design of concrete structures, University of Waterloo, Ontario, Canada, August 7-9, 1979.

Cohn, M. Z., and Franchi, A. 1979. A computer system for structural plasticity. ASCE Journal of the Structural Division, Vol. 105, No. ST4, 1979, pp. 789-804.

Cohn, M. Z., and Lounis, Z. 1991. Moment redistribution in structural concrete codes. CAN. J. CIV. ENG. Vol. 18, 1991, pp. 97-108.

Cohn, M. Z., and Riva, P. 1992. Yield safety, cracking control, and moment redistribution. Journal of Structural Engineering, Vol. 118, No. 2, February, 1992, pp. 447-468.

Corley, G. W. 1966. Rotational capacity of reinforced concrete beams. ASCE Journal of the Structural Division, 92, ST5, 121-146.

Cosenza, E., Greco, C., and Manfredi, G. 1991. Theoretical evaluation of inelastic rotations and displacements in the reinforced concrete monodimensional elements (in Italian). Atti dell'Academia Nazionale dei Lincei, serie IX, Volume II, Fascicolo 3.

CSA A23.3-94. Design of Concrete Structures for Buildings. Canadian Standards Association, Rexdale, pp. 281.

Dilger, W. 1966. Veranderlichkeit der Biege-und Schubsteifigkeit bei Stahlbetontragwerken und ihr EinfluB auf Schnittkraftverteilung und Trablast bei statisch unbestimmter Lagerung. Ddeutscher Ausschuss Fur Stahlbeton, Heft 179, Berlin, pp101.

DIN 1045-78, German Standards, 1978.

266

Dishongh, B. E. 1995. Inelastic moment redistribution for bridges. Journal of Structural Engineering, Vol. 121, No. 2, February, 1995, pp. 378-382.

DS 411-1986. Structural Use of Concrete. Danish Standard, 1986.

Eifler, H. 1969. Bericht uber die Vorvesuche fur die Ermittlung des Werkstoff- und Verbundverhaltens im Bereich plastischer Gelenke von Stahlbetonplatten bei statischer Belastung, Bundesanstalt fur Materialprufung (BAM), Az.: 2.2/11 9311, Berlin.

Furlong, R. W. 1970. Design of concrete frames by assigned limit moments. ACI Journal, Vol. 67, No. 4, April 1970, pp. 341-353.

Furlong, R. W., and Rezende, C. 1979. Alternate to ACI analysis coefficients. ASCE Journal of the Structural Division, Vol. 105, No. ST11, November 1979, pp. 2203-2221.

Hillerborg, A. 1988. Rotational capacity of reinforced concrete beams. Norwegian Concrete Research, Publication No. 7, 1988, pp. 121-134.

JSCE-1986. Standard Specifications for Design and Construction of Concrete Structures, Part 1: Design. Japanese Society of Civil Engineers, Tokyo, Japan, 1986.

Kang, Y., and Scordelis, A. C. 1980. Non-linear analysis of prestressed concrete frames. ASCE Journal of the Structural Division, Vol. 106, No. ST2, Feb. 1980, pp. 445-462.

Kaufmann, W., and Marti, P. 1998. Structural concrete: cracked membrane model. Journal of Structural Engineering, ASCE, 124, No. 12, December 1998, pp1467.

Kemp, A. R. 1981. Ductility and moment redistribution in reinforced concrete beams. The Civil Engineer, South Africa, May 1981, pp. 177-181.

Kemp, A. R. 1998. The achievement of ductility in reinforced concrete beams. Magazine of Concrete Research, June 1998, 50, N0. 2, pp. 123-132.

Kent, D. C., and Park, R. 1971. Flexural members with confined concrete. Journal of the Structural Division, ASCE, Vol. 97, ST7, July 1971, pp. 1969-1990

Langer, P. 1987. Vedrehfahigkeit plasticizer Tragwerksbereiche im Stahlbetonbau. Ph.D Thesis, University of Stuttgart, Institut fur Werkstoffe in Bauwesen.

Li, L. 1995. Rotationsfahigkeit von plastischen Glenken im Stahl-und Spannbetonbau. Ph.D Thesis, University of Stuttgart, Institut fur Werkstoffe in Bauwesen.

Macchi, G. 1960. A proposal of analysis based on the theory of imposed rotations. Bulletin d'Information du Comite Euro-International du Beton Paris,No. 21, January, 1960.

Mander, J. B., Priestly, M. J. N.,and Park, R. 1988. Theoretical stress-strain model for confined concrete. Journal of Structural Engineering, Vol. 114, No. 8, August 1988, pp. 1804-1826.

Marti, P. 1980. Zur plastischen Berechnung von Stahlbeton (plastic analysis of reinforced concrete). Coll. StruReport No. 104, Zurich Institute of Structural Engineering, ETH, 1990.

Marti, P. 1991. Dimensioning and detailing. Coll. Structural Concrete, Zurich International Association for Bridge & Structural Engineering, Vol. 62, 1991, pp.411.

Marti, P. 1999. A simple, consistent approach to structural concrete. Paper presented to the Institution of Structural Engineers, May 25, 1999.

Marti, P., Alvarez, M., Kaufmann, W., and Sigrist, V. 1998. Tension chord model for structural concrete. Structural Engineering International, 8, No. 4, November 1998, pp 287.

Mattock, A. H. 1959. Redistribution of design bending moments in reinforced concrete continuous beams. Proceedings of the Institution of Civil Engineers, pp. 35-46.

Mattock, A. H., 1964. Rotational capacity of hinging regions in reinforced concrete beams. Proceedings of the International Symposium on Flexural Mechanics of Reinforced Concrete, ACI SP-12, 143-182.

Mattock, A. H. 1967. Discussion of Rotational capacity of reinforced concrete beams, by Corley, W. G. ASCE Journal of the Structural Division, Vol. 93, ST2, April 1967, pp. 519-522.

Mattock, A. H. 1983. Secondary moments and moment redistribution in ACI 318-77 code. Proceedings International Symposium on Nonlinearity and Continuity in Prestressed Concrete. Preliminary publication, 3, University of Waterloo, Ontario, Canada, 1983, pp. 27-48.

Michalka, C. 1986. Zur Rotationsfahigkeit von plastischen Glenken in Stahlbetontragem. Ph.D Thesis, University of Stuttgart, Institut fur Massivbau.

Naaman, A. E., Harajli, M. H., and Wight, J. K. 1986. Analysis of ductility in partially prestressed concrete flexural members. Prestressed Concr. Inst. J., 1986, 31, No. 3, pp 64-87.

Nguyen, D. H. 1984. CEPAO- an automatic program for rigid-plastic and elastic-plastic analysis and optimization of frame structures. Struct. Eng., Vol. 6, January 1984, pp. 33-51.

Park, R., and Paulay, T. 1975. Reinforced Concrete Structures. John Wiley & Sons, New York, 1975.

Park, R., Priestly, M. J. N., and Gill, W. D. 1982. Ductility of squared-confined concrete columns. Journal of the Structural Division, ASCE, Vol. 108, No. ST4, April 1982, pp. 929-950.

Pisanty, A., and Regan, P. E. 1998. Redistribution of moments-from serviceability to ultimate limit state. Structural Engineering International, January 1998, pp. 35-39.

Rangan, V. B., and Hall, A. S. 1984. Moment Redistribution in Flat Plate Floors. ACI Journal, Vol. 81, No. 6, November-December 1984, pp 601-607.

Riva, P., and Cohn, M. Z. 1994. Rotation capacity of structural concrete members. Magazine of Concrete Research, 46, No. 168, 223-234.

Roy, H. E. H., and Sozen, M A. 1964. Ductility of concrete. Flexural Mechanics of Reinforced Concrete, Sp-12, ACI/ASCE, Detroit, pp. 213-224.

Saatcioglu, M., and Razvi, S. R. 1992. Strength and ductility of confined concrete. Journal of Structural Engineering, Vol. 118, No. 6, June 1992, pp. 1590-1607.

Sargin, M. 1971. Stress-Strain relationships for concrete and the analysis of structural concrete sections. Study No, 4, Solid Mechanics Division, University of Waterloo, 167 pp.

Sawyer, H. A. 1964. Design of concrete frames for two failure stages. Proceedings of the International Symposium on Flexural Mechanics of Reinforced Concrete, ACI SP 12, 405-438.

Scholz, H. 1993. Contribution to redistribution of moments in continuous reinforced concrete beams. ACI Structural Journal, Vol. 90, No. 2, March-April 1993, pp. 150-155.

Scott, B. D., Park, R., and Priestley, M. J. N. 1982. Stress-strain behavior of concrete confined by overlapping hoops at low and high strain rates. ACI Journal, Vol. 79, No. 1, January-February 1982, pp. 13-27.

Sheikh, S. A. 1982. A comparative study of confinement models. ACI Journal, Vol. 79, No. 4, July-August 1982, pp. 296-306.

Sheikh, S. A., and Uzumeri, S. M. 1980. Strength and ductility of tied columns. ASCE Journal of Structural Division, V106, St5, 1079-1102.

Sheikh, S. A., and Yeh, C. C. 1986. Flexural behavior of confined concrete columns. ACI Journal, Vol. 83, No. 3, May-June 1986, pp. 389-404.

Sigrist, V., and Marti, P. 1994. Ductility of structural concrete, a contribution. Workshop on development of EN 1992 in relation to new research results and the CEB-FIP Model code 1990, Czech Technical University, Prague, Czechoslovakia, pp 211-223.

Soliman, M. T. M., and Yu, C. W. 1967. The flexural stress-strain relationship of concrete confined by rectangular transverse reinforcement. Magazine of Concrete Research, Vol. 19, No. 61, pp. 223-238

Sveinson, T. N. 1989. Non-linear behaviour and redistribution of moments in continuous concrete structures. MSc. Thesis, Department of Civil Engineering, University of Calgary.

Vallenas, J., Bertero, V. V., and Popov, E. P. 1977. Concrete confined by rectangular hoops and subjected to axial loads. Report No. UCB/EERC-77/13, Earthquake Engineering Research Centre, University of California, Berkley, Aug. 1977, 114 pp.

Walraven, J. C., 1999. Tension stiffening and moment curvature in structural concrete. Text Book on Behaviour, Design and Performance, Updated Knowledge of the CIB/FIP Model Code 1990. FIP Bulletin 1, Vol. 1, Federation Internationale du Beton, Lausanne, pp. 189-205.

Wyche, P. J., Uren, J. G., and Reynolds, G. C. 1992. Interaction between prestress secondary moments, moment redistribution, and ductility- A treatise on the Australian concrete codes. ACI Journal, Vol. 89, No. 1, Jan.-Feb. 1992, pp. 57-70.

APPENDIX A

SPREAD SHEET SOLUTION FOR DUCTILITY MODEL

INPUT DATA

Structure Geometry

Span length	L =	12	m

Section Properties

Height	h =	800	mm
Web Width	b =	300	mm
Clear Cover	ccl =	50	mm
c/c Cover	cct =	60	mm
Effective Depth	d =	740	mm
Distance to Compression Steel	dc =	65	mm

Material Properties

Concrete

Cylinder Strength	fc =	30	MPa
Modulus of Elasticity	Ec =	2.46E+04	MPa
Ultimate Strain	ecu =	0.005	

Steel

Tension Steel

Yield Strength	fy =	400	MPa
Ultimate Strength	fu =	540	MPa
Modulus of Elasticity	Est =	2.00E+05	MPa
Yield Strain	esy =	2.00E-03	
Ultimate Strain	esu =	0.1	
Strain Hardening Modulus of Elasticity	Esh =	1.43E+03	MPa

Compression Steel

Yield Strength	fyc =	400	MPa
Ultimate Strength	fuc =	600	MPa
Yield Strain	esyc =	0.002	
Ultimate Strain	esuc =	0.1	
Strain Hardening Modulus of Elasticity	Eshc =	2.04E+03	MPa

Stirrrups

Yield Strength	fys =	400	MPa

273

Amount of Reinforcement

Tension Reinforcement

Number of bars	nb =	6	
Dia. of Bar	db =	20	mm
Area of Reinforcement	As =	1800	mm^2
	roht=	0.0081	

Compression Reinforcement

Number of bars	nbc =	0
Dia. of Bar	dbc =	0
Area of Reinforcement	Asc =	0

STIRRUPS

	nleg =	2	
Dia. of Bar	dbs =	10	
Spacing	s =	150	mm
	Abs =	100	
	Avs =	200	

Reinforcement Index $\omega =$ 0.1081

Crack spacing $S_m =$ 150 mm

Compression strut angle $\alpha =$ 45 degree = 0.785 rad

cotα= 1

v= 0.8

Magnitude of bond shear stress

$$\tau_{b1} = 0.6^*(v^*fc)^{\wedge}(2/3) = 5.0$$

$$\tau_{b2} = 0.3^*(v^*fc)^{\wedge}(2/3) = 2.5$$

RESULTS OF ANALYSIS

Bar dia.	no. of bars	c/d	ω	qu	Mu	θp	β
				kN/m	kNm	rad	%
20	6	0.1348	0.1081081	56.32884	581.0	0.0280318	42.7

274

DETAILED CALCULATIONS

1. Calculation of Depth of Neutral Axis , Steel Strain, and Support Moment

$\alpha_1 = 0.85 - 0.0015*fc$ =   0.805

$\beta_1 = 0.97 - 0.0025*fc$ =   0.895

ε_s (Steel Strain)		c	a	fs	T	dv	M_a
(Av steel strain from plane-sections analysis)							
0.03209 ◄——┘							
0.0469	(assumed ε_s)	99.76	89.28	464.14	835.46	695.41	581.0
0.026629 ◄——┐							
(Av steel strain from bond-model)							

2. Assume a value of   q   =   56.33   kN/m

                          Mel =   1013.92   kNm

                          Ma =   580.99   kNm

3. Calculation of Tension Force and Stress in Steel at Crack Locations

Ru= (reaction at support)   386.39   kN   Vu=   386.39   Vc=   145.91

                                                                   kN   kN

x	Vx	Mx	Ft	σ_{cr}	Eqn for computing Ft
0	386.39	580.99	835.46	464.14	Eq. 4.64
0.15	377.94	523.66	826.47	459.15	Eq. 4.64
0.3	369.49	467.61	799.50	444.17	Eq. 4.64
0.45	361.04	412.82	754.56	419.20	Eq. 4.64
0.6	352.59	359.29	691.64	384.24	Eq. 4.64
0.75	344.14	307.04	613.59	340.88	Eq. 4.65
0.9	335.69	256.05	536.05	297.80	Eq. 4.65
1.05	327.24	206.33	460.32	255.74	Eq. 4.65
1.2	318.79	157.88	386.42	214.68	Eq. 4.65
1.35	310.34	110.69	314.35	174.64	Eq. 4.65
1.5	301.90	64.77	244.09	135.61	Eq. 4.65
1.65	293.45	20.12	175.66	97.59	Eq. 4.65
1.8	285.00	-23.26	109.05	60.58	Eq. 4.65
1.95	276.55	-65.38	44.26	24.59	Eq. 4.65
2.1	268.10	-106.22	-18.70	-10.39	Eq. 4.65
2.25	259.65	-145.80	-79.84	-44.36	Eq. 4.65
2.4	251.20	-184.12	-139.16	-77.31	Eq. 4.65
2.55	242.75	-221.16	-196.66	-109.25	Eq. 4.65
2.7	234.30	-256.94	-252.33	-140.19	Eq. 4.65
2.85	225.85	-291.45	-306.19	-170.10	Eq. 4.65
3	217.40	-324.70	-358.21	-199.01	Eq. 4.65
3.15	208.95	-356.68	-408.42	-226.90	Eq. 4.65
3.3	200.50	-387.38	-456.81	-253.78	Eq. 4.65
3.45	192.05	-416.83	-503.37	-279.65	Eq. 4.65
3.6	183.60	-445.00	-548.11	-304.50	Eq. 4.65
3.75	175.16	-471.91	-591.02	-328.35	Eq. 4.65
3.9	166.71	-497.55	-632.12	-351.18	Eq. 4.65
4.05	158.26	-521.92	-671.39	-372.99	Eq. 4.65
4.2	149.81	-545.02	-708.84	-393.80	Eq. 4.65
4.35	141.36	-566.86	-744.47	-413.59	Eq. 4.65
4.5	132.91	-587.43	-778.27	-432.37	Eq. 4.65

275

Computation of Distances, XL1, XL2, XR1, XR2

Case 1: $\sigma_{scrL} > f_y$; $\sigma_{scrR} > f_y$; $\sigma_{smin} > f_y$

	XL2	XL1	XR1	XR2
crack 1	80.0	0	0	70.0
crack 2	90.0	0	0	60.0
crack 3	100.0	0	0	50.0
crack 4	110.0	0	0	40.0
crack 5	118.4	0	0	31.6
crack 6	118.1	0	0	31.9
crack 7	117.1	0	0	32.9
crack 8	116.1	0	0	33.9
crack 9	115.1	0	0	34.9
crack 10	114.1	0	0	35.9

Case 2: $\sigma_{scrL} > f_y$; $\sigma_{scrR} > f_y$; $\sigma_{smin} < f_y$

	XL2	XL1	XR1	XR2
crack 1	128.5	-48.5	-48.5	118.5
crack 2	118.5	-28.5	-28.5	88.5
crack 3	88.5	11.5	11.5	38.5
crack 4	38.5	71.6	71.6	-31.6
crack 5	-31.6	150.0	150.0	-118.4
crack 6	-118.4	236.6	236.6	-204.7
crack 7	-204.7	321.8	321.8	-289.0
crack 8	-289.0	405.1	405.1	-371.2
crack 9	-371.2	486.3	486.3	-451.4
crack 10	-451.4	565.5	565.5	-529.6

Case 3: $\sigma_{scrL} > f_y$; $\sigma_{scrR} \leq f_y$; $\sigma_{smin} < f_y$

	XL2	XL1	XR1	XR2
crack 1	128.5	-18.9	40.4	0
crack 2	118.5	-6.4	37.9	0
crack 3	88.5	21.1	40.4	0
crack 4	38.5	63.7	47.9	0
crack 5	-31.6	120.4	61.2	0
crack 6	-118.4	185.4	83.0	0
crack 7	-204.7	249.6	105.1	0
crack 8	-289.0	312.3	126.7	0
crack 9	-371.2	373.5	147.8	0
crack 10	-451.4	433.1	168.3	0

276

Case 4: $\sigma_{scrL} < f_y$; $\sigma_{scrR} < f_y$; $\sigma_{smin} < f_y$

	XL2	XL1	XR1	XR2
crack 1	0	77.5	72.5	0
crack 2	0	82.5	67.5	0
crack 3	0	87.5	62.5	0
crack 4	0	92.5	57.5	0
crack 5	0	96.7	53.3	0
crack 6	0	96.6	53.4	0
crack 7	0	96.1	53.9	0
crack 8	0	95.6	54.4	0
crack 9	0	95.1	54.9	0
crack 10	0	94.5	55.5	0

STRESSES

Case 1: $\sigma_{scrL} > f_y$; $\sigma_{scrR} > f_y$; $\sigma_{smin} > f_y$

Left	Left Int	Int	Right Int	Right
464.1	424.2	424.2	424.2	459.1
459.1	414.2	414.2	414.2	444.2
444.2	394.2	394.2	394.2	419.2
419.2	364.3	364.3	364.3	384.2
384.2	325.1	325.1	325.1	340.9
340.9	281.9	281.9	281.9	297.8
297.8	239.3	239.3	239.3	255.7
255.7	197.8	197.8	197.8	214.7
214.7	157.2	157.2	157.2	174.6

Case 2: $\sigma_{scrL} > f_y$; $\sigma_{scrR} > f_y$; $\sigma_{smin} < f_y$

Left	Left Int	Int	Right Int	Right
464.1	400.0	448.4	400.0	459.1
459.1	400.0	428.4	400.0	444.2
444.2	400.0	388.5	400.0	419.2
419.2	400.0	328.6	400.0	384.2
384.2	400.0	250.2	400.0	340.9
340.9	400.0	163.8	400.0	297.8
297.8	400.0	78.7	400.0	255.7
255.7	400.0	-4.5	400.0	214.7
214.7	400.0	-85.6	400.0	174.6
174.6	400.0	-164.6	400.0	135.6

Case 3: $\sigma_{scrL} > f_y$; $\sigma_{scrR} \leq f_y$; $\sigma_{smin} < f_y$

Left	Left Int	Int	Right Int	Right
459.1	400.0	406.4	444.2	444.2
444.2	400.0	378.9	419.2	419.2
419.2	400.0	336.4	384.2	384.2
384.2	400.0	279.8	340.9	340.9
340.9	400.0	214.9	297.8	297.8
297.8	400.0	150.8	255.7	255.7

255.7	400.0	88.2	214.7	214.7
214.7	400.0	27.1	174.6	174.6
174.6	400.0	-32.4	135.6	135.6
135.6	400.0	-90.5	97.6	97.6

Case 4: $\sigma_{scrL} < f_y$; $\sigma_{scrR} < f_y$; $\sigma_{smin} < f_y$

Left	Left Int	Int	Right Int	Right
464.1	464.1	386.8	459.1	459.1
459.1	459.1	376.8	444.2	444.2
444.2	444.2	356.8	419.2	419.2
419.2	419.2	326.8	384.2	384.2
384.2	384.2	287.7	340.9	340.9
340.9	340.9	244.5	297.8	297.8
297.8	297.8	201.9	255.7	255.7
255.7	255.7	160.3	214.7	214.7
214.7	214.7	119.8	174.6	174.6
174.6	174.6	80.2	135.6	135.6

Determination of Applicable Case

crack 1	CASE 1
crack 2	CASE 1
crack 3	CASE 2
crack 4	CASE 3
crack 5	CASE 4
crack 6	CASE 4
crack 7	CASE 4
crack 8	CASE 4
crack 9	CASE 4
crack 10	CASE 4

4. Calculation of stress-strain distribution within cracked elements and total angle of rotation

	dx	x	σ_s	ε_s	θ_i	θ_{tot}	ε_{sm}
crack 1		0.0	464.1	0.0469			
	128.49	128.5	400.0	0.0020			
	-48.48	80.0	448.4	0.0359			
	-48.48	31.5	400.0	0.0020			
crack2	118.48	150.0	459.1	0.0434	0.00624	0.0160358	0.0266
	118.48	268.5	400.0	0.0020			
	-28.48	240.0	428.4	0.0219			
	-28.48	211.5	400.0	0.0020			
crack 3	88.47	300.0	444.2	0.0329	0.00555		
	100.01	400.0	394.2	0.0020			
	0.00	400.0	394.2	0.0020			
	0.00	400.0	394.2	0.0020			
crack 4	49.99	450.0	419.2	0.0154	0.00340		
	38.46	488.5	400.0	0.0020			
	63.66	552.1	336.4	0.0017			
	47.88	600.0	384.2	0.0019			
crack 5	0.00	600.0	384.2	0.0019	0.00084		
	0.00	600.0	384.2	0.0019			

278

	96.71	696.7	287.7	0.0014			
	53.29	750.0	340.9	0.0017			
crack 6	0.00	750.0	340.9	0.0017	0		
	0.00	750.0	340.9	0.0017			
	96.57	846.6	244.5	0.0012			
	53.43	900.0	297.8	0.0015			
crack 7	0.00	900.0	297.8	0.0015	0		
	0.00	900.0	297.8	0.0015			
	96.07	996.1	201.9	0.0010			
	53.93	1050.0	255.7	0.0013			
crack 8	0.00	1050.0	255.7	0.0013	0		
	0.00	1050.0	255.7	0.0013			
	95.56	1145.6	160.3	0.0008			
	54.44	1200.0	214.7	0.0011			
crack 9	0.00	1200.0	214.7	0.0011	0		
	0.00	1200.0	214.7	0.0011			
	95.05	1295.1	119.8	0.0006			
	54.95	1350.0	174.6	0.0009			
crack 10	0.00	1350.0	174.6	0.0009	0		
	0.00	1350.0	174.6	0.0009			
	94.55	1444.5	80.2	0.0004			
	55.45	1500.0	135.6	0.0007			

5. Total rotation (Both sides)　　　　　　θ_{tot}= 0.032072

6. Yield rotation　　　　　　　　　　　θ_y= 0.00404

7. Plastic rotation　　　　　　　　　　θ_p= 0.028032

8. Stiffness of plastic hinge

　　　　　　　　　　k_s=　　　3.64E+09

9. Cracked moment of inertia

　　　　　　Ig=　　　1.28E+10 mm^4
　　　　　　Icr=　　　5.01E+09 mm^4
　　　　　　EIcr=　　 1.24E+14
10. Recalculate the load "q"

　　　　　　q=　　　　56.32884

Iterate till the values of q from step 2 and 10 converge.

279

Calculation of Yield Rotation

n=	8.114408
roh=	0.008108

1. Depth of neutral axis

c_y=	224.1254
la=	665.2915

2. Yield Moment

May=	479.0099 kN.m

3. Yield load

qy=	26.61166 kN/m

4. Calculation of Tension Force and Stress in Steel at Crack Locations

x (m)	Vx (kN)	Mx (kN.m)	Ft (kN)	σsy (Mpa)
0	199.59	479.0099	720	400
0.15	195.60	449.37116	714.92704	397.1817
0.3	191.60	420.33119	699.70814	388.7267
0.45	187.61	391.88997	674.34332	374.6352
0.6	183.62	364.04752	638.83258	354.907
0.75	179.63	336.80384	596.06436	331.1469
0.9	175.64	310.15891	554.01848	307.788
1.05	171.65	284.11275	512.87261	284.9292
1.2	167.65	258.66535	472.62673	262.5704

5. Stress-strain distribution within cracked elements and total yield rotation

	dx	x	σsy	εsy	dcr	wcr	qyi
crack 1		0	400	0.002			
	0	0	400	0.002	0		
	76.41135807	76.411358	323.70783	0.001619	0.1382487		
	73.58864193	150	397.18169	0.001986	0.1326232		
crack 2	0	150	397.18169	0.001986	0	0.2708719	0.000525
	0	150	397.18169	0.001986	0		
	79.2340742	229.23407	318.0712	0.00159	0.141681		
	70.7659258	300	388.72675	0.001944	0.125043		
crack 3	0	300	388.72675	0.001944	0	0.266724	0.000517
	0	300	388.72675	0.001944	0		
	82.05679034	382.05679	306.79795	0.001534	0.1426813		
	67.94320966	450	374.63518	0.001873	0.1157469		
crack 4	0	450	374.63518	0.001873	0	0.2584282	0.000501
	0	450	374.63518	0.001873	0		
	84.87950647	534.87951	289.88807	0.001449	0.141011		
	65.12049353	600	354.90699	0.001775	0.1049734		
crack 5	0	600	354.90699	0.001775	0	0.2459844	0.000477
	0	600	354.90699	0.001775	0		

280

	86.89861989	686.89862	268.14391	0.001341	0.1353557		
	63.10138011	750	331.14686	0.001656	0.0945402		
crack 6	0	750	331.14686	0.001656	0	0.2298958	0
	0	750	331.14686	0.001656	0		
	86.6976552	836.69766	244.58444	0.001223	0.1247864		
	63.3023448	900	307.78805	0.001539	0.0874162		
crack 7	0	900	307.78805	0.001539	0	0.2122026	0
	0	900	307.78805	0.001539	0		
	86.44726465	986.44726	221.47562	0.001107	0.1143835		
	63.55273535	1050	284.92923	0.001425	0.0804585		
crack 8	0	1050	284.92923	0.001425	0	0.194842	0
	0	1050	284.92923	0.001425	0		

Computation of Average Steel Strain and Depth of Neutral Axis From Plane-Section Analysis

Specified Axial Load	$P =$	0
Specified Moment	$M =$	
Specified Level of Strain	$ecc =$	0.005

Assumed Depth of N.A	$x =$	99.758608
Width of Stirrup c/c	$bs =$	210
Height of Stirrup c/c	$hs =$	710
Width of Stirrup Outside	$bso =$	220
Height of Stirrup Outside	$hso =$	720
Volumetric Ratio of Stirrups	$rohs =$	0.0077441
Confinement Index	$kcon =$	1.1032548
Slope of Falling Branch	$zm =$	60.096422

Distance From Neutral Axis "y_i"	Strain ε_{ci}	Stress f_{ci} (MPa)	Force C_{ci} (kN)	Force Arm y_{ci} (mm)	Moment M_{ci} (kNm)
0	0	0			
4.99	0.0003	7.08	5.29	2.493965	0.01
9.98	0.0005	13.30	15.24	7.481896	0.11
14.96	0.0008	18.68	23.92	12.46983	0.30
19.95	0.0010	23.20	31.33	17.45776	0.55
24.94	0.0013	26.88	37.47	22.44569	0.84
29.93	0.0015	29.70	42.33	27.43362	1.16
34.92	0.0018	31.68	45.93	32.42155	1.49
39.90	0.0020	32.81	48.25	37.40948	1.80
44.89	0.0023	33.01	49.24	42.39741	2.09
49.88	0.0025	32.51	49.03	47.38534	2.32
54.87	0.0028	32.02	48.28	52.37327	2.53
59.86	0.0030	31.52	47.54	57.3612	2.73
64.84	0.0033	31.02	46.79	62.34913	2.92
69.83	0.0035	30.52	46.05	67.33706	3.10
74.82	0.0038	30.03	45.30	72.32499	3.28
79.81	0.0040	29.53	44.56	77.31292	3.45

281

84.79	0.0043	29.03	43.82	82.30085	3.61
89.78	0.0045	28.54	43.07	87.28878	3.76
94.77	0.0048	28.04	42.33	92.27671	3.91
99.76	0.0050	27.54	41.58	97.26464	4.04

Compression Force in Concrete $C_c =$ 797.37308 kN

Moment of Concret Force About Neutral Axis $M_c =$ 43.991903 kNm

Centroid of Compression Force from N.A $y_c =$ 55.171041 mm

Lever Arm to Centroid of Tension Steel $larm =$ 695.41243 mm

Concrete Stress-Strain Relationship

Concrete Stress Variation
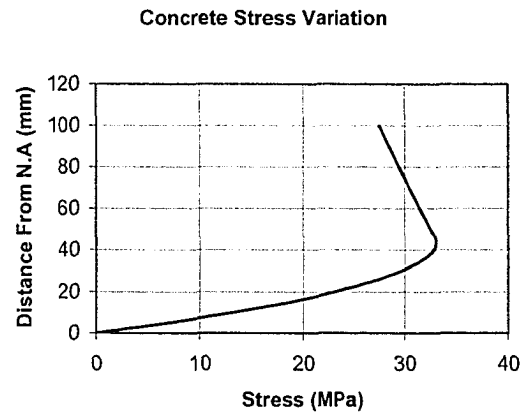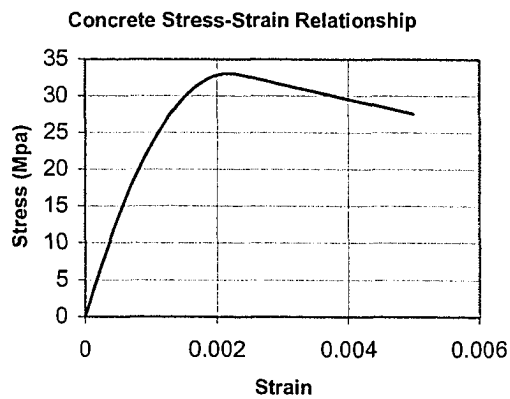
Srain and Stress in Compression Steel

Strain in Compression St $e_{sc} =$ 0

Stress in Compression St $f_{sc} =$ 0 MPa

Force in Compression St $C_s =$ 0 kN

Strain and Stress in Tension Steel

Strain in Tension Steel $e_{st} =$ 0.0320895

Stress in Tension Steel $f_{st} =$ 442.98504 MPa

Force in Tension Steel $F_t =$ 797.37308 kN

Computation of Factors α_1 and β_1

$$\beta_1 = \quad 0.8939092$$
$$\alpha_1 = \quad 0.993517$$

Computation of Depth of Neutral Axis

$$x = \quad 99.758608$$

Equilibrium of Forces

Summation of Axial Forces $P =$ Ft-(Cc+Cs)

                                                 $P =$ 0 kN

Summation of Moment $M =$ 554.50315 kNm

Depth of Neutral Axis, Moment of Resistance, and Curvature

Depth of Neutral Axis	$x =$	99.758608 mm	Correct Solution
Av Curvature	cur =	5.012E-05	Correct Solution
Av Moment of Resistance	Mr =	554.50315 kNm	Correct Solution

283